DEVELOPMENT OF NOVEL TRANSDERMAL DRUG DELIVERY TECHNOLOGIES FOR THERAPEUTIC PEPTIDES

Submitted to Waterford Institute of Technology for the Degree of Doctor of Philosophy August 2017

By Colin Dillon

Pharmaceutical and Molecular Biotechnology Research Centre (PMBRC)

Waterford Institute of Technology

Waterford

Ireland

Prepared under the supervision of Dr. Helen Hughes, Dr. Niall O'Reilly and Dr. Peter McLoughlin

DECLARATION

I hereby certify that this material, which I now submit for assessment is entirely my own work and has not been taken from the work of others save and to the extent that such work has been cited and acknowledged within the text of my work.

Signed: _____

ID No.: _____

Date: _____

ACKNOWLEDGEMENTS

The journey I undertook that ended with the completion of this thesis began on a fateful day in November 2008 when the opportunity to change the direction of my life was presented to me. I seized the chance and apprehensively started on a new path as a student of science. 8 years later, I write this while thinking back to that day and the incredible direction my life was about to take. It has been a very interesting 8 years with both highs and lows but always a deep feeling of gratitude to have been given this opportunity in the first place. My journey through this academic adventure has not been alone however, and I am eternally grateful for all the help, support, friendship, guidance and love that I have received along the way.

First, I want to thank my undergraduate classmates for pulling me through those early years. The long lunches spent in the canteen poring over chemical structures and spectra were as good as any lecture! A special thanks to my postgraduate and postdoctoral friends in the PMBRC. It was a pleasure working with you all every time that I set foot in those labs and these are the days I will miss the most.

To Helen, Niall and Peter: Where do I start? I cannot thank you all enough for giving me the opportunity to undertake this project. Every step of the way has been with your expert guidance, advice, patience, motivation and mentoring. I will be truly forever grateful to you all.

A big thank you to my parents, Christopher and Breda, for all your support over the years. It took a while, but I hope you have saved a spot on the sitting room wall for my enrobed mugshot! To Carla and Robert: I shall now be joining your enrobed mugshots on the wall!

To my wonderful children: Eva, Kate and Eoin. I am so proud of you and so grateful to be your Dad. I look forward to seeing you grow and take those first steps on your own epic journeys. But don't be afraid to change course – you never know where it will take you…

Finally, I want to thank my beautiful wife Louise for all your love, support, patience and friendship. We have had quite a journey together, especially over the last 8 years. It has been far from easy but I know that those difficult times only served to show us how resilient we are as a family and how we can overcome anything that life throws at us. My name is on the cover of this thesis but it belongs to you as much as it does to me. I love you very much and I look forward to the next exciting chapter with you which I'm sure will be an interesting one.

"The journey of a thousand miles begins with one step"

Lao Tzu

TABLE OF CONTENTS

LIST OF FIGURES

LIST OF EQUATIONS

LIST OF TABLES

LIST OF ABBREVIATIONS

ALA	5-aminoevulinic acid
AMP	Antimicrobial Peptide
BHA	Benzhydrylamine
BHI	Brain Heart Infusion
Boc	Butyloxycarbonyl
BSA	Bovine Serum Albumin
COX	Cyclooxygenase
CMC	Carboxymethyl Cellulose
DBU	1,8-Diazabicyclo (5,4,0) undec-7-ene
DCM	Dichloromethane
DIPEA	N,N-Diisopropylethylamine
DLS	Dynamic Light Scattering
DMF	Dimethylformamide
DNA	Deoxyribonucleic Acid
DSC	Differential Scanning Calorimetry
DVS	Dynamic Vapour Sorption
EMA	European Medicines Agency
FDA	Food and Drug Administration
FLD	Fluorescence Detector
Fmoc	Fluorenylmethyloxycarbonyl
FTIC	Fluorescein isothiocyanate
FTIR	Fourier Transform Infrared
GI	Gastrointestinal
GRAS	Generally Recognised as Safe
HBTU	2-(1H-benzotriazole-1-yl)-1,1,3,3-tetramethyluronium hexafluorophosphate
HEM	Human Epidermal Membrane
HF	Hydrogen Fluoride
HOBt	Hydroxybenzotriazole
HPLC	High Performance Liquid Chromatography
ICH	International Conference on Harmonisation
LC-MS	Liquid Chromatography-Mass Spectrometry

LOD	Limit of Detection
LOQ	Limit of Quantitation
MDR	Multidrug Resistant
MTC	Medullary Thyroid Cancer
NCL	Native Chemical Ligation
NMF	Natural Moisturising Factor
NMR	Nuclear Magnetic Resonance
OCT	Optical Coherence Tomography
PBS	Phosphate Buffered Saline
PDMS	Polydimethylsiloxane
PEG	Polyethylene Glycol
PGA	Polyglycolic Acid
PI	Polydispersity Index
PLA	Polylactic Acid
PLGA	Polylactic-co-glycolic Acid
PS	Polystyrene
PS-PAA	Polystyrene-*block*-poly(acrylic acid)
PVA	Polyvinyl Alcohol
PVP	Polyvinylpyrrolidone
RH	Relative Humidity
SC	Stratum Corneum
SEM	Scanning Electron Microscopy
SLP	Synthetic Long Peptide
SPS	Solution Phase Synthesis
SPPS	Solid Phase Peptide Synthesis
T_g	Glass Transition Temperature
TFA	Trifluoroacetic Acid
TGA	Thermogravimetric Analysis
UV	Ultra Violet
W/O	Water in Oil
W/O/W	Water in Oil in Water
WIT	Waterford Institute of Technology
XLF	Xtreme Laser Facility
ZOIs	Zones of Inhibition

ABSTRACT

The enormously rich chemical and biological diversity of peptides makes them extremely exciting targets as therapeutic entities. Delivery of these biologically active drugs is limited, however, to mainly parenteral intravenous injection or infusion which limits their potential, particularly for the treatment of less severe conditions. Transdermal drug delivery is an attractive proposition given that it represents a non-invasive means of administering pharmaceuticals. The highly effective barrier properties provided by the stratum corneum (SC), however, limits the application of transdermal delivery to relatively small, lipophilic molecules.

A dissolving microneedle system was developed using a combination of biocompatible polymers and stabilising sugars. In order to avoid loss of drug activity, the formulation process was carried out in aqueous solutions and at ambient temperatures. A variety of characterisation techniques were carried out and, with the aid of statistical analysis, an optimum polymer/sugar formulation was selected. Further characterisation work was carried out to examine needle strength, needle sharpness, drug diffusion within the array matrix, skin penetration and the stability of a model peptide, polymyxin B, encapsulated in the formulation. Franz diffusion cells were then used to carry out *in vitro* diffusion studies utilising porcine skin. These studies demonstrated that the microneedle system successfully delivered the peptide drug-load without loss of activity. In addition, 2 synthesised analogues of existing therapeutic peptides were also incorporated into the microneedle arrays and subsequently delivered through porcine skin to examine the effectiveness of the microneedle system to deliver peptides of various sizes and chemical properties.

Finally, a sustained drug release system based on the dissolving microneedle formulation was investigated which incorporated drug loaded polylactic-co-glycolic acid (PLGA) particles into the PVP/trehalose microneedles. These arrays were subsequently characterised and skin diffusion testing carried out to determine the ability of the microneedles to deliver the particles through porcine skin. Drug release studies were also carried out to examine the release profile of polymyxin B encapsulated in the PLGA particles.

CHAPTER 1. INTRODUCTION

1.1. Introduction

Transdermal drug delivery has been utilised for thousands of years for the treatment of various ailments and most recently, has been successfully employed as a means of administering many drugs for the treatment of a wide variety of conditions such as pain, travel sickness, smoking cessation and heart problems. The excellent barrier properties of the skin however, limits the range of drugs that can successfully permeate through its outer layer and as such, greatly reduces the potential of the transdermal route as a mode of drug administration [1, 2].

The ever growing numbers of pharmaceutically active peptides and proteins possess a broad range of therapeutic effects and have the ability to effectively treat a wide range of medical conditions. Exploiting the full potential of these biomolecules depends largely on the development of alternative delivery methods. The delivery of bio-therapeutic drugs such as peptides and proteins is almost exclusively via traditional hypodermic injection or intravenous infusion due to the fact that these drugs are generally metabolised by the GI tract, are poorly absorbed and suffer from poor bioavailability if administered orally. These therapeutic peptides and proteins are generally too large to passively diffuse through the barrier layer of the skin, unlike smaller drug molecules which possess larger diffusion coefficients and are capable of diffusion into the skin more easily [3, 4].

Microneedle technology offers a means of delivering a wide variety of pharmaceutical agents across the skin in a minimally invasive and virtually pain free manner. By utilising microneedle fabrication technology with biocompatible polymers in a dissolving microneedle system, it is envisioned that large hydrophilic macromolecules such as therapeutic peptides and proteins, which would normally not permeate through the skin, can be successfully delivered both systemically or in a targeted and controlled fashion.

1.2. The Skin and Transdermal Delivery

1.2.1. Skin Function and Structure

Skin is the heterogeneous integument of the human body and is also the largest organ, comprising approximately 10% of total body mass, covering roughly 1.7 m^2 [1]. The skin is composed of tissue that is in a constant state of growth, differentiation, renewal and death. The structure of the skin contains more than 5 different cell types and within the skin itself, transient cells from the circulatory and immune systems are present [5]. It performs many functions within the body including protection from toxic environmental chemicals and microorganisms, protection from ultra violet (UV) radiation, regulation of body temperature, synthesis of vitamin D (cholecalciferol) and the retention of bodily fluids [5, 6]. Human skin consists of three main and distinct anatomical layers (Figure 1.1) namely the epidermis, the dermis and subcutaneous tissues (also known as the hypodermis). The epidermis is the outer layer which serves as a barrier to the outer world and protects the body from external elements such as water, heat and cold, bacteria and sunlight. It also serves as a barrier which retains bodily fluids and keeps vitamins, minerals, hormones, proteins and heat within the body [7].

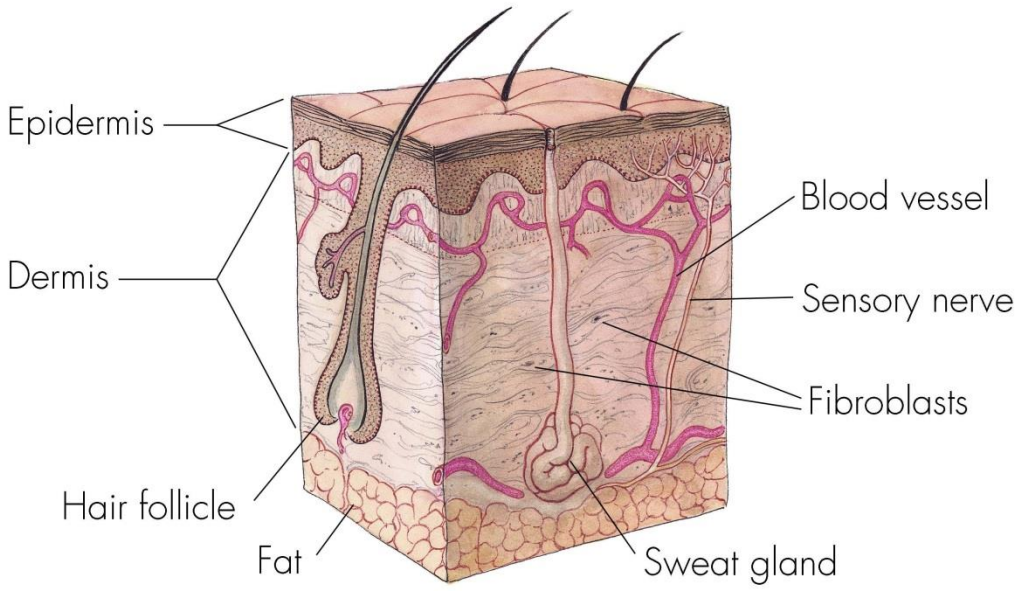

Figure 1.1: Cross section illustration showing the layers of the skin [8] .

In addition, the skin has immunological functions, synthesises vitamin D in the body and is important in social interaction and sexual attraction [2]. The skin is approximately 3 mm thick however thickness varies depending on a number of factors including age, health and the site of the body (thicker at the soles of the feet/palms of the hands, thinner at the eyelids). Appendages contained within the skin include sweat glands, sebaceous glands and hair follicles [9].

1.2.2. Epidermis

The epidermis is a layer approximately 100 µm in thickness and is defined as a stratified squamous epithelium. The epidermis is derived from the embryonic ectoderm, or outer gem layer, of the human embryo and it can range in thickness from approximately 0.06 mm on the eyelids to approximately 800 µm on the palms of the hands and soles of the feet [10]. It is extremely active and can completely regenerate itself over a period of between 45 to 74 days [7]. The epidermis is composed of several well-defined sub-layers (in reverse order from the surface): the stratum basal, stratum spinosum, stratum granulosum, stratum lucidum and the stratum corneum. As there are no blood vessels in the epidermis, all nutrients and waste are transported across the epidermal-dermal layer via diffusion [1]. The epidermis contains 4 cell types including melanocytes (which produce melanin - the body's main pigment and natural sunscreen) [11], Langerhans cells and merkel cells. However, it consists primarily of cells called keratinocytes which are produced by cell division in the deepest layer of the epidermis. These keratinocyte cells migrate up through the epidermal layers, eventually dying and forming the outer barrier layer. The rate of keratinocyte cell production is roughly equal to the rate of keratinocyte cell death in a healthy individual [10].

1.2.2.1. Stratum Basal

The stratum basal, also referred to as the stratum germinativum [6], is the deepest layer of the epidermis, is roughly 1 to 3 cells in thickness and is unevenly attached to the dermis via a basement membrane [12]. All the layers of the epidermis are composed mainly of keratinocytes and each layer is the site of a different level of

cellular differentiation. There are two types of keratinic cells in this layer: one type which anchors the epidermis to the basement membrane and the other type which have the ability to divide and produce new keratinocytes [13]. These cells are responsible for the synthesis of keratin and cytokines [14] and are only found in the stratum basal or basal layer and once produced, these keratinocytes are then carried up through the other layers to the surface of the skin. This migration of the keratinocytes from the basal layer to the surface layer takes approximately 12 to 24 days [15]. During this journey, the cells undergo a series of morphological and biochemical changes called keratinisation which results in the formation of the skins outer layer, the SC. Included in these changes are the synthesis of lipid structures and the synthesis of the proteinaceous keratin material.

1.2.2.2. Stratum Spinosum

The next epidermal layer above the stratum basal is the stratum spinosum or prickle cell/spinous layer. The keratinocytes become flatter as they move up to this layer, connected via desmosomes, and are referred to as prickle cells [14]. In addition to the keratinocytes, the stratum spinosum also contains Langerhans cells which play an important role in the skins immunological function, acting as the first line of defence against external antigens [10]. Lipids present in this layer are also similar to those found in the basal layer [7].

1.2.2.3. Stratum Granulosum

The stratum granulosum or granular layer is composed of flattened keratinocytes and also contains lipids which differ from those found in the lower layers. These lipids include free sterols, ceramides, cholesterol sulphate and glycolipids and are discharged by cells into the intercellular space of the granular layer acting as a type of ‘cement’ to hold together the cellular ‘bricks’ of the tissue structure [7, 10]. It is in this layer that the keratinocytes begin to lose cellular functions and die.

1.2.2.4. Stratum Lucidum

The stratum lucidum is a layer that is only present in areas of thickened palmoplantar skin in the body namely the palms of the hands or soles of the feet. It consists of layers of clear, flat, keratinocytes however, these cells are referred to as transitional as they remain nucleated [12, 14].

1.2.2.5. Stratum Corneum

The SC is the outer layer of the epidermis and is often referred to as the "horny layer" (Figure 1.2). It provides a mechanical barrier of protection against water loss and foreign materials to the epidermis beneath [6]. It is a composite material composed primarily of a fibrous coil shaped protein called keratin. Keratin consists of coiled polypeptide chains which are joined together into supercoils of polypeptides linked together by disulphide bonds between neighbouring cysteine amino acids [14]. The SC is only 15 – 150 µm thick and is composed primarily of approximately 8 to 16 layers of flattened, stratified and tightly packed dead keratinocyte cells called corneocytes.

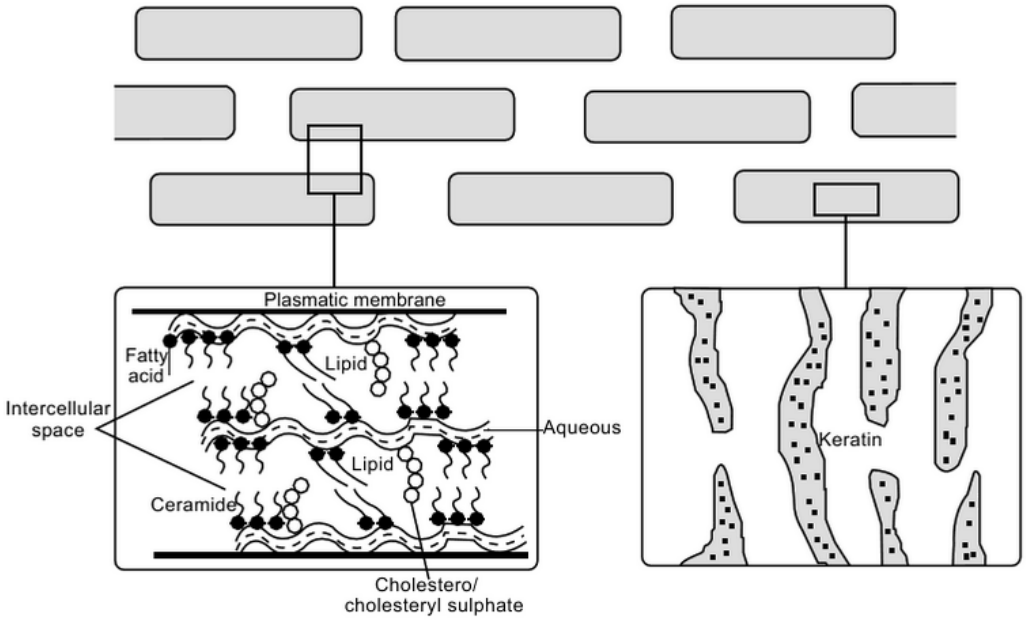

Figure 1.2: Simplified structural diagram of the layers comprising the stratum corneum [13].

The SC is highly dense (approximately 1.4 g/cm^3) and has a much lower level of hydration (approximately 15-20%) when compared with the rest of the body (approximately 70%) [13, 15]. It is in the SC that the keratinocytes undergo programmed cell death, a form of apoptosis known as terminal differentiation [6] - fully changing into flattened corneocytes, losing their nucleus and organelles as well as their plasma membrane which is replaced by a cornified cell envelope [12]. These corneocytes are held together by keratin filaments which form crosslinked disulphide macrofibres and by intercellular lipids which form the main part of the permeability barrier [14]. The overall composition of the SC is approximately 60% structured proteins, 20% lipids and 20% water [15]. The corneocytes are arranged in bilayers along with the intercellular lipid phase which contains ceramides, free sterols, free fatty acids, triglicerides, sterol esters and cholesterol sulphate. This structure of the SC is akin to a brick wall with the corneocytes functioning as the bricks and the lipids as the mortar [7, 10]. Without the SC, the body would rapidly lose significant amounts of water to the environment and become dehydrated. The tightly packed overlapping cells and lipids block the diffusion of water and retain it within the body. Removal of the SC layer from the skin increases water loss approximately ten fold [10]. The SC is replaced fully in approximately 14 days in young individuals and in about 37 days in adults over 50 years old [7].

The SC is a highly effective barrier, protecting the body from water loss and external contaminants such as chemicals and microorganisms. In addition to its barrier properties, the acid pH of sweat, the presence of anti-microbial peptides (Aparticles) and sebaceous secretions also contribute to the antimicrobial properties of the SC [10]. Two main types of Aparticles are produced in the epidermis namely defensins and cathelicidins, and these are effective at killing both Gram-positive and Gram negative organisms as well as fungi and certain viruses. [14]. The SC is not totally impermeable however, and must allow certain materials generated in the skin tissue to escape such as gases, oils and other hydrophobic materials [7].

1.2.3. Dermis

The dermis is a fibrous layer of connective tissue about 1 to 3 mm thick which lies directly beneath the epidermis. It provides protection to the body from mechanical

injury, helps with thermal regulation and contains many receptors and sensory stimuli [6]. The dermis forms the main bulk of the total skin mass (about 90%) and the structure of the dermis consists of a matrix of loose connective tissue which is mainly composed of 2 types of fibrous proteins called collagen and elastin. Collagen is responsible for most of the tensile strength of the skin and makes up about 77 % of the dry weight and up to 30% of the volume of skin [11, 14]. These proteins are produced by the main cells of the dermis known as fibroblasts [13, 15] and are embedded in an unstructured ground substance composed of water, ions and complex carbohydrate mucopolysaccharides (glycosaminoglycans) which are attached to the collagen and elastin proteins and it is these proteins which give skin its strength and elastic properties. In addition to these, the dermis also contains blood vessels, nerves, sensory receptors, hair follicles, sebaceous and sweat glands [7, 10, 15]. The dermis comprises of two main sections: the papillary dermis and the reticular dermis.

The papillary dermis is the outer section of the dermis and is in direct contact with the epidermis. It contains many blood vessels and is the main source of nutrition for the epidermis. Nutrients are transported to and from the dermis via a network of blood capillaries which are composed of a series of loops originating from arteries which gradually become smaller and smaller, eventually forming minuscule vessels measuring only a number of microns in size near the top of the papillary dermis. The vessels eventually reverse direction and form venules, enlarging as they return to the dermis [7].

The reticular dermis is situated below the papillary dermis and although it contains less cells and blood vessels than the papillary dermis, it is composed of densely packed bundles of collagen and elastin fibres which give the skin its physical strength and resistance to tearing (in fact, leather is manufactured from the reticular dermis of animals). The skin appendages, namely sweat/oil glands and hair follicles, are situated here also [7].

1.2.4. Subcutaneous Layer

The subcutaneous layer lies directly beneath the dermis and is composed of loose, fibrous connective and adipose tissue. The level of adipose tissue varies from person

to person but is generally thicker in the abdominal region and non-existent on the eyelids. The main functions of the subcutaneous layer are as a heat insulator, shock absorber and as a reserve energy store for the body. The base of hair follicles and the secretory area of sweat glands are located here in addition to cutaneous nerves and various blood and lymph networks. The cutaneous nerves are abundant within the skin, with approximately 57,000 nerve fibres embedded in every cubic millimetre of nerve which join to sensors and it is these nerves which enable the detection of sensations such as pressure, pain, heat and cold [12, 15]. As nerve fibres are contained within the dermis, they can be up to 800 μm below the skin surface, depending on the location, ending around hair follicles and the papillary dermis [6].

1.3. Transdermal Drug Delivery

For thousands of years, many ailments have been treated by the application of compounds to the skin. Today, transdermal drug delivery devices have been employed in the treatment of a wide variety of conditions including travel sickness, cardiovascular disorders, pain management, smoking cessation and hormone replacement therapy [9]. Advantages associated with transdermal drug delivery include the potential for steady state drug levels, hepatic first pass metabolism avoidance, improved patient compliance and no gastrointestinal side effects [16].

Transdermal drug delivery devices are an attractive alternative to invasive injection-based delivery methods and additionally, tend to be more efficient – using less drug per application and are typically less variable compared with some oral pharmaceuticals which can undergo degradation in the GI tract [17]. Drug loaded patches are usually the most recognisable transdermal delivery system. These patches are typically polymer based, contain a reservoir of drug in addition to an adhesive layer and facilitate controlled, steady delivery of the drug for up to a week [16, 18]. The first transdermal drug delivery patch to be brought to the market was a scopolamine (Figure 1.3) delivery system developed by the Alza Corporation to treat motion sickness [2, 19]. Transdermal nicotine patches emerged a decade later and proceeded to become the first widely used transdermal drug delivery system, subsequently raising the profile of transdermal drug delivery in the process [2].

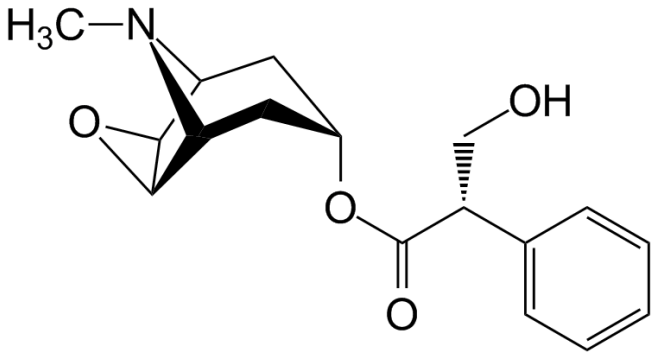

Figure 1.3: Chemical structure of scopolamine [20].

The delivery of pharmaceuticals through the skin offers many advantages over the more traditional oral route most notably the avoidance of first past metabolism and the GI tract which can inactivate the drug before it reaches the intended target site. Similarly, unlike the parenteral route, transdermal drug delivery is non-invasive, allows the patient to self-administer and also offers the ability to provide controlled and prolonged release of the drug into the body [1, 2, 19]. In addition, delivery of vaccines transdermally is an attractive alternative to parenteral delivery with the added advantage that transdermal immunisation stimulates both systemic and mucosal immunity. Mucosal immunity is significant given that most pathogenic organisms enter the body through mucosal surfaces. The presence of immunocompetent cells in the skin such as keratinocytes and Langerhans cells contribute to a potent immune response from this type of vaccination also [21].

The SC provides the main barrier to skin permeation and as such, limits the therapeutic effectiveness of any topically applied compounds [1, 17]. The rate of percutaneous drug transport across the skin is directly limited by the SC, which is much more effective as a barrier to drug delivery than the epithelial barriers of gastrointestinal, buccal, nasal, vaginal or rectal delivery paths [9]. Any permeation is limited to lipophilic or hydrophobic compounds due to the SC's high lipid content and as the SC is effectively composed of dead tissue, the mode of transport is via passive diffusion as per Fick's Law (Equation 1.1).

Fick's Law of Diffusion in relation to transport of drug across the SC [9] is given as:

$$\frac{dM}{dt} = \frac{D.\Delta C.K}{h} \qquad \textbf{Equation 1.1}$$

Where: *dM/dt* is the steady state flux across the SC

D is the diffusion coefficient of drug molecules

ΔC is drug concentration gradient across the SC

K is the partition coefficient of the drug between skin and formulation medium, and

h is the thickness of the SC

In contrast, the viable epidermis is hydrophilic and as such, acts as rate limiting barrier in the case of particularly lipophilic compounds [15]. However, in general, once the drug molecules have passed through the SC layer, passage into the other dermal layers and subsequent systemic delivery occurs quite rapidly and with ease [9, 19].

There are a very limited number of drugs which possess the ability to successfully permeate across the SC in a sufficient quantity to have a therapeutic effect (Table 1.1). Size, shape and chemical properties all have a major influence on the ability of a molecule to effectively pass through the SC with passive diffusion generally limited to potent hydrophobic drug molecules with low molecular weights (<500 Da) [3, 19]. To overcome this, a range of methods have been investigated to enhance transdermal drug absorption and these include physical techniques such as iontophoresis, electroporation, thermal ablation, ultrasound, biochemical methods such as enzyme inhibition and liposomal vesicles, microneedles and chemical permeation enhancing techniques [13, 18].

Table 1.1 Transdermal drugs approved by the U.S. FDA [2].

Drug (Trade name, year of FDA approval)	Indication	Patch design	Duration of application
Buprenorphine (Butrans®, 2010)	Chronic pain	Drug in Adhesive	7 days
Clonidine (Catapres-TTS®, 1984)	Hypertension	Reservoir/Membrane	7 days
Oestradiol (Estraderm®, 1986)	Female HRT	Reservoir/Membrane	3–4 days
Oestradiol (Climara®, 1994)	Female HRT	Drug in Adhesive	7 days
Oestradiol (Vivelle®, 1994)	Female HRT	Drug in Adhesive	3–4 days
Oestradiol (Alora®, 1996)	Female HRT	Drug in Adhesive	3–4 days
Oestradiol (Vivelle-Dot®, 1999)	Female HRT	Drug in Adhesive	3–4 days
Oestradiol (Menostar®, 2004)	Female HRT	Drug in Adhesive	7 days
Oestradiol (Minivelle®, 2012)	Female HRT	Drug in Adhesive	3–4 days
Oestradiol (E)/Norethindrone (NT) (Combipatch®, 1998)	Female HRT	Drug in Adhesive	3–4 days
Ethinyl oestradiol (EE)/Norelgestromin (NL) (Ortho Evra®, 2001)	Female contraception	Drug in Adhesive	7 days
Oestradiol (E)/Levonorgestrel (L) (Climara Pro®, 2003)	Female HRT	Drug in Adhesive	7 days
Fentanyl (Duragesic®, 1990)	Chronic pain	Drug in Adhesive	72 h
Granisetron (Sancuso®, 2008)	Chemotherapy-induced nausea and vomiting	Drug in Adhesive	Up to 7 days
Methylphenidate (Daytrana®, 2006)	ADHD	Drug in Adhesive	Up to 9 h in a day
Nitroglycerin (Nitro-Dur®, 1995)	Angina pectoris	Drug in Adhesive	12–14 h
Nitroglycerin (Minitran®, 1996)	Angina pectoris	Drug in Adhesive	12–14 h
Oxybutynin (Oxytrol®, 2003)	Over-active bladder	Drug in Adhesive	3–4 days
Rivastigmine (Exelon®, 2007)	Alzheimer's and Parkinson's disease	Matrix	24 h
Rotigotine (Neupro®, 2007)	Parkinson's disease Restless legs syndrome	Drug in Adhesive	24 h
Scopolamine (Transderm Scōp®,1981)	Motion sickness	Reservoir/Membrane	72 h
Selegiline (Emsam®, 2006)	Major depressive disorder	Drug in Adhesive	24 h
Testosterone (Androderm®, 1995)	Hypogonadism	Reservoir/Membrane	24 h
Nicotine (Nicoderm CQ®, 1991)	Smoking cessation	Reservoir/Membrane	24 h
Nicotine (Nicorette®)	Smoking cessation	Matrix	16 h

Nicotine (Nicorette® Invisipatch®)	Smoking cessation	Matrix	16 h
Nicotine (Habitrol®, 1990)	Smoking cessation	Matrix	24 h
Sumatriptan (Zecuity®, 2013)	Migraine	Iontophoretic system	4 h
Capsaicin (Qutenza®, 2009)	Neuropathic pain	Drug in Adhesive	Single 60 min application of up to four patches
Diclofenac epolamine (Flector®, 2007)	Topical treatment acute pain	Drug in Adhesive	12 h
Lidocaine (Lidoderm®, 1999)	Post-herpetic neuralgia pain	Drug in Adhesive	Up to three patches only once for up to 12 h within a 24 h period
Lidocaine (L)/Tetracaine (T) (Synera®, 2005)	Local dermal analgesia	Eutectic mixture – CHADD® technology	20–30 min
Menthol (M)/Methyl salicylate (MS) (Salonpas®, 2008)	Muscles and joints pain	Drug in Adhesive	Up to 8–12 h
Oestradiol (Evamist®, 2007)	Menopausal symptoms	Cutaneous solution	One spray once daily (starting dose)
Testosterone (Axiron®, 2010)	Hypogonadism	Cutaneous solution	2 pump actions once daily (starting dose)

1.3.1. Chemical Enhancers

Chemical penetration enhancers, also referred to as accelerants or sorption promoters, have been used to enhance the penetration of therapeutic and cosmetic materials across the SC. In most cases, chemical enhancers disrupt the lipid area of the SC which results in fluidisation that allows permeation through the SC layers [22]. An array of drugs have been effectively delivered transdermally in conjunction with chemical percutaneous enhancers, however the inclusion of such chemicals in transdermal formulations has been limited as the mode of action of these enhancers is complex and not fully understood [23]. In addition, although a wide range of chemical enhancers have been employed in this way, none have proved to be ideal. Attributes of an ideal chemical permeation enhancer include non-toxicity, non-irritating and non-allergenic. An ideal permeation enhancer should work rapidly once applied and the activity of the enhancer should be predictable and reproducible. The enhancer should have no pharmacological effect and work uni-directionally by allowing drug into the body but preventing endogenous material from permeating out through the skin. The barrier property of the skin should recover quickly and fully after removal of the enhancer and the chemical enhancer needs to be fully compatible with the drug and any excipients used in the formulation [2, 13, 24].

Three routes are available for percutaneous permeation: transappendageal (through hair follicles or sweat and sebaceous glands), transcellular and intercellular (both of which involve permeation through the intact SC) [1] (Figure 1.4). It is believed however, that the predominant routes by which molecules permeate through the skin are transcellular or interecellular given that follicle orifices and sweat/sebaceous glands account for less than 0.1% of total skin area [13, 24]. The mechanism of intercellular diffusion involves the lateral movement of the drug molecules through the inter-lamellar spaces present between the corneocytes of the SC. These spaces contain less ordered lipids and more flexible hydrophobic chains and have higher water content, allowing for the transport of hydrophilic molecules. Transcellular diffusion involves the permeation of the drug molecules through the corneocytes. However, this mode of diffusion is practically unimportant for transdermal drug transport [13].

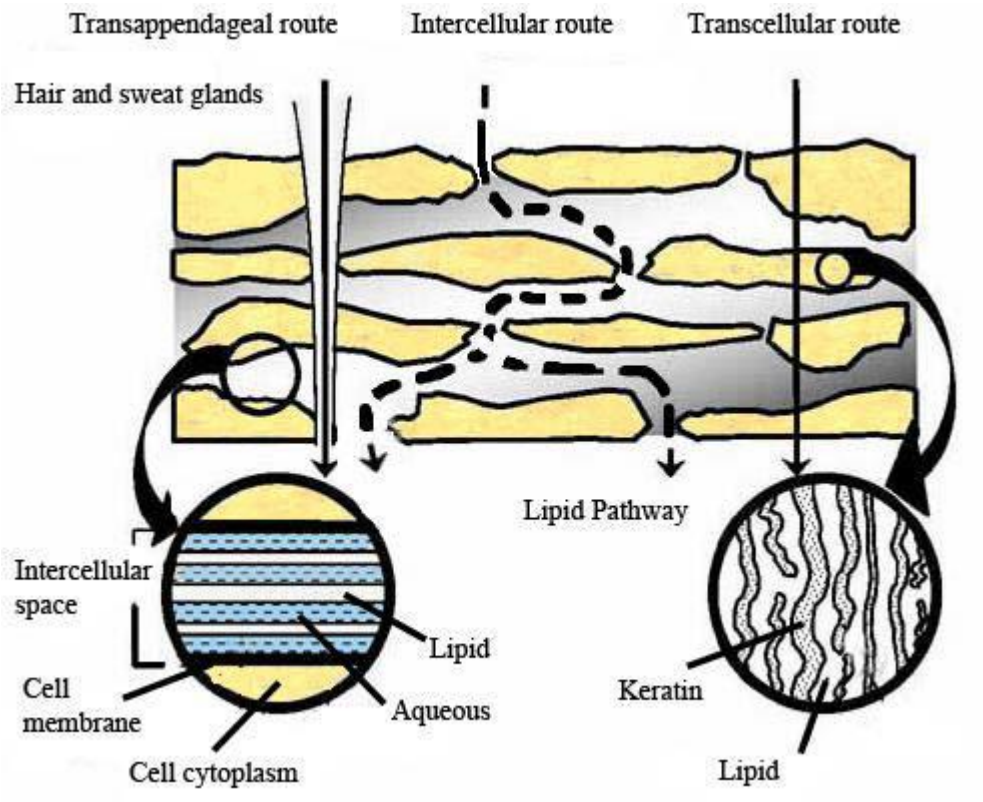

Figure 1.4: Illustration of the three pathways of diffusion across the SC into the dermis: transappendageal, intercellular and transcellular [22].

Chemical permeation enhancers can work in a variety of ways in order to increase diffusion across the skin by altering the proteins and lipids of the SC. Direct effects include denaturing or modifying the conformation of intercellular keratin of the SC, after which swelling and increased hydration can occur. In addition, the packing of the corneocytes can be disrupted by the chemical enhancer acting on the desmosome cells which hold the corneocytes together. The barrier properties of the lipid bilayers can also be reduced by the modification of the intercellular lipid domains. The solvent nature of the SC can also be changed which assists in the permeation of the drug into the skin. Examples of commonly used permeation enhancers include water, urea, alcohols, surfactants, terpenes and fatty acids. Water is the most natural of all permeation enhancers and the hydration of the skin above the normal water content of the human SC of 15-20% via direct soaking of the skin or exposure to high humidity, results in an increase in the permeability and transdermal absorption of both hydrophilic and lipophilic permeants [23].

1.3.1.1. Occlusion

Covering the skin with impermeable films or substances can cause occlusion. This is utilised effectively by many transdermal patch systems and topical applications. Occlusion of the skin can result in an increase in SC hydration which causes swelling of the corneocytes, disrupting the barrier structure and increasing the intercellular spaces between cells, increasing permeability. The SC is extremely hygroscopic and can absorb up to 500% of its dry weight in water in less than one hour if immersed but the enhanced permeability of the skin after hydration is limited to mostly non-polar and lipid soluble molecules [25]. Occlusion over an extended period (48 h) however, has been shown to swell the intercellular spaces of the SC to such an extent that a continuous channel is formed, allowing the permeation of both polar and non-polar molecules [13].

1.3.1.2. Short Chain Alcohols

Of all the alcohols utilised as skin permeation enhancers, ethanol and isopropyl alcohol are the most widely used [26]. Ethanol is used extensively in the formulation of transdermal patch systems due to its ability to increase the permeation of many pharmaceutical materials. It can be used as a solvent to increase the solubility of a drug or can alter the solubility properties of the skin tissue. Used in high concentrations over extended periods of time, its properties as a volatile solvent may result in the extraction of some lipid from the SC, resulting in improved drug flux through the skin [13].

1.3.1.3. Fatty Acids

A large number of fatty acids have been investigated as skin permeation enhancers including straight chain saturated, monounsaturated and polyunsaturated acids. Their efficacy is directly related to their structure, in particular the length of their carbon chains – as fatty acids with shorter chain lengths possess insufficient lipophilicity for adequate SC permeation. The most popular and effective of this type of permeation enhancer for both polar and non-polar drugs is oleic acid [23]. It is generally recognised as safe (GRAS) listed and Food and Drug Administration (FDA)

approved [13]. Along with its methyl and ethyl esters, oleic acid is used widely as a fatty acid permeation enhancer and is often used in conjunction with propylene glycol which increases its permeation enhancing qualities (Figure 1.5). Oleic acid works by causing alterations to the membrane structure and the interface between solid and liquid areas of the SC. This results in a shortening in the diffusional path length for permeants or a reduction in the resistance properties of the SC [26].

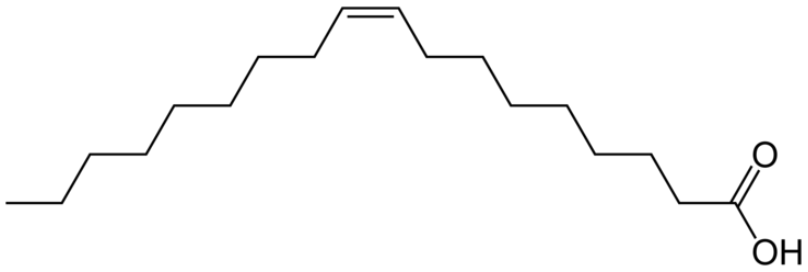

Figure 1.5: Chemical structure of oleic acid [27].

1.3.1.4. Surfactants

Surfactants are used extensively in many pharmaceutical and cosmetic formulations as emulsifiers, stabilisers, wetting and suspending agents, but they also possess the ability to alter the permeability of the skin. Surfactants are composed of a lipophilic long chain carbon tail group and a hydrophilic head-group and are classified according to the charge on the head-group as anionic, cationic, non-ionic or zwitterionic surfactants. Cationic and anionic surfactants have marked permeability enhancing effects on skin. However, by swelling the SC and interacting with intercellular keratin, they can damage and irritate the skin. Non-ionic surfactants have lower toxicity than cationic or anionic surfactants and are regarded as safe, resulting in their frequent use for topical formulations [26]. As such, coupled with their effect on skin permeability, non-ionic surfactants show great potential as effective transdermal drug delivery enhancers [13]. Polyoxyethylene-23-lauryl ether, polyoxyethylene-2-oleyl ether, polyoxyethylene-2-stearyl ether and polysorbate 80 (Figure 1.6) are examples of non-ionic surfactants that have been investigated as permeation enhancers for transdermal drug delivery [28]. In addition, Lechitin, a phospholipid which acts as a surfactant, is a natural non-toxic and biocompatible permeation enhancer used in the cosmetic industry [22].

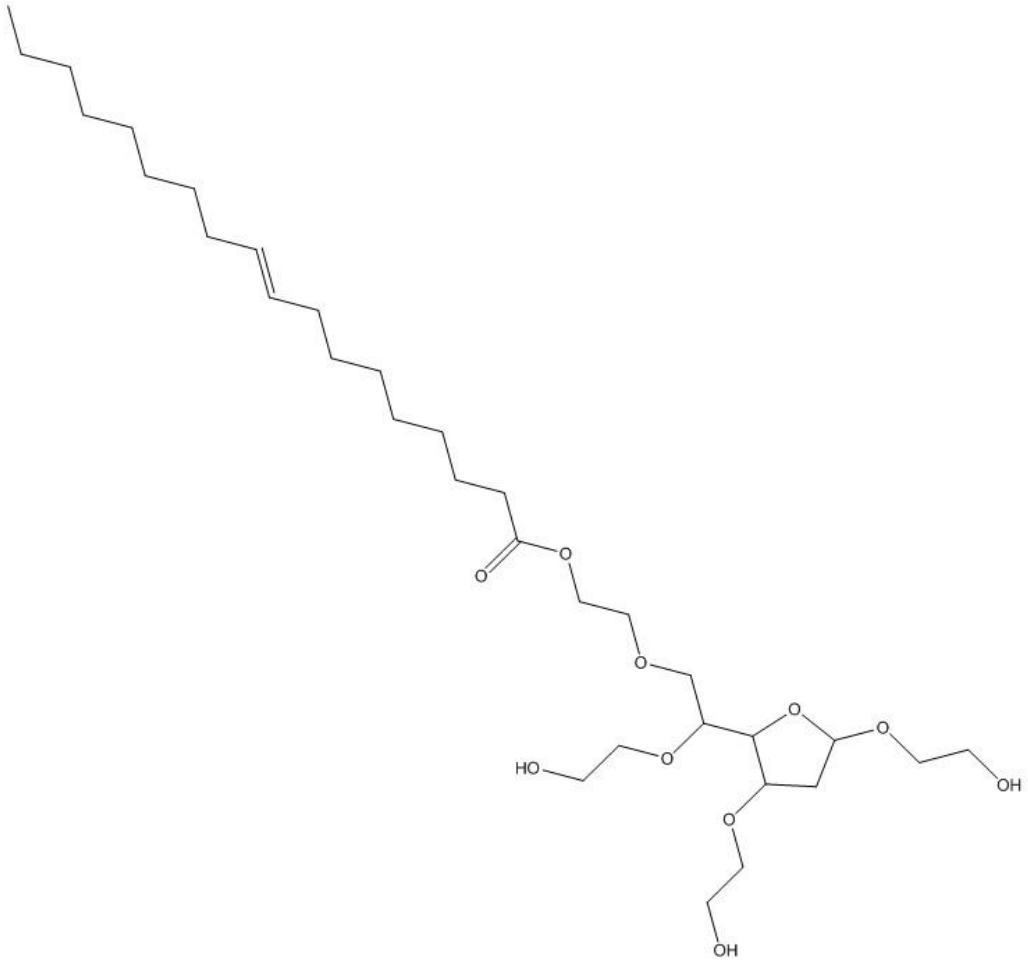

Figure 1.6: Chemical structure of non-ionic surfactant polysorbate 80 [29].

1.3.1.5. Terpenes

Terpenes consist of repeating isoprene (C_5H_8) units and are classified according to the number of isoprene units, chemical groups and whether they are linear, monocyclic or bicyclic (Figure 1.7). They are FDA approved and although have been known to cause skin irritation, are non-toxic and do not cause lasting erythema. In addition to their use as antispasmodics, carminatives and antiseptics, terpenes have been used to enhance the permeation of both lipophilic and hydrophilic drugs.

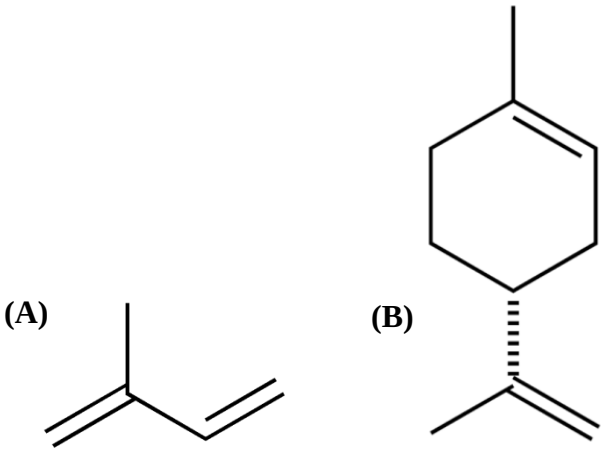

Figure 1.7: Structure of (A): a single isoprene unit and (B): limonene, a cyclic terpene consisting of 2 isoprene units [30].

Smaller terpenes have been shown to be more effective permeation enhancers than larger terpenes; however, their effectiveness is related to the actual chemical structure of the terpene in addition to the properties of the drug in the formulation [13].

1.3.2. Iontophoresis, Electroporation, Phonophoresis, and Thermal Ablation

Iontophoresis is the use of low level electrical current which is passed through the skin to increase the transport of both neutral and charged molecules and provides an efficient, non-invasive, local and pain free method of transdermal drug delivery [31, 32]. Controlled drug delivery is possible using this technique given that the volume of drug delivered is directly proportional to the current which is applied as well as current duration, which also allows for the use of pre-programmed delivery rates [2, 33]. In addition, it is a technique which can be used for targeted or systemic delivery. Iontophoresis has been successful in transdermal delivery of ionized and hydrophilic drug molecules that otherwise would not passively diffuse into the skin [34]. Katikaneni *et al*., 2010 [35] have investigated the delivery of daniplestim using a combination of iontophoresis and microneedles. Another technique which utilises electricity for transdermal enhancement is electroporation, which involves the application of high voltage pulses to create temporary structural disruption of the lipid layers of the SC [36].

The use of ultrasound to enhance the delivery of drugs across the skin has been used for many years and is referred to as sonophoresis or phonophoresis. Sonophoresis utilises either high frequency ultrasound between 20kHz and 16MHz or low frequency ultrasound in the range of 10 to 100kHz [37]. Low frequency ultrasound was shown to be more effective, however, for the delivery of larger molecules such as proteins and nucleotides. This technique causes nano-scale structural disruption within the lipid layers of the SC which in turn results in increased permeability [32].

Thermal ablation or thermophoresis, is the application of heat to selectively remove the SC while avoiding causing damage to the deeper layers of the skin. By applying rapid temperature increase to the SC, surface tissue is vaporised with ablation restricted to the SC leaving the underlying tissue undamaged. Another application of heat to enhance transdermal delivery is thermoporation or microporation which involves heating metallic filaments which are in contact with the skin to create micropores in the SC [38]. Similarly, laser ablation involves the directed application of optical energy to the SC which instantly evaporates water from the structure and creates microchannels. Using this technique, the depth of the channels can be carefully controlled to avoid damage to the lower layers and drug formulation can then be applied over the microchannels to facilitate enhanced transdermal delivery [32].

1.4. Peptides

1.4.1. Amino Acids and Peptide Formation

Peptides are biopolymers which are derived from serial condensation reactions that occur between various natural amino acid monomers (Figure 1.8) [39]. Amino acids are organic compounds which are composed of amine (-NH_2) and carboxylic acid (-COOH) functional groups in addition to a side chain which is specific for each amino acid. Over 700 amino acids have been discovered to exist in nature however, only 20 of these (Figure 1.9) are utilized in the biosynthesis of proteins [39, 40]. As such, these particular amino acids are essentially the building blocks of all life on earth. The general formula of these 'elementary' amino acids can be given as: $RCH(NH_2)COOH$, with the amino group located on the α carbon atom. With the exception of glycine, all of these amino acids are chiral molecules with an asymmetric centre at the α carbon.

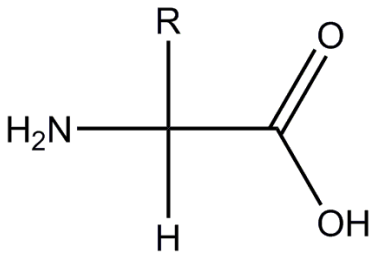

Figure 1.8: General structure of an α – amino acid where R refers to the specific side chain for each amino acid [40].

The remaining non-protein forming amino acids and peptides formed from them can carry out numerous biological functions as neurotransmitters or intermediates in metabolic pathways. In fact, the majority of these non-protein amino acids have been found in prokaryotes and lower eukaryotes such as algae, fungi, yeasts and sponges and the amino acids can often impart unusual properties on the peptides, many of which are utilised in the production of biochemical tool molecules, antibiotics and other therapeutic biologics [41].

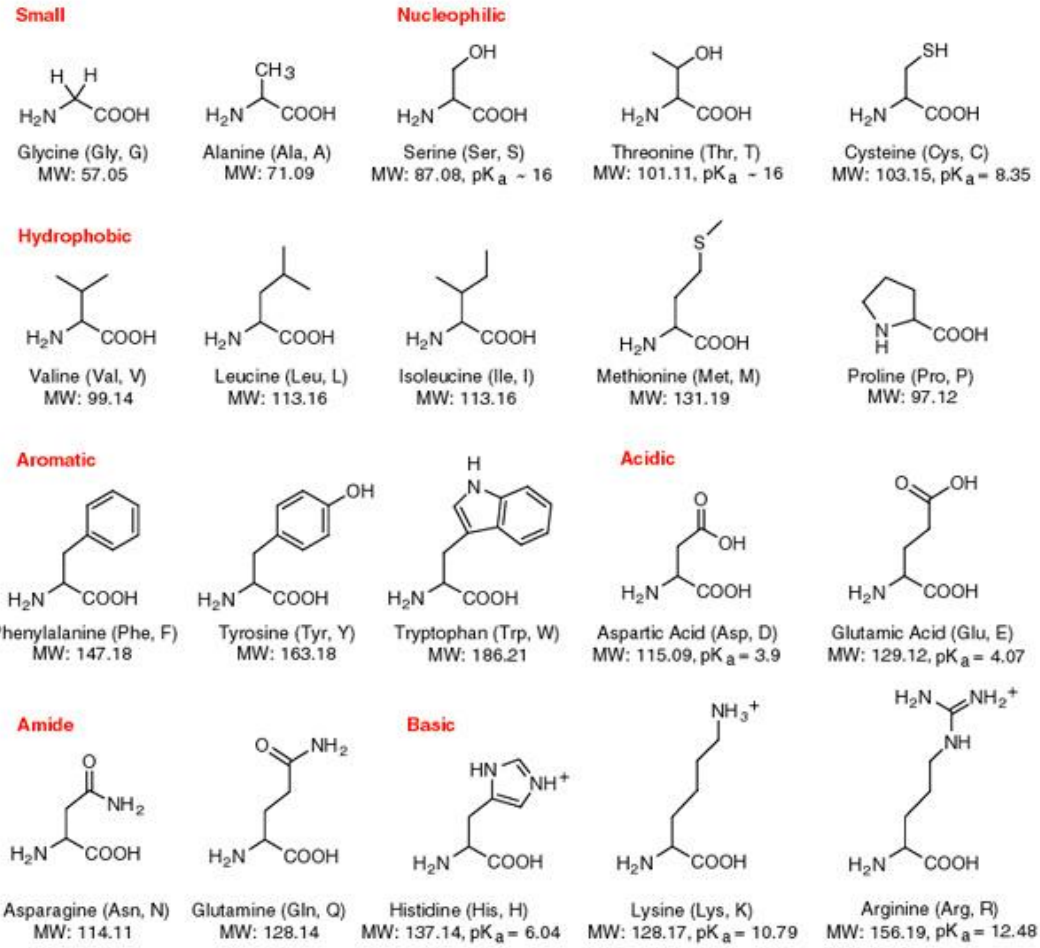

Figure 1.9: List and structures of the 20 amino acids found naturally in proteins [42].

Polymers of these amino acids are formed through the condensation reactions between respective carboxyl and amino groups with polymers consisting of 50 or less amino acid residues referred to as peptides, and those with more than 50 amino acid residues referred to as proteins [40]. The hydrophobic or hydrophilic properties of an amino acid depend upon its side chain and it is this combination of side chains within a peptide which give its characteristic set of properties. Peptides have the greatest variation in structure and function of all classes of bioactive macromolecules and they are essential to all biological processes. The amino acid sequences in both peptides and proteins are responsible for all cellular function and intercellular communication [43]. Peptides can be involved in these processes in a number of roles; as enzymes, antibodies, hormones, kinins, cytokinins and neurotransmitters to name but a few. Peptides display high specificity and potency and can undergo rapid metabolism, all of which are properties that are essential for these biological

functions [39]. In short, the chemical diversity of peptides and proteins is unmatched by any other type of biological molecule [43].

1.4.2. Pharmaceutical Peptides

Therapeutic peptides have emerged as promising pharmaceutical contenders largely due to advancement in molecular biology and biotechnology. Natural peptides exhibit an enormous range of biological activities and this makes them ideal candidates for use in the development of new therapeutic drugs. In nature, the roles of peptides are vast and varied ranging from immunity, stress, growth, homeostasis, reproduction and defence. In fact, many promising antimicrobial peptides have been isolated from the skin of frogs and toads where their natural function is to protect from predators and pathogens. Numerous peptides isolated from venomous creatures such as snakes and spiders are being investigated for the treatment of pain, diabetes, neurological disorders and cancer [44].

Compared with conventional therapeutics, peptides have many advantages including high activity, high specificity and typically are effective at low concentrations [45-47]. In addition, peptides degrade into amino acids which are far less biologically harmful than the toxic metabolites which can accumulate in the body often as a product of side effects from small molecule drugs [48]. Where side effects occur as a result of therapeutic peptide administration, these are generally related to dosage or confined to local reactions at the site of injection [43]. Most physiological processes are regulated by peptides acting as endocrine or paracrine signals at certain sites and as neurotransmitters or growth factors at others. To date, peptides have been employed therapeutically in a wide range of areas including neurology, endocrinology and haematology [49]. The increase in targeting metabolic disorders with peptides has resulted in the development of longer and more complex molecules however, interest continues in the development of shorter peptides with less than 10 residues in the area of peptide based vaccines [43] which highlights the scope of these therapeutic molecules.

The first peptide to be successfully isolated and therapeutically administered was insulin and to date, it is still the most widely prescribed therapeutic peptide, having

been available for over 50 years. Insulin (Figure 1.10) has a molecular weight of 5808 Da and consists of 51 amino acid residues divided into a pair of peptide chains that are connected via two disulphide bonds [50, 51].

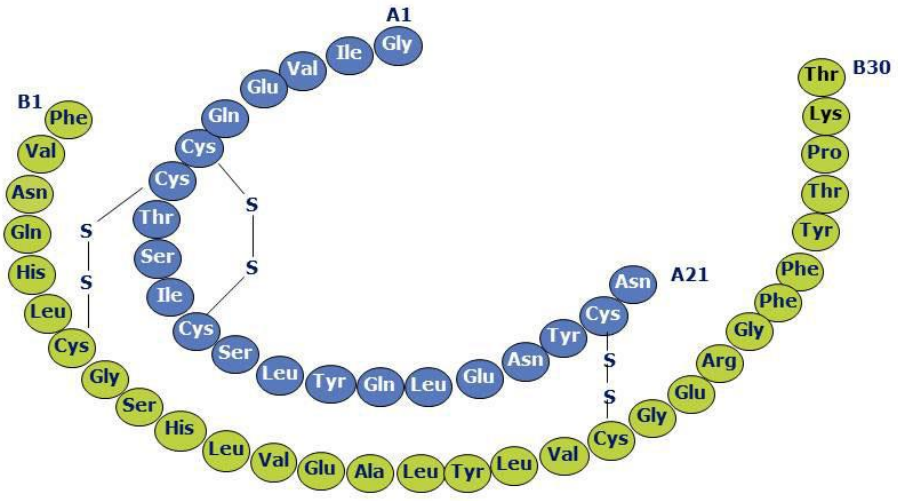

Figure 1.10: Primary structure of human insulin showing disulphide bonds, amino acid residues and pair of peptide chains A (blue) and B (green) [52].

Given their poor oral bioavailability, peptides were often overlooked as potential therapeutic agents however, pharmaceutical companies have since come to accept the potential of orally unavailable drugs [53]. Research continues into novel analogues and delivery methods with inhaled, buccal, intranasal, rectal and sub-lingual preparations of the drugs being explored [49, 54]. Recent advances in the areas of molecular biology, immunology and enzymology in addition to progress in synthetic biotechnology, have increased the potential for peptide use in pharmaceutical product development [39]. As such, research is ongoing into peptide therapeutics in a wide number of areas with a large number of peptide drugs entering clinical trials for the treatment of metabolic disorders such as diabetes, obesity, osteoporosis and certain cancers [48, 55]. As of 2013, there were approximately 60 approved peptide drugs [43, 56, 57], four of which have reached global sales exceeding US$1 billion. These include glatiramer acetate (Copaxone; $3.18 billion), leuprolide acetate (Lupron;

$2.12 billion), goserelin acetate (Zoladex; $1.14 billion), and octreotides acetate (Sandostatin; $1.12 billion) [55] (Table 1.2).

Table 1.2: Approved peptide drugs [58-64].

Drug	Product Name	Indications	Description	Route	Dose
Glatiramer	Copaxone	Multiple sclerosis	Random copolymer of 4 amino acids average MW 5000-9000 Da	SC	20 mg daily
Exenatide	Byetta	Type 2 diabetes	39mer peptide MW 4186 Da	SC	5 µg daily
Teriparatide	Forsteo	Osteoporosis, Pagets disease	Recombinant form of parathyroid hormone MW 4117 Da	SC	20 µg twice daily
Calcitonin salmon	Miacalcin	Osteoporosis, Pagets disease	32mer peptide	SC or IV	100 units daily
Octreotide	Sandostatin	Carcinoid tumours	8mer peptide Mimics somatostatin	SC or IV	50-200 µg up to 3 times daily
Leuprorelin	Prostap	Prostate cancer	MW ≈1200 Da GnRH agonist	SC or IM	3.75 mg every 28 days
Goserelin	Zoladex	Prostate and breast cancer	MW 1269 Da GnRH agonist	SC	3.6 mg every 28 days

As the main function of the GI tract is to metabolise dietary proteins into either dipeptide/tripeptide subunits or amino acids in order to facilitate nutritional absorption [65], therapeutic peptides and proteins are rapidly metabolised and inactivated by gastrointestinal enzymes and are poorly transported across the intestinal epithelium [49]. In addition, the hydrophilic nature of the peptides would result in poor intestinal absorption either transcellularly or via paracellular transport [47]. As a result, oral administration of peptides and proteins, although traditionally a desirable route for delivery of pharmaceuticals, is generally ineffective [66]. Exceptions to this are the micro-emulsion formulation of cyclosporine and DDAVP® (a desmopressin tablet) which are approved oral peptide formulations (Figure 1.11).

These represent exceptions and are effective due to the peptides' unique physiochemical characteristics [67].

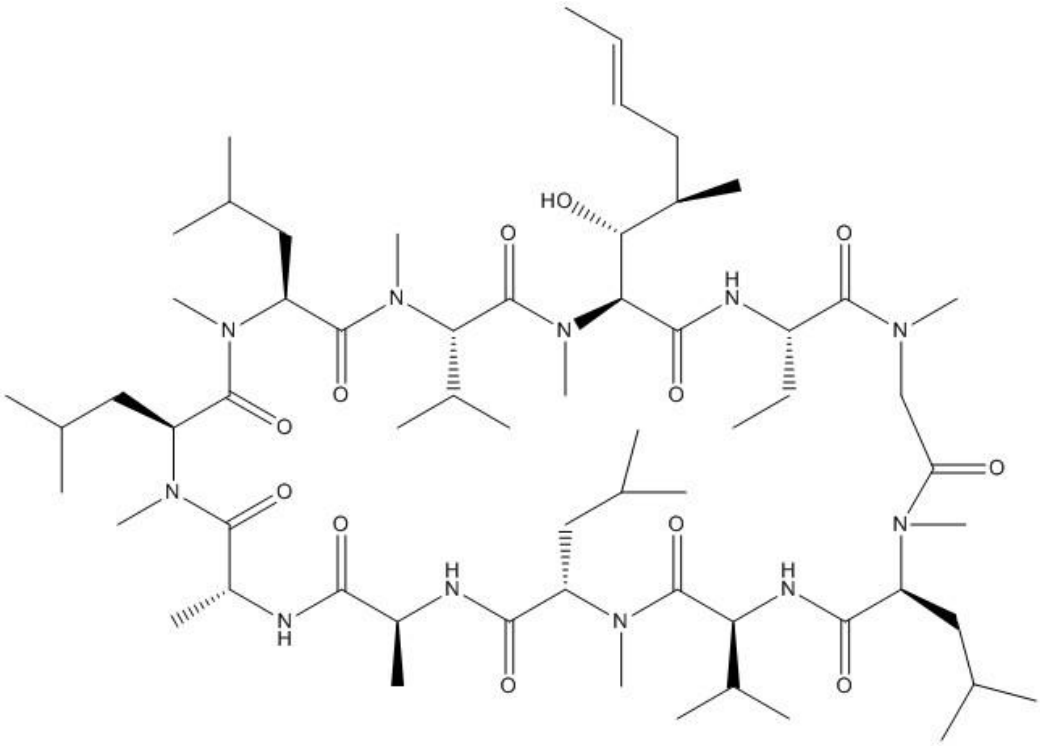

Figure 1.11: Chemical structure of cyclosporine A [68].

Given, however, that administering pharmaceuticals orally is usually associated with high patient compliance, ease of self-administration, low cost and overall convenience, especially for prolonged and repeat treatments, there is ongoing research into developing an oral delivery system for peptides and proteins [46]. Christopherson *et al.* [69] have investigated the area of utilising solid lipid particles as drug carriers for oral peptide/protein delivery and Parmentier *et al.* [70] have also utilised tetraether lipid liposomes to improve the oral bioavailability of the octapeptide octreotide. Gastrointestinal Permeation Enhancement Technology™ (GIPET™) is an enteric coated, solid dose microemulsion based technology for oral peptide delivery developed by Merrion Pharmaceuticals. The development of this technology was influenced by research into permeation enhancement utilising medium-chain fatty acids [67].

Indeed the development of pharmaceuticals using recombinant technology and genetic engineering, in addition to creating a surge of interest in therapeutic peptides, also initiated a major focus on developing alternative drug delivery systems to

injections [43]. As such, research has focussed on alternative non-invasive delivery methods such as nasal, buccal, pulmonary and transdermal [47, 49, 71].

As peptides are generally large hydrophilic macromolecules, often containing charged side groups (e.g. aspartic acid, lysine (Figure 1.12)), they do not easily permeate across the skin and typically require additional enhancement techniques to facilitate their transport through the SC barrier.

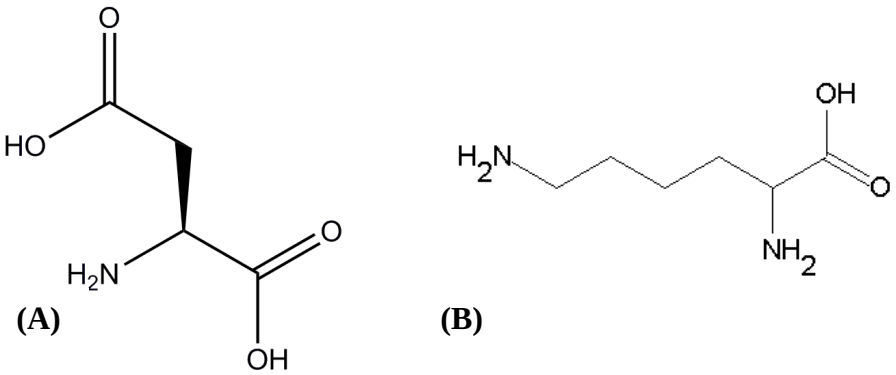

Figure 1.12: Chemical structures of (A) aspartic acid [72] and (B) lysine [42].

Physical disruption of the SC through the use of radiofrequency ablation, thermal microporation or microneedles are techniques which can potentially allow these molecules to traverse the barrier layer of the skin and penetrate into the body [73]. Combining these techniques may also provide a viable method of achieving effective transdermal delivery of peptides, with studies carried out using microneedle technology combined with iontophoresis increasing transdermal flux 100-fold compared with iontophoresis alone (0.08 µg to 8.08 µg) [74].

1.4.3. Peptide Synthesis

Therapeutic peptides have normally been obtained from either natural sources (plants, animals, humans), isolated from genetic libraries or chemically discovered. The technology to chemically synthesise peptides ranging from 5 to 50 residues is now widely available and as such, synthetic peptides are used extensively as pharmaceutical or commercial products ranging from aspartame (a dipeptide sweetener) to hormones such as oxytocin, calcitonin and adrenocorticotropic

hormone [53, 75]. Peptides that consist solely of natural amino acids are generally poor therapeutics given that they generally possess low plasma stability, are highly sensitive to proteases and are rapidly metabolised. As such many natural peptides require chemical modification before they are suitable for therapeutic use, mainly to increase stability or molecular longevity and this is usually achieved through the addition of D-amino acids, pseudo amino acids or cyclisation [40, 76]. The technology to synthesise peptides has been around for many years with small peptides such as bradykinins, oxytocin and vasopressin and larger peptides such as insulin, calcitonin and secretin successfully chemically synthesised for medical purposes [39]. Glatiramer (also known as Copolymer 1 (Cop -1)) is a therapeutic peptide marketed by Teva Pharmaceuticals used in the treatment of multiple sclerosis (Figure 1.13). It is a mixture of synthetic peptides composed of the amino acids alanine, glutamic acid, lysine and tyrosine [49].

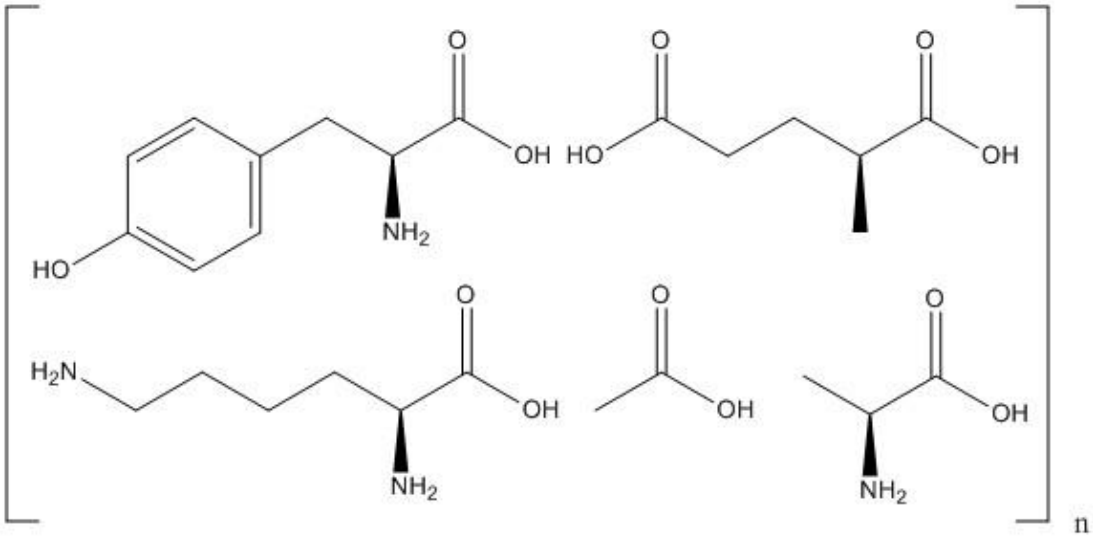

Figure 1.13: Chemical structures of the peptide components of glatiramer [77].

Synthetic production of peptides utilising stepwise assembly has been carried out for almost a century. The methodology involves coupling reactions between amino acids which result in peptide formation after which reversible protecting groups are removed [75]. There are two general methods of peptide synthesis currently incorporated today, namely solution phase and solid phase.

1.4.3.1. Solution Phase Peptide Synthesis

Classical solution phase synthesis (SPS) is a technique which employs typical organic synthesis methods to couple single amino acids together in solution. It is predominantly utilised in large-scale peptide manufacturing, typically with yields ranging from tens of grams to tens of kilograms. The main advantage this method has is that during synthesis, intermediate products can be de-protected and purified which results in a highly pure final product peptide [46]. In addition, this method is more economical and environmentally friendly than the solid phase method but is more time-consuming and labour intensive, especially during the early stages of method development. The reason for this is that many aspects of the process require optimisation and validation in order to obtain the required product and to ensure it is of high quality. The steps involved which require optimisation include the reaction conditions, yields and purification procedures for all intermediates in addition to the finished product itself. [39]. Peptides which have been synthesised using SPS include oxytocin (a neuromodulator peptide) (Figure 1.14) and human insulin [46].

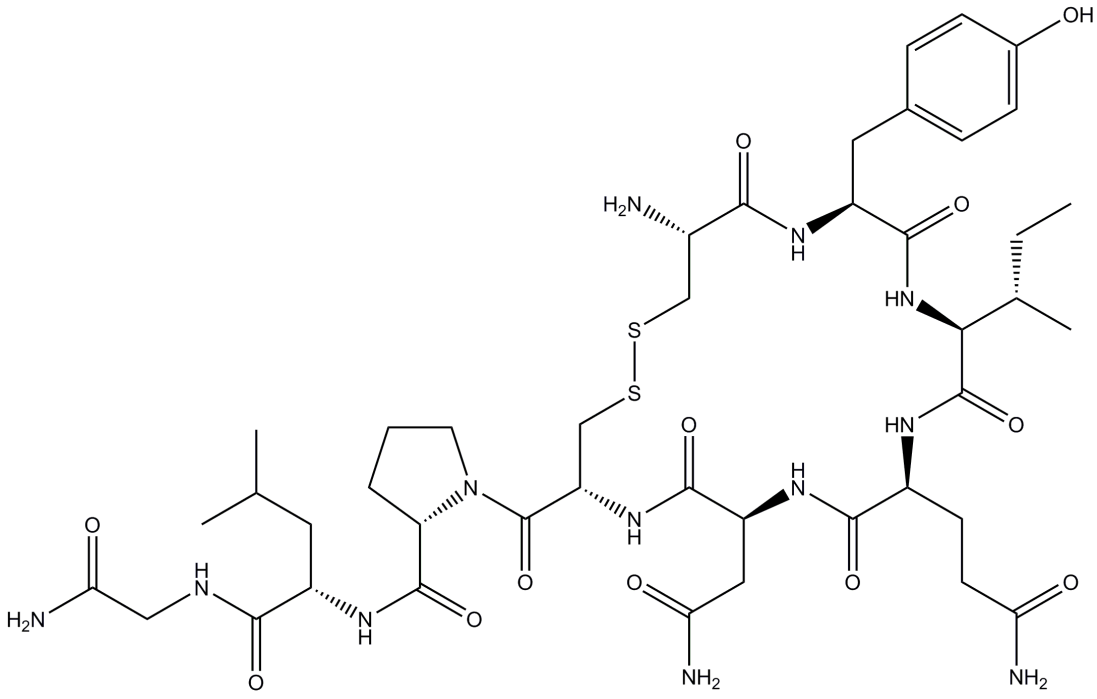

Figure 1.14: Chemical structure of oxytocin molecule [78].

1.4.3.2. Solid Phase Peptide Synthesis

Solid phase peptide synthesis (SPPS) is a method which is particularly suited for research purposes, providing a means of peptide synthesis which is both rapid and accessible. Developed by R. Bruce Merrifield in the 1960's, SPPS incorporates the chemistry of the solution phase method but involves a stepwise system whereby amino acids are assembled in a predetermined sequence through a series of addition reactions on one end of the peptide chain while the other end is typically anchored to an insoluble polymer support [41]. The anchored peptide continues to be extended by further addition reactions until at the end of the synthesis the polymer support, in addition to unwanted by-products and reagents, are removed by washing and filtration [75]. The advantages of SPPS over the solution phase method include the fact that purification steps at intermediate stages of the synthesis are minimised or avoided and the technique is suitable for automation given that the synthesis steps are quick and simple and are carried out in the same reaction vessel at typically ambient temperatures [39]. Solid phase synthesis is particularly suitable for the synthesis of smaller peptides ranging in size from 20 to 30 amino acids with larger peptides and proteins synthesised using a combination of solid and solution phase methods. With the development of new resins, automated techniques, coupling agents and protecting groups in addition to advances in biochemistry, it is now possible to synthesise almost any peptide in a laboratory environment [79].

Rapid growth in the area of therapeutic peptide development is evident by the array of companies that provide high quality peptide products such as Bachem and Lonza (Switzerland), Biomatik (Canada), Gennscript and AmbioPharm (USA), Polypeptide Laboritories (Europe, USA) and Shym-Pharma (China). The development of SPPS over the years since its original concept by Merrifield has resulted in lower cost, faster methods and the use of generic chemical and purification processes [46].

1.5. Microneedles

1.5.1. History

The oral delivery of certain drugs at therapeutic levels has been a challenging endeavour due to poor absorption, low bioavailability and degradation which occurs at various stages in the GI tract [3, 18]. Some drugs, such as therapeutic peptides and proteins, cannot reach the bloodstream in therapeutically effective concentrations when delivered orally and are merely metabolised within the GI tract or are poorly absorbed via this route [80]. For drugs such as these, as well as most vaccines and biopharmaceuticals, delivery through the skin via hypodermic needle injection or intravenous infusion is the most commonly used means of drug delivery providing a cheap, rapid and direct route of administration [4]. However, this method suffers from a number of disadvantages including the stringent need for a trained medical expert to administer the drug, tissue trauma, increased chance of infection, needle phobia and the fact that it can be quite painful which in turn can also result in poor patient compliance [13]. In addition, parenteral and oral delivery methods are restricted to bolus drug delivery with the full dose administered into the body in one delivery. In order to avoid potentially toxic effects of high doses of particularly potent drugs, oral and parenteral delivery of lower doses are sometimes required multiple times daily [18]. As such, transdermal drug delivery has emerged as a viable alternative delivery method and holds a number of advantages over oral or hypodermic needle delivery.

Transdermal drug delivery bypasses the harsh conditions of the GI tract and as such, in addition to being safe and painless, can result in higher bioavailability depending on the properties of the drug in question [81]. It can provide a means of maintaining the concentration of the drug in the bloodstream at therapeutic levels for longer periods of time in addition to providing controlled release of the drug. Transdermal patches have been in use for decades providing easy to use, safe and painless ways of administering drugs such as nicotine, scopolamine and nitroglycerin [13].

The highly efficient barrier properties of the SC mean that the effective delivery of pharmaceuticals across the skin at therapeutic rates is a difficult undertaking, with only low doses of small lipophilic molecules successfully administered

transdermally. Many methods exist which seek to increase the permeability of the skin and allow the delivery of large hydrophilic macromolecules such as peptides and proteins [82]. The aim of these techniques is to create micro-channels in the SC large enough to facilitate the transport of molecules into the skin. To be effective however, chemical permeation enhancers usually require concentrations which can cause skin irritation [83].

Microneedle technology (Figure 1.15) has emerged as a practical and less invasive method of overcoming the barrier properties of the SC and delivering drugs effectively across the skin, including high-molecular weight and/or hydrophilic drugs [2, 84].

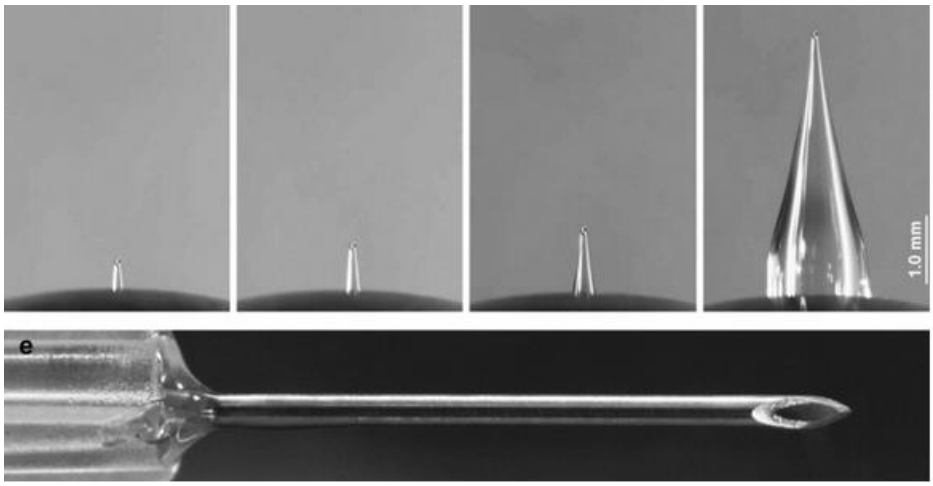

Figure 1.15: Microneedles measuring 500 μm, 750 μm, 1 mm and 4 mm in length under the same magnification as a hypodermic needle with intradermal-bevel (26-gauge) [85].

Studies have been carried out on the use of microneedle systems to deliver a wide variety of pharmaceuticals including small drug molecules, therapeutic peptides and proteins, oligonucleotides, deoxyribonucleic acid (DNA) and vaccines to name a few [82]. Akin to a hybrid system of both hypodermic needle and transdermal patch technologies, microneedles typically consist of an array of micron sized needles, usually less than 1 mm in length [86, 87], which when applied to the surface of the skin, breaches the SC and epidermis without reaching the pain receptor nerves in the deeper tissues of the dermis [13, 88]. Diffusion of the drug then occurs through the epidermis, via the micro-conduits created by the needles, to the dermis from where the drug is then absorbed by capillaries into the bloodstream. Factors which influence

the diffusion rate of the drug across the skin include the density of needles in the array, the length and sharpness of the microneedle shafts, site of application, amount of drug administered, and the concentration of drug administered [89, 90]. The micro-conduits created by the arrays allow higher molecular weight compounds to penetrate the skin barrier that would normally be unable to passively permeate through [86]. Using this method, drugs can be administered in a variety of ways and microneedles have also been utilised in conjunction with other skin permeation enhancement techniques [73, 91].

Microneedle methodologies have the potential not only to increase the rate of delivery and permeability of many drugs into the skin but also may lead to faster pharmacological effects by overcoming the lag time associated with more conventional transdermal drug delivery methods [92]. To date, microneedles have been investigated for a variety of transdermal medical applications including the administering of vaccinations [93, 94], pain relief [95], cutaneous fluid extraction and glucose monitoring, and for delivering insulin and nano-particles [13, 96]. In addition to the area of transdermal drug delivery, microneedles have also been utilised for ocular and intracellular drug delivery [4, 97].

1.5.2. Types of Microneedles

Microneedles are generally described as *in-plane* or *out-of plane* depending on the fabrication process. *In-plane* microneedles are fabricated with the needle shaft being parallel to the base and *out-of-plane* microneedles protrude perpendicular to the substrate surface [80, 98]. Microneedles can be fabricated from a wide range of materials such as silicon, metal, glass, sugars and synthetic polymers and various microneedle designs have been developed in an attempt to maximise the effectiveness of each delivery method. The main types of microneedles currently developed for transdermal drug delivery can be categorised into four main groups; solid, coated, dissolving and hollow microneedles (Figure 1.16) with each type offering a different mode of drug delivery [3, 4, 99].

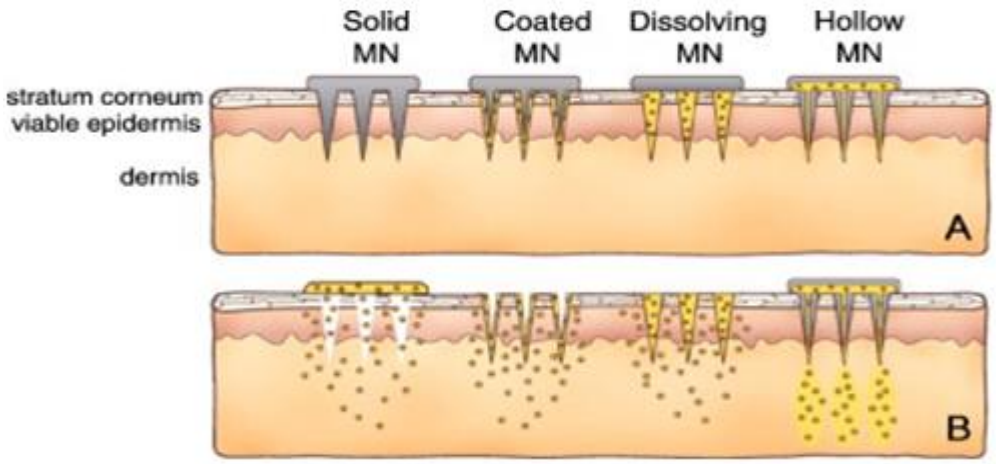

Figure 1.16: Main methods of microneedle mediated drug delivery [4].

1.5.2.1. Solid Microneedles

Solid microneedles are typically made from silicon, metals (such as stainless steel and titanium) or polymers and are used to disrupt the SC in a skin pre-treatment strategy commonly referred to as 'poke and patch' where the microneedle array is applied to the skin to increase permeability prior to the application of drug material [100]. Compared with other microneedle types, such as hollow or dissolving, solid microneedles are easier to manufacture and generally possess greater mechanical strength [13]. Once the microneedles have been inserted into and removed from the skin, tiny micro-channels are created which then facilitate the passive diffusion of molecules from a drug formulation applied either topically (e.g. solution, cream, gel) or via a traditional transdermal patch [98]. This method was initially demonstrated by Henry *et al.* (1998) [101] using silicon microneedles (Figure 1.17) to increase the transdermal permeation of calcein. This study concluded that by applying a force of approximately 10 N (roughly equivalent to the force required to push an elevator button), sufficient penetration of the skin was achieved using a 20 x 20 microneedle array with needle length of 100 µm. The permeation of the calcein model drug into the skin was increased by almost four orders of magnitude by utilising the microneedles in this way [101].

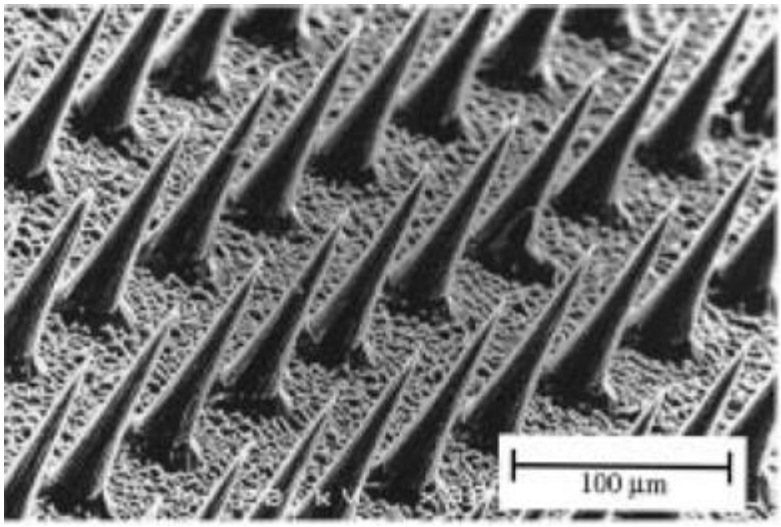

Figure 1.17: Section of a 20 x 20 solid silicon microneedle array as used by Henry *et al.* [101].

As mentioned above, the initial studies into solid microneedle technology for transdermal drug delivery used silicon to manufacture the microneedles, however, silicon has been shown to break easily when inserted into the skin and is relatively expensive when compared with other materials used such as polymers or metals. Metals utilised to date for solid microneedle studies include stainless steel, nickel and titanium. Positive features of such needles include the increased mechanical strength of the needles and lower cost of production. Similarly, various polymers have been tested as alternative materials for solid microneedles as they are generally cheaper and stronger than silicon [13]. Many studies have been carried out using the poke and patch method to deliver a number of drug molecules including naltrexone (a small hydrophilic drug) [17, 102], nanoparticles [103, 104], acetylsalicyclic acid [100], insulin [105] acyclovir [85] verapamil hydrochloride, amlodipine besylate [89] and a number of vaccines [90, 106].

The transdermal delivery of 'cosmeceutical' peptides utilising solid microneedles has been investigated by Mohammed *et al.* (2014) [51] who employed stainless steel arrays consisting of 3 needles each measuring 700 µm length and 250 µm in width on average. The peptides examined were melanostatin, rigin and palmitoylpentapeptide (Pal-KTTKS) with 3, 4 and 5 amino acid residues respectively (Figure 1.18). Results indicated that melanostatin and rigin delivery was enhanced by the use of microneedle pre-treatment however, the delivery of the larger Pal-KTTKS

was not significantly affected by this method indicating that delivery of larger peptides may require additional delivery enhancement techniques [51].

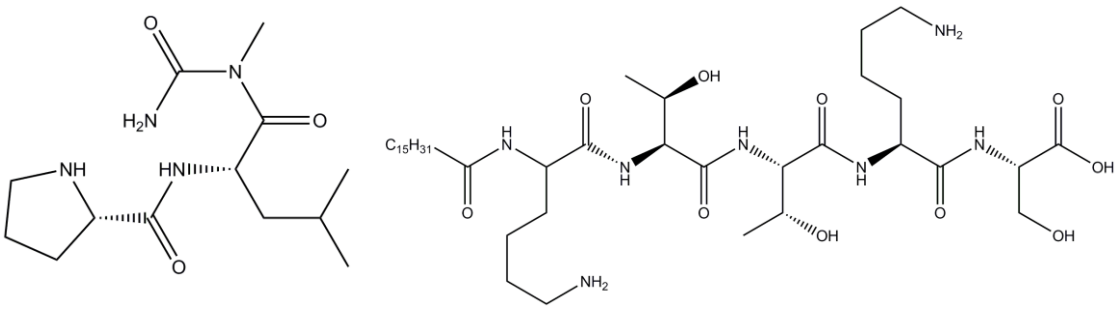

(A) **(B)**

Figure 1.18: Chemical structures of (A) melanostatin [107] and (B) Pal-KTTKS [108].

The effectiveness of using solid microneedles depends upon the ability of the microneedles to penetrate the SC and form micro-conduits through which the applied drug formulation can diffuse, in addition to the length of time these micro-pores remain open. The healing time of the skin after microneedle treatment has been measured at anywhere from 15 min [86] to 2 h [94] to 48-72 h [17, 98] however, Banks *et al.* (2012) carried out studies which indicated an increase in micro-pore lifetime to 200 h using daily applications of a non-specific cyclooxygenase (COX) inhibitor, Solaraze® after microneedle treatment [102]. In addition, Li *et al.* (2009) reported that micropores remained open after 24 h *in vivo* when occluded with a penetration enhancer formulation [73]. Other factors such as microneedle length and the age of the patient can affect the rate of micro-pore closure with longer needles and aging skin associated with longer closure times [109].

1.5.2.2. Coated Microneedles

Coated microneedles are used in an application method referred to as ‘coat and poke’ whereby a drug formulation is applied to the surface of solid microneedles and after insertion into the skin, the formulation dissolves, releasing the drug into the body [19]. Coated microneedles are generally fabricated from silicon or metal with the drug applied as a coating layer in a dried state. The methods used to coat the

microneedles include roll coating, dip coating and spray coating typically using an aqueous solution with a higher viscosity which allows more of the formulation to be retained on the needle surface after drying [4]. Unlike solid microneedles, coated microneedles require a simple one step application process. This method is particularly suited to the administration of low dose drugs such as vaccines given the limited area on the microneedles which is available for coating the formulation [92, 98]. Even so, coated microneedles offer a viable route to rapid bolus delivery of low dose/high molecular weight drugs through the skin and in addition, the stability of active ingredients may be maintained by storing the drug formulation as a solid phase coating on the microneedles [3, 97]. Administering vaccines using coated microneedles is of particular interest given that lower dosage may be applied and a more potent immune response can be achieved through the delivery of antigens directly to epidermal Langerhans cells and dermal dendritic cells in the skin [3, 110].

The methods of coating the drug formulation onto the microneedle arrays mostly involve a process of either dipping or spraying the needles with an aqueous solution of the drug formulation. The drug formulation used for microneedle coating must facilitate controlled and uniform application onto the microneedle surface in addition to allowing rapid dissolution once inserted into the skin. The coating must remain adhered to the needles during insertion and all excipients and solvents used during the coating process must be safe for human use and not affect the active ingredient. Typical formulations used for coated microneedles often incorporate surfactants to enable wetting of the needle surface, stabilising agents to protect the active ingredient during drying and storage and must have sufficient viscosity to allow more of the formulation to be retained on the array after drying. In addition, the coating process used must not be damaging to the active ingredient by avoiding high processing temperatures and utilising aqueous solutions to avoid denaturing of biological molecules [3, 4].

To overcome disadvantages of dip coating such as uncontrollable deposition weight variations of coated arrays, material waste and scale-up limitations, Uddin *et al.* (2015) [111] investigated inkjet printing as a method of coating solid microneedles with a formulation of anti-cancer drugs (5-fluorouracil, *cis*-platin and curcumin) and polymer (Soluplus®, a co-polymer of polyvinyl caprolactame-polyvinyl acetate-

polyethylene) by applying the formulation in the form of tiny droplets, allowing for a more uniform distribution onto the needle surface (Figure 1.19).

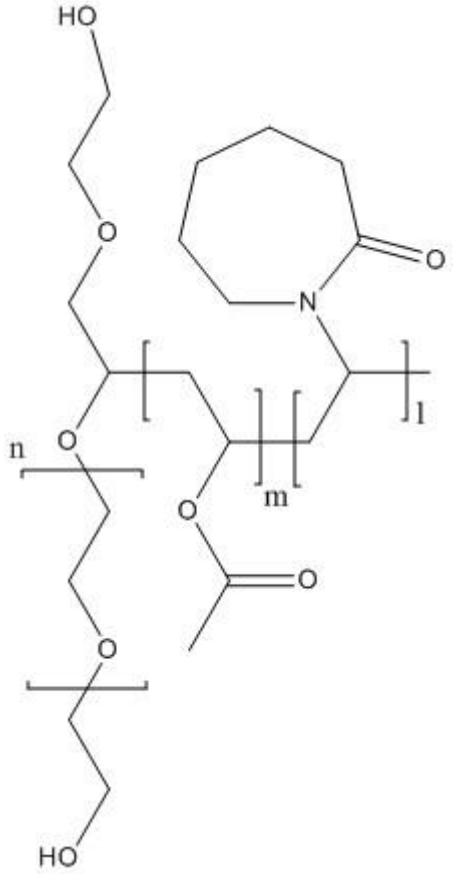

Figure 1.19: Chemical structure of Soluplus® (polyvinyl caprolactam-polyvinyl acetate-polyethylene glycol graft copolymer (PCL-PVAc-PEG)) [112].

The results obtained indicated highly uniform, reproducible and accurate coating of the drug-polymer formulation onto the microneedles with rapid release rates obtained for all three model drugs [111].

A wide variety of microneedle designs have been developed to facilitate this coating process including three-dimensional groove embedded microneedles to enable greater coating amounts and pocketed microneedles which also increase coating quantities and facilitate the application of liquid coatings and improved drug targeting [4]. Gill *et al.* (2008) [82] examined a dip coating method incorporating pocketed microneedles for controlled transdermal drug release (Figure 1.20). Laser etching techniques were incorporated to fabricate the microneedles from 75 µm stainless steel sheets and also to cut the pockets in the shafts.

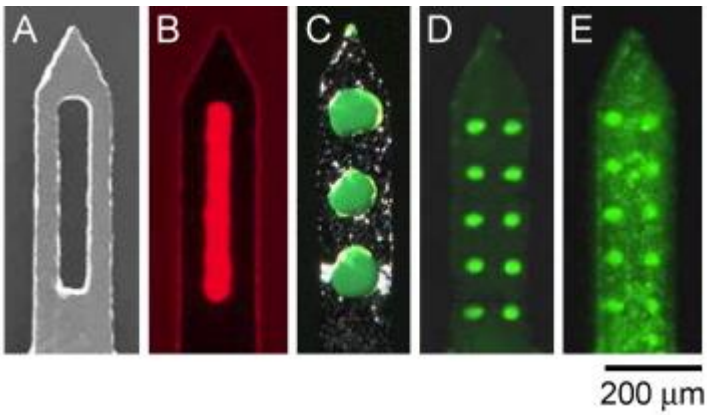

Figure 1.20: Various pocketed microneedles: A) representative microneedle with large central pocket, B) microneedle with pocket filled with sulforhodamine, C) microneedle pocket filled with fluorescein, D) filled with plasmid DNA as a model drug and E) microneedle showing pocket filled with plasmid DNA which also coats the surface, as used by Gill *et al.* (2008) [82].

The pockets of the microneedles were filled with drug formulation during the coating process and as the drug was confined to one area of the microneedle shaft, this facilitated targeted delivery to a specified skin depth which may be desirable for selective delivery to less vascularised areas of the skin, such as the middle of the dermis, which would reduce systemic delivery. This particular technique also allows for further coating of the microneedles with additional drug or a protective layer to preserve the activity of the pharmaceutical ingredient [82]. Similarly, Khandan *et al.* (2015) investigated the application of fenestrated titanium solid microneedles coupled with a fast dissolving drug coating for ocular drug delivery. The needles used ranged from 500 to 1500 µm in length. The drug carrying capacity of the microneedle design was found to be 5 times greater than standard solid microneedles of similar size and a model drug, rhodamine B, was uniformly delivered *ex vivo* [113].

A wide range of compounds have been successfully coated onto microneedle arrays and these include small molecules such as calcein [114], vitamin B, flourescin and lidocaine, larger macromolecules such as desmopressin, ovalbumin, bovine serum albumin [115] and horseradish peroxidase, numerous vaccines including inactivated influenza virus and hepatitis B surface antigen and various kinds of DNA such as plasmid DNA encoding protein vaccines against hepatitis C virus [4]. The transdermal delivery of desmopressin, a synthetic peptide used to treat enuresis in

young children (Figure 1.21), was investigated by Cormier *et al.* (2004) utilising a coated microneedle patch system [83].

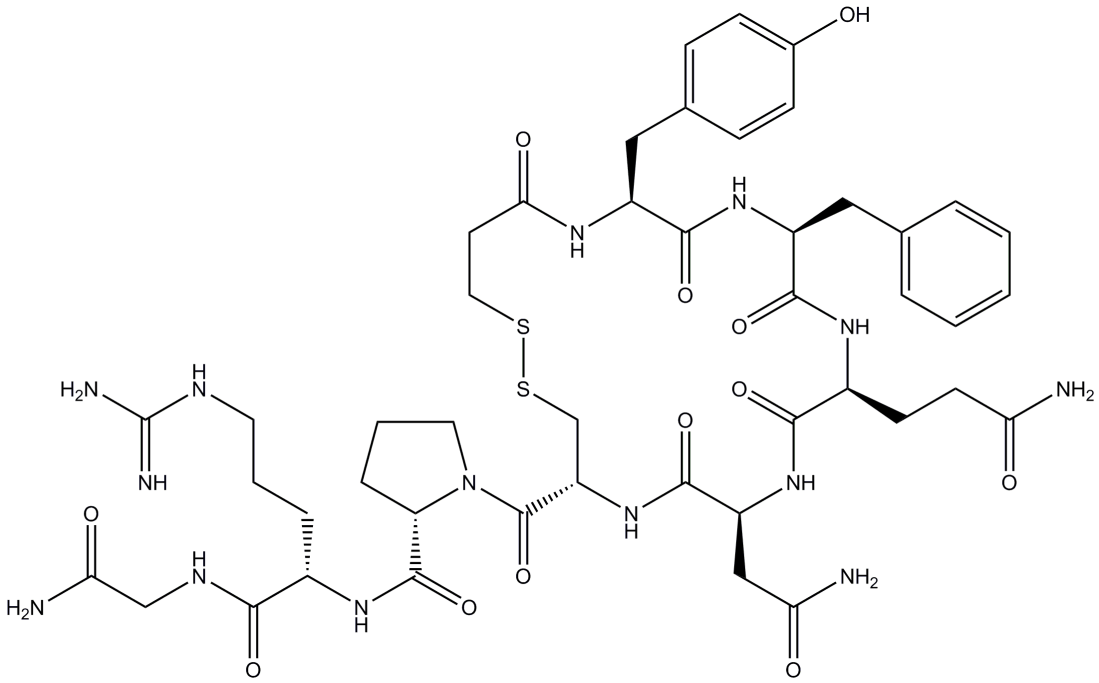

Figure 1.21: Chemical structure of desmopressin [116].

The drug was coated onto the solid needles in an aqueous formulation also containing polysorbate 20 and via partial immersion, discarding arrays where the coating extended to the base. The results obtained indicated that although the target dose of 20 µg was delivered, an increase in drug loading (up to 82 µg) did not result in a significant increase in drug delivery. Limited availability of interstitial fluid to allow the dissolution of the drug into the skin was surmised as the reason for the reduced bioavailability of higher dosed applications [83]. This highlights one of the main limitations of coated microneedles; limited dosage.

1.5.2.3. Hollow Microneedles

Hollow microneedles function in a similar manner to traditional hypodermic needles in that a fluid formulation containing the drug is injected into the body through the microneedle arrays. This method is referred to as ‘poke and flow’ [98]. Materials used in the fabrication of such microneedles include silicon, metal, polymers and glass. Hollow microneedles can facilitate the continuous delivery of liquid drug

formulation across the skin either by diffusion or driven flow (pressure or electrical) and as such, are capable of delivering greater volumes of drug than solid or coated microneedles with the ability to control the flow rate [13, 98]. The most common method of drug delivery using hollow microneedles is with the use of a syringe as with hypodermic needles. However, some systems incorporate an actuator which can control the delivery through the hollow needles by CO_2 gas pressure, piezo-electric micropumps, syringe pumps or micro-gear pumps [4]. Martanto *et al.* [117] investigated methods which could increase and control micro-infusion through the skin using hollow glass microneedles (Figure 1.22) with an injection system consisting of high pressure CO_2 and a 1 mL glass syringe.

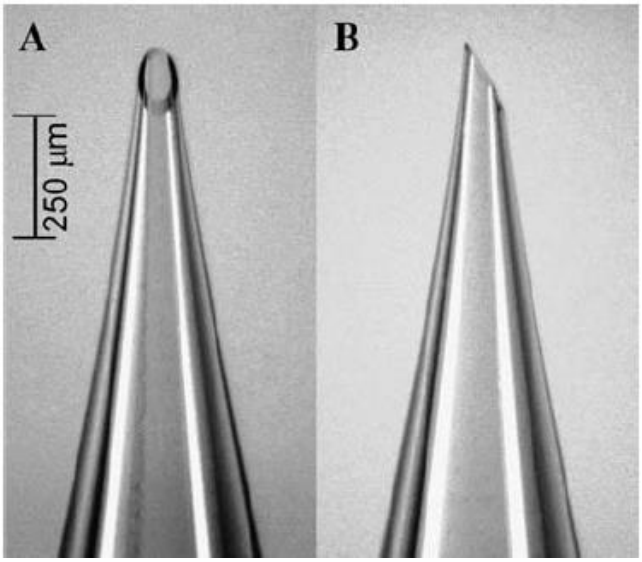

Figure 1.22: (A) Front and (B) side views of a representative hollow, glass microneedle as utilised by Martanto *et al.* illustrating the bevelled tip [117].

They concluded that by infusing at high pressure in addition to utilising a bevelled tip microneedle and retracting almost completely after insertion, infusion of the drug into the skin was optimised with flow rate increasing from 28 µL/ h for fully inserted needles to 326 µL/ h for retracted arrays. This last parameter overcame problems associated with flow resistance due to the compression of dense dermal tissue ant the needle tips during insertion [117].

In addition to the above, other problems associated with this type of microneedle strategy include the potential for clogging in the microneedle bores and reduced mechanical strength of the microneedle structure. However, these limitations may be

overcome through improved microneedle design and use of more robust materials. Clogging of the needle tip can be avoided by positioning the bore opening at the side of the shaft rather than the tip and this has been shown to also increase the area of tissue exposed to the drug, as well as maintaining the sharpness of the tip [92, 118]. The main advantage of utilising hollow microneedles for transdermal drug delivery is that they offer a means of continuous infusion of drug into the skin which cannot be achieved using other microneedle designs [13]. However, the complexity of the diffusion system remains an issue for this particular microneedle system [119]. With the use of 3 mL syringes with mounted hollow metal microneedles, Norman *et al.* (2013) [120] delivered 0.1 mL of sulforhodamine B (a fluorescent dye) into porcine skin. Delivery of the dye was confirmed using fluorescence microscopy on a skin cross-section post injection. Similarly, but using controlled pressure delivery, Vinyakumar *et al.* (2014) [121] delivered 50µL of liquid into the skin in 2 s with an array of 100 hollow microneedles.

1.5.2.4. Dissolving Microneedles

Solid microneedles and coated microneedles remain intact after insertion into the skin and subsequent drug application which can result in biohazardous sharps waste. Dissolving microneedles on the other hand are designed to completely dissolve in the interstitial fluid of the skin during the application process [4]. Dissolving microneedles are typically fabricated from biocompatible and biodegradable polymeric materials which house the drug payload within the matrix of the microneedles themselves and are used in a method commonly referred to as ‘poke and release’ [98]. After insertion in the skin, the needles dissolve when in contact with interstitial fluid, subsequently releasing the drug into the body. Depending on the constituents used, dissolving microneedles can fully degrade within 5 min in the case of water soluble materials or may take several days for some biodegradable polymers [4]. In fact, delivery of the encapsulated drug can be tailored by adjusting the formulation used giving a predetermined release rate and subsequent sustained and controlled delivery [122]. These types of microneedles can also be used without an incorporated drug load as a skin pre-treatment method to increase skin permeability prior to drug application, in the same manner as solid microneedles [4]. A notable advantage of dissolving microneedles over coated ones is the increased

dosage that can be delivered given that the drug is encapsulated within the microneedle matrix as opposed to merely coating the surface of the shafts [123, 124].

In all cases, the polymers used for dissolvable microneedles must be biocompatible and biodegradable and must include materials with long established medical safety profiles such as polylactic acid (PLA), polyglycolic acid (PGA), polylactic-co-glycolic acid (PLGA), PVP (Figure 1.23), biopolymers such as sodium hyaluronate, chondroitin sulphate and carbohydrates such as sugars, carboxymethyl cellulose (CMC) and amylopectin. [87, 92]. Consideration needs to be given to the properties of the polymers used as the component materials need to retain sufficient tensile strength and sharpness to penetrate the skin after the formulation process [125].

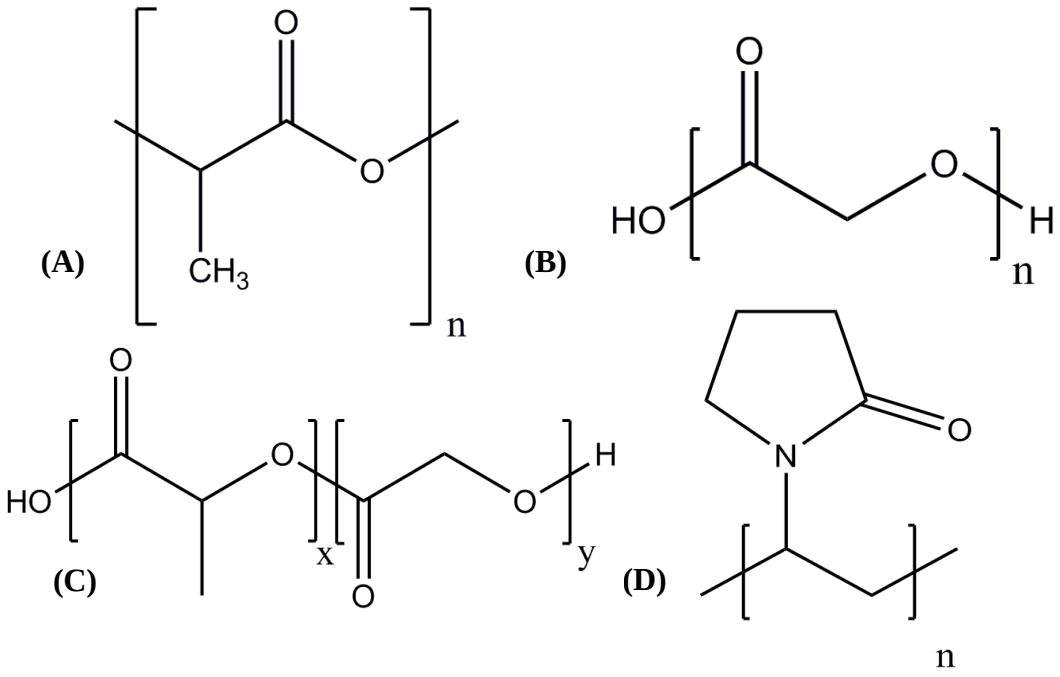

Figure 1.23: Chemical structures of some biodegradable/biocompatible polymers: (A) PLA, (B) PGA, (C) PLGA and (D) PVP [126, 127].

The time required for dissolving microneedles to fully dissolve and release their drug payload in the skin after insertion can vary greatly depending on the polymeric material or formulation used, with dissolution times ranging from minutes to several days. These properties can be manipulated and designed to facilitate either immediate or controlled/sustained release as required [128].

Limitations associated with this type of microneedle design include compromising the mechanical strength of the needles due to the loading of drug material into the needle structure and the potential for drug degradation during the microneedle fabrication process [92]. The formulation process for dissolving microneedles also needs to be suitable for the active ingredients used. Peptides, proteins and antigens are all sensitive to temperature and require benign formulation conditions to avoid damaging their pharmaceutical activity [119]. As such, encapsulation and solidification of microneedles incorporating these drugs must be carried out at lower temperatures and in many cases, avoiding harsh environments such as high or low pH, high pressure and organic solvents [9]. UV curing has been proposed as a method of casting polymer microneedles at ambient temperatures, however this method may also cause damage to the drug and also raises the issue of the use of potential toxic photo-initiators during the curing process [119]. In addition, due to the mechanical weakness of water soluble components of dissolvable microneedles, wider needle bases are needed to increase mechanical strength. This can result in the microneedles not fully inserting into the skin during application due to skin deformation, which may lead to impediment of the wider base, resulting in the full drug payload not being administered [129, 130]. This limitation may be overcome by encapsulating the drug in the microneedle tips only. However, this further complicates the manufacturing process and reduces the available dose of the drug [4].

Chu *et al.* [129] proposed a two-tiered dissolvable microneedle system which incorporated a separable arrowhead design where a sharp tipped polyvinyl alcohol (PVA)/PVP polymer arrowhead encapsulating sulforhodamine was mounted on a blunt stainless steel microneedle shaft (Figure 1.24). Upon insertion into the skin, the polymer arrowhead remained embedded in the skin and the blunt shafts were removed and discarded. The rapid separation of the arrowheads from the shaft allowed for full administration of the sulforhodamine drug payload with release kinetics controlled by the polymer formulation.

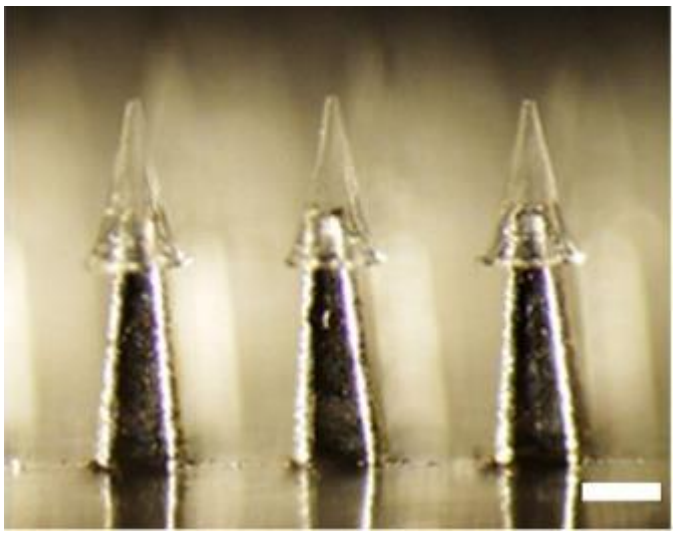

Figure 1.24: Separable arrowhead microneedles comprising 600 μm-tall metal shafts capped with water-soluble PVA/PVP arrowheads encapsulating sulforhodamine [129].

This technique addressed three problems that can be encountered when applying microneedle technology to transdermal drug delivery. Firstly, as the polymer tips were completely embedded in the skin, the whole intended dose was administered once the needles were applied and secondly, as the polymer tips remained in the skin, the administration time took only seconds after which the blunt shafts were removed. Finally, as the discarded metal shafts were blunt, initial indications were that they generated no bio-hazardous sharp waste and could be disposed of relatively easily. However, the preparation of the drug/polymer formulation during this study utilised a 10 min heating step at 195^{o} C which would make this method unsuitable for peptide or protein drugs [129].

Similarly, Chen *et al.* (2013) [94] developed antigen encapsulated biodegradable chitosan microneedles mounted onto PLA supports (Figure 1.25), which offered greater mechanical strength during insertion.

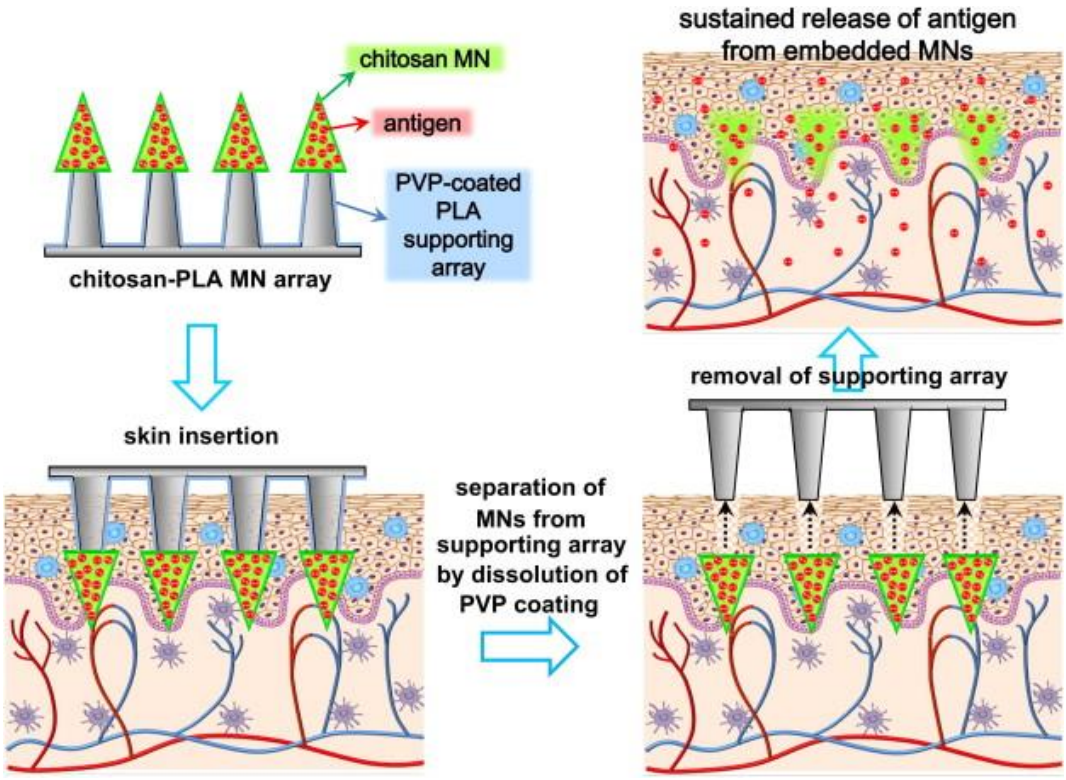

Figure 1.25: Schematic illustration detailing the administering of antigen using an embeddable chitosan microneedle and PLA support delivery system [94].

As with the arrowhead needles developed by Chu *et al.*, after insertion, the chitosan needles detached from the PLA base and remained embedded in the skin, allowing sustained release of the antigen for up to 14 days. A notable advantage of this particular two-tiered system is the use of ambient temperatures and mild formulation conditions during the formulation process which makes this method more suitable for biologically active pharmaceuticals [94]. A similar study also incorporated solid microneedles composed of biodegradable PLA utilising PVA and sucrose to fabricate a rapidly separating dissolving polymer gel mounted onto the solid microneedle supports [131].

Another interesting application of the dissolving microneedle system was investigated by Kim *et al.* (2012) [122] who designed PLGA microneedles which housed hydrogel micro-particles within the microneedle matrix with the view to delivering sustained release of both hydrophobic and hydrophilic drug molecules (Figure 1.26). Swelling of the hydrogel particles due to moisture absorption after insertion in the skin facilitated the mechanical failure of the PLGA needles due to the

difference in volume expansion and resulted in the release of the drug material within the hydrogel particles.

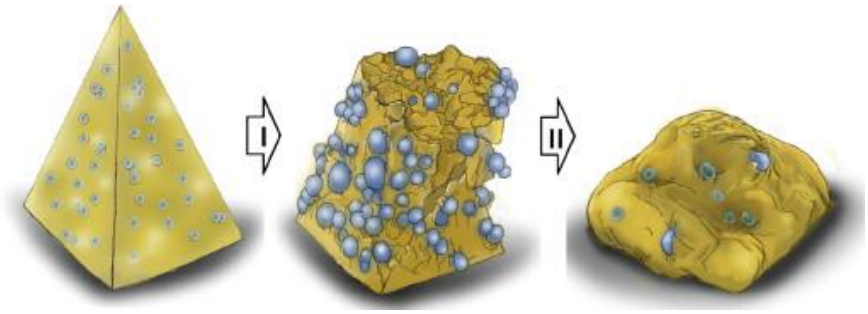

Figure 1.26: Schematic diagram detailing the mechanism of hydrogel swelling and subsequent mechanical failure of PLGA microneedles developed by Kim *et al.* [122].

Studies utilising various dissolving microneedle designs have been carried out for the delivery of a wide range of therapeutics including ferric pyrophosphate for the treatment of iron deficiency [132], lidocaine for pain management [95], aspirin, lisinopril dehydrate and atorvastatin calcium trihydrate in a combined fixed dose for cardiovascular disease [133], insulin [134-136] and vaccines [137-141]. In fact, it is in the area of transdermal immunisation that the first phase 1 human trial incorporating dissolving microneedles was conducted. Rouphael *et al* (2017) carried out a phase 1 clinical trial to deliver inactivate influenza vaccine utilising a dissolving microneedle patch with results indicating a robust antibody response after 28 days, comparable to intramuscular vaccine administration [142].

1.5.2.5. Other Microneedle Designs

A number of studies have investigated microneedle systems which utilise mechanisms that differ from more common solid, coated, hollow or dissolving needle designs. In one such study, Seong *et al* (2017) developed a dual function, double layered microneedle system utilising a swellable polystyrene-*block*-poly(acrylic acid) (PS-PAA) outer layer and non-swellable polystyrene (PS) inner layer designed for the delivery of protein drugs. The bullet shaped PS-PAA needles expanded to 8 times initial volume on application, forming arrowhead shaped tips which facilitated mechanical interlocking with skin tissue (Figure 1.27).

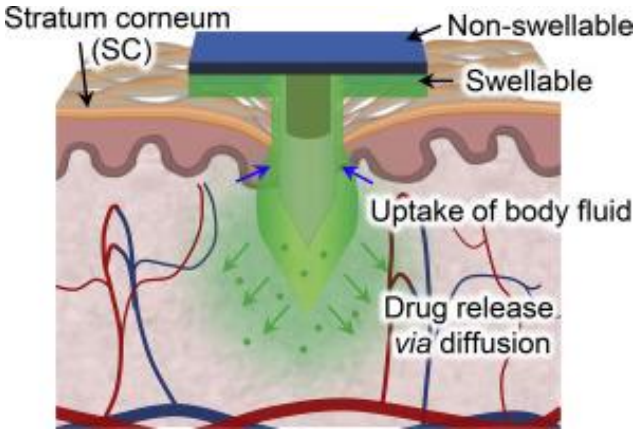

Figure 1.27: Schematic illustrating the mode of action of double layered PS-PAA and PS based swellable microneedles [143].

In conjunction with the tip swelling, prolonged delivery of insulin encapsulated in the swellable microneedles was also achieved at a constant rate for 6 h without an initial burst release, facilitating a gradual decrease in blood glucose levels [143]. Employing a similar drug release mechanism, Kearney *et al.* (2016) carried out studies to determine the effectiveness of a hydrogel based microneedle system to deliver of donepezil hydrochloride for the treatment of Alzheimer's disease. Utilising Gantrez® based arrays and a drug loaded reservoir, the swelling of the hydrogel needles on insertion into the skin resulted in the formation of a porous, aqueous network through which diffusion of drug from the reservoir patch occurred [144].

1.5.3. Advantages and Limitations of Microneedles

The use of microneedles to facilitate transdermal drug delivery has numerous advantages over more traditional drug delivery methods. In addition to all the advantages associated with transdermal drug delivery as mentioned previously, microneedles require no medical expertise to apply and due to their micron sized shafts, are painless by avoiding nerve receptors in the dermis and present little or no risk of infection, unlike normal hypodermic needle delivery [4, 88].

Traditional delivery of vaccines is intramuscular via hypodermic needle injection however, this method does not deliver the drug to the optimum location to stimulate an immune response given that, compared with the skin, muscle contains far less immunologically sensitive cells [130]. The use of microneedles has been shown

experimentally to dramatically increase the permeation properties of the skin and the presence of Langerhans cells, dendritic cells and other immunocompetent cells in the skin make the microneedles highly suitable as a vaccine delivery system [13].

Microneedles can also facilitate the controlled release of drugs by either encapsulating the drug within a biodegradable polymer matrix or coating solid needles with a drug formulation and can enable targeted drug delivery to particular sites. In addition, microneedles can increase the bioavailability of therapeutic agents by directly introducing the drugs into the bloodstream, bypassing the GI tract and may also result in faster pharmacological effects by removing the lag time normally encountered with typical transdermal drug delivery methods [92]. In addition, scaling up the production of microneedles would likely be inexpensive resulting in microneedle devices which are disposable and user friendly [88].

The small size of the microneedles means that, in the case of coated and dissolving needles particularly, these methods are only suitable for high potency, low dose drugs. In addition, coating microneedles consistently and uniformly is a difficult process requiring considerable research with optimisation of the formulation and coating methods varying from drug to drug [92]. The skin's viscoelastic properties resulting from the underlying fat and muscle may also affect the ability of the needles to adequately pierce through the SC, which has been associated with microneedles of shaft lengths less than 300 μm [85]. The ability of microneedles to penetrate the skin, particularly in the case of shorter, blunter arrays, may be affected by the robustness and elastic properties of the skin. A 'bed of nails' effect, caused by the distribution of force on the needles, especially where many needles are used, may reduce the insertion depth however this may be avoided by utilising a less rigid back-layer on the needle array [145]. Folding of the skin over the arrays during application and insertion forces exceeding the tensile strength of the needles may result in penetration failure and damage to the shafts [98]. Skin thickness can also be affected by a number of factors including age, race, sex and also varies depending on the area of the body. As such, the successful application of the microneedles and delivery of the drugs in question may vary depending on one or more of these factors. This is particularly relevant in the case of dissolving microneedles where failure of the device to fully penetrate the skin would lead to delivery of a much lower than

intended dose [13, 130]. Microneedles may also cause localised erythema and irritation of the skin depending on needle length, with 400 µm needles causing higher levels or erythema and blood flow than 200 µm needles [4]. Also, the two-step ‘poke and patch’ process associated with solid microneedles is potentially inconsistent in relation to dosage, especially during home usage and can result in bio-hazardous sharps waste [92].

1.6. Research Objectives

This study aims to develop and optimise a method of successfully delivering a range of therapeutic peptides transdermally utilising microneedle technology. The research will investigate a number of formulations with the view to generating dissolving microneedle arrays from biodegradable polymers and sugars which will release the drug rapidly and systemically during the degradation process. For dissolving microneedles to be effective as drug delivery devices, however, a number of factors must be considered:

- The microneedles need to have sufficient mechanical strength and suitable design to penetrate through the SC without breaking or bending in order to deliver the drug into the viable epidermis [125];
- The microneedles need to be sufficiently sharp to penetrate the SC;
- The microneedle formulation process must not cause any loss of efficacy to the active drug encapsulated within the matrix. In the case of biological therapeutics, this usually involves the use of ambient temperatures, aqueous environments and mild pH conditions;
- Full administering of the drug payload must be accomplished;
- The materials used must be biocompatible and not cause any adverse effects on the patient;
- The formulation needs to be stable enough to allow for long-term storage;
- The arrays also need to possess a degree of flexibility in order to overcome contours in the skin [146].
- The formulation process should be relatively uncomplicated to be economical and allow ease of scale up [125].

To develop a rapid and systemic release system, a variety of polymers and sugars will be examined initially including PVP, CMC, PVA, PLGA, trehalose and sucrose to determine the optimum formulation for microneedle fabrication. The chemical stability of proteins and peptides in a dry state can be enhanced by incorporating amorphous sugars which prevent loss of activity from either chemical or thermal denaturation. Of these sugars, trehalose is regarded as the best stabiliser for biological materials and prevents dehydration and desiccation in peptides and proteins [147].

Characterisation of the microneedles will be carried out using texture analysis, scanning electron microscopy (SEM), differential scanning calorimetry (DSC), thermogravimetric analysis (TGA), dynamic vapour sorption (DVS) and fluorescence microscopy. These analytical techniques will be used to examine the physical characteristics of the needles including strength and morphological properties. Using the data from these techniques, statistical analysis will be carried out to determine the optimum formulation.

Once the optimum formulation has been established, further characterisation will be carried out to determine the mechanical strength of the needles in addition to the ability of the arrays to successfully penetrate the skin. Porcine skin penetration studies will be carried out using texture analysis, optical coherence tomography (OCT) and micro-sectioning to determine the depth of penetration of the needles. Microbiological disc diffusion studies will also be carried out to determine the effect, if any, of the formulation process on the activity of the model antibiotic drug.

Due to the high cost and often high potency (toxicity) of therapeutic peptides, a model peptide, polymyxin B will be selected initially with synthetically developed model peptides incorporated at a later stage.

Fmoc based solid phase peptide synthesis techniques will be utilised to synthesise these peptides which will then be incorporated into the microneedle arrays. Drug release studies consisting of Franz cell based skin diffusion tests will be carried out on the peptide drug loaded microneedle arrays to determine the effectiveness of the microneedles in delivering the 3 model peptides through porcine skin.

Finally, in conjunction with the rapidly dissolving PVP/trehalose microneedles, a sustained release drug delivery system will be investigated utilising peptide loaded PLGA particles which will be rapidly deposited in the skin and slowly release the drug payload through polymer degradation in a controlled manner over time.

CHAPTER 2. FORMULATION AND CHARACTERISATION OF POLYMERIC MICRONEEDLES FOR THE TRANSDERMAL DELIVERY OF PEPTIDES

2.1. Introduction

Delivering therapeutic peptides transdermally presents a significant challenge. However, dissolving microneedle technology appears to provide a highly viable method to facilitate the delivery of therapeutic macromolecules [148]. As per Section 1.5.2.4, many types of dissolving microneedles have been developed utilising a wide range of designs, materials and modes of delivery.

A number of studies have been carried out on the viability of carbohydrates for the fabrication of dissolving microneedles. One investigation into the use of sugar as a material for microneedle fabrication was carried out by Li *et al.* (2010) [149] who utilised maltose microneedles to create micro-channels in the skin which successfully increased the permeation of human immunoglobulin G. While this study demonstrated the ability of sugar microneedles to successfully penetrate the skin, the maltose microneedles contained no drug payload and merely created micro-channels which facilitated the delivery of the drug after it was applied to the treated skin.
Donnelly *et al.* (2010) [150] examined the use of galactose hot melts for microneedle fabrication and subsequent delivery of 5-aminoevulinic acid (ALA) and bovine serum albumin (BSA). This study showed that the galactose hot melts were difficult to mould and the galactose arrays once formed, were extremely susceptible to ambient relative humidity conditions (43%), rapidly deforming after 1 h and being completely melted after 6 h. In addition, drug loss during the fabrication process occurred which was attributed to degradation of the drug due to the high processing temperatures (160 ºC) and also due to possible reaction between the amino groups of the drugs and the *R*-hydroxy carbonyl group of the galactose [150]. Given these drawbacks, the study indicated that utilising hot melts of carbohydrates appeared to be unsuitable as a method of fabricating dissolving microneedle arrays and specifically for the delivery of biologically active pharmaceuticals.

Martin *et el* (2012) [87] investigated a variety of sugar glasses for the low temperature fabrication of dissolving microneedles, subsequently utilising a trehalose and sucrose formulation which was selected based on the ability of the formulation to reproducibly form non-crystalline sugar glasses and partially stabilise a model protein, β-galactosidase enzyme, in the sugar glass matrix. The microneedles fabricated from this formulation (Figure 2.1) were successfully capable of

penetrating the SC and dissolved rapidly on insertion, depositing marker dye into deeper layers of skin. The design of the needles used was octagonal pyramidal with a base of approximately 200 µm and a length of approximately 250 µm [87].

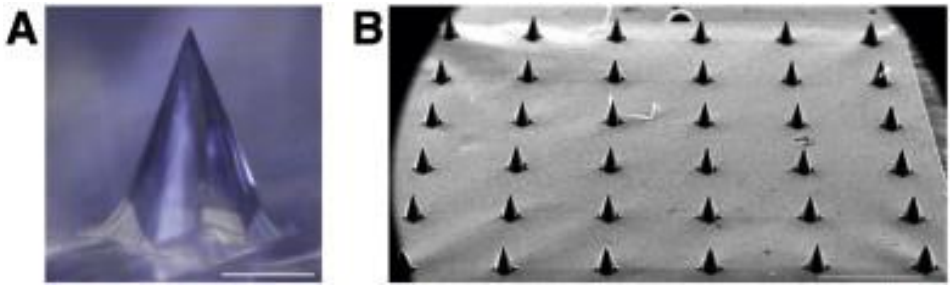

Figure 2.1: (A) Light photomicrograph of an individual sugar glass microneedle (Bar = 100 µm), and (B) scanning electron micrograph of entire sugar glass microneedle array (Bar = 1 mm) as used by Martin *et al.* [87].

Given however, that the drug payload was encapsulated within the needle matrix, the low available volume of these needles would limit the deliverable dose of drug that could be potentially administered with this design. In addition, the physical strength of sugar glass microneedles may not be sufficient to utilise with longer microneedle arrays.

Loizidou *et al.* (2014) [151] examined the structural properties of sugar microneedles composed of carboxymethyl cellulose (CMC) and a variety of sugars namely trehalose, sucrose and maltose. The microneedles used in this study consisted of an array of 18 x 18 cone-shaped needles each with base diameter of 200 µm and needle height of 750 µm. Tests carried out on the 1:1 CMC/sugar formulations examined the mechanical strength of the microneedles in addition to their ability to penetrate the SC and deliver a dose of propranolol hydrochloride (Figure 2.2) into the skin. Results from this study indicated that CMC/trehalose and CMC/maltose possessed greater structural strength than the CMC/sucrose needles with a fracture force of 15 N required for CMC/maltose needles and 11 N for CMC/trehalose needles compared with 0.04 N for the CMC/sucrose needles. Despite the results of the mechanical tests, the drug delivery studies indicated that the CMC/sucrose needles were almost as effective as the CMC/maltose needles in terms of the proportion of drug delivered. Additionally, the CMC/trehalose needles showed no statistical difference in drug delivery compared with the control (flat discs of the same formulation). These results

were attributed to either the dissolution rates of the sugars in the skin or possible interactions between the drug and components within the microneedle formulation.

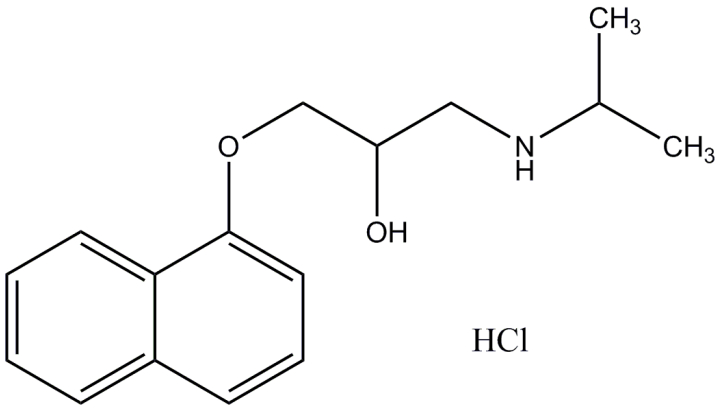

Figure 2.2: Chemical structure of propranolol hydrochloride, a beta blocker [152].

The formation of multiple hydrogen bonds between sugars and biomolecules, which can lead to the stabilisation of the biomolecules, may also affect the dissolution rate of the molecules from the microneedles to the skin. As trehalose provides extra stability in such instances, due to a larger hydration sphere, hydrogen bonded complexes between trehalose and propranolol may have adversely affected the diffusion rate of the drug.

2.1.1. Trehalose

The use of amorphous carbohydrates, particularly disaccharides such as sucrose, lactose and trehalose, is common in the pharmaceutical industry where they are utilised to encapsulate, stabilise and release labile biological active ingredients [153]. Their use as cryoprotectants during freeze drying processes and stabilisers during dehydration is widespread. Reasons for their use in these areas include the fact that they have low toxicity, are readily available at high purity levels and have high glass transition temperatures (T_g) [147, 154].

Trehalose (Figure 2.3) is a homodisaccharide which consists of two molecules of glucose which are bonded together via a symmetrical, low energy α α-1, 1 linkage. It is a non-reducing sugar due to the fact that the reducing end of the glucosyl residues

of both glucose units are connected to each other and therefore unavailable for reduction [155]. In addition, as it is a non-reducing saccharide, it does not undergo a Maillard browning reaction with amines, amino acids, peptides or proteins [156].

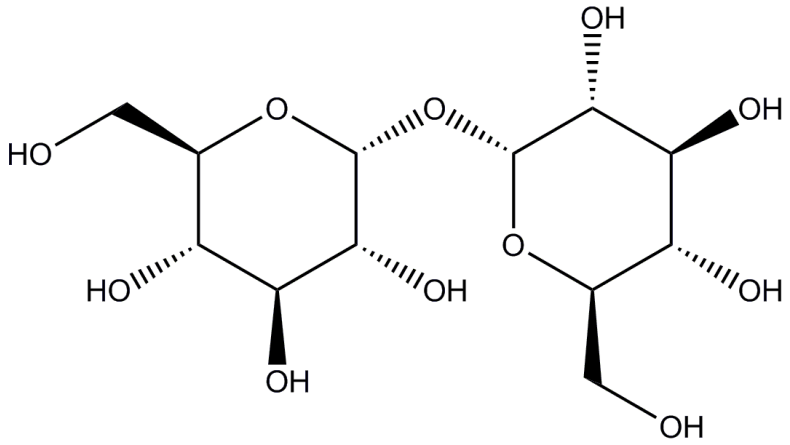

Figure 2.3: Chemical structure of trehalose [147].

Trehalose is also the most thermodynamically and kinetically stable naturally occurring disaccharide and has a high pH stability range (resisting degradation between pH 3.5 and 10 for 24 h at 100 ºC) [155]. Trehalose is extensively found in many organisms including bacteria, insects, plants, invertebrates and fungi (with mushrooms containing up to 25% trehalose by dry weight) however, it is not found in mammals [155, 156]. In nature, trehalose carries out a wide variety of functions including use as a carbon/energy source (providing high levels of blood glucose in winged insects as an energy source for flight [155]), osmoregulation, as a structural component in bacterial cell walls, desiccation protectant, cryoprotection, immunogenicity and as a growth regulator in plants [157]. Although trehalose is not found in mammals, the enzyme trehalase has been found in the intestinal villi of mammals which allows dietary trehalose to be cleaved into two molecules of glucose [155]. In humans, trehalase is found in the epithelial membrane brush border cells within the small intestine and in the proximal tubules of the kidneys which is surprising given the absence of cellulase, the hydrolysing enzyme used to break down the more commonly occurring polysaccharide, cellulose, [158].

One function which is of particular interest is its role in stabilising membranes and protecting the integrity of cells and other macromolecules of organisms under

conditions of extreme environmental stress [155, 156]. Up until quite recently, trehalose was understood to be a storage molecule which facilitated the release of glucose for the cellular functions however, it is now known that trehalose is synthesised in many organisms when exposed to environmental stresses such as cold, heat, oxidation and desiccation. In particular, unicellular organisms synthesise large amounts of trehalose in response to stress and this helps to maintain cell viability by protecting proteins from denaturation [157]. Many organisms when experiencing forms of environmental stress undergo a state known as cryptobiosis whereby metabolic indicators are evident and the organism becomes ametabolic (the slowing down or reversible ceasing of signs of life). The terms associated with this form of 'suspended animation' as a result of environmental stresses are anhydrobiosis (desiccation), anoxybiosis (lack of oxygen), cryobiosis (low temperatures) and osmobiosis (high pressure). Trehalose, (Table 2.1) along with other non-reducing disaccharides, has been implicated in the ability of many organisms to undergo these processes [155].

Table 2.1: Properties of trehalose [156, 157].

Chemical formula	$C_{12}H_{22}O_{11}\cdot 2H_2O$
Molecular weight	378.3 g/ mol^{-1}
Melting point	97.0 ºC
Relative density	1.22 g/cm^{-3} (at 25 ºC and weight fraction = 0.5)
T_g	117 ºC
Hygroscopicity	None at <90% RH
Solubility	68.9 g/100 g H_2O at 20 ºC
Relative sweetness	45 % of sucrose
Digestibility	Digested and absorbed by the small intestine
pH stability of solution	>99 % (pH 3.5-10, at 100 ºC for 24 h)
Heat stability of solution	>99 % (at 120 ºC for 90 min)

The exceptional protection properties of trehalose have been attributed to a number of physical qualities one of which is its T_g which is widely given as ≈115 - 117 ºC [157, 159], which is the highest T_g of all disaccharides. The T_g of an amorphous material is the temperature above which the substance changes from a viscous to a fluid state and is related to its physical stability [153]. With carbohydrates, once melted, they can cool to room temperature, without crystallising, into a glassy state. Glasses can encapsulate molecules as a result of having typically high viscosity and as such, the encapsulated molecule becomes immobile and, therefore, stable and protected from environmental stresses [157]. This is facilitated by the amorphous characteristic of the glass which allows enough contact between the biomolecule and the glass to allow sufficient hydrogen bonding to occur [160]. Each trehalose molecule has 4 hydroxyl sites per ring which allows for hydrogen bonding to occur with polar head groups of phospholipids and functional groups of proteins that would normally be hydrated [161, 162]. However, given that other good glass forming sugars such as the polysaccharides dextran and hydroxyethyl starch are not effective at biomolecule preservation suggests that other properties are required other than the formation of amorphous glass [147].

In relation to the ability of trehalose to act as a biomolecule protectant, 3 theories have emerged; glassy immobilisation, preferential exclusion and water replacement hypothesis [155, 157, 158]. In the case of the glassy immobilisation theory, it is thought that trehalose entraps the molecule in a glassy matrix which inhibits the movement of the protein molecules. The ability of trehalose to reversibly transition between dihydrate and anhydrous crystalline forms without relaxing structural integrity is believed to be the mechanism by which the biomolecules are trapped. The second theory, preferential exclusion, states that the trehalose does not interact with the biomolecule directly but in fact exclusion of water molecules from the solvation layer of the biomolecule occurs and the water instead orders around the trehalose, now acting as a kosmotrope which results in stabilisation of the biomolecule. The third theory is water replacement which proposes that water molecules are replaced by trehalose molecules around the biomolecule which can mimic the hydrogen bonding patterns for water [163]. The three dimensional structure of the biomolecule is then retained through hydrogen bonding between the trehalose and hydrogen-bonding species of the biomolecule [155, 157, 158, 161].

As a result of these remarkable properties, trehalose has found uses in a wide variety of industries including medical (organ preservation), pharmaceutical (stabilisation of vaccines, antibodies and other therapeutic biomolecules), cosmetics (as a moisturiser and stabiliser) and in the food industry as a preservative, sweetener and masking agent [155].

2.1.2. PVP

PVP is a synthetic polymer which is widely used in the cosmetic, food and pharmaceutical industries in addition to being utilised for various technical applications [164]. It is a polymer lactam which possesses an internal amide bond (Figure 2.4) and is classed as a poly-N-vinylamide [127]. PVP is readily soluble in water, biologically compatible, temperature resistant, pH stable, is non-ionic and chemically inert [165]. Soluble PVP is commonly obtained through the process of radical polymerisation of vinylpyrrolidone in an aqueous solution using hydrogen peroxide as an initiator whereby the molecular weight of the polymer product is determined by the volume of hydrogen peroxide used, with higher volumes of hydrogen peroxide resulting in lower molecular weight of polymer and vice versa [164].

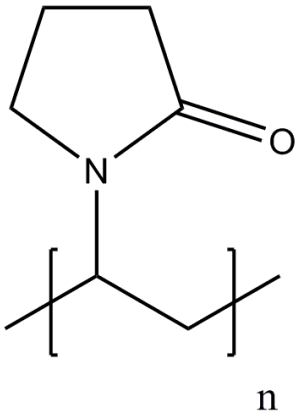

Figure 2.4: Chemical structure of polyvinylpyrrolidone [164].

One of the distinct characteristics of PVP is that it has amphoteric properties and is universally soluble in both water and a variety of organic solvents due to the presence of hydrophilic and hydrophobic functional groups in its structure; the amide group of its monomer unit is highly polar and the methylene groups of its main chain

and ring are non-polar [127, 164]. As a result of its distinctive properties, both physical and chemical, PVP is used in the pharmaceutical industry in a wide range of applications including as an adhesive, as a toxicity reducer, in regulating the controlled release of active ingredients, cryoprotection, lyophilisation and enzyme stabilisation [165].

PVP is produced in a wide range of viscosity grades ranging from low to high molecular weight and these are differentiated by K-numbers (e.g. PVP K 12, K 17, K 25, K 30). The K numbers characterise the mean molecular weight of the polymer which is calculated from the relative viscosity of the polymer in water [165]. PVP of high mean molecular weight (such as K 25, K 30, K 90) is widely used in the pharmaceutical industry as a binder in tablets and granulates. Lower molecular grades such as K 12 and K 17 are widely used as solubilisers, dispersants and crystallisation inhibiting agents particularly in parenteral formulations [165]. In the case of parenteral drug delivery, molecular weight is an important factor as it directly affects the rate and extent of polymer elimination from the body. Parenterally administered polymers are excreted via a size-dependent process of renal filtration with a generally accepted size threshold of 40 kDa to prevent accumulation of polymer in the body after multiple administrations [166].

2.2. Objectives

The focus of this chapter was to develop and characterise a dissolving microneedle formulation for the rapid systemic delivery of high potency therapeutic peptides. The formulation utilised biologically stabilising sugars in addition to biocompatible polymers with a view to enhancing the stability, mechanical strength and drug delivery capability of the microneedle system. As such, a number of polymers and sugars were initially tested to determine which would prove most suitable. In addition to selecting the materials, other parameters needed to be considered including the fact that the microneedles chosen needed to be long enough to deliver the drug effectively without sacrificing structural integrity or inducing pain in the patient.

2.3. Experimental

2.3.1. Materials

The materials used for the formulation of the microneedles were as follows:

- Poly(vinylpyrrolidone) (PVP) average weight 40 kDa supplied by Sigma Aldrich Ireland
- Poly (vinyl alcohol) (PVA) average weight 61 kDa supplied by Aldrich Chemistry
- Poly (lactic-co-glycolic) acid PLGA Purasorb PDLG obtained from Purac Biomaterials
- Polydimethylesiloxane (PDMS) Sylgard® 184 Silicone Elastomer Kit supplied by Sigma Aldrich Ireland
- Carboxymethylcellulose (CMC) low viscosity
- Trehalose D(+)-trehalose dihydrate (≥98 %) obtained from Fisher Scientific
- Sucrose
- Trypan Blue from Sigma Aldrich Ireland
- Glycerol – ACS grade obtained from Reagecon
- Polyethylene Glycol PEG 400 supplied by Merck-Schuchardt
- Ethanol 96% v/v supplied by Lennox Laboratory Supplies.
- Sylgard ® 184 elastomer kit supplied by Fischer Scientific.

2.3.2. Methods

2.3.2.1. Microneedle Master Mould Fabrication

The microneedle master moulds used for this research were designed and fabricated using the Xtreme Laser Facility (XLF) in Cardiff University by David Barrow, Professor of Micro- and Nano-Technology. To fabricate the moulds, silicon sheets were laser ablated to create pre-programmed inverse patterns of the arrays.

Two microneedle designs were examined for this research: one design consisted of an array of 18 x 18 needles each with 750 µm shaft length, 200 µm base width and 600 µm spacing between needles. The second design used was an array of 18 x18

needles each with a shaft length of 650 µm, 200 µm base width and 600 µm spacing between needles. These microneedles were chosen because of the high aspect ratio of the designs.

2.3.2.2. PLGA and PDMS Mould Fabrication

PLGA moulds were fabricated from the silicon master moulds supplied by Cardiff University by placing PLGA granules over the mould which was then heated to 150 ºC in a vacuum oven at low vacuum (<5 mbar) for 1 h. After this, the vacuum was broken and the melted PLGA was pressed over the silicon moulds using a glass microscope slide and left in the oven for a further 10 min. The PLGA and silicon moulds were removed and left to cool to room temperature after which the silicon mould was peeled carefully away from the PLGA microneedle master arrays. Following this, a batch of PDMS was prepared using a Sylgard ® 184 elastomer kit by mixing the PDMS with the supplied curing agent in a ratio of 10 parts PDMS to 1 part curing agent. PDMS was selected as the mould material as it is flexible and produces accurate reproduction moulds of the master structure [146]. This mixture was then de-gassed in a vacuum desiccator until bubbling of the mixture ceased. The degassed PDMS was then poured over the PLGA moulds in a petri dish carefully to avoid any bubble formation and then placed in an oven to cure at 100 ºC for 45 min as per the manufacturer's instructions. Once the PDMS had set, the PLGA moulds were carefully peeled away leaving PDMS inverse moulds which would be used to cast the polymer/sugar microneedle arrays (Figure 2.5).

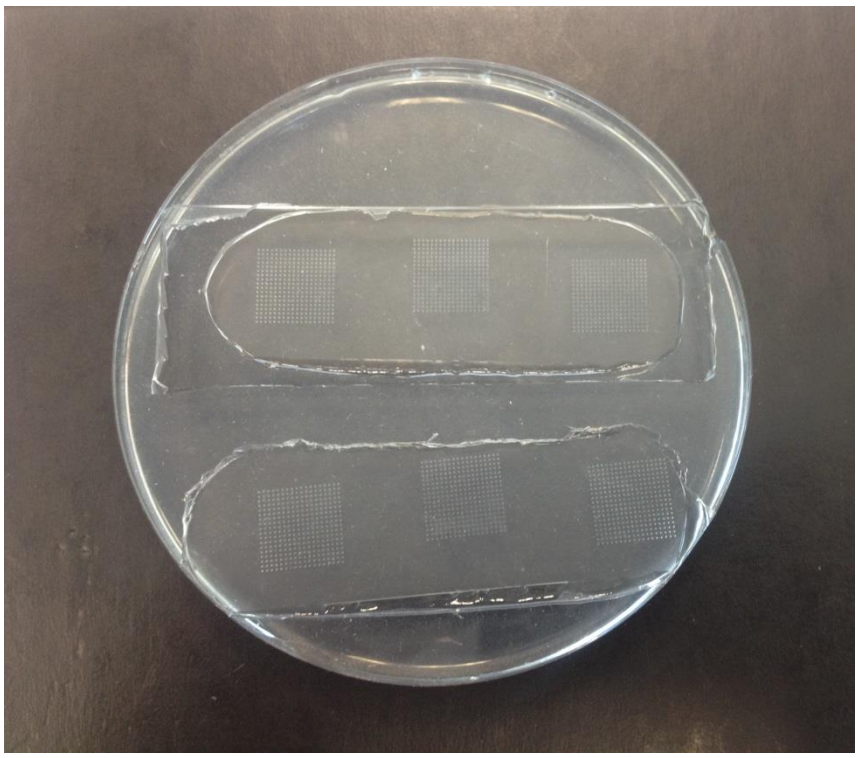

Figure 2.5: Image of set PDMS mould containing 6 microneedle inverse moulds.

2.3.2.3. Formulation Preparation

A number of different polymers and sugars were tested to determine which would be the most suitable as components of the dissolving microneedles. The polymers tested included PVP, PVA, and CMC with trehalose and sucrose comprising the sugars used. In addition, glycerol and PEG 400 were utilised as plasticisers for the polymer/sugar formulations to prevent the arrays from becoming too brittle and to facilitate ease of removal of the arrays from the moulds. For each formulation, the polymer and sugar components were carefully weighed using an analytical balance and transferred into a 100 mL beaker. 10 mL of DI water was added using a micropipette and the solution was thoroughly mixed. Plasticiser was then added and the beaker was placed in a sonicator for 20 min to ensure total dissolution of the components. Once fully dissolved, the formulation was pipetted over the PDMS microneedle moulds ensuring total coverage of each mould. The formulations were then held under vacuum to fill the mould cavities and cast the microneedle arrays.

A number of methods were employed to fill the PDMS moulds with the polymer/sugar formulations. These included a benchtop vacuum flask method, a vacuum desiccator/pump method and a vacuum oven method.

2.3.2.4. Vacuum Flask Method

The vacuum flask method employed was the method developed by Martin *et al.* [87] which consisted of placing an individual PDMS micromould into a vacuum flask sealed with a rubber stopper (Figure 2.6). Double sided tape was placed on the base of the vacuum flask and the mould placed on the tape to prevent it from becoming dislodged. The micromould was then held under vacuum using an aspirator attached to a water tap for approximately 30 min after which the microneedle formulation was applied directly onto the PDMS mould by injecting with a syringe through a septum in the stopper. Once the formulation was applied to the mould, the vacuum was immediately released and the micromould removed from the flask and placed in an incubator at 22 ºC for 24 or 48 h to dry, depending on the formulation.

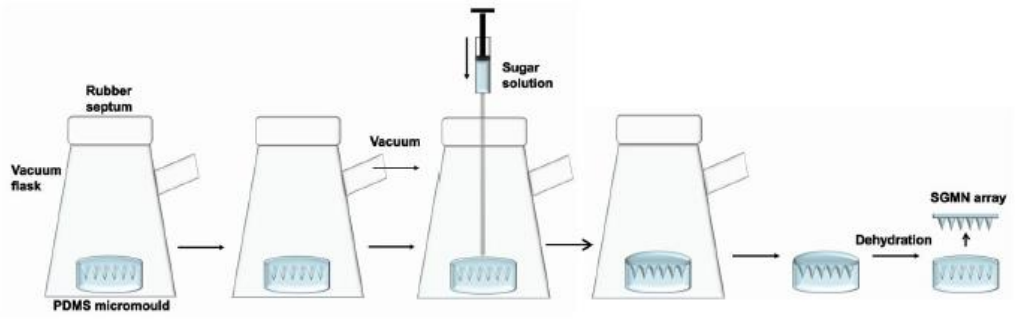

Figure 2.6: Schematic of vacuum flask method developed by Martin *et al.* [87].

2.3.2.5. Vacuum Chamber Method

The formulations were sonicated for 20 min to ensure total dissolution of the formulation components and the solution was then degassed in a chamber attached to a vacuum pump until the majority of the gas was removed, indicated by the cessation of bubbling from the mixture. The micro-moulds were then placed into the chamber and the microneedle formulation was micro-pipetted onto the micro-mould surface. The chamber was sealed and the vacuum was applied for approximately 5 min. The

vacuum was then released and the mixture was gently agitated on the mould surface to remix the formulation and remove any bubbles from the formulation droplet (Figure 2.7). Additional formulation was applied where required to prevent the solution from drying out. The vacuum was applied again for another 5 min and the process was repeated until the formulation ceased bubbling, indicating that the mould cavities had been fully filled. The vacuum was then released and the micromoulds were removed and immediately placed in an incubator at 22 ºC for 24 or 48 h until dried, depending on the formulation.

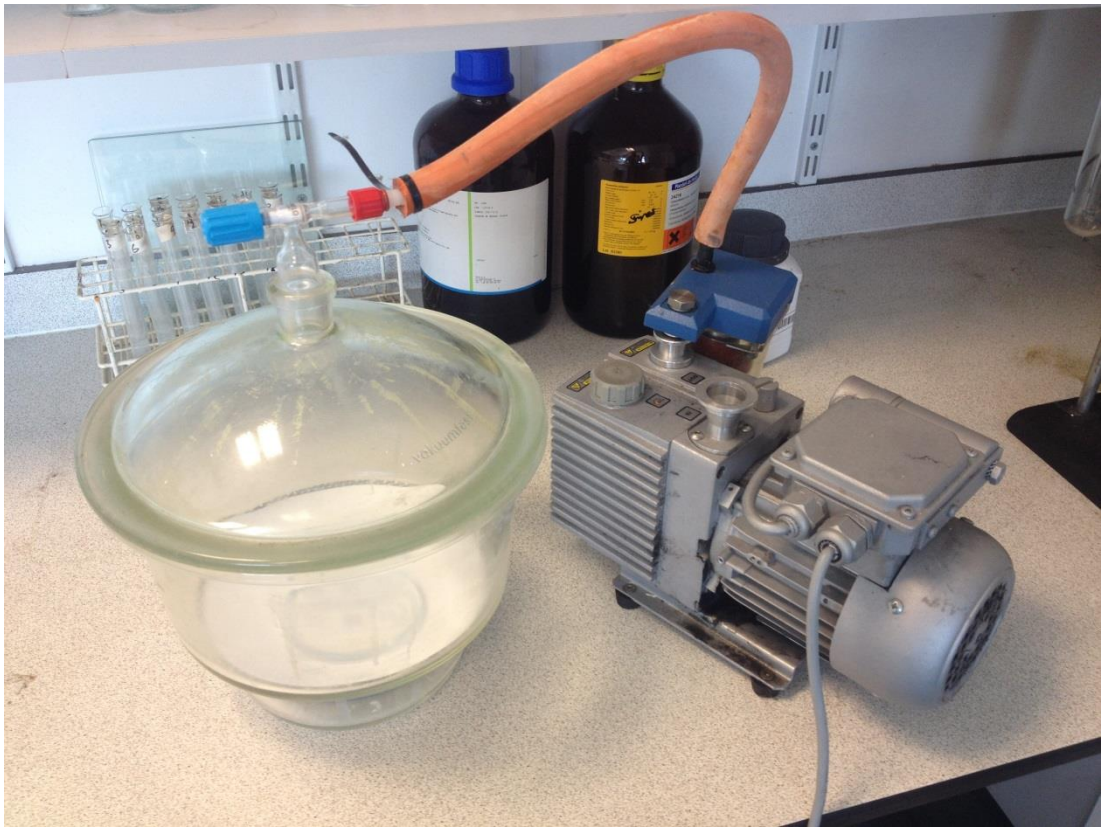

Figure 2.7: Image detailing the apparatus set-up of the vacuum chamber casting method.

2.3.2.6. Vacuum Oven Method

The formulations were sonicated for 20 min to ensure total dissolution of the components in the formulation. The sugar/polymer formulation was then carefully micro-pipetted directly onto the micro-mould surface and the micro-moulds were placed in a vacuum oven set at 22 ºC with the vacuum pressure set to 5 mbar. Once the oven was set, the vacuum was applied and the moulds were left for 15 min. After this, the vacuum was released and the moulds were removed. The formulation was

gently agitated on the mould surface to remix the formulation and remove any bubbles from the formulation droplet. The moulds were returned to the oven and the process was repeated until the formulations ceased bubbling under vacuum, indicating that the mould cavities had been fully filled by the formulation. The vacuum was then released and the micro-moulds were placed in an incubator at 22 ºC and left for 24 or 48 h to dry, depending on the formulation. Once the formulations had dried sufficiently, each microneedle array was carefully peeled off the PDMS mould using a tweezers, the entire batch placed in a petri dish and then stored in a desiccator prior to subsequent analysis.

2.3.2.7. Scanning Electron Microscopy (SEM)

SEM was carried out on each batch to examine the morphology of the arrays. The instrument used for this experiment was a Hitachi S-2460N SEM. For sample analysis, the emission current was set to 80 µA and the accelerating voltage was set at 22 kV. Prior to SEM analysis, each sample was affixed to a metal stub using carbon adhesive tabs before being gold coated using a K550 Emitech Sputter coater with deposition current set to 35 mA and a coating time of 3.5 min.

2.3.2.8. Thermogravimetric Analysis (TGA)

TGA was carried out to determine the moisture content and decomposition temperatures of the various components of the formulations. The instrument used for this experiment was a TA Instruments Q50 TGA. A standard heating programme was selected incorporating a heating rate of 10 ºC / min from ambient temperature up to 500 ºC with the balance purge flow set to 5 mL/ min and the sample purge flow also set at 5 mL/min. All samples were run in triplicate and the thermograms were analysed using TA Instruments Universal Analysis 2000 software.

2.3.2.9. Differential Scanning Calorimetry (DSC)

DSC was carried out to examine the thermal behaviour of the formulations, particularly the T_g of the polymer/sugar formulations. Calibration of the instrument

was carried out using indium. The instrument used for this experiment was a TA Instruments QS 2000 DSC. All formulations were tested in triplicate with sample weights ranging from 5 to 10 mg. All samples tested were accurately weighed and placed into Tzero aluminium pans which were hermetically sealed using a crimper. A pin hole was placed on the lid of the pans to allow the release of water vapour. The programme used for all samples, carried out under nitrogen, incorporated an equilibration step at 20 ºC followed by a series of heating and cooling cycles initially starting with a ramp of 10 ºC/ min up to 180 ºC. The next stage was a cooling cycle of 10 ºC down to 20 ºC and finally, another heating cycle consisting of a ramp of 10 ºC up to 180 ºC. TA Instruments Universal Analysis 2000 software was used to analyse the thermograms with the T_g being measured as the inflection point between the initial and final T_g's in each case [167].

2.3.2.10. Dynamic Vapour Sorption (DVS)

DVS analysis was carried out on the polymer/sugar formulations to examine the rate of moisture sorption. The instrument used for this experiment was a Surface Measurements Systems DVS Intrinsic. The instrument was programmed to increase the RH in steps with each step held for 120 min. The RH stages used ranged from 0 % up to 75 % and back down to 0% in 10 % increments. The flow rate was set at 200 sccm and the temperature was maintained throughout each experiment at 25 ºC. Each sample measured was between 10-20 mg.

2.3.2.11. Rate of Disintegration

The instrument used for disintegration testing was a triple basket testing Pharma Test Dist-3. The stroke rate was 30/min and the water bath temperature was set to 37 ºC. The samples tested were 500 µL discs of each formulation incorporating approx. 20 µL of trypan blue solution to allow the discs to be more easily seen in the baskets. Each polymer/sugar formulation was prepared as before however, instead of moulding into microneedles, 500 µL aliquots of formulation and trypan dye were applied to a flat PDMS mould surface and dried in an incubator overnight at 25 ºC to form discs. 6 discs of each formulation were tested simultaneously and the elapsed

time was monitored on the instrument display. The time required for each disc to fully dissolve was recorded and the procedure was repeated for each formulation prepared.

2.3.2.12. Statistical Analysis

Minitab 16 Statistical Software was used to examine the effect of each variable in the formulation to aid in determining the optimum formulation for the PVP/trehalose microneedles. The explanatory variables were polymer/sugar formulation, % plasticiser and plasticiser type. The response variables examined were disintegration time, T_g and percentage mass increase.

2.4. RESULTS & DISCUSSION

2.4.1. Microneedle Preparation

The vacuum flask method (Figure 2.6) had a number of limitations including the fact that each array had to be cast individually, with each mould requiring approx. 30 min to prepare and fill. In addition, the moulds needed to be secured to the inner base of the flask with double sided tape to avoid the mould hopping inside the flask once the vacuum was released. This process itself was tricky and cumbersome, resulting in difficulty when removing the moulds without spilling the formulation after the filling process.

Although the vacuum desiccator method (Figure 2.7) allowed for rapid filling of a large batch of microneedle moulds, it was difficult to control and the high vacuum often resulted in the formulation bubbling and spilling out over the moulds. Releasing the vacuum also often caused the moulds to jump within the desiccator and spill the formulation. In addition, as moisture was driven off the formulations rapidly under vacuum, drying across the arrays was often uneven and the microneedles were often too dry and broke on removal from the moulds after setting.

The vacuum oven method proved to be the most suitable cast filling method employed. This method allowed the operator to control the temperature and vacuum level and, unlike the previous casting methods, applied the vacuum gradually to the samples which prevented the solutions from drying out too quickly. It also allowed a large batch of moulds to be filled and cast together which enabled an entire batch of 18 arrays to be prepared and ready for drying in under an hour.

Once the microneedle arrays had been removed from the moulds, placed in the desiccator and were sufficiently dried, SEM images were taken to examine the morphology of the arrays. Each array being examined was placed on a metal sample stub, affixed to an adhesive carbon tab, sputter coated and placed in the SEM for analysis.

2.4.1.1. Initial Formulations

The SEM images provided information on the arrays such as the formation of the needles (i.e. whether they were fully representative of the inverse master moulds), whether they were solid or hollow and, where needles hadn't formed, whether they had broken off at the base during removal from the moulds or had not formed at all during the casting process (Figure 2.8). The SEM images also provided information on how quickly the needles softened and deformed as a result of atmospheric moisture and temperature.

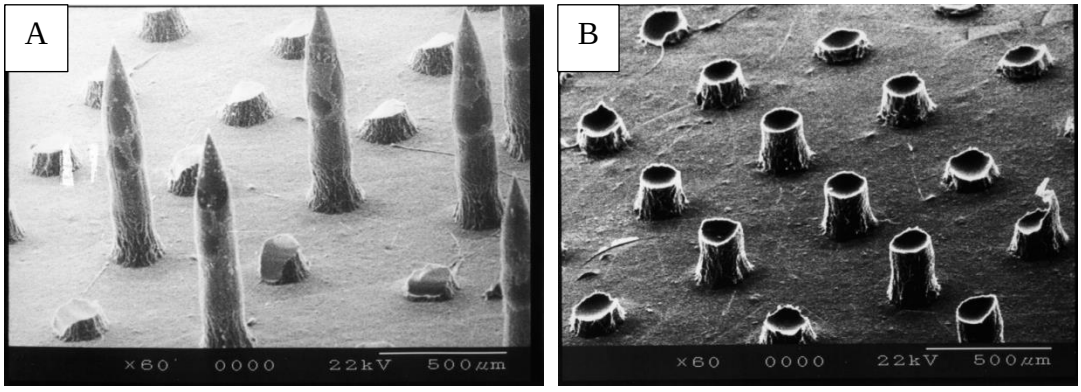

Figure 2.8: SEM images of (A) trehalose/CMC microneedles broken when removed from micro-mould after casting and, (B) trehalose/CMC microneedles not fully formed during the casting process.

General parameters observed during the fabrication process included the need to optimise the drying time to prevent the arrays from either drying out too much prior to removal from the moulds which often lead to needle breakage, or insufficient drying time, which caused the needles to stretch and deform on removal from the moulds. In addition, during the casting stage, care was required to ensure that the formulation did not dry out too much under vacuum which caused the formulation to solidify too quickly and crack. This was more easily achieved when using the vacuum oven casting method.

In relation to the initial formulations tested, CMC/trehalose microneedles were often brittle and hollow and this may have been due to the fact that the CMC formulations were extremely viscous. This may have prevented the formulation from filling the moulds fully under vacuum. The result of this being that initially, the microneedles

appeared to have formed in line with the inverse moulds however on closer inspection, the needles were determined to be hollow (Figure 2.9).

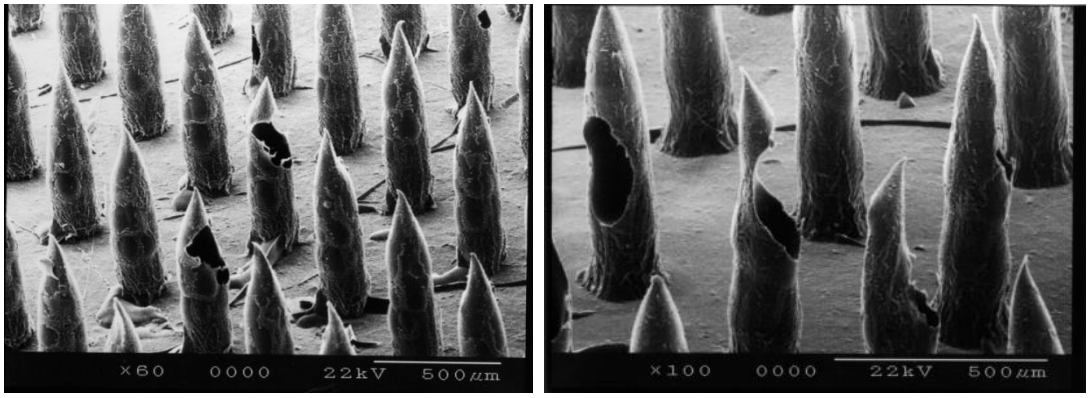

Figure 2.9: SEM images of CMC/trehalose microneedles.

Another formulation tested used PVA in conjunction with PVP however, as with the CMC needles, the PVA/PVP formulation was too viscous to fill the moulds completely. As a result, the needles formed were hollow and in this case, still quite soft after 48 h drying which was evident from the SEM images which showed the shafts had started to collapse (Figure 2.10). After storage in a dessicator for a number of days in which the needles dried out, the arrays were also quite brittle.

Trehalose was also used without any additional components to examine its suitability alone for microneedle fabrication. However, attempts to cast arrays using a trehalose only formulation were unsuccessful (Figure 2.10). The trehalose needles failed to fully form and were extremely brittle. Additionally, the trehalose liquid formulation was too fluid, and it would often draw off the mould in places leaving unfilled cavities on the microneedle mould which needed to be recovered during the filling process.

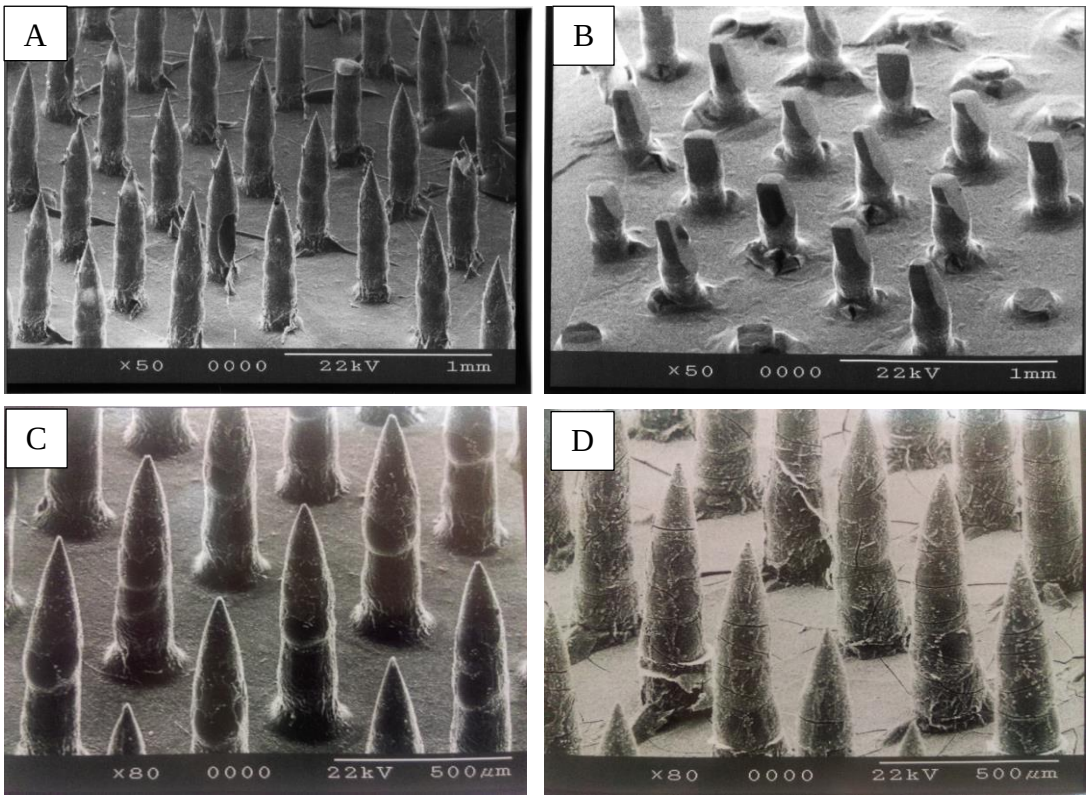

Figure 2.10: SEM of (A) PVA/PVP microneedles detailing the hollow shafts, (B) trehalose microneedles which failed to fully form, (C) PVA/PVP microneedle array detailing collapsing shafts and (D) brittle PVA/PVP array after desiccator storage.

From these SEM images, in addition to the experimentation carried out on casting the various formulations into arrays, PVP and trehalose were selected as the most suitable combination of materials with which to fabricate the dissolving microneedles. Microneedles fabricated utilising PVP were generally firm, sharp and fully formed and the arrays were consistently representative of the inverse moulds (Figure 2.11). PVP and trehalose needles formulated with either glycerol or PEG 400 as plasticisers were successfully cast and SEM images confirmed these formulations produced solid, fully formed arrays that were easily removed from the moulds after drying. As such, it was decided to continue the research into developing the dissolving microneedles using combinations of PVP and trehalose in various ratios in conjunction with the addition of either PEG 400 or glycerol as a plasticiser. This study represented the first time that such formulations had been tested together to determine suitability for use in the fabrication of dissolving microneedles.

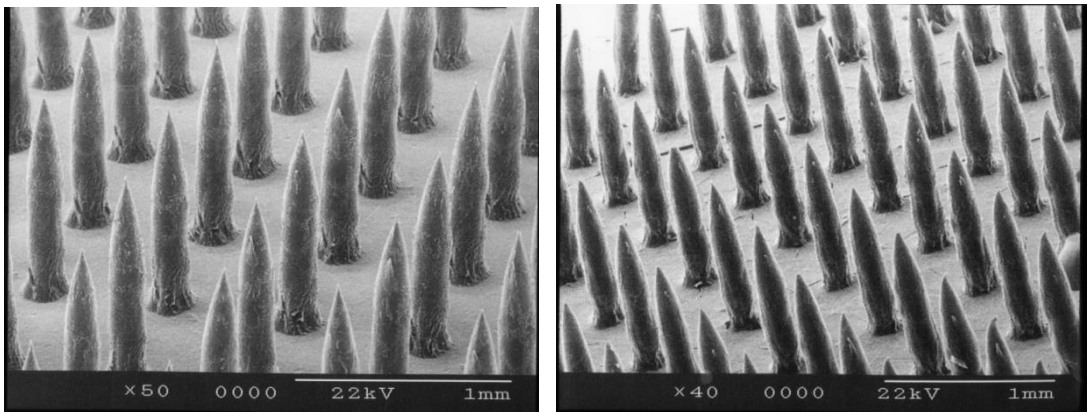

Figure 2.11: SEM images of various PVP/trehalose microneedles.

2.4.2. PVP and Trehalose Formulations

Based on the results obtained from the experiments carried out with various polymer and sugar combinations, PVP and trehalose were selected as the components for the dissolving microneedle system. PVP was chosen as it hardens well on drying, with each monomer ring providing intermolecular rigidity and subsequently, increased mechanical strength [168]. In addition, the fact that PVP is sufficiently hydrophilic and highly water soluble indicated that it should dissolve rapidly after insertion into the skin [169]. It is also biocompatible and has been used extensively in the medical, pharmaceutical and food industries [165]. Trehalose was selected due to its cryoprotectant properties to help stabilise biopharmaceuticals embedded in the microneedle matrix [170]. Trehalose has also found uses in the medical, food and pharmaceutical industries, particularly as a stabiliser for vaccines and other biologically active ingredients [155, 157]. In addition, initial experiments utilising PVP and trehalose combinations for microneedle formulations resulted in consistently solid, fully formed needles which were easily removed from the moulds without damage with the addition of PEG 400 or glycerol.

In order to determine the optimum formulation of PVP/trehalose and plasticiser, an experimental design process was utilised incorporating a variety of formulations. These consisted of PVP, 1:1 blends of PVP/trehalose and trehalose. Each formulation included the addition of either 1% or 2% w/w of glycerol or PEG 400 (Table 2.2).

Table 2.2: PVP/trehalose microneedle formulations used for further characterisation testing and analysis.

No.	PVP (g)	Trehalose (g)	Plasticiser (w/w)
1	3.6	0	1% Glycerol
2	3.6	0	1% PEG 400
3	3.6	0	2% Glycerol
4	3.6	0	2% PEG 400
5	1.8	1.8	1% Glycerol
6	1.8	1.8	1% PEG 400
7	1.8	1.8	2% Glycerol
8	1.8	1.8	2% PEG 400
9	0	3.6	1% Glycerol
10	0	3.6	1% PEG 400
11	0	3.6	2% Glycerol
12	0	3.6	2% PEG 400

Given that previous experiments with PVP and trehalose combinations had consistently produced arrays which were solid and fully formed, further characterisation was required. The characterisation techniques employed to evaluate the formulations were TGA, DSC, DVS and disintegration testing. These techniques were used to determine disintegration time, degradation profile, T_g and moisture sorption profile of the various combinations. Using this data, statistical analysis was carried out to determine the optimum PVP/trehalose/plasticiser combination.

2.4.2.1. Vacuum Oven Casting

Of the three casting methods employed, the vacuum oven method was chosen as it was the most easily controllable. This ensured that each formulation was prepared under the same casting conditions.

2.4.2.2. Disintegration Testing

The disintegration testing method used provided a simple means of determining the rate of disintegration of each formulation in an aqueous environment with each formulation subjected to the same conditions. This method provided useful data in relation to the rate at which each formulation would dissolve. This information was important as the optimum formulation needed to remain intact long enough to penetrate through the SC before dissolving and releasing the active ingredient. As such, if the formulation dissolved too rapidly, the needles would fail to pierce the skin.

The formulations tested were as per Table 2.2 and were tested at random with each formulation tested six times. The results obtained demonstrated that the trehalose only formulations dissolved extremely rapidly which was as expected with similar rates all below 1 min. The PVP formulations took the longest to dissolve with 507 s the mean disintegration time for formulation No. 1. Figure 2.12 illustrated the decrease in disintegration time relative to decreasing polymer/increasing sugar content but additionally indicated an effect on disintegration time as a result of the increase in plasticiser content for the PVP and PVP/trehalose formulations.

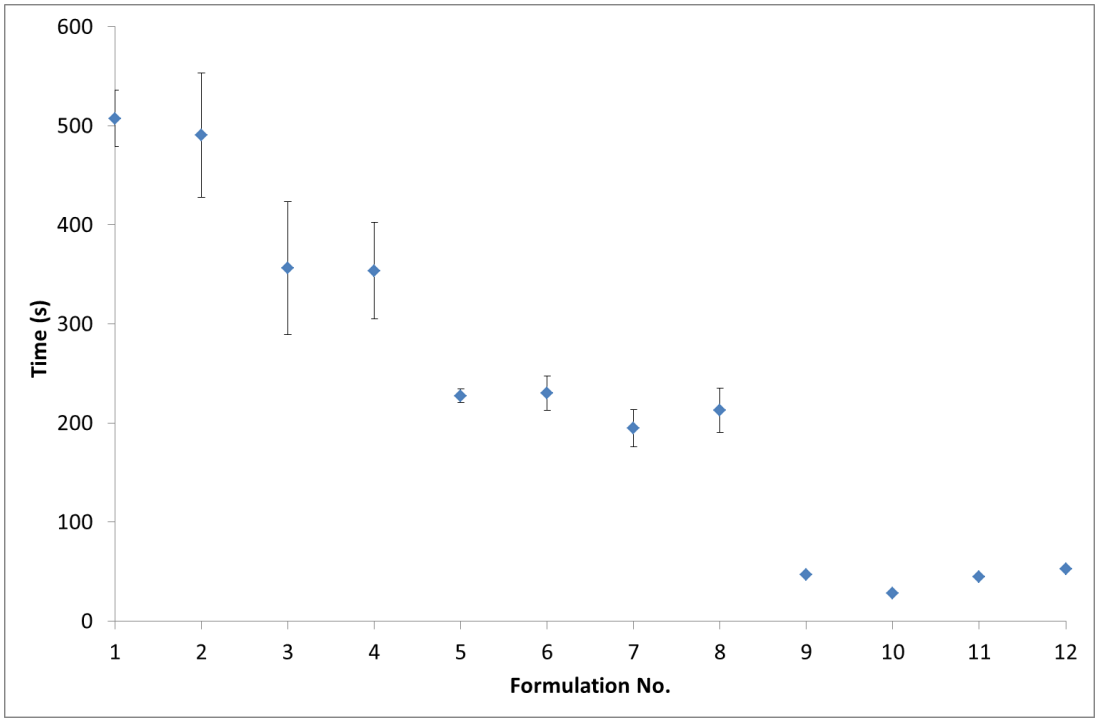

Figure 2.12: Plot detailing the disintegration time (s) of each formulation (n=6). Error bars for formulations 9 to 12 are smaller than the data points.

The plasticiser content for the PVP formulations (1-4) appeared to greatly affect the disintegration time with the formulations containing 2% of each plasticiser dissolving much quicker than those containing 1% plasticiser. These effects were as a result of hydrogen bonding between the hydroxyl groups of the plasticisers and the carbonyl oxygens of the PVP. Due to the basic nature of the PVP amide groups, these are good proton acceptors which facilitate hydrogen bonding with the hydroxyl groups of both PEG 400 and glycerol. In addition, both plasticisers can behave as crosslinking agents and this crosslinking results in enhanced free volume within the polymer/plasticiser matrix [171, 172]. As such, this free volume would cause greater uptake of water into the matrix, facilitating a more rapid disintegration time in an aqueous environment. The 1:1 formulations (5-8) also showed this trend but to a much lesser extent. The results of these tests also indicated that trehalose only microneedles would probably dissolve too rapidly on contact with the surface of the skin and would likely fail to penetrate the SC. This was as expected given that trehalose, along with most carbohydrates, is highly hydrophilic and can strongly interact with water [154]. PVP microneedles would however, remain intact long enough to penetrate into the skin and would then dissolve rapidly to effectively deliver the drug payload. The 1:1 formulations (5-8) dissolved after an average of 216 s which also indicated that microneedles with a PVP content of at least 50% would remain intact long enough the penetrate the skin.

2.4.2.3. Thermal Analysis: TGA & DSC

By definition, thermal analysis refers to the examination of property changes in a sample as a result of subjection to changes in temperature [173]. The main purpose of utilising TGA was to examine the temperature degradation profile of the sample (Figure 2.13). Step 1 indicated the loss of water, step 2 was indicative of the trehalose degradation and finally, step 3 indicated the degradation of the PVP component of the sample. Running the TGA analysis was a precursor to running the sample on the DSC. By determining the temperature at which the formulation started to degrade, the DSC programme could be set to avoid this degradation temperature during analysis given that the sample was being heated and cooled in 3 cycles during each run.

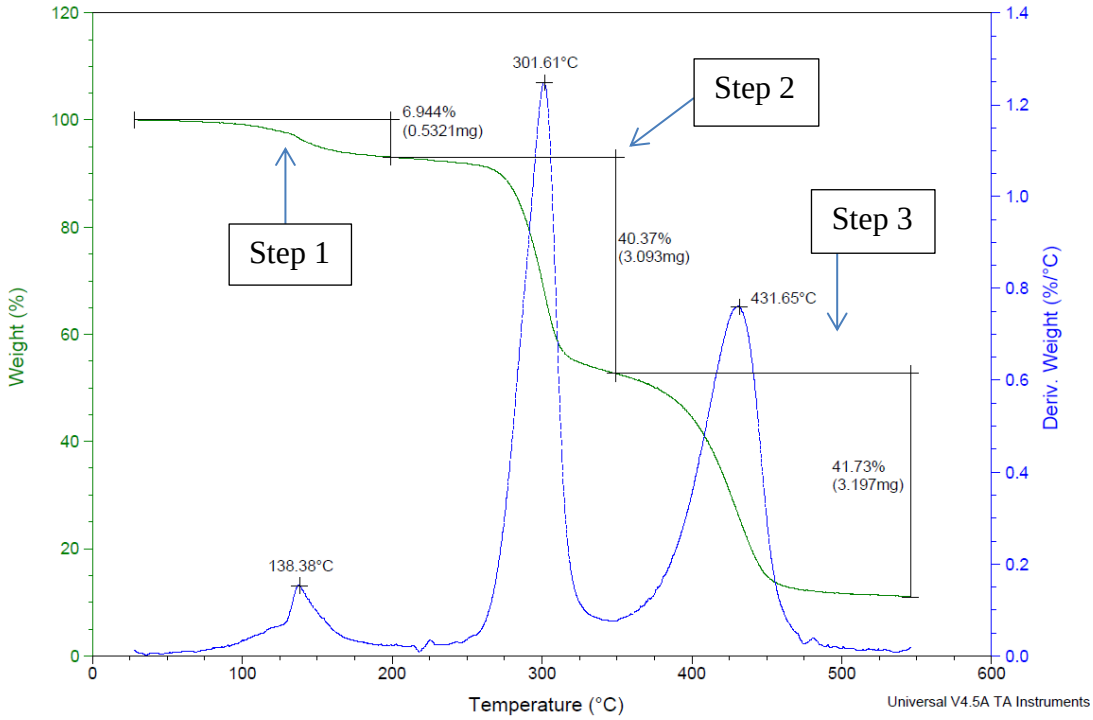

Figure 2.13: TGA thermogram detailing the heat degradation profile of a 7.6 mg sample of a 1:1 PVP/trehalose formulation with 1% w/w glycerol with % weight loss as a function of temperature increase.

Initially, thermal analysis was conducted on the trehalose dihydrate material used. By combining both TGA and DSC analysis of the trehalose dihydrate sample, the degradation of the sample was seen to be consistent with the stoichiometry of trehalose dihydrate and the melting point observed on the DSC thermogram corresponded with the expected melting point of the crystalline carbohydrate [157] occurring at approx. 97 ºC (Figure 2.14).

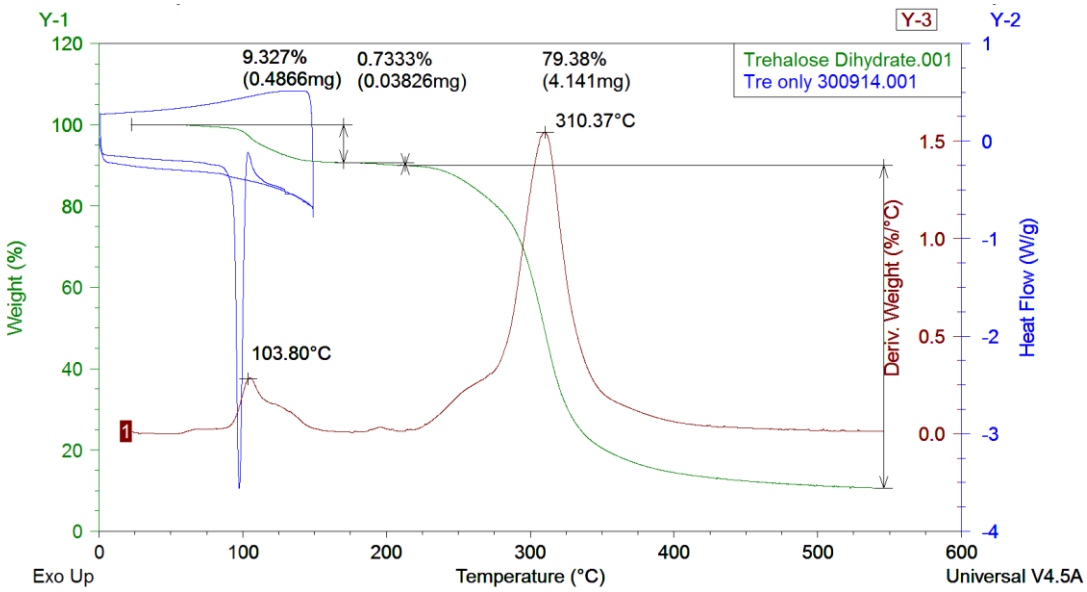

Figure 2.14: Overlaid DSC and TGA thermograms for trehalose dihydrate.

Finally, SEM images of the trehalose (Figure 2.15) confirmed the crystalline form of the material, clearly indicating the rhomboid crystals typically formed by trehalose dihydrate [174].

Determination of the T_g of polymers is a useful indication of stability and relates directly to both the packing density and cohesive energy of the polymer [172] . T_g is an important thermophysical property of polymers given that materials are generally hard, brittle and rigid (glassy state) below T_g and in a highly viscous/rubbery state at temperatures above the T_g (rubbery or viscoelastic state) [175, 176]. For amorphous formulations, the T_g is an indication of physical stability and in relation to pharmaceutically active ingredients, stability should be achieved through storage below the T_g. This is achieved because of the fact that molecular mobility is extremely reduced below the T_g [153, 154]. In relation to binary blends and co-polymers, T_g analysis can also provide information on whether components are miscible or compatible with miscibility of a blend indicated by a single T_g [177].

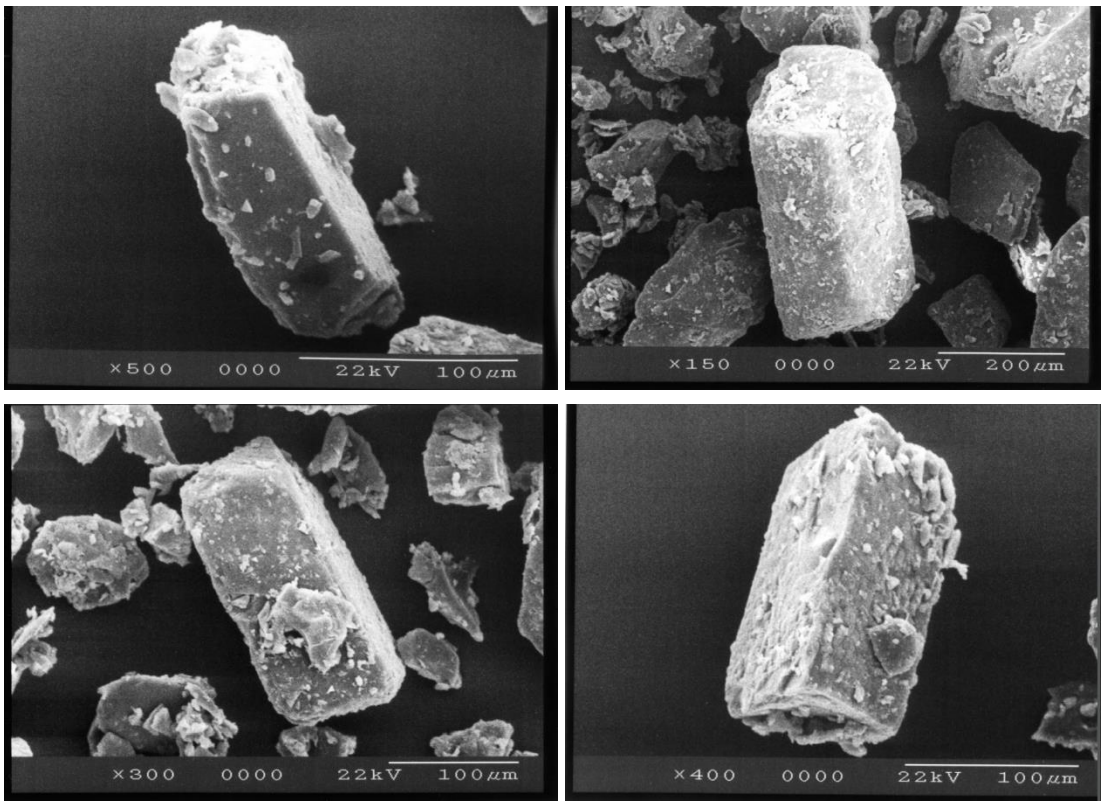

Figure 2.15: SEM images of trehalose dihydrate crystals.

Given that many reactions require the reactants to possess an adequate degree of mobility, reducing such mobility can reduce the likelihood of any chemical reactions from occurring [178]. Indeed, the pharmaceutical industry goes to enormous lengths to optimise the encapsulation, storage and release of active ingredients and incorporating excipients with relatively high T_g's is required in order to offset the effects of buffers, salts and moisture which can lower the T_g [153].

In relation to dissolving microneedle formulations, a number of factors are considered in relation to T_g. In addition to maintaining the stability of the encapsulated active ingredient, the structural stability of the needles must also be preserved. Essential to the effectiveness of the microneedles is the ability of the polymer/sugar formulation to maintain structural integrity at ambient temperatures. Although other factors such as moisture and the addition of plasticisers can affect this, establishing the T_g for each formulation was carried out to determine which formulation was potentially the most physically stable. Lai *et al.* (1999) [178] carried out studies on the deamidation of Asn-hexapeptide in lyophilised polymers (namely

PVP and PVA) and suggested that although the stability of the peptide in the glassy polymer formulations was higher when kept below the T_g of the polymer formulation, some chemical activity did occur at temperatures below the T_g. While other factors such as water content and polymer type were also thought to affect the deamidation of the peptide, a higher T_g may be associated with a greater decrease in mobility within the matrix at temperatures below the T_g, adding to the stabilising properties of the formulation. Similarly, Dirama *et al.* (2005) [161] proposed that the improved stability of a biomolecule in a glassy matrix was as a result of retarded dynamics, causing a slowing effect on the denaturation process and other reactions such as aggregation, deamidation and oxidation of peptide side chains [160].

On DSC thermograms, T_g is indicated by changes in the shape of the baseline as opposed to readily distinguishable peaks. In polymers, the Tg results in a change in heat capacity as a result of the transition from the rigid glassy to the more flexible rubber-like states and this is indicated by sudden changes in the baseline position on the thermogram [173]. The measured T_g value for PVP was determined as 160 ºC (Figure 2.16) which was in line with the literature value which was given as 163 ºC [179].

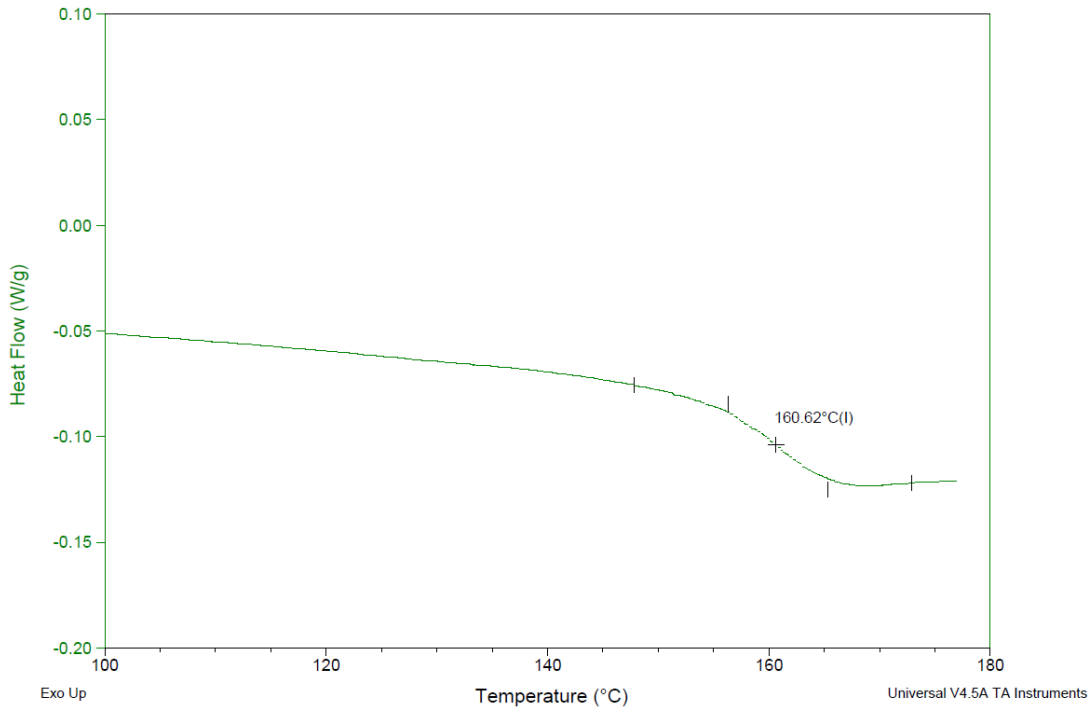

Figure 2.16: DSC thermogram showing the T_g of an unaltered PVP sample.

T_g values for amorphous trehalose vary in the literature from 73 ºC to 115 ºC which may be due to differences in sample purity and/or residual water content [170]. A 20% w/v aqueous solution of trehalose was prepared and dried in a fume hood for 24 h to form a trehalose glass. This was then examined using DSC and an experimental T_g value of 91.1 ± 1.8 ºC (n=3) for trehalose was obtained (Figure 2.17).

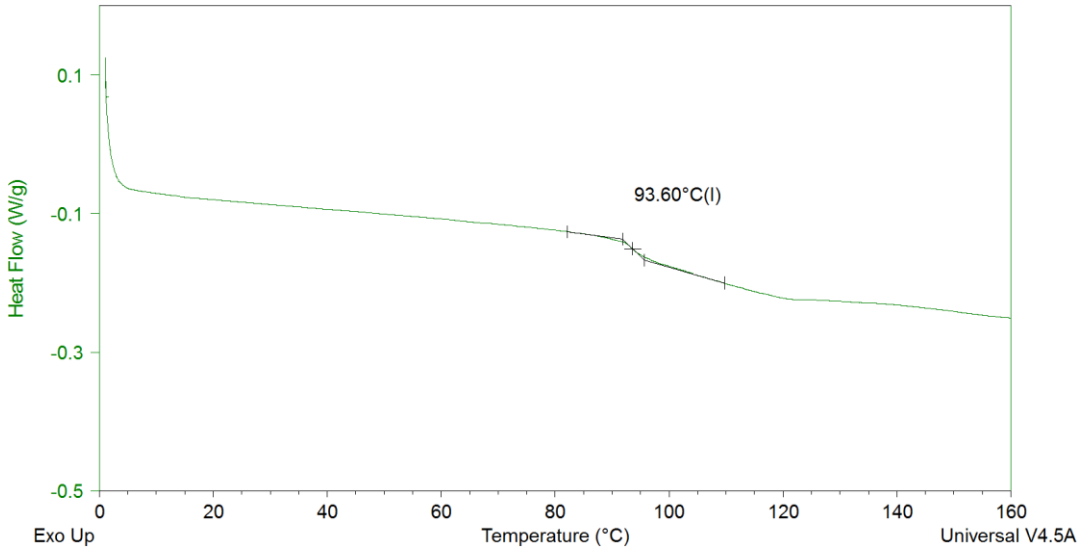

Figure 2.17: DSC thermogram illustrating the measured T_g of 93.6 ºC of an amorphous trehalose glass sample.

As discussed above, the addition of plasticisers shift the T_g to lower temperatures but are required in order to reduce brittleness [175]. Plasticisers, such as glycerol and PEG 400 (Figure 2.18), are generally non-volatile, low molecular weight substances and they improve the flexibility of a polymer, lowering the T_g by penetrating the polymer matrix, reducing the cohesive forces of attraction between the polymer chains and subsequently increasing the polymer chain mobility [176].

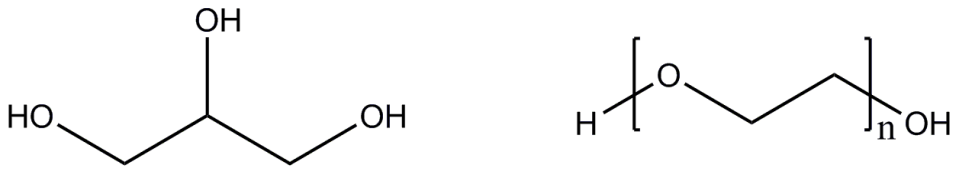

Figure 2.18: Chemical structures of glycerol [180] and PEG [181].

They interact with polymers much like solvents but are used in much lower quantities, essentially being absorbed into the polymer, forming a material with

lower T_g [182]. In this case, the plasticisers were utilised to reduce the brittleness of the polymer/sugar formulations and allow for the removal of the arrays from the moulds without causing damage to the needle shafts. In addition, studies have found that the addition of small amounts of low T_g plasticisers, such as glycerol, to carbohydrate glasses resulted in increased stability of encapsulated proteins in the glass matrix [160, 183].

The Gordon-Taylor equation [170] can be used to predict the T_g of binary mixtures based on the T_g of the individual pure components and the volume fraction of each component in the mixture. The Gordon-Taylor equation (Equation 2.1) is given as:

$$\boldsymbol{T_g = [w_1 T_1 + k w_2 T_2]/[w_1 + k w_2]} \qquad \textbf{(Equation 2.1)}$$

Where:

T_1 and T_2 are the glass transitions of the two components,
w_1 and w_2 are their mass fractions (or mol. fractions),
and k is an adjustable parameter which can be derived as $V_1/w_2 + V_2/w_1$ (where V refers to specific volume).

This equation was limited for the purposes of predicting the T_g of the formulations, however, given that each formulation consisted of three components namely polymer, sugar and plasticiser. In addition to this, water can invariably be present in most samples (even dried samples) and as such, should be taken into account as a component of the mixture [184]. The Gordon-Taylor equation predicted the T_g of the mixture based on the PVP and trehalose content of the formulations only and did not allow for the amount of plasticiser or residual water present. As such, using the Gordon-Taylor equation, formulations 5 – 8, (Table 2.2) were predicted to each have a T_g of 103 ºC. As the experimentally derived T_g values obtained varied for each of the four formulations (Table 2.3), the limitations of using the Gordon-Taylor equation to predict the T_g of mixtures containing more than two components was evident.

The amounts of plasticiser and water present in each sample was quite low however, and as such, it was reasonable to accept that the T_g values obtained experimentally closely matched the T_g values as predicted by the Gordon-Taylor equation and were

as expected given the components of each formulation. When used to predict the T_g of the PVP/plasticiser formulations 1-4 (Table 2.2), the equation calculated a T_g value of 159 ºC for all four formulations. This seemed to indicate again that the Gordon Taylor equation was limited in this instance when the concentration of one of the components of the mixture was quite low.

Prediction of T_g in mixtures can also be carried out using the Fox equation (Equation 2.2) [171]. This can be used for ternary and quaternary blends where the specific volume of each component is similar [185].

$$\frac{1}{T_g} = \frac{W_1}{T_{g1}} + \frac{W_2}{T_{g2}} + \frac{W_3}{T_{g3}} \qquad \textbf{(Equation 2.2)}$$

Where:

W refers to the weight fraction of each component;

T_g refers to the glass transition temperature of each component;

By taking the T_g values of glycerol and PEG 400 as 200 ºK and 206 ºK [171] respectively, and using the experimentally derived T_g values for PVP and trehalose, the calculated T_g values for the four 1:1 formulations were compared with the experimentally derived values (Table 2.3).

Table 2.3: Comparison of predicted and experimentally derived T_g values for all four 1:1 formulations.

Formulation	Predicted T_g (ºC) – (GT)	Predicted T_g (ºC) (Fox)	Experimental T_g (ºC)
1:1 with 2% Glycerol	103	95	96
1:1 with 2% PEG 400	103	97	98
1:1 with 1% Glycerol	103	108	114
1:1 with 1% PEG 400	103	109	105

Using the Fox Equation, the calculated T_g values obtained across all four of the 1:1 formulations closely matched the experimentally derived figures with the exception of the formulation containing 1% glycerol which yielded an experimental value of 114 ºC which was higher than the predicted value of 108 ºC. This suggested that the

plasticising effects may be suppressed where the glycerol concentrations are extremely low, possibly due to interactions with the PVP or trehalose. Given that the Fox equation can be used for ternary or quaternary mixtures, and in this instance enabled the inclusion of the plasticisers in the calculation, the results obtained from this equation indicated that the experimentally derived T_g values for the 1:1 formulations were as expected given the individual components.

The results obtained from running DSC analysis on the 12 formulations indicated a definite trend towards decreasing T_g in line with decreasing PVP/increasing trehalose content (Table 2.4).

Table 2.4: Data obtained from DSC triplicate experiments to determine the T_g for each PVP/Trehalose formulation.

No.	Formulation	T_g (°C)	T_g (°C)	T_g (°C)	Mean T_g (°C)	Std Dev (°C)
1	PVP 1% Gly	149.41	148.58	148.41	148.8	0.54
2	PVP 1% PEG	142.43	146.71	146.31	145.15	2.36
3	PVP 2% Gly	135.46	135.75	135.45	135.55	0.17
4	PVP 2% PEG	124.09	128.19	129.05	127.11	2.65
5	1 to 1 1% Gly	115.59	114.1	114.7	114.80	0.75
6	1 to 1 1% PEG	98.99	107.91	108.24	105.05	5.25
7	1 to 1 2% Gly	99.41	92.63	98.83	96.96	3.76
8	1 to 1 2% PEG	98.49	98.47	99.18	98.71	0.40
9	Tre 1% Gly	87.72	89.08	98.56	91.79	5.91
10	Tre 1 % PEG	94.12	88.5	92.24	91.62	2.86
11	Tre 2% Gly	98.61	99.14	98.14	98.63	0.50
12	Tre 2% PEG	90.58	89.44	88.69	89.57	0.95

As trehalose has a lower T_g than PVP, a drop in T_g for the 1:1 formulations would be as expected [186]. In relation to the PVP only formulations (1-4), the mean T_g was below that obtained for PVP (161 ºC) which was also as expected as the addition of plasticiser and water in the sample would be expected to cause a drop in T_g. In addition, the plasticiser used greatly affected the T_g particularly the quantity used, with the 2% w/w formulations (3, 4) causing a drop in T_g of up to 18 ºC compared

with the 1% w/w formulations (1, 3) in the case of PEG 400. In fact, the addition of PEG 400 caused a greater drop in T_g than glycerol across the PVP formulations.

The crosslinking that can occur as part of the complexation mechanism between PVP and both glycerol (Figure 2.19) and PEG 400 (Figure 2.20) could explain this drop in T_g associated with PEG 400 use.

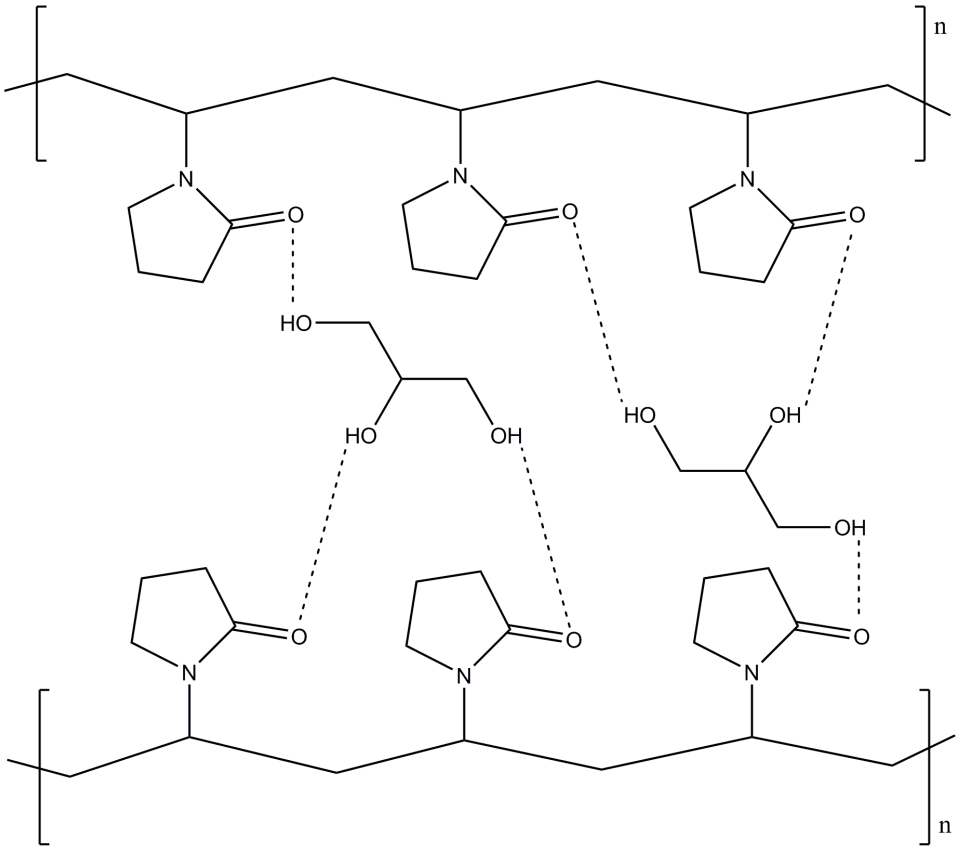

Figure 2.19: Diagram of proposed hydrogen bonding between PVP carbonyls and hydroxyl groups of glycerol.

Given that each glycerol molecule consists of a 3 carbon chain with an hydroxyl group on the C_1, C_2 and C_3 carbons whereas the PEG 400 units contain much longer chains with two terminal hydroxyl groups, the greater free volume created within the PVP/PEG matrix in addition to the flexibility of the PEG chains would be expected to increase the molecular mobility of the polymer segments in between adjacent hydrogen bond formations in the PVP/PEG complex [171].

This trend was evident in the 1:1 formulations also with the exception of formulations 7 and 8 which were relatively similar in this case however, the 2% glycerol formulation resulted in a slightly lower T_g than the 2% PEG formulation.

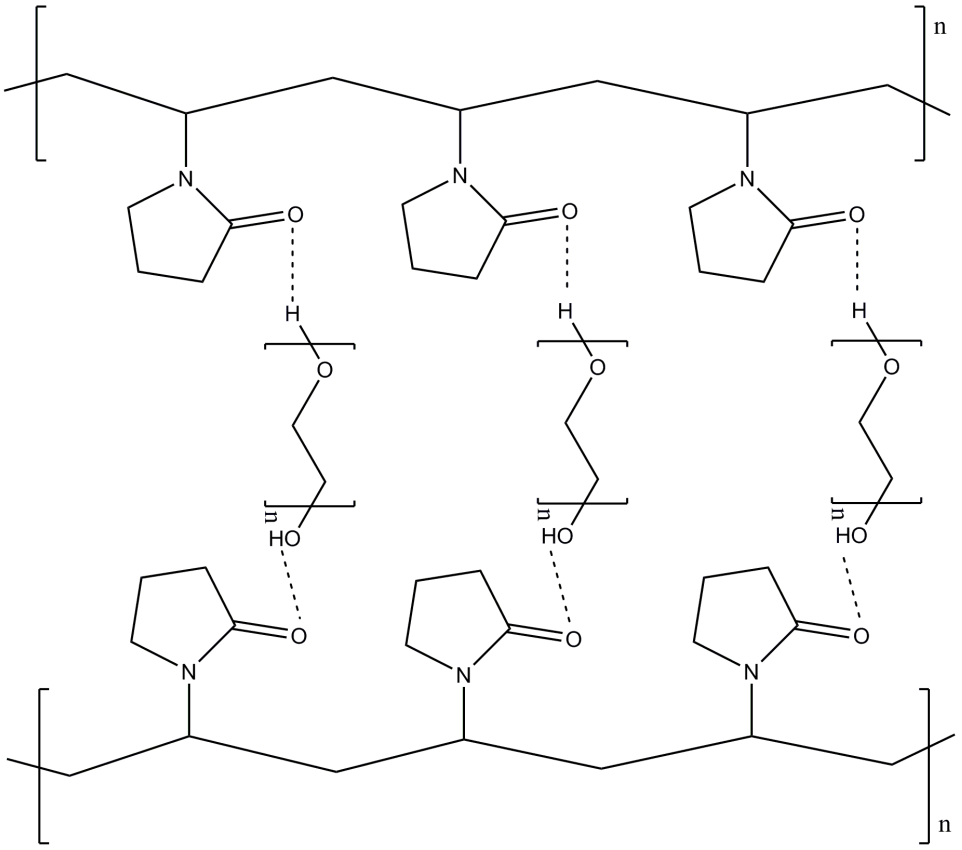

Figure 2.20: Proposed illustration of hydrogen bonding between PVP carbonyls and PEG hydroxyl groups**.**

A plot of the T_g for each formulation (Figure 2.21) illustrated the general trend of decreasing T_g as a result of decreasing PVP content in addition to the drop in T_g due to increased plasticiser content.

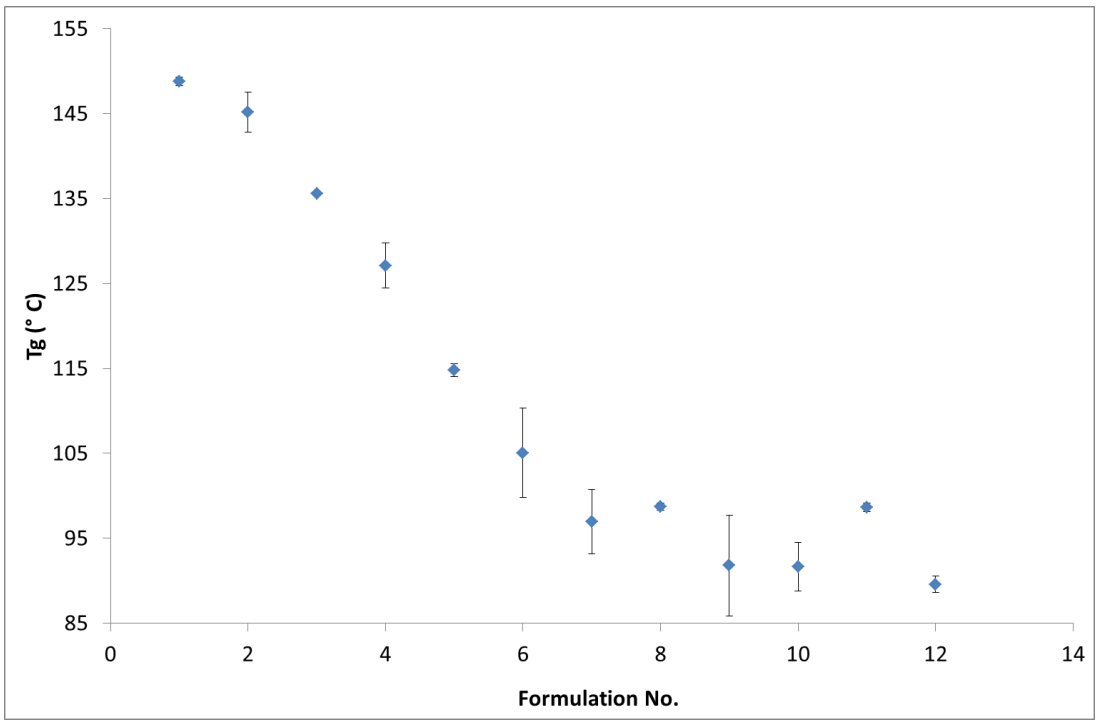

Figure 2.21: Plot of T_g values obtained for each of the 12 PVP/trehalose formulations (n=3) numbered as per Table 2.2. Analysis was carried out on 3 separate samples of each formulation.

The trehalose formulations (9-12) did not display a similar trend in lowering T_g temperatures as a result of the addition of plasticisers and each formulation remained relatively unchanged with the exception of formulation 11 which showed a higher T_g with 2% glycerol than formulation 9 with 1% glycerol, which was against the trend observed for the other formulations. Each sample was tested in triplicate and the low standard deviation obtained for this formulation discounted the possibility that this may have been an outlier. Given that each formulation was prepared in an aqueous environment, it was possible that residual water in the formulation may have caused plasticising effects that affected the T_g across the range, however, TGA analysis of the 4 formulations revealed that the water content of formulation 11 was approx. 10%, slightly higher than formulations 9 (9.4%) and 10 (9.6 %) but lower than formulation 12 (10.8%).

Dirama *et al.* (2005) [161] carried out a study on hydrogen bonding in trehalose and glycerol mixtures suggesting that strong hydrogen bonds are formed between glycerol and the hydroxyl groups of trehalose. They proposed that the addition of up to 5% glycerol to a trehalose mixture can increase the T_g by either reducing the motion of the trehalose rings or causing greater alignment between trehalose

molecules through glycerol bridges. They proposed that the initial addition of glycerol to trehalose resulted in the formation of these robust hydrogen bonds up to a concentration of 5% however, further addition of glycerol caused the liquid nature of the plasticiser to dominate and weaken the hydrogen bonding network. As such, this may have accounted for the increased T_g observed with the trehalose formulation containing 2% glycerol.

When the data obtained from the DSC was plotted with the disintegration data (Figure 2.22), a trend was evident which indicated that the drop in T_g across the formulations generally corresponded with the drop in disintegration time, in line with decreasing polymer/increasing sugar content of the formulation. The trend across the 1:1 formulations was particularly interesting, however, as the drop in T_g which corresponded with increasing plasticiser content did not correspond with a drop in disintegration time. In fact, the graph clearly illustrated that the disintegration time for all four of the 1:1 formulations remained relatively similar, regardless of plasticiser or amount used. The disintegration time for the trehalose formulations (9-12) was too rapid to gauge whether plasticiser content had any meaningful effect with each of the four trehalose formulations dissolving in under 1 min.

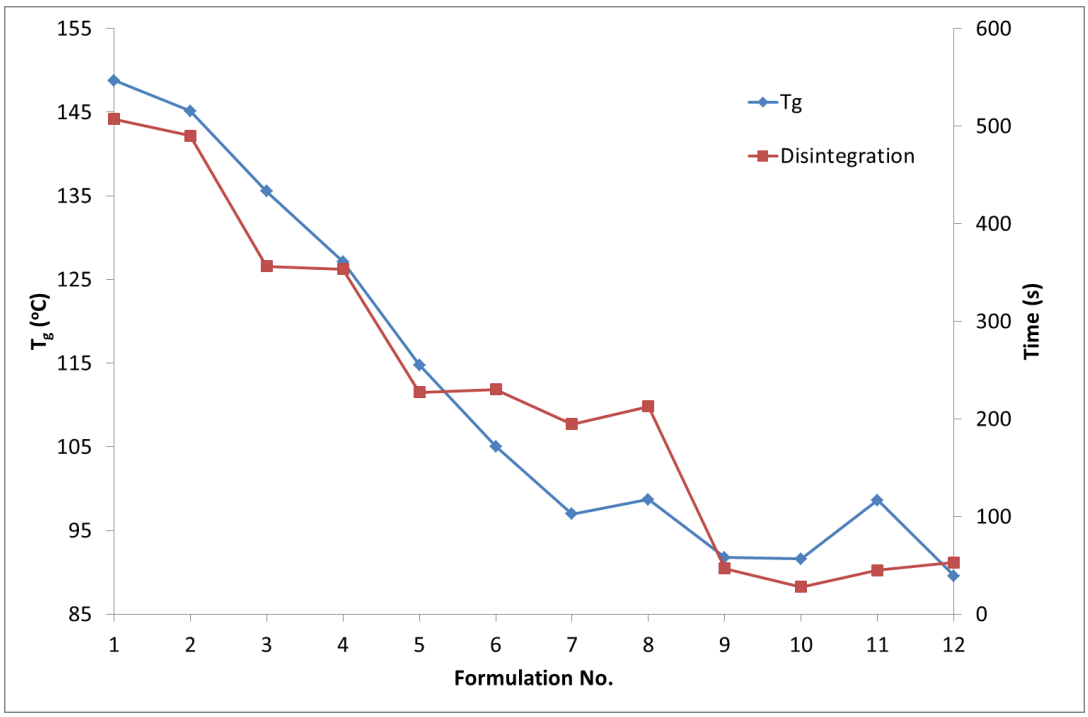

Figure 2.22: Plot of glass transition temperature and disintegration time for each PVP/trehalose formulation numbered as per Table 2.2.

2.4.2.4. DVS

DVS is routinely utilised in the pharmaceutical industry for the characterisation of materials such as active ingredients, excipients, formulations and packaging solutions. Such testing is driven by the requirement to gain an understanding of the surface chemistry, material stability and polymorph characterisation of pharmaceutical solids [187]. A water sorption isotherm illustrates the functional relationship between RH and the equilibrium water content of an amorphous solid. A sorption isotherm includes both absorption and desorption data and the difference measured between each is referred to as hysteresis.

The purpose of these experiments was to examine the level of water sorption across all 12 of the PVP/trehalose formulations at varying levels of RH. This information would help to determine two important characteristics of the formulations. The first being that the amount of moisture absorbed by the formulations would have an effect on the physical structure of the needles in that higher levels of moisture would cause plasticising effects on the needles, softening and deforming the shafts resulting in the arrays being unable to penetrate the skin. Secondly, the amount of moisture absorbed could indicate the rate of dissolution of the formulations, particularly once the arrays have been applied to the skin.

Each formulation was examined using the same programme which increased the RH of the test chamber in 10 ºC increments every 2 h from 0 % up to 75 % and back down to 0 %. As such, as each sample run took approx. 38 h, only one run per formulation was carried out. In order to validate the reproducibility of this technique, a triplicate run of one formulation was carried out (Table 2.5).

Table 2.5: DVS data obtained from triplicate runs of a 3 to 1 PVP/Trehalose formulation to verify the repeatability of the DVS technique.

Target RH (%)	dm (%) 1	dm (%) 2	dm (%) 3	Mean dm (%)	STD Dev (%)
0	0	0	0	0	0
5	0.162	0.232	0.187	0.194	0.035
10	0.453	0.596	0.530	0.526	0.072
20	1.116	1.351	1.179	1.215	0.121
30	2.175	2.529	2.215	2.306	0.194
40	4.114	4.569	4.050	4.245	0.283
50	7.991	8.624	7.822	8.146	0.423
60	13.967	14.692	14.173	14.277	0.374
70	21.062	21.742	20.946	21.250	0.430
75	27.029	27.713	26.736	27.160	0.501
70	25.484	25.943	25.472	25.633	0.268
60	20.467	20.686	20.697	20.617	0.130
50	16.567	16.655	16.876	16.699	0.159
40	13.941	13.877	14.255	14.024	0.202
30	12.133	12.018	12.464	12.205	0.232
20	10.675	10.548	11.026	10.750	0.248
10	9.310	9.164	9.667	9.381	0.259
5	8.176	8.036	8.537	8.250	0.259

Data from these 3 runs showed that the DVS technique was a highly repeatable method (Table 2.5) and the data obtained from the single runs of all 12 formulations could be relied upon without resorting to running triplicate experiments (Figure 2.23). The low standard deviation values for each data point highlighted the repeatability of the analysis.

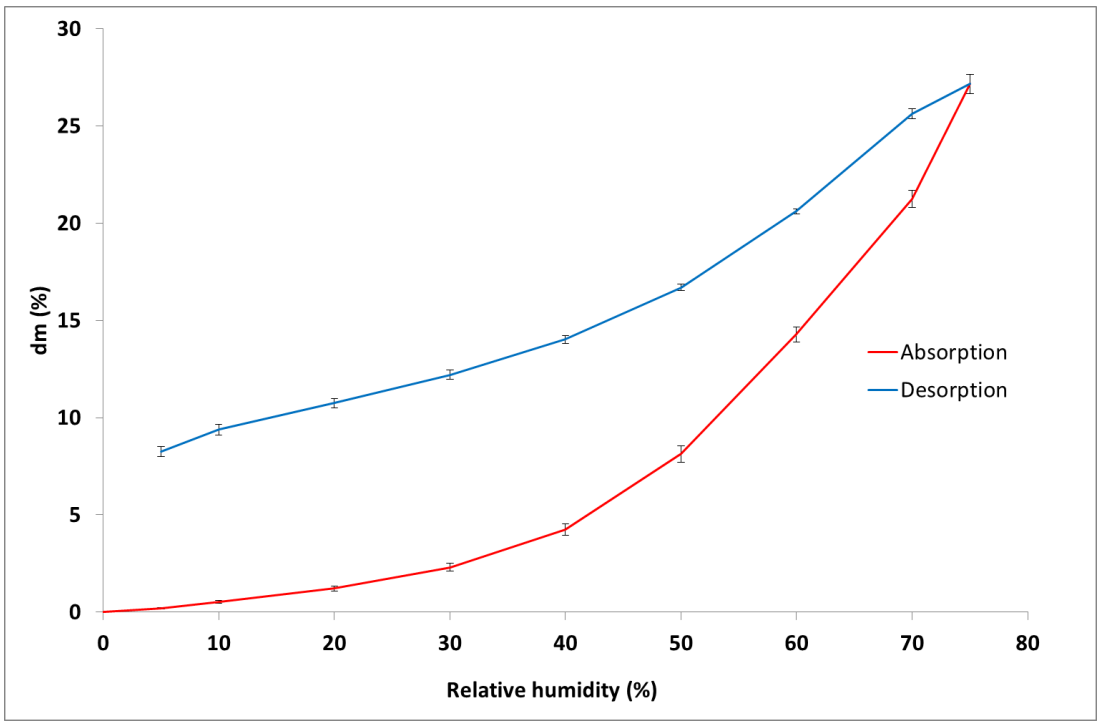

Figure 2.23: Plot of water sorption isotherm obtained from experiments on a 3 to 1 PVP/trehalose formulation (n=3). Change in mass % (dm) vs. relative humidity (%).

The results obtained across all formulations containing 1% PEG were examined together and the sorption isotherms for each were compared (Figure 2.24).

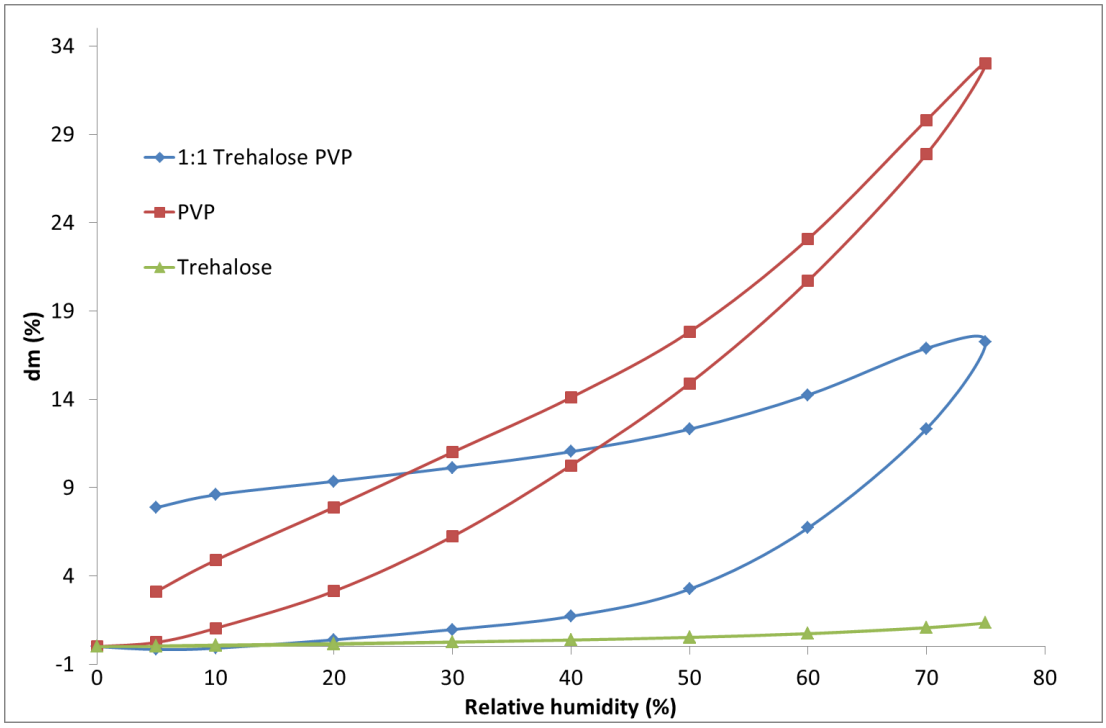

Figure 2.24: Comparison between water sorption isotherms for trehalose, PVP and 1:1 formulations with 1% PEG.

The water sorption isotherms when plotted together highlighted the high level of hysteresis for the 1:1 formulation and almost total absence of hysteresis for the trehalose formulation. The PVP formulation showed significant mass increase with a moderate level of hysteresis. This trend was evident across all the formulations tested. The reason for this high level of hysteresis may have been due to complexation between the carbonyl groups of the PVP and the hydroxyl groups of the trehalose (Figure 2.25) [188, 189], similar to the complexation with the plasticisers as previously discussed [171].

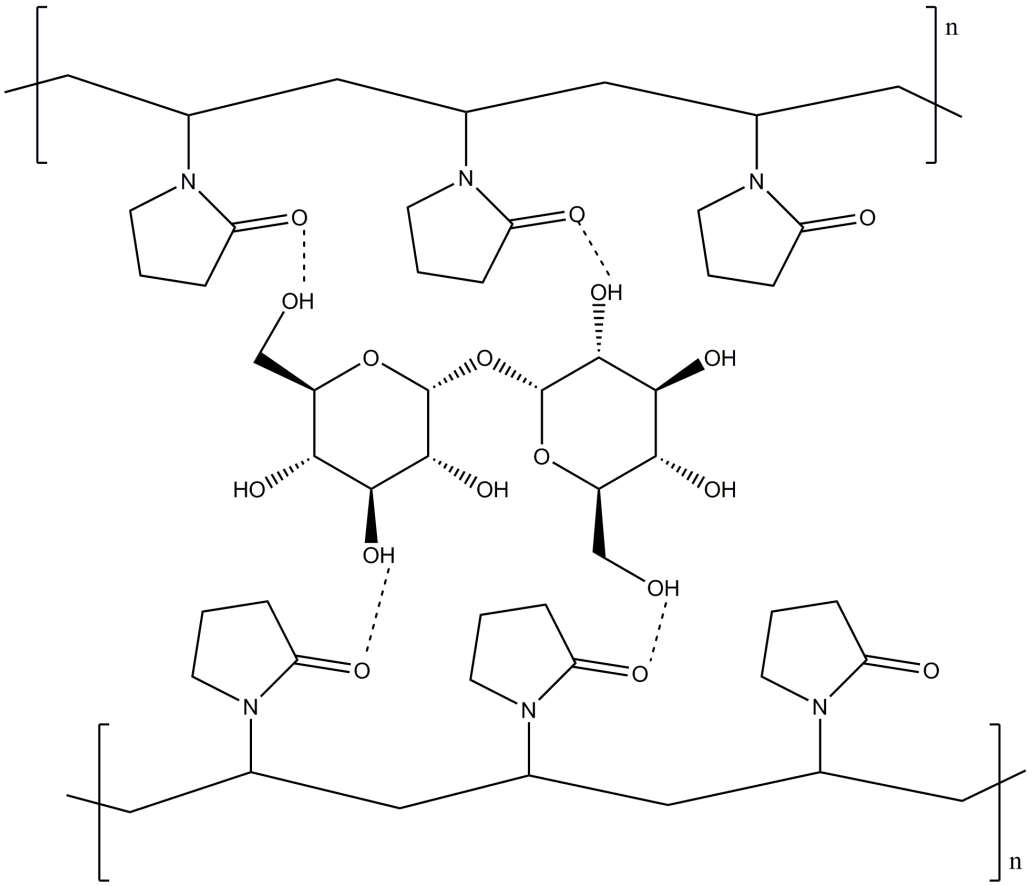

Figure 2.25: Proposed illustration of complexation between PVP carbonyls and trehalose hydroxyl groups.

Zhang *et al.* (2000) [186], after carrying out water vapour absorption studies on amorphous sucrose/PVP and trehalose/PVP mixtures, concluded that hydrogen bonding interactions between the sugars and the polymer were insufficient to affect the accessibility of water to the mixture. They surmised that water vapour absorption of co-lyophilised amorphous dispersions of these sugar/polymer mixes could be predicted by the weighted average of the isotherm of each individual component. They did not, however, report any data in relation to the desorption isotherms which,

as per this study, indicated that the trehalose/PVP interactions resulted in an increase in water retention for the 1:1 formulations.

Taking a RH value of 50% as typical of ambient conditions, the % mass increase across all 12 formulations at 50 % RH was examined (Figure 2.26). Formulations 1-4 showed greatest mass increase (and variability) as expected given the high PVP content and its high hygroscopicity [164].

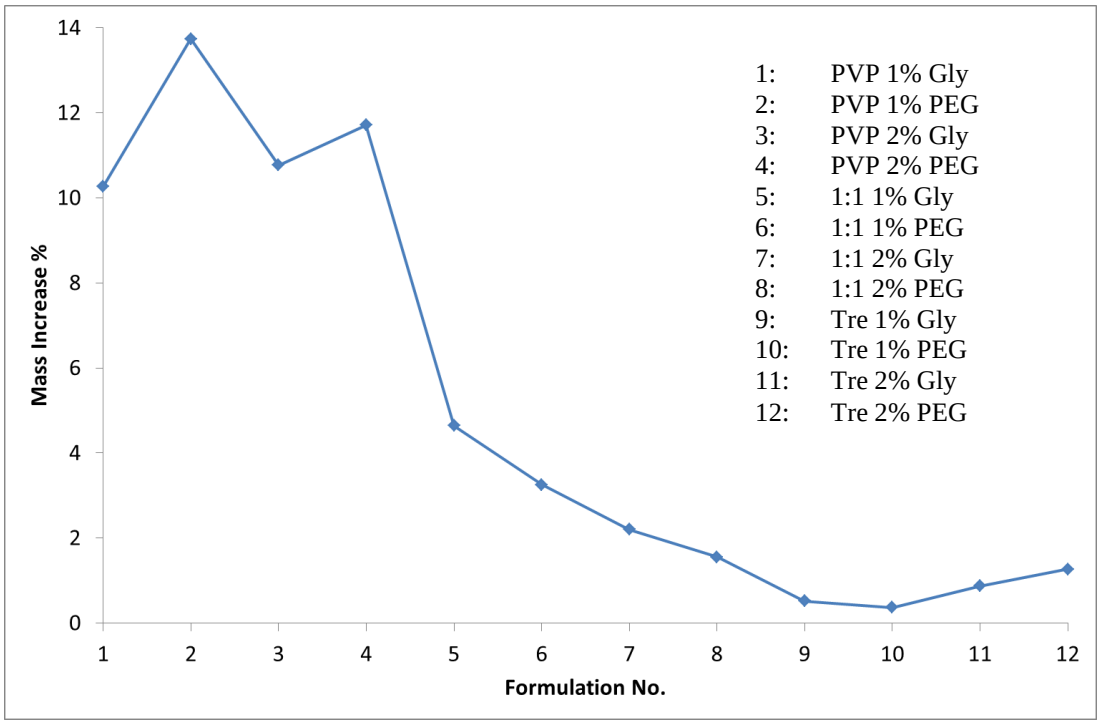

Figure 2.26: Plot of % mass increase for each formulation at 50% RH, exposure time 2 h.

The 1:1 formulations (5-8) showed much lower mass increase and were only marginally higher than the sugar only formulations (9-12). The results indicated that the addition of plasticiser to the PVP formulations affected the mass increase greatly with the addition of PEG resulting in higher % mass increase than the glycerol formulations. As discussed earlier, complexation between the PVP and PEG 400 can result in crosslinking which, given the longer chain length of the PEG compared with glycerol, would result in greater space between PVP chains possibly allowing for greater interaction with water molecules. In contrast, crosslinking between PVP and the shorter 3 carbon chain of glycerol would result in a tighter matrix which could

limit the amount of interaction with water molecules via steric hindrance, resulting in less of a mass increase as observed here [171, 172, 190].

DVS analysis of the 1:1 formulations showed a high degree of hysteresis and moderate mass increase for all 4 formulations (Figure 2.27). As discussed previously, complexation between the PVP and trehalose may have resulted in the formation of a matrix capable of retaining water molecules longer than PVP only formulations.

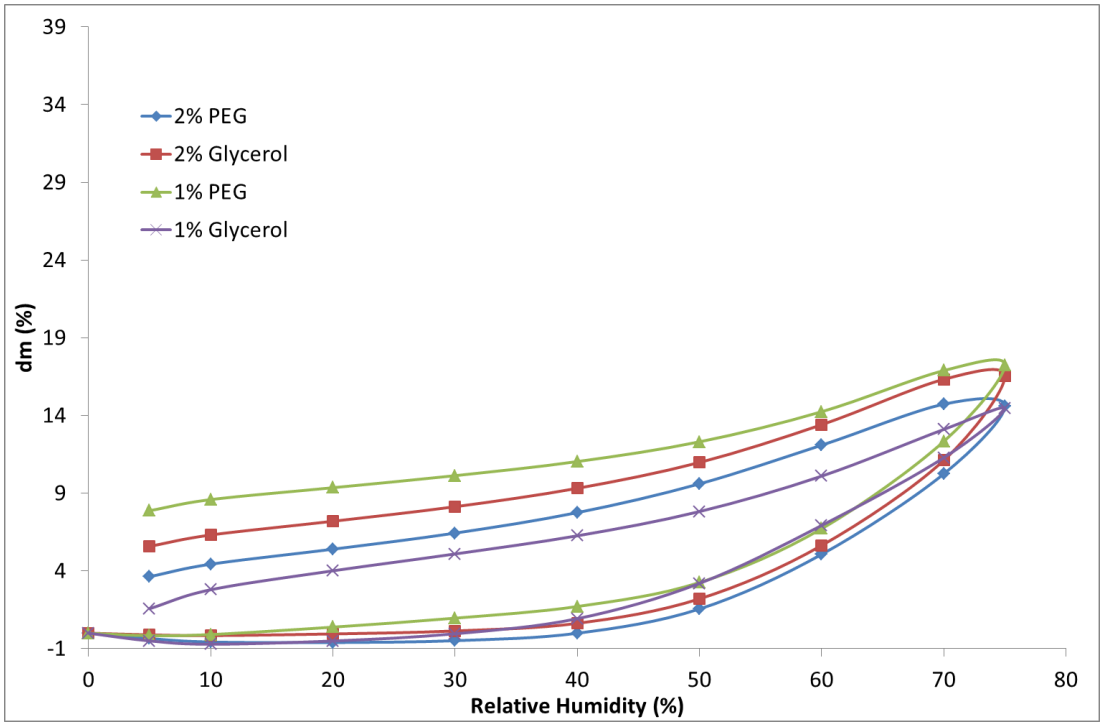

Figure 2.27: Plot detailing water sorption isotherms for the 1 to 1 formulations.

The data indicated that the plasticiser and amount used had only moderate effects on the hysteresis of the formulations. The formulation containing 1% PEG 400 had the greatest level of hysteresis with the 1% glycerol formulation showing the lowest hysteresis level.

Analysis of the water sorption isotherms for the PVP formulations showed moderate levels of hysteresis but large % mass increase across all 4 formulations (Figure 2.28). The PVP formulations absorbed more moisture than both the 1:1 and trehalose formulations, which was as expected for an amorphous hygroscopic polymer.

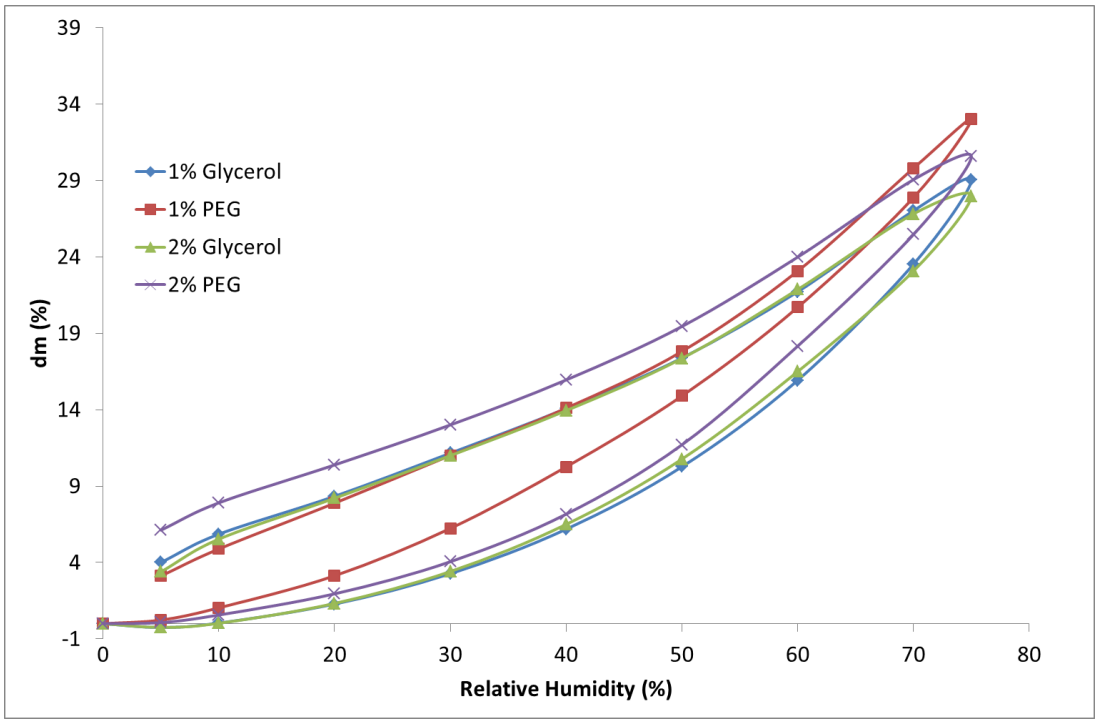

Figure 2.28: Plot detailing water sorption isotherms for the PVP formulations.

However, as discussed above, the hysteresis observed was slightly less than the 1:1 formulations possibly due to hydrogen bond interactions between the PVP and trehalose in the 1:1 formulations. In addition, the type or amount of plasticiser used in the PVP formulations had a minimal effect on the hysteresis or % mass increase of the formulations.

DVS analysis of the trehalose only formulations (Figure 2.29) showed low % mass increase and almost complete absence of hysteresis for all 4 formulations and, given that trehalose is not hygroscopic below 90% RH, this was as expected [157]. The sorption isotherm also indicated the presence of crystalline material in the sample.

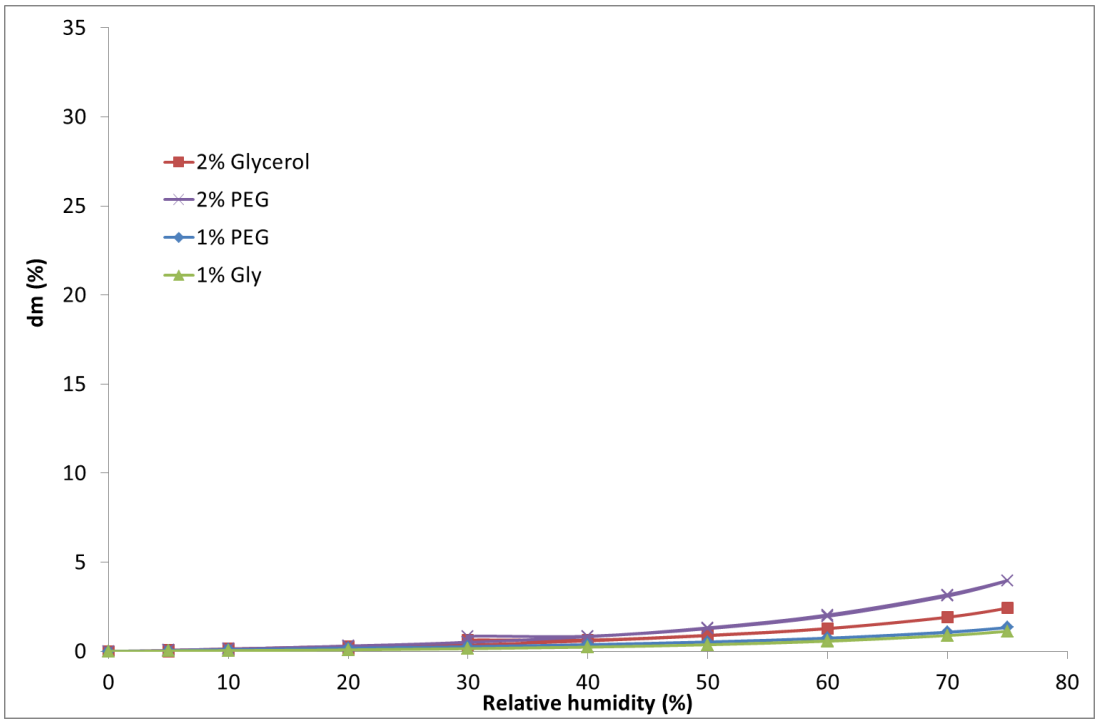

Figure 2.29: Plot detailing water sorption isotherms for the trehalose formulations, typical of crystalline material.

The results obtained from the DVS in relation to % mass increase were compared with the DSC results examining the T_g across all 12 formulations (Figure 2.30). As can be seen from Figure 2.30, the decreasing T_g values generally corresponded with a lower % mass increase.

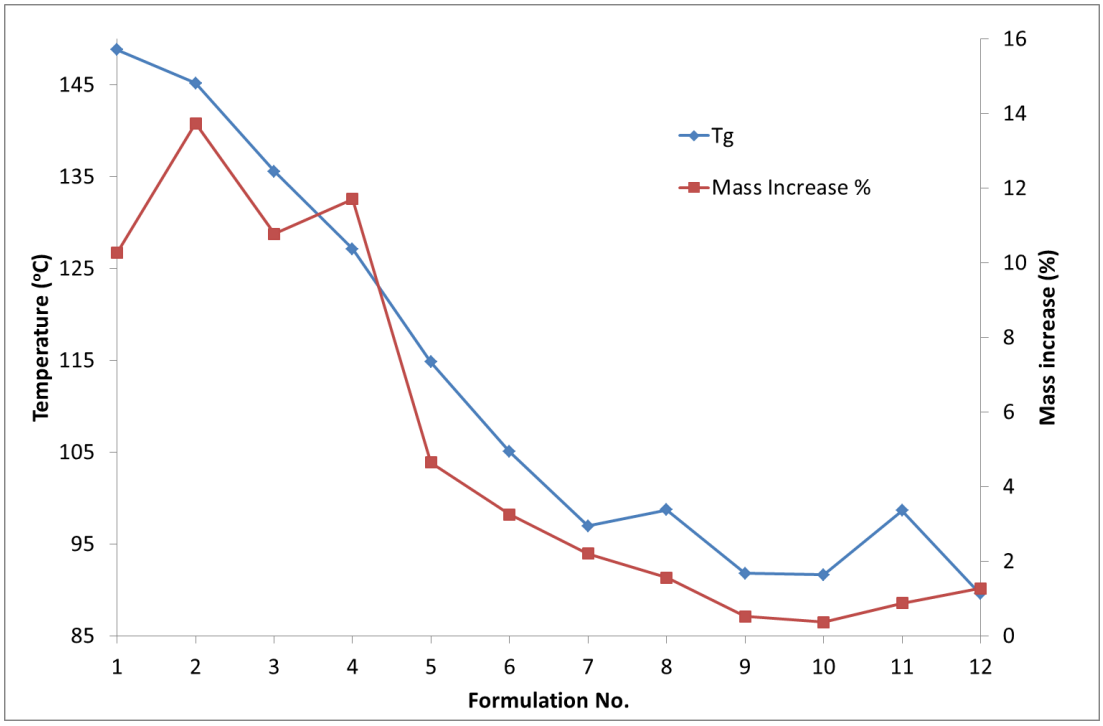

Figure 2.30: Plot of % mass increase at 50% RH with T_g for each formulation.

2.4.2.5. Statistical Analysis

The results of the 3 experiments (disintegration test, glass transition determination via DSC and water sorption analysis using DVS) were input on Minitab 16. The disintegration tests were run 6 times for each formulation and the glass transition experiments were carried out in triplicate. The explanatory variables examined were polymer/sugar formulation (PVP or 1:1), percentage plasticiser used (1% or 2%) and plasticiser type (glycerol or PEG). The desirable outcomes were high disintegration time value, high glass transition temperature and low mass increase as a result of sorption. As the results obtained for the trehalose only formulations produced very low disintegration times, this data was excluded from the analysis.

In relation to disintegration time, the output of the analysis on Minitab indicated that the average effect on disintegration time between the PVP formulations and the 1:1 formulations was -210.6 s. This could be regarded as a statistically significant difference given the p value was <0.001. Similarly, the difference between the amounts of plasticiser used was statistically significant with p <0.001 however the effect for this variable was lower, determined as 84.5 s. In the case of plasticiser type (PEG or glycerol), a p value of 0.977 was calculated indicating that this variable had no statistically significant difference on the outcome (Figure 2.31).

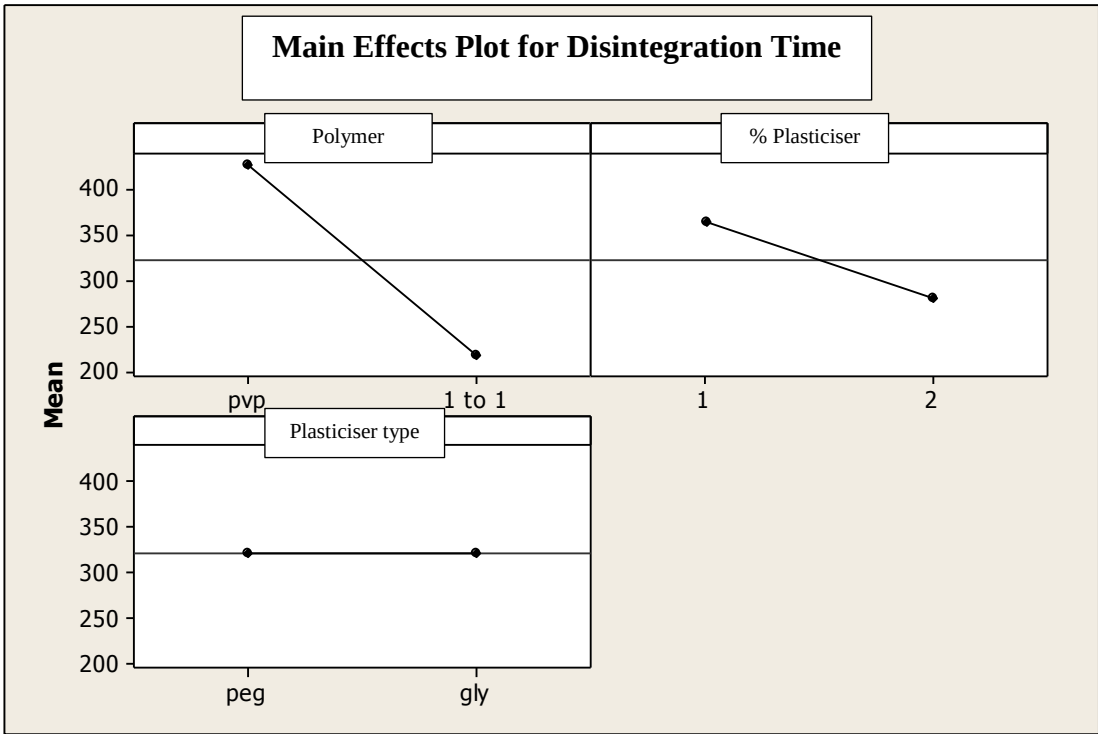

Figure 2.31: Graphs detailing the mean effects of each variable on the disintegration outcome for each formulation, illustrating the statistical significance for each variable.

Analysis of the glass transition data (Figure 2.32) showed that the effect of formulation type (either PVP or 1:1) was -36.19 ºC with p <0.001 indicating a statistically significant difference for this variable. Also, in relation to amount of plasticiser used, the effect was calculated as -12.95 ºC which again was significant with p <0.001. In this case however, the type of plasticiser used also had a significant effect on the outcome with a value of 5.93 ºC. Although relatively low, this was still a statistically significant variable with p <0.001.

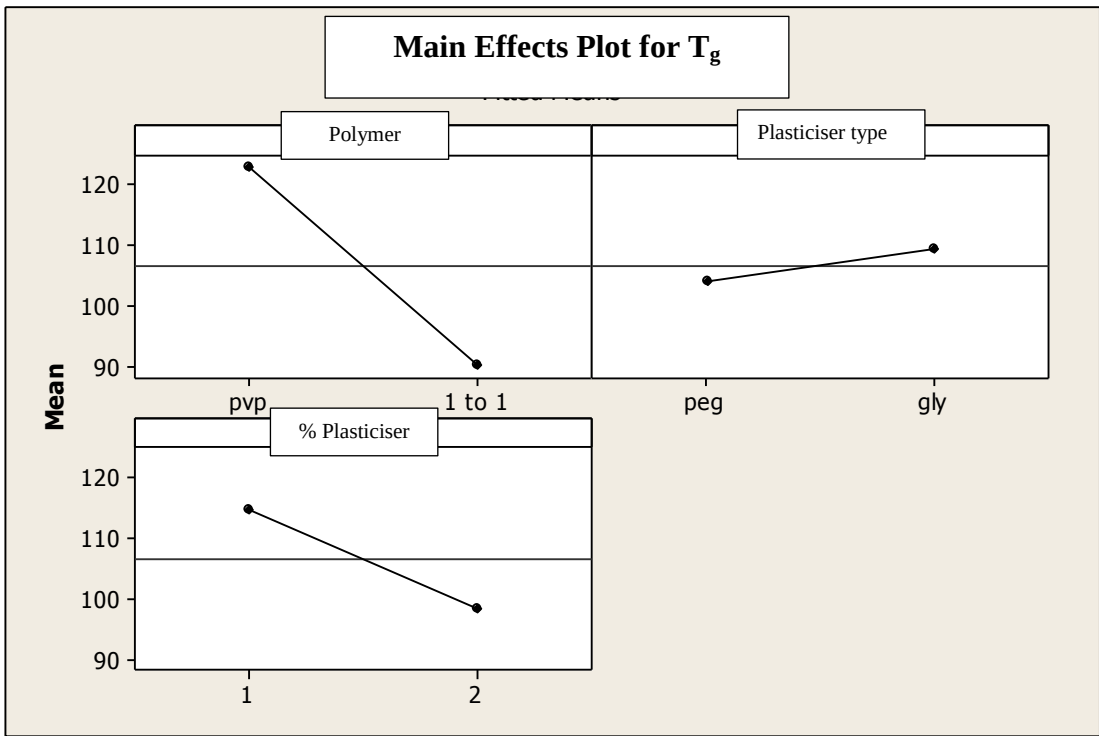

Figure 2.32: Minitab output graphs detailing the mean effects of each variable on the T_g outcome for each formulation illustrating the statistical significance for each variable.

The % mass increase due to water sorption was the final variable examined. As only one replicate for each formulation was run, no statistical table was obtained however the results of the single runs were plotted (Figure 2.33). The repeatability of the DVS technique was examined by running triplicate runs of one formulation which resulted in a low average standard deviation across all the data points. As such, the data used on Minitab for these experiments was input as if triplicate runs had been carried out. The graphs illustrated that 1:1 formulations were preferable in order to minimise mass increase due to water sorption. In relation to plasticisers, the data indicated that although plasticiser type and % amount did not cause much effect, utilising 2% glycerol was a preferable combination.

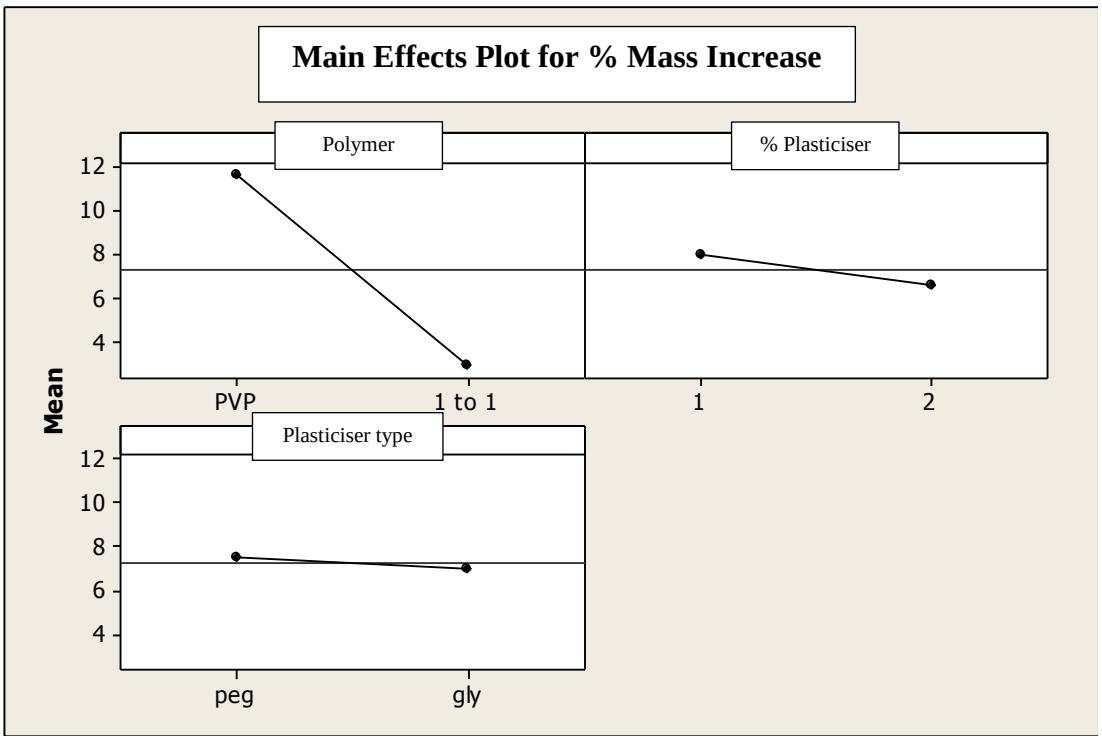

Figure 2.33: Minitab output graphs detailing the mean effects of each variable on the % mass increase (dm %) outcome for each formulation illustrating the statistical significance for each variable.

The statistical analysis of the data indicated that all 3 of the desired outcomes (high disintegration time, high T_g and low mass increase due to water sorption) could not be simultaneously obtained utilising the factors at the existing levels. As such, by modifying the factor levels, an optimum formulation could be determined. To achieve a high disintegration time and to maintain a high T_g, the polymer content needed be kept relatively high. Similarly, the addition of 2% w/w plasticiser caused a lowering of both the T_g and disintegration time compared with 1% but seemed to cause a lowering of % mass increase. Utilising glycerol was associated with higher T_g and lower mass increase compared with PEG but was associated with lower disintegration times. Plasticiser type had little effect on the mass increase of the formulations and no effect on the disintegration time but was statistically significant in relation to T_g with glycerol use resulting in higher T_g values.

2.5. Conclusions

The aim of this study was to determine which combination of PVP, trehalose and plasticiser would produce microneedle arrays most suited to the systemic transdermal delivery of therapeutic peptides. Attributes of such a microneedle system included mechanical strength, stability and suitable dissolution on application. The results obtained from the characterisation testing of the various PVP/trehalose formulations and subsequent statistical analysis has shown the effects each component has on the physical properties of each of the formulations. In addition to the morphological examination of the moulded microneedle arrays using SEM, the parameters of the various formulations investigated included disintegration time, T_g and water sorption behaviour. By examining each parameter, the effects of the polymer, sugar and plasticiser content was determined and statistical analysis also indicated the statistically significant factors for each property.

Zhang *et al.* (2000) [186] indicated that, after carrying out studies on amorphous trehalose/PVP mixtures, specifically water vapour absorption, water has greater plasticising effects on trehalose than PVP and that plasticising effects on such amorphous mixtures can be decreased through increasing the PVP content of the mixture. Similarly, the glass to rubber transition of amorphous sugars, which can lower the stabilising effect of the sugar, can be suppressed through the addition of a polymer [188]. As such, a formulation which contains a higher proportion of PVP would have a higher T_g indicating greater stability in addition to enhancing the stabilising effect of the trehalose. Coupled with the data obtained from this study which indicated that higher PVP content was associated with higher disintegration times and higher T_g values, this would suggest that the optimum formulation should consist of a higher ratio of PVP.

The main function of trehalose in the formulation was to act as the main stabilising agent for the peptide in the microneedle matrix but utilising this disaccharide alone proved impractical given the rapid disintegration of the trehalose only formulations. This indicated that trehalose needles would disintegrate too rapidly on application resulting in failure of the needles to penetrate fully into the skin, if at all.

In relation to plasticisers, studies into trehalose-glycerol mixtures have shown that the addition of glycerol to trehalose, while decreasing the T_g of the trehalose, actually increased the stabilising effects of the mixture through the suppression of local dynamics [159, 160]. In fact, Barreca *et al.* (2013) [159] suggested that glycerol concentrations of 2.5 % resulted in the most notable suppression of diffusive dynamics in trehalose out of the investigated values of 0%, 2.5%, 5% and 10% glycerol. In addition, utilising glycerol in the formulation over PEG resulted in higher T_g value and lower % mass increase both of which were desirable characteristics.

Taking into account the experimental and statistical data obtained from this study in addition to the data obtained from literature, it was determined that the optimum formulation to proceed with in relation to this dissolving microneedle system would consist of a 3:1 formulation of PVP/trehalose incorporating 2% w/w concentration of glycerol.

This study represents the first investigation into PVP/trehalose based microneedle formulations designed for systemic transdermal delivery of therapeutic peptides. In addition, the characterisation procedures utilised have never been combined to determine an optimum formulation before in this manner. By investigating the morphological and physical characteristics of the various formulations, an indication of optimum formulations was determined. In addition, by applying the data obtained in this study, it may be possible to alter the PVP/trehalose formulations, adjusting the factors (i.e. disintegration time, T_g, water sorption) to facilitate the delivery of therapeutic peptides of various sizes and properties – essentially tailoring the formulation to the peptide being delivered.

CHAPTER 3. CHARACTERISATION AND SKIN INSERTION STUDIES OF PVP/TREHALOSE MICRONEEDLES FOR THE TRANSDERMAL DELIVERY OF PEPTIDES

3.1. Introduction

In order to successfully develop dissolving microneedles for the delivery of therapeutic peptides, a number of essential factors need to be addressed during the design and formulation process. Solid, coated or hollow microneedles can be made of materials such as ceramics or metals and as such, these microneedle designs possess mechanical strength which is generally not compromised during the application process [18]. Dissolving microneedles however, must be fabricated from materials that will be sufficiently strong to penetrate the skin in addition to subsequently dissolving in the interstitial fluid. The design of such a formulation can be difficult, particularly where the target drug is biologically labile and potentially sensitive to high temperatures, organic solvents and extreme pH conditions. As such, the fabrication of these microneedle systems generally needs to be carried out in aqueous solutions, ambient temperatures and mild pH conditions which, in turn, make the process extremely challenging [4, 191].

There are certain key requirements which must be addressed when developing a dissolving microneedle system that will produce an effective means of delivering the encapsulated drug payload. Initially, the formulation process must not cause any loss of efficacy to the active ingredient and should also stabilise the drug for prolonged periods to allow for storage etc. On application, the microneedles must administer the drug as intended, either as a bolus delivery or sustained release, without any loss of efficacy [192]. Finally, the needles must be sufficiently strong to penetrate the SC on application [125, 129] and should not bend or break which would lead to insufficient dose delivery. Suffice it to say, determining the fracture strength of the microneedles is required to establish the physical limits of the system [193].

Park *et al.* (2005) [18] investigated the failure force of biodegradable PLA, PGA and PLGA microneedles fabricated using a vacuum moulding method. To determine whether the polymer needles were mechanically strong enough to pierce the skin without breaking, the failure of the needles under axial load (force applied parallel to vertical axis of the needles) was determined. This was achieved by the measurement of force and displacement as the needles were pressed against a solid metal surface at a rate of 1.1 mm/s. An abrupt drop in force was observed on needle failure and the maximum force applied immediately prior to the needle failure was regarded as the

needle failure force. The results showed that all the polymer needles tested had failure force measurements above that required to penetrate the skin. Measured failure forces ranged from 0.06 to 0.32 N/needle with the majority of designs tested having failure forces significantly greater than expected insertion forces (approx.0.06 N/needle).

Similarly, Donnelly *et al.* (2010) [194] examined the mechanical strength of a polymeric dissolving microneedles formulation consisting of 20 % w/w aqueous solution of Gantrez® AN-139. This formulation produced microneedle arrays which were rigid and mechanically robust, losing only approx. 20 % of needle height on the application of compression force of 0.36 N per needle. In addition, the microneedles were capable of penetrating skin *in vitro* at a relatively low insertion force of 0.03 N/needle. However, optical coherence tomography (Figure 3.1) indicated that the needles only penetrated approx. 460 µm into the skin, leaving a gap of approx. 136 µm between the base of the array and the SC surface. Controlling the depth of penetration of the microneedle array is essential considering that drug may only be delivered from the part of the microneedle embedded in the skin [195]. Failure to fully insert may result in reduced drug delivery efficiency and drug wastage [94].

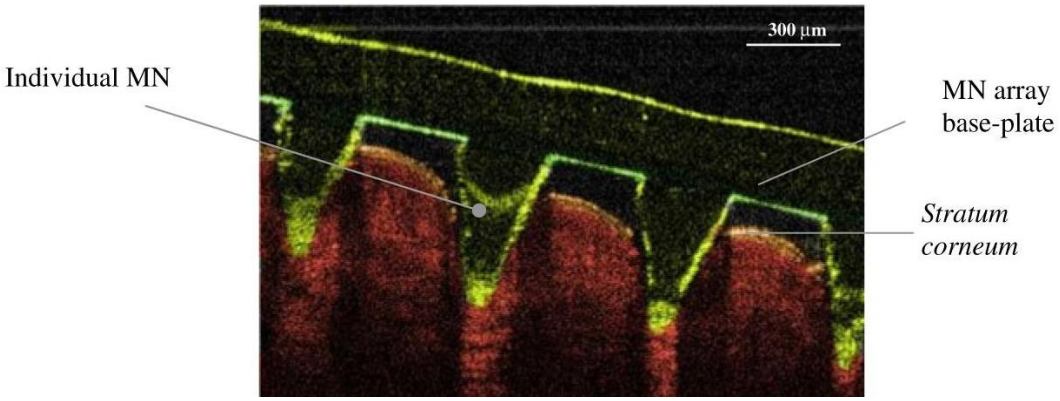

Figure 3.1: Optical coherence tomography cross sectional image illustrating the penetration depth of 600 µm length cone-shaped polymeric microneedles into human skin *in vivo* [194].

For dissolving polymeric microneedles to be effective, the need to use strong and robust fabrication materials is evident. However, the geometry of the needles must also facilitate successful skin penetration during the application process. These geometric factors include needle shape, needle tip radius, needle height, base

diameter and microneedle density (the number of needles per unit area) [19, 84]. By carrying out tests on the fracture strength of fibroin microneedles using axial loading, You *et al.* (2011) [196] concluded that the needle strength could be improved with an increase in needle base diameter and a decrease in tip radius and shaft length [196]. Studies have been carried out utilising microneedles with tip radii ranging from 2.5 µm up to 80 µm which also suggest the decreasing tip size correlated to a decrease in required insertion force [128, 195, 197]. In fact, Roxhed *et al.* developed ultra-sharp hollow silicon microneedles with a tip radius below 100 nm (Figure 3.2) and they determined that the insertion force per needle to successfully penetrate human skin was only 10 mN per needle [198].

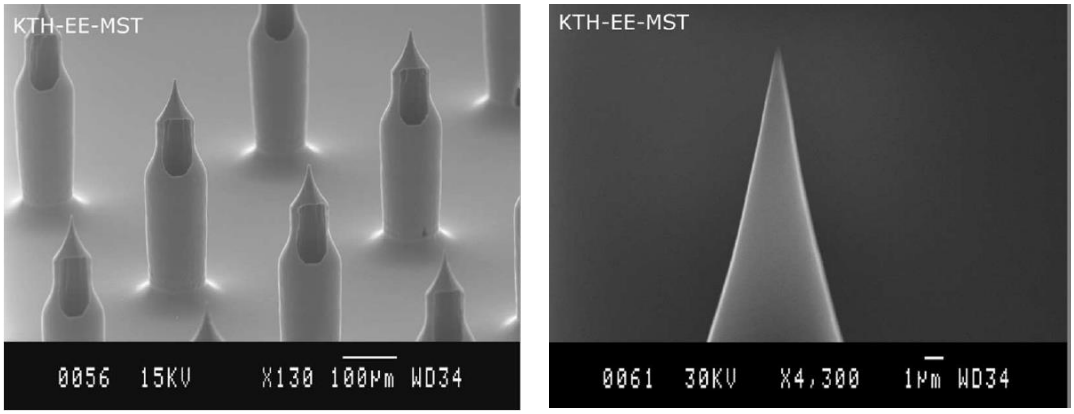

Figure 3.2: SEM images of ultra-sharp silicon hollow microneedles showing (A) microneedle array, needle shaft length of 400 µm and (B) microneedle apex with tip radius < 100 nm [198].

In addition to the successful penetration of the needles, penetration depth was an important factor which needed to be considered. Applying a microneedle array to the skin initially causes indentation on the skin surface prior to penetration and insertion depth can, as a result, range from 10 to 80 % of the actual needle length. Factors which impact on penetration depth include application velocity, application force, and needle length [195]. The needle density of the array must also be considered as another major factor affecting the insertion force required to penetrate the skin. It was determined that insertion forces required ranged from 0.1 to 3 N, similar to previous studies [197] and this force was determined as sufficiently low to allow manual application by hand.

Yan *et al.* (2010) [85] carried out a study on the effect that microneedle length and array density had on skin penetration utilising solid silicone microneedle arrays with needle lengths ranging from 100 µm to 1100 µm and arrays with densities which ranged from 400 to 11,900 needles/ cm^2. The study utilised the various microneedles to pre-treat human epidermal membrane (HEM) prior to the application of the antiviral drug, acyclovir, to the skin surface. Results indicated that a significant increase in flux was observed when arrays with needle lengths > 600 µm were used compared with smaller length needles. A flux of 3.7 µg/cm^2/h was achieved with 650 µm length needles compared with 0.5 µg/cm^2/h which was achieved with 100 µm length needles. The highest level of flux was seen when needles measuring 1100 µm were utilised however, needles of this length would be likely to cause pain to the patient [199]. They observed that an increase in needle density on the array correlated with a decrease in drug delivery which was attributed to the "bed of nails" effect. As a result of the increased number of needles on the array, a smaller force was applied to each individual needle and, as the overall force was distributed across the entire array, the needles therefore failed to penetrate the skin. Overall, the findings of this study indicated that utilising needles longer than the sufficient length of 600 µm did not significantly increase drug flux and that it was more effective to utilise lower needle density arrays [85].

Encapsulating the drug material in the microneedle formulation has many advantages over other microneedle drug delivery systems such as increased volume of drug material and the potential to control the release rate by adjusting the formulation [122]. One possible disadvantage of the dissolving microneedle system is the fact that drug material in the needle may diffuse from the needles into the backing layer of the array which could result in failure to administer the full intended dose. Conversely, Lee *et al.* (2008) [200] carried out studies on CMC dissolving microneedles with model drug loaded in both the needles and the backing layer. They demonstrated a sustained release of drug from the microneedle system over a number of days, indicating that utilising the backing layer as a drug reservoir was a potentially viable delivery method. It was hypothesised that the release rate of drug diffusion from the backing layer into the skin could be tailored through altering the array material [200], just as controlled delivery can be predetermined by the needle formulation [122].

Effectively delivering biologically active pharmaceuticals using a dissolving microneedle system places severe limitations on the materials and conditions that are available for use in the formulation process. The materials used must be biocompatible as the needles will dissolve and be absorbed into the biological milieu of the skin. Additionally, the formulation process must not cause any degradation of the active ingredient. Given that therapeutic peptides and proteins can be easily damaged in extreme conditions, mild pH and ambient temperatures must be employed. In addition, harsh organic solvents must be avoided and as such, the formulations must be prepared in aqueous solutions. The fragility of biological molecules cannot be underestimated however and slight deviations in temperature or pH can potentially cause irreversible damage to peptides and proteins which in turn can affect their activity [98, 169]. Determining the activity of the drug once encapsulated in the microneedle formulation is critical in developing the system, to ensure that the efficacy of the drug payload is preserved.

As such, polymyxin B was selected as a suitable model peptide drug to incorporate into the microneedle arrays in order to monitor any effect on activity due to the formulation process. Polymyxin B is a cationic amphiphatic lipopeptide antibiotic produced by a strain of *Bacillus polymyxa* and which possesses bactericidal activity against Gram-negative bacteria [201, 202]. Originally developed in the 1940's, polymyxins became less popular as antibiotics mainly due to nephrotoxicity and adverse neurological effects associated with their use and they were gradually replaced by less toxic antibiotics. The recent emergence of multidrug-resistant (MDR) Gram-negative bacteria however, has resulted in a resurrection of the parenteral use of polymyxins as they are often one of the few treatments to which these MDR organisms are susceptible. Less toxic derivatives were developed however, although their toxicity was reduced, so too was their antibacterial effects [203, 204].

The structure of polymyxin B (Figure 3.3) consists of a cyclic heptapeptide which is linked by a tripeptide chain to a fatty acyl tail [205]. There are three main components in polymyxin B namely B_1, B_2 and B_3 which differ in the fatty acyl residue in the tripeptide side chain which is attached to the cyclic heptapeptide. As a result, quantitation of the drug can be challenging [206]. The advantage of utilising

polymyxin from a microneedle formulation point of view is that one can readily monitor the activity of the peptide during formulation and following delivery through the skin using well diffusion studies.

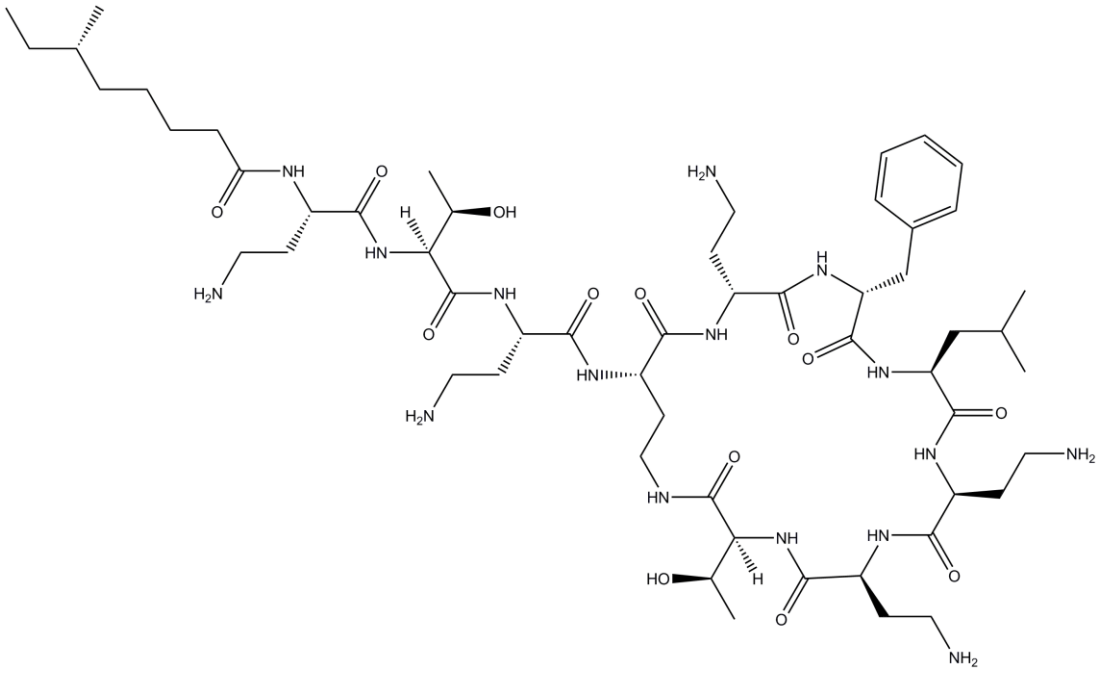

Figure 3.3: Chemical structures of polymyxin B_1 [207].

3.1.1. Objectives

The focus of this chapter was to evaluate the morphology, T_g and moisture sorption properties of the optimum microneedle formulation of 3:1 PVP/trehalose, 2% glycerol utilising the thermal techniques and SEM imaging applied to the formulations investigated in the previous chapter. In addition, further characterisation techniques were employed to examine the needle fracture force, needle tip sharpness, skin penetration, diffusion of material from the needles to the backing layer of the array and the activity of a model drug within the formulation.

3.2. Materials and Methods

3.2.1. Materials

Polymyxin B Sulphate supplied by Sigma Aldrich
Poly(vinylpyrrolidone) (PVP) average weight 40,000 supplied by Sigma Aldrich
Trehalose D(+)-trehalose dihydrate obtained from Fisher Scientific
Glycerol – ACS grade obtained from Reagecon
Brain heart infusion obtained from Oxoid Microbilogy Products
Salmonella typhimurium (LT2) from Waterford Institute of Technology (WIT) culture collection
Sodium Fluorescein supplied by Sigma Aldrich
Sodium Bromide obtained from Fisons Scientific
Methelyne Blue Hydrate 96+ % obtained from Acros Organics
Epoxy Resin + Curing agent
Porcine ear skin (untreated) – supplied by Dawn Pork and Bacon
Phosphate buffered saline (PBS) solution obtained from Fischer Scientific

3.2.2. Methods

3.2.2.1. Well and Disc Diffusion

Well and disc diffusion methods were used based on the Kirby-Bauer Disc Diffusion method [208]. *Salmonella typhimurium* was chosen as the target microorganism given that it is a Gram negative bacterium which should be highly susceptible to polymyxin B. Six agar plates were used: Four were tested using the polymyxin B incorporated into the 3:1 PVP/trehalose formulation, one was the formulation without the drug and one was the drug alone. Standard antibiotic sensitivity testing using the Kirby-Bauer method indicated that polymyxin should have a concentration of 300 units per disc with zones of inhibition (ZOIs) ranging from $\leq$ 8 mm for resistant, 9-11 mm for intermediate and $\geq$ 12 mm indicating that the microorganism is susceptible to the antibiotic [208].

3.2.2.2. Well Diffusion

A formulation of 3:1 PVP/trehalose (3.6 g) with glycerol (2% w/w) was dissolved in 8 mL of deionised water. 8 mg of polymyxin B sulphate was then added and the solution was sonicated for 15 min until all components were completed dissolved. A control formulation was also prepared as before but without the addition of the polymyxin.

Once the formulations were prepared, 7.4 g of brain heart infusion (BHI) agar was added to 200 mL of water and the agar solution was melted in a waterbath at 45 ºC. The BHI agar was then seeded with 500 µL of the Salmonella culture and gently inverted to mix, taking care to avoid the formation of froth or bubbles. Once mixed, the seeded medium was carefully poured into petri-dishes and left to solidify for 30 min. Wells were placed in the solidified agar plates using flamed glass capillary tubes and 50 µL of the liquid formulation was added to each well. The plates were then incubated at 37 ºC overnight and then examined the following day for ZOI's.

3.2.2.3. Disc Diffusion

For this experiment, a formulation of 3:1 PVP/trehalose (3.6 g) with glycerol (2% w/w) was dissolved in 8 mL of deionised water as per the well diffusion experiment. 8 mg of polymyxin B sulphate was then added and the solution was sonicated for 15 min until all components were completed dissolved. Using a micropipette, 20 x 50 µL aliquots were pipetted onto a flat PDMS surface and allowed to dry in an incubator at 22^{o} C overnight. In addition, microneedle arrays containing the polymyxin were also prepared using the remaining formulation. As per the well diffusion experiment, a control formulation was prepared as before only without the addition of the polymyxin. The BHI medium was prepared as per the well diffusion experiment and once the seeded agar plates had solidified, three of the formulation discs were placed an equal distance apart on the surface of the agar plates. The drug infused microneedles were also spread over the surface of the agar plates. The plates were then incubated at 37 ºC overnight and then examined the following day for ZOI's.

3.2.2.4. Thermogravimetric Analysis (TGA)

The instrument used for this experiment was a TA Instruments Q50 TGA. The experiments were carried as per Section 2.2.2.8 with no deviation in the settings.

3.2.2.5. Differential Scanning Calorimetry (DSC)

The instrument used for this experiment was a TA Instruments QS2000 DSC. The experiments were carried out as per Section 2.2.2.9 with no deviation in the settings.

3.2.2.6. Dynamic Vapour Sorption (DVS)

The instrument used for this experiment was a Surface Measurements Systems DVS Intrinsic. The programme settings used were as per Section 2.2.2.10 with no deviation in the settings.

3.2.2.7. Scanning Electron Microscopy (SEM)

The instrument used for this experiment was a Hitachi S-2460N SEM with all settings as per Section 2.2.2.7.

3.2.2.8. Fluorescence Microscopy

Fluorescence microscopy was used to determine whether the model drug in the needles diffused into the base of the arrays after the formulation and casting process. The instrument used for this analysis was an Olympus BX51 Fluorescence Microscope and the samples were viewed using a fluorescein isothiocyanate (FTIC) filter cube.

To prepare the fluorescein needles, approx. 20 µL of a sodium fluorescein solution was added to a batch of microneedle formulation prepared as before using the 3:1 PVP/trehalose mix and incorporating 2% glycerol. Once the components dissolved,

the solution was then pipetted onto the PDMS microneedle moulds and placed in the vacuum oven as per Section 2.3.2.6. After the moulds had been filled, excess formulation was removed from the mould surface using a glass microscope slide and the moulds were left in an incubator for 4 h to allow the microneedles to set. PVP/trehalose formulation without the added fluorescein was then pipetted over the moulds and left to dry for 24 h. The microneedle arrays were then removed from the moulds and immediately stored in a desiccator prior to examination under the fluorescence microscope.

3.2.2.9. Needle Sharpness

This experiment was carried out to determine the effect that 60 % RH would have on the tip sharpness of the microneedles. The instruments used for this experiment were a Zeiss Micro-imaging Axiocam Keyence VHX Digital Microscope with a Zeiss Micro-imaging Axiocam and a Hitachi S-3400N VP Scanning Electron microscope.

A controlled humidity container was set up by placing a saturated solution (1.16 g/mL) of sodium bromide [209] in a desiccator which kept the RH between 58 and 61 % at room temperature. A Microlog Pro II data logger was placed in the humidity chamber to monitor temperature and humidity to ensure both remained within the parameters required for the duration of the experiment. A batch of the 3:1 PVP/trehalose microneedles with 2% w/w glycerol was prepared and once cast, half the batch was placed in the humidity chamber for 5 h and the other half was kept in a desiccator. Both batches were then examined using SEM and digital microscopy. The tip radius and tip angle were measured using the digital microscope software.

3.2.2.10. Needle Fracture Force

For the needle fracture force tests, a similar method to that of Donnelly *et al.* (2011) [194] was employed and the instrument used for this experiment was a TA XT Plus Texture Analyser. The instrument test mode was set to compression, the pre-test speed was set at 1 mm/sec, test speed at 0.5 mm/sec and post-test speed at 0.5 mm/sec. The target mode was set to distance and the distance set to 1 mm with a

hold time of 30 s. The trigger type was set to auto (force) with a trigger force of 0.049 N. The microneedle arrays were attached to a SEM metal stub with a carbon adhesive tab using parafilm and double-sided adhesive tape.

3.2.2.11. Skin Penetration

The method used for the skin penetration tests was again similar to that employed by Donnelly *et al.* (2011) [194], utilising the TA XT Plus Texture Analyser. The instrument test mode was set to compression, the pre-test speed was set at 1 mm/sec, test speed at 0.5 mm/sec and post-test speed at 0.5 mm/sec. The target mode was set to force and the force setting to 20 N with a hold time of 30 s. The trigger type was set to auto (force) with a trigger force of 0.049 N.

Porcine ears were supplied freshly excised and untreated by Dawn Pork and Bacon. These were immediately stored in a freezer at -20 ºC until required. The ears were removed from the freezer and stored at 4 ºC for 24 h before use. Immediately prior to the experiment, the ears were placed in a large beaker of water to remove any debris from the skin surface. Following this, the ears were dried using paper towels and the skin was carefully dissected into squares approx. 2 cm^2 in size while also carefully removing all subcutaneous non-dermal fat and tissue material from the sample.

To prepare the methylene blue needles, a batch of microneedle formulation was prepared as before using the 3:1 PVP/trehalose mix with 2% w/w glycerol. Once the components had been dissolved, 4 mL of the solution was pipetted into a separate beaker and 0.5 % w/w of methylene blue dye was added and thoroughly mixed into the formulation. This solution was then pipetted onto the PDMS microneedle moulds and placed in the vacuum oven as before. After the moulds had been filled, excess formulation was removed from the mould surface using a glass microscope slide and the moulds were left in an incubator for 4 h to allow the microneedles to set. The remaining formulation without the added dye was then pipetted over the moulds and left to dry for 24 h. After this, the microneedle arrays were removed from the moulds and immediately stored in a desiccator prior to use.

The method used for the skin penetration test consisted of attaching one of the methylene blue containing microneedle arrays to a metal cylinder probe attachment as per Donnelly *et al.* [194] with a porcine skin sample placed on the instruments' metal base. The microneedle array was then pressed onto the skin sample as per the instrument settings for 30 s and removed. The skin sample was then wiped with paper towel to remove excess dye and formulation and an image of the skin was obtained. In addition to the above, non-dye containing microneedles were utilised for the same procedure with the methylene blue dye applied to the surface of the skin for 10 min after microneedle insertion. As before, excess formulation was wiped from the skin surface with paper towel prior to staining with methylene blue.

3.2.2.12. Micro-sectioning

The instruments used for this experiment were a Buehler EcoMet 250 Pro Grinder Polisher, a Buehler Isomet 5000 Linear Precision Saw with blade speed set to 2500 rpm and a feed rate of 1.2 mm/min and a Zeiss Stemi 2000-C Stereomicroscope.

After skin penetration studies had been carried out using the methylene blue microneedles, the skin samples were prepared for micro-sectioning. The skin sample was affixed to a plastic stand and placed upright in a 3 cm diameter plastic cylinder mould. Prior to this, the walls of the mould were coated in a thin layer of silicon grease to allow the sample to be removed easily from the mould once set. An encapsulating material consisting of a mixture of epoxy resin and curing agent were combined in a ratio of 4:1 resin to curing agent and this was carefully poured into the cylinder mould to avoid formation of bubbles, until the skin sample was completely covered. The resin was left to cure overnight after which the resin-encapsulated sample was removed from the mould.

The encapsulated skin sample was then affixed to the precision saw and a section of the sample was cut through the sample parallel to the microneedles penetration trajectory in the skin. The sample was then polished until a row of microneedles could be seen clearly on the resin encapsulated sample surface. The sectioned sample was then viewed under the digital microscope and the penetration depth of the needles was measured using the system software.

3.2.2.13. Optical Coherence Tomography (OCT)

OCT analysis was carried out under the supervision of Prof. Ryan Donnelly at the School of Pharmacy at Queens University Belfast. The analysis was carried out using a VivoSight® EX1301 OCT Microscope (Michelson Diagnostics Ltd., Kent, UK). The swept-source Fourier domain OCT system has a laser centre wavelength of 1305.0 ± 15.0 nm, allowing for real-time high-resolution imaging of the upper skin layers with 7.5 μm lateral and 10.0 μm vertical resolution. Scanning of the skin samples was carried out at a frame rate of up to 15 B-scans (2D cross-sectional scans) per second (scan width = 2.0 mm). Analysis of the 2D skin images was carried out using the imaging software ImageJ® (National Institute of Health, USA). The scale of the image files obtained was 1.0 pixel = 4.2 μm, which facilitated accurate measurements of the depth of microneedle penetration, the width of pore created, and the distance between the microneedle base plate and the SC.

Neonatal porcine skin was utilised for the OCT analysis and was obtained from stillborn piglets. The skin was immediately (<24.0 h after birth) excised and trimmed to a thickness of 500 μm using an electric dermatome (Integra Life Sciences TM, Padgett Instruments, Plainsboro, NJ, USA). Skin was then stored in aluminium foil at − 20.0 °C until further use. Prior to use, the skin was re-hydrated in PBS solution for 5 min and then dried with paper towels after which any hair was removed from the skin surface with a razor. The prepared skin sample was then incubated at 37 ºC before use. Analysis was carried out on a single sample of skin with an approx. area of 36 cm^2.

3.3. Results and Discussion

3.3.1.1. SEM

SEM images were taken of the 3:1 PVP/trehalose needles to examine the morphological properties of the arrays (Figure 3.4). Casting microneedle arrays from the 3:1 formulation consistently resulted in the formation of full arrays of solid and perfectly formed microneedles which were fully representative of the inverse moulds. The dimensions of the arrays used were 324 needles with 750 µm length shafts with a base width of 200 µm and inter-needle spacing of 600 µm. These arrays were chosen due to the high aspect ratio and sufficient length of the needles [85].

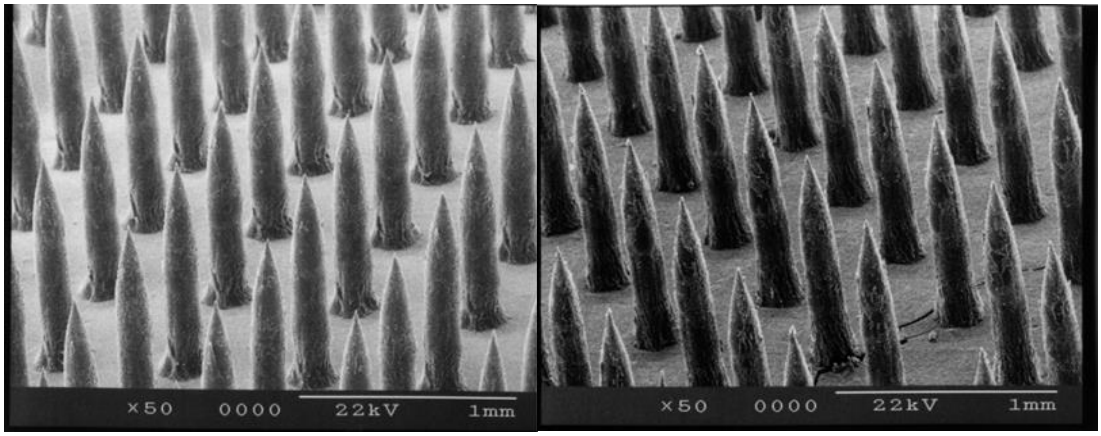

Figure 3.4: SEM images of 3:1 PVP/trehalose microneedles with needle length of 750 µm, base width of 200 µm and 600 µm inter-needle spacing.

3.3.1.2. DSC and TGA

Thermal analysis was carried out on the 3:1 formulation as per Section 2.4.2.3. The TGA analysis indicated the degradation profile of the mixture in accordance with expected values. The thermogram (Figure 3.5) showed bound and unbound water loss from the mixture amounting to over 5.6 % of the formulation. The PVP and trehalose content was as expected at approx. 3:1. The T_g of the formulation was measured as 112.4 ± 1.4 ºC (n=3). Using the Fox equation (Equation 2.2) [171], the predicted T_g, was determined as 113 ºC which indicated that the experimental value obtained was reasonable for the formulation used.

The relatively high T_g confirmed the physical stability of the formulation even though this value was significantly lower than the obtained value for the equivalent PVP only formulation of 135.6 ºC (Table 2.4). As 25 % of the formulation consisted of trehalose in addition to 2 % glycerol, both of which have T_g values much lower than that of PVP (and as a result would act as plasticiers), a drop in T_g for this formulation was as expected [186]. Plasticisers with two or three hydroxyl groups, such as PEG or glycerol, cause negative deviations in the T_g of PVP blends far greater than predicted by the Fox equation. This suggests that the drop in T_g is proportional to the fractions of hydroxyl groups as opposed to the weight fractions of the plasticisers [171]. As such, the fraction of hydroxyl groups in a blend containing both trehalose and glycerol as plasticisers would be quite high and a significant drop in T_g would be expected in such a composition. This drop in T_g was not predicted to impact on the physical stability of the microneedles however, as it remained relatively high in comparision to standard storage conditions.

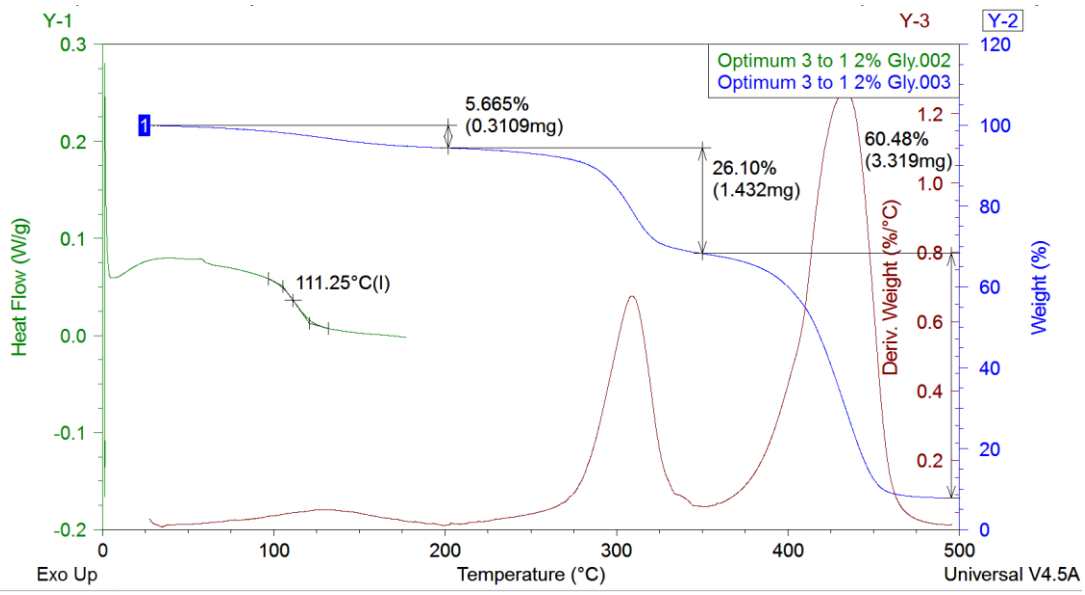

Figure 3.5: Overlaid TGA and DSC thermograms for the 3:1 PVP/trehalose formulation.

3.3.1.3. DVS

DVS analysis of the 3:1 formulation (Figure 3.6) indicated that the mixture absorbed moisture at a rate similar to the PVP only formulation. At 75 % RH, the mass increase reached approx. 25 % compared with 28 % for PVP only with the hysteresis level similar to that observed for the 1:1 formulations (Section 2.4.2.4). As such, this

indicated that, on insertion, the needles should then begin to absorb moisture from the interstitial fluid of the skin and this in turn would facilitate a relatively rapid dissolution rate of the needles. Such a rapid dissolution rate would be advantageous for systemic bolus delivery in addition to reducing the length of time a patient would need to apply the microneedles to obtain the full intended dose. This study also represented a novel approach to utilising DVS for characterising dissolving microneedles by examining the moisture sorption profile of the microneedle formulation.

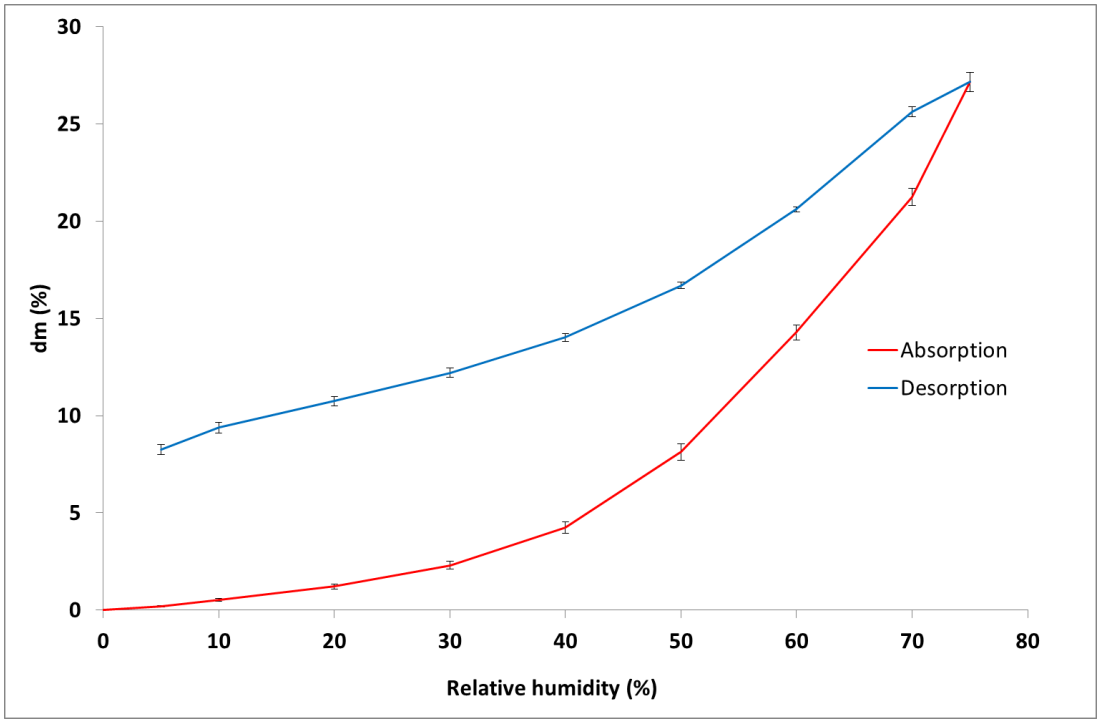

Figure 3.6: Plot of water sorption isotherm obtained from experiments on a 3 to 1 PVP/trehalose formulation (n=3).

3.3.1.4. Diffusion into Base Layer

Encapsulating drug material in a dissolving microneedle array implies that a specific dose is housed within each array. To be viable as a drug delivery device, the microneedle system must be capable of delivering the intended dose with each application. Where the microneedle system contains the drug payload in the needles only, any diffusion of drug material from the needles into the base of the arrays may result in a decrease in drug delivery and would render the dissolving microneedle system inefficient. In addition, this could lead to problems during scale-up, manufacturing and clinical use [191]. Although research has been carried out

whereby drug payload has been housed within the base to facilitate sustained release [200], this may not be suitable for a system designed for bolus delivery.

In order to examine whether any drug diffusion into the base layer of the arrays was taking place within the microneedle array, sodium fluorescein (Figure 3.7) was added to the microneedles and the base of the arrays consisted only of the polymer/sugar formulation.

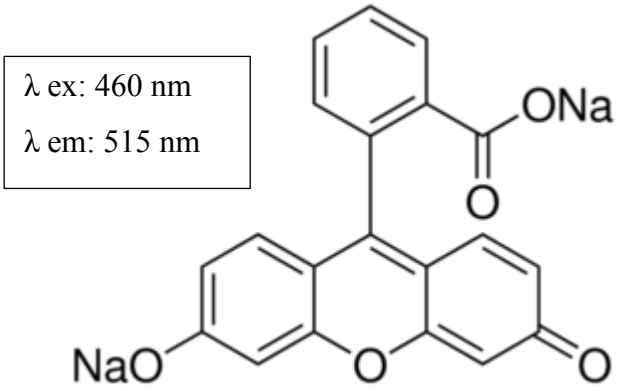

Figure 3.7: Chemical structure of sodium fluorescein [210].

After casting, the arrays were examined under a fluorescence microscope to determine whether diffusion of any fluorescein into the base of the arrays had occurred. Images obtained from the fluorescence microscope (Figure 3.8) showed that the fluorescein remained in the needles and no diffusion into the base of the arrays had occurred. This indicated that the dissolving microneedle system would retain the drug payload in the needles and that the drug payload would not diffuse into the base layer. Given however, the physiochemical differences between sodium fluorescein and peptides, this study provided a guideline only as to the diffusion characteristics of an encapsulated molecule in the microneedle formulation. Further studies would be required to examine the diffusion of therapeutic peptides once encapsulated in the microneedle matrix.

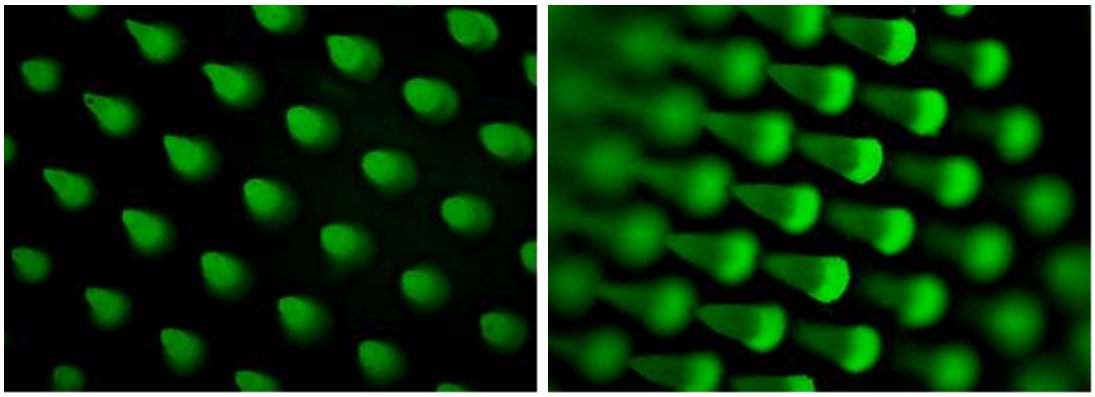

Figure 3.8: Fluorescence microscopy images of PVP/trehalose microneedles with added sodium fluorescein in the needles.

3.3.1.5. Needle Strength

In order to penetrate the SC, the microneedles needed to be sufficiently strong. Dissolvable microneedles can only be effective as a drug delivery system if the needles can effectively penetrate the skin and insert to a sufficient depth in order to deliver the full dose of the drug payload. As such, testing must be carried out to determine the maximum direct force required to cause the mechanical failure of the needle shafts [95]. The typical amount of force used to manually press a microneedle patch into the skin is between 5 and 10 N which equates to approx. the same force used to press an elevator button [101, 211]. Using microneedles 720 µm in length, Davis *et al.* (2004) [197] determined that insertion forces between 0.1 – 3 N for needles with tip radii ranging from 30 to 80 µm were sufficient to penetrate the skin of human subjects, measured by monitoring changes in the electrical resistance of the skin during the application process.

The microneedles used in this experiment were 750 µm in length and 200 µm in base diameter. The spacing between needles was 600 µm and each array consisted of 324 needles (18 x 18). The results obtained from these experiments displayed a high degree of variability between each array. This was attributed to slight variations in the thickness and surface smoothness of the base of the arrays. As such, the positioning of the arrays may not have been uniform for each array and this may have contributed to the variation in results obtained. Despite the variations observed, the lowest fracture force was recorded as 1900 g/ 18.6 N which was significantly above the calculated upper insertion force of ≈ 10 N. The highest fracture force

measured was 4500 g/ 44.1 N (n=3) (Figure 3.9). These results were comparable to previous studies on PVP microneedles which reported fracture forces of approx. 0.1 N/needle [169] (or 29 N for an array of 324 needles). The slight drop in force which initially occurred on the plot was taken as the fracture force and after this, the subsequent force drops were attributed to breaking of the array base. As such, the PVP/trehalose microneedles would be expected to successfully penetrate the skin without bucking or breaking given that the lowest fracture force measured was almost double the calculated upper insertion force required [101].

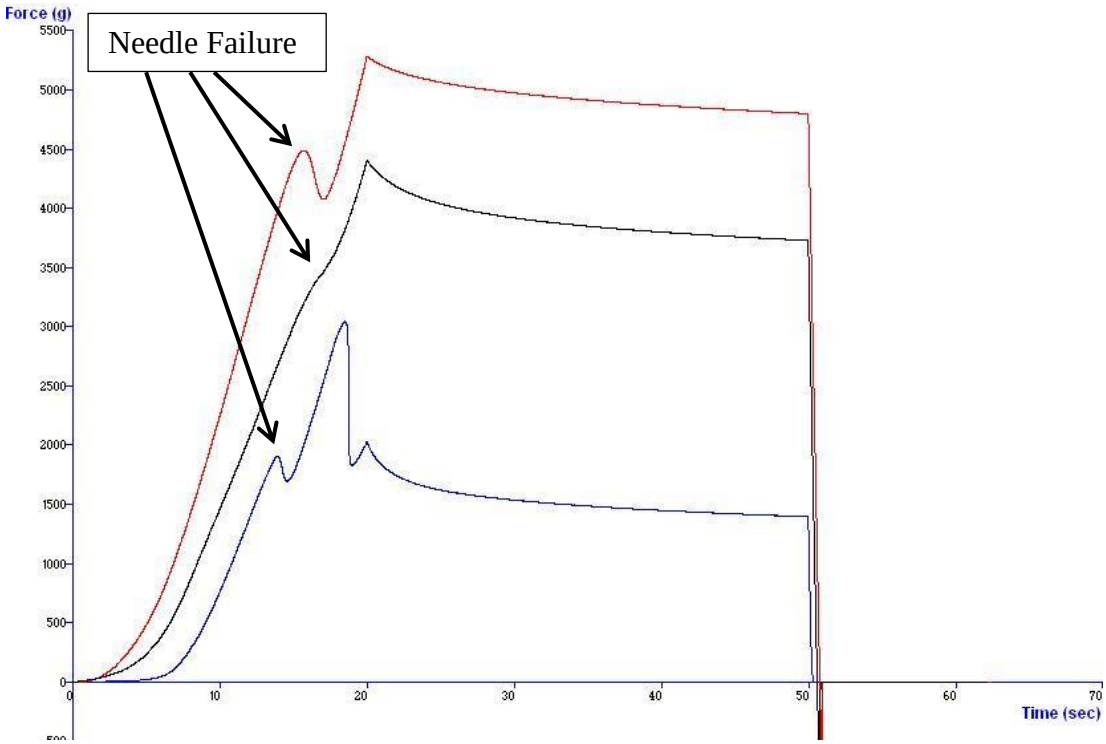

Figure 3.9: Plot of applied force vs time illustrating the fracture force of PVP/trehalose microneedle arrays (n=3).

3.3.1.6. Needle Sharpness

In order to effectively penetrate the skin, the microneedles must remain sufficiently sharp [128]. While protection of the needles during prolonged storage can be achieved in a sealed environment (e.g. packaging), once exposed to ambient conditions, the integrity of the arrays must remain for a sufficient period of time to allow for effective application. As such, this experiment utilised a controlled

humidity chamber (Figure 3.10) to test the sharpness of the PVP/trehalose needles after a prolonged period of exposure to a relatively high level of humidity, above what would normally be experienced under ambient conditions. The effect this exposure had on the sharpness of the needles was then examined to determine if the tip sharpness had degraded beyond an acceptable level, taken as > 80 µm [197].

Figure 3.10: Image of sealed humidity chamber set-up with saturated sodium bromide solution and data logger.

Romgens *et al.* (2014) [195] carried out studies on the penetration performance of a number of individual solid glass microneedles 3 mm long with tip diameters of 5, 15, 24 and 37 µm. It was determined that the smallest tip diameter needles penetrated the skin more smoothly and with a linear increase in depth compared with microneedle displacement. Conversely, needles with larger tip diameters had smaller penetration depths initially due to skin indentation followed by a rapid increase in penetration depth. From this, it was determined that smaller tip diameter needles were required to allow for controlled skin penetration [195] with radius curvature of <10 µm required for ease of penetration with manual insertion [128]. These findings were particularly relevant to the use of the PVP/trehalose dissolvable microneedles given that dissolution of the needles would begin immediately on application to the skin

surface. As such, sharp tips would be required to facilitate full skin penetration, allowing for maximum delivery of the drug payload.

The mean tip radius of the microneedles that were kept in the desiccator for the duration of the experiment was determined by measuring the tip radius of a total of ten microneedles from two arrays. The mean tip radius of the arrays that were kept in the humidity chamber at 60 % RH for the duration of the experiment was calculated in the same manner (Table 3.1).

Table 3.1: Tip radius measurements for both microneedle batches obtained from digital microscopy images. Microneedle arrays were stored in a desiccator/humidity chamber for 5 h.

Desiccator	**Humidity Chamber (60% RH)**
Tip Radius (µm)	**Tip Radius (µm)**
6.2	16.7
7.3	26.4
12.2	26.7
10	21.9
9.1	15.7
10.1	15.0
5.6	13.7
9.3	27.3
11.3	38.6
7.6	43.4
Mean: 8.9	**Mean: 24.5**
Std. Dev: 2.04	**Std. Dev: 9.4**

SEM was used to examine both sets of arrays – those kept in a desiccator and those kept in the humidity chamber. Figure 3.11 illustrated that the loss of sharpness attained by the arrays exposed to the elevated RH was not immediately obvious. The arrays that had been subjected to the elevated RH showed no initial signs of deformation or structural deviation from the unaffected arrays after a period of 5 h.

In fact, both arrays looked remarkably similar with no obvious loss of needle sharpness visible from the SEM images alone.

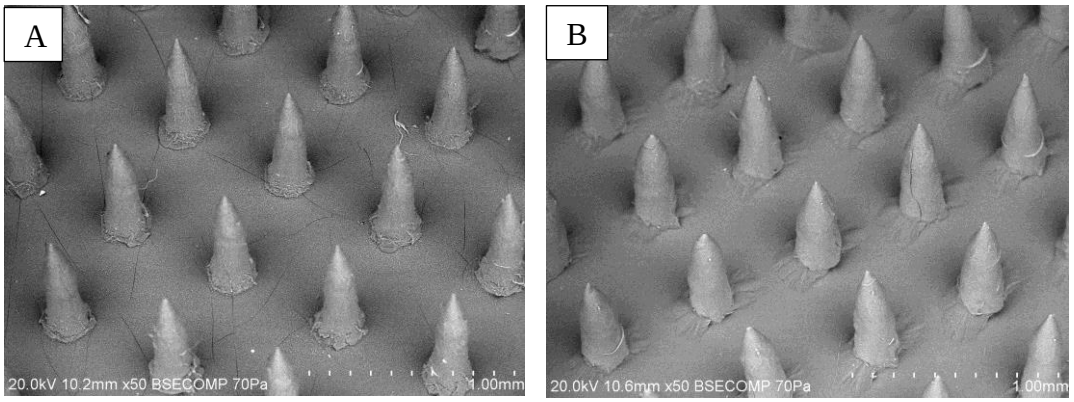

Figure 3.11: SEM Images of 3:1 formulation microneedles where (A) were stored in a desiccator and (B) subjected to 60% RH in a humidity chamber for 5 h.

The digital microscopy images of the needle tips (Figures 3.12, 3.13) did, however, illustrate the level of tip deformation as a result of the elevated RH conditions. The results of the experiment indicated that exposure of the microneedles to an elevated RH (≈60 %) environment for 5 h caused the mean tip radius to degrade from 8.9 ± 1.9 µm to 24.5 ± 9.5 µm (n=10).

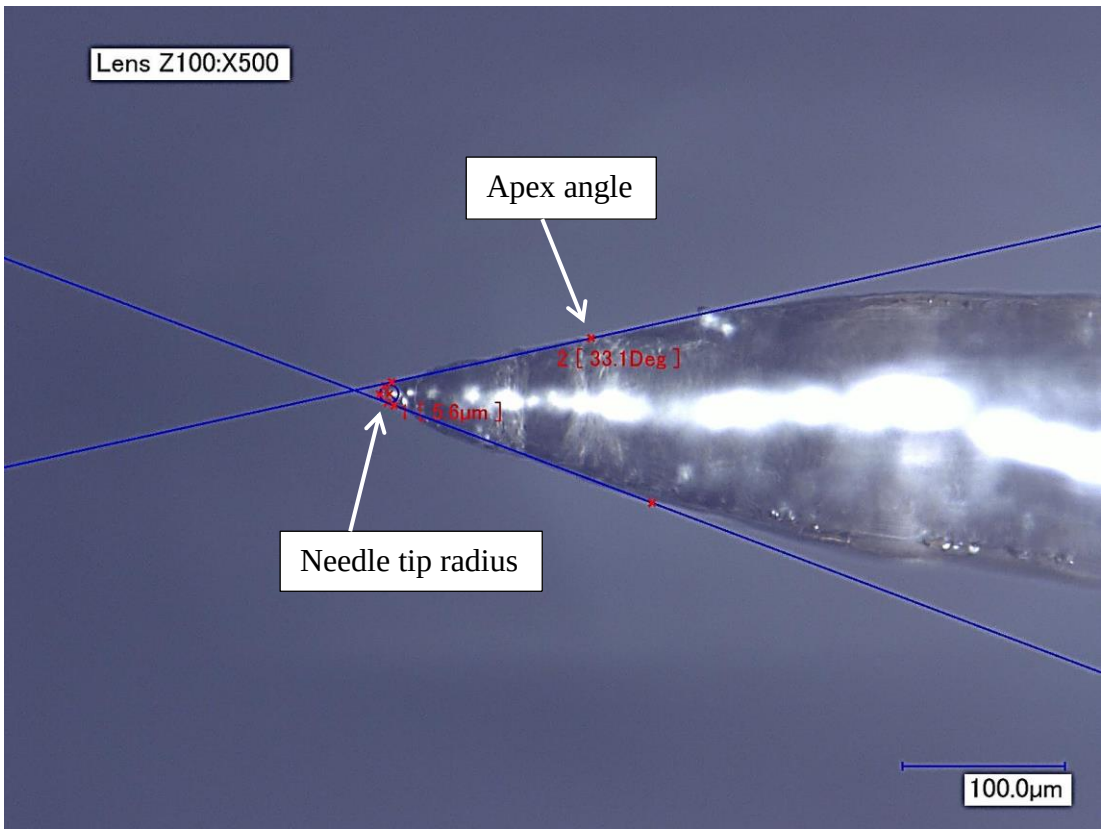

Figure 3.12: Digital microscopy image of PVP/trehalose microneedle tip illustrating apex angle and needle tip radius. This sample was taken from the batch kept in a desiccator for the duration of the experiment.

Previous studies have shown that microneedles with tip radii of up to 80 µm can effectively penetrate the skin, depending on application force [197]. In this study, exposure of the PVP/trehalose microneedles to elevated RH conditions resulted in a mean loss of tip sharpness, determined by tip radius, of only 15.6 µm. As such, the average tip radius of the microneedles after exposure to the high RH was only 24.5 µm. This indicated that the PVP/trehalose needles would remain effective after such exposure and, more likely, could be used without any loss of function after a short period of exposure to ambient temperatures and RH.

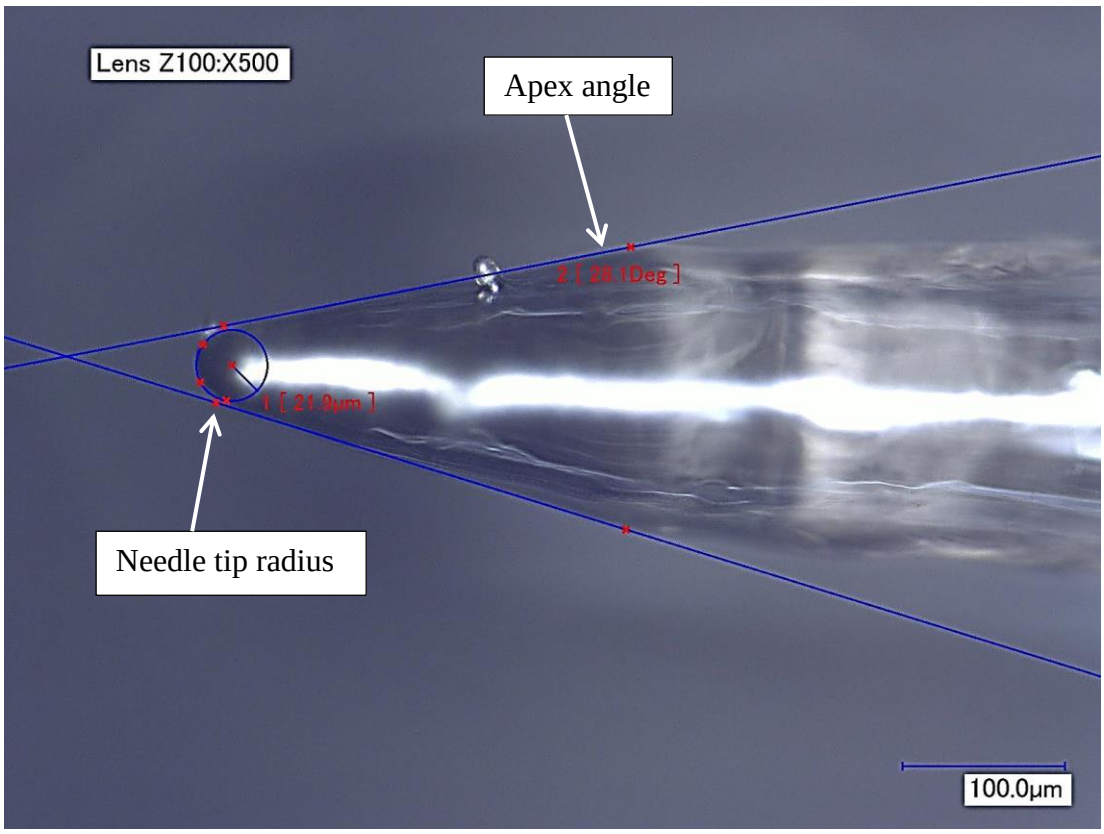

Figure 3.13: Digital microscopy image of PVP/trehalose microneedle tip illustrating apex angle and needle tip radius. This sample was taken from the batch kept in a humidity chamber at ≈ 60% RH for the duration of the experiment.

3.3.1.7. Skin Penetration

The crux of dissolvable microneedle drug delivery is the ability of the needles to effectively penetrate the SC of the skin and administer the drug payload as intended. As such, the failure force of the microneedle arrays must exceed the insertion force required to penetrate the skin otherwise the needles will fail to penetrate the SC. In order to facilitate effective penetration, the needles must be sufficiently long and sharp, however increasing both of these features decreases the mechanical strength of the needles [212]. Having determined that the fracture force of the 750 µm needles was sufficiently high (≈ 20 N), tests were carried out to evaluate the ability of the microneedles to penetrate porcine skin samples. Micro-sectioning and OCT techniques were utilised to examine the skin penetration abilities of the microneedle arrays.

The micro-sectioning technique employed to examine the skin samples was modified from a technique normally utilised to examine metallic samples and other technological components (Figure 3.14). As such, to the authors' knowledge, it has never been used to examine organic material before.

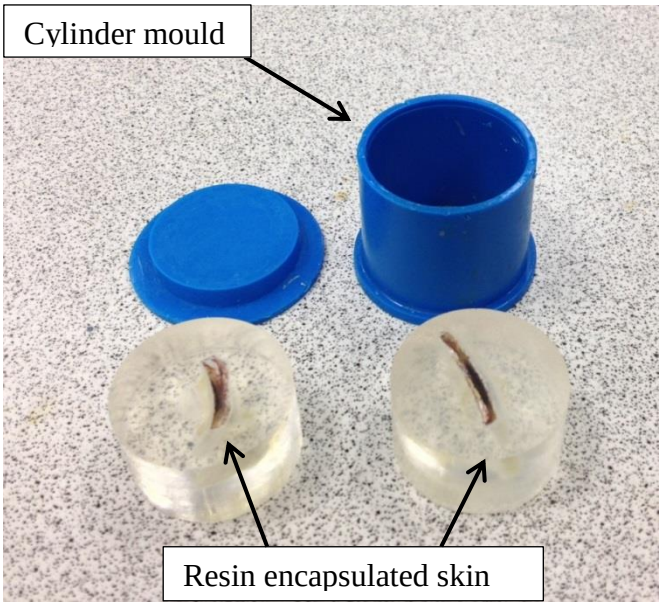

Figure 3.14: Resin mould with epoxy resin encapsulated skin samples prior to microsectioning.

Previous skin penetration studies utilised methylene blue dye to visualise micro-channels in the skin created after pre-treatment of the skin with microneedles [73, 87]. Conversely, other studies have incorporated the methylene blue dye directly into the needles [87]. You *et al.* demonstrated the drug delivery capabilities of dissolving fibroin microneedles by mixing powdered methylene blue dye into the needle formulation. Their study, however, utilised the methylene blue as a model drug given its' use in the treatment of neurodermatitis and malaria [196].

In this study, the methylene blue dye was utilised both ways with one test carried out using dye loaded needles and another with standard needles for pre-treatment followed by skin staining after application. After insertion of the dye loaded arrays, the needles dissolved in the skin leaving the dye embedded in the micro-channels (Figure 3.15). The micro-channels were easy to visualise on the skin surface and therefore it was possible to determine the level of penetration achieved by the arrays. In addition, the embedded dye was used as an indicator to determine the depth of

penetration after the skin samples were micro-sectioned. Similarly, after the application of the standard formulation array and surface staining, the micro-channels are clearly visible indicating a high percentage of the needles successfully penetrated the skin.

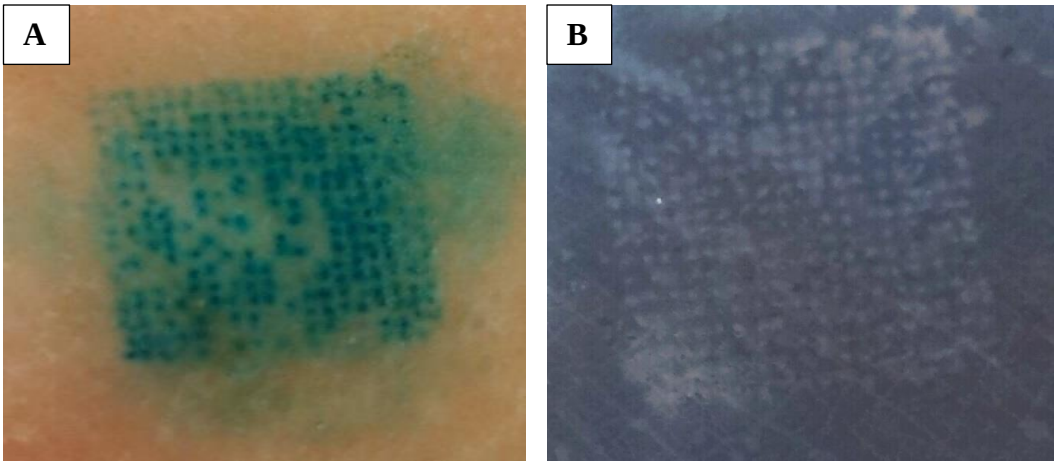

Figure 3.15: Porcine skin samples after (**A**) application of methylene blue infused microneedles and (**B**) skin surface staining after application of standard formulation microneedle array.

Figure 3.16 illustrated penetration depths of 590 µm, 450 µm and 380 µm for selected microneedles, determined by the concentrated levels of methylene blue dye visible in the micro-sectioned sample. Similarly, Figure 3.17 illustrated another cross section of the skin sample with measured penetration depths ranging from 370 µm to 450 µm. Given that the shaft length of the microneedles was 750 µm, this suggested that, at most, only 90 % of the full length of the needles had penetrated into the skin. In an array containing 324 drug loaded needles, this indicated that a significant amount of the drug payload may not be effectively administered. However, previous studies have reported that, as a result of the elastic properties of the skin, undissolved portions of the microneedles ranging from 5 – 20 % remain after application [130]. Factors such as skin occlusion and maintaining the microneedle array on the skin for longer periods may result in further drug uptake, however, additional studies would need to be carried out to determine this.

A number of issues, however, were encountered during the micro-sectioning process. During the resin encapsulation stage, particularly as the resin hardened on curing, the

skin sample appeared to have slightly deformed from its initial state. As such, the measured penetration depths may not have been fully representative of the actual depth of the needles in the skin. This suggested that the actual depth that the needles had penetrated may have been greater than the measured depths.

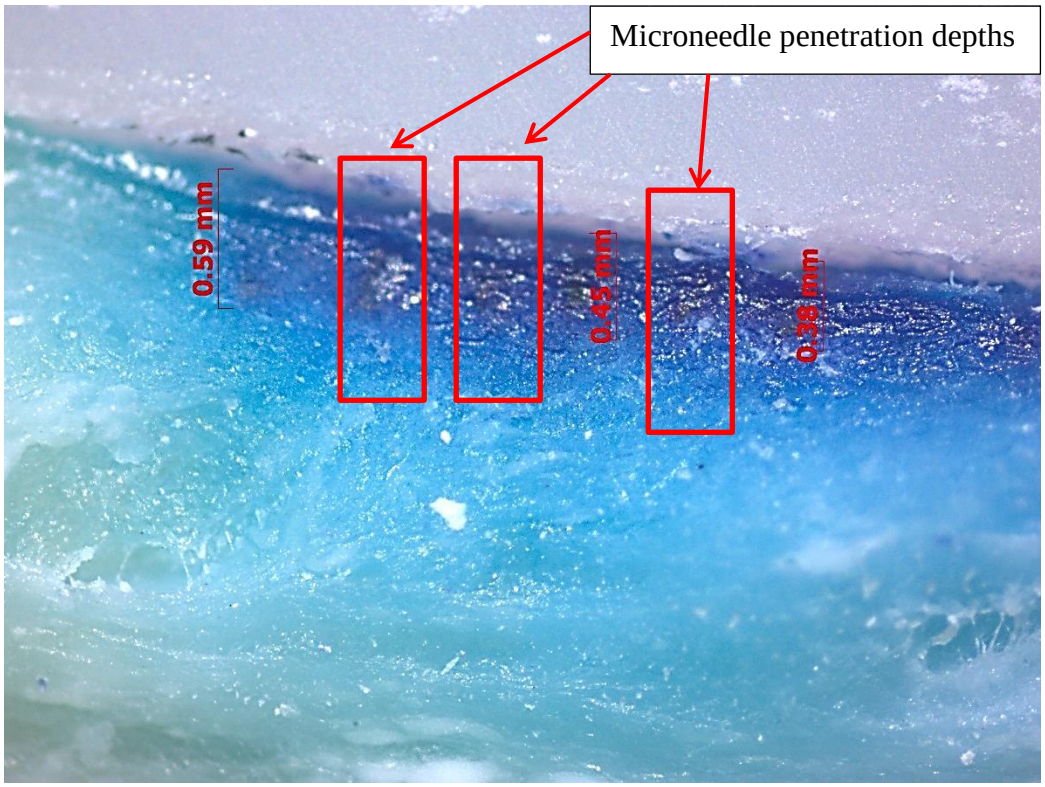

Figure 3.16: Cross section of resin encapsulated skin sample detailing measured depth of methylene blue microneedles.

Another issue also arose during the polishing stage. It was observed that dye embedded in the skin began to leech out and contaminated the surrounding material causing the blue tinge visible through the entire material cross section. Although the penetration points of the microneedles were still visible, the results may have been much clearer had the leeching not occurred. As such, it was determined that further optimisation of this technique was required in order to improve the results obtained.

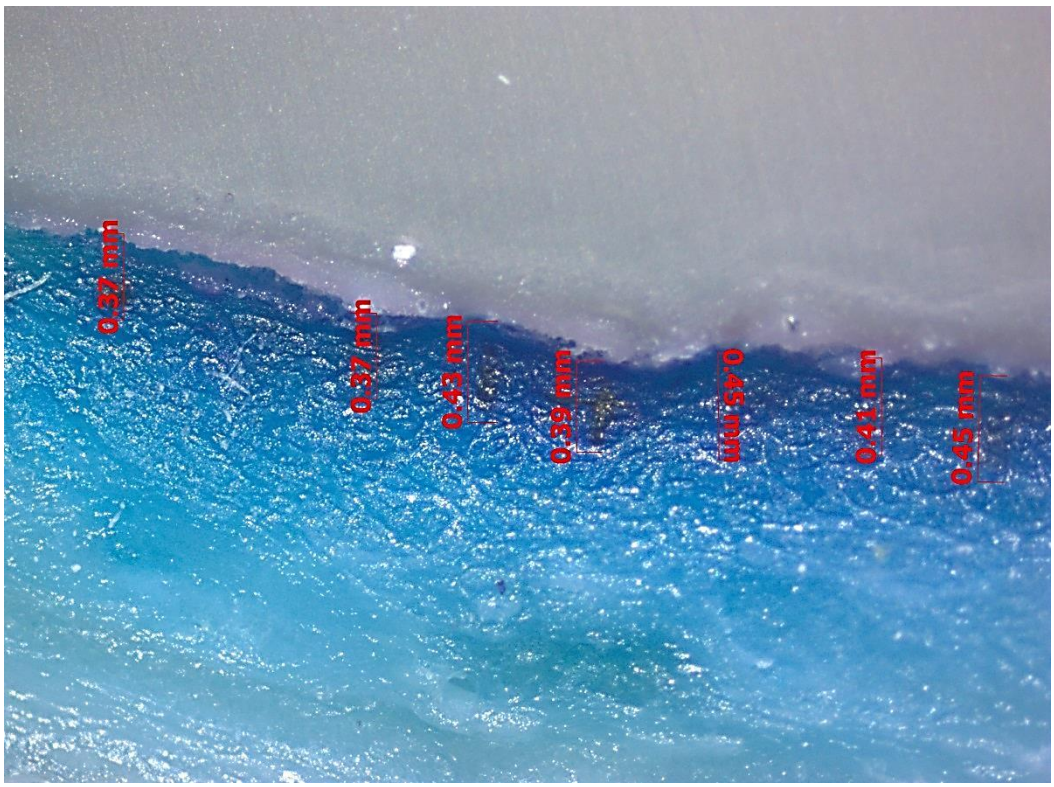

Figure 3.17: Cross section of resin encapsulated skin sample detailing measured depth of methylene blue microneedles.

3.3.1.8. OCT

OCT analysis provided a more accurate method of determining the depth of penetration of the microneedle arrays. OCT is a non-invasive optical imaging technique that maps variations in reflected light as a function of depth in biological samples, similar to ultrasound. Light scattering in skin tissue however, results in significantly lower penetration depths than those obtained with ultrasound, with depths of approximately 2 mm possible with OCT. Compared with confocal microscopy, which is capable of depths of only approximately 0.25 mm, OCT provides a valuable technique for real time cross sectional imaging of the epidermis and upper dermis which is particularly suited to measuring microneedle penetration depth [84, 213].

Immediately after insertion into porcine skin, the rapid dissolution of the PVP/trehalose microneedles resulted in a low level of contrast in the OCT image between the skin and the arrays. Despite this, the penetration depths for the microneedles were clear and the image (Figure 3.18) illustrated that the

PVP/trehalose microneedles penetrated the skin to an average depth of 384 µm, which was over half the needle length and corresponded with the results obtained from the epoxy resin micro sectioning method (Section 3.2.2.12). The OCT technique however, provided more accurate measurements and facilitated the analysis of not only the penetration depth but also the average width of the micro-conduits and the average distance between the base layer of the arrays and the surface of the skin sample.

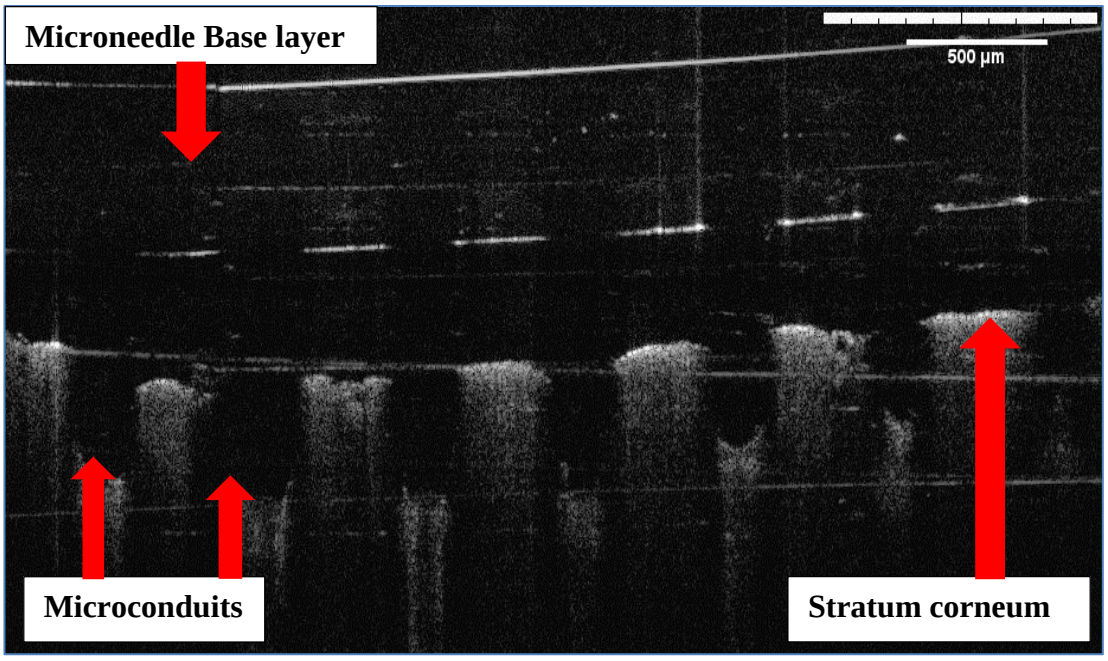

Figure 3.18: OCT image detailing the penetration depth of PVP/trehalose microneedles into porcine skin. This image shows needle penetration with an average depth of 358 ± 31 µm, average micro-conduit width of 246 ± 6.7 µm and the average distance between the microneedle base and skin surface of 290 ± 18 µm (n=6).

Lee *et al* (2016) utilised OCT to examine the penetration depths of spin coated PVP microneedles. They observed that needles with a length of 300 µm were capable of penetrating to an approx. depth of 250 µm, representing over 80 % of the total needle length [213]. As longer needles most likely experience a greater elastic resistance from the epidermal and dermal layers as they penetrate more deeply, lower penetration depths relative to overall needle length would be expected [84]. This hypothesis could therefore explain the penetration depths of approx. 50 % needle length for the 750 µm microneedles observed in this study.

3.3.1.9. Drug Activity in Formulation

Encapsulating therapeutic peptides into a dissolving microneedle system requires that the stability of the peptides is not compromised either during the formulation process or while the drug is embedded in the microneedle matrix [124]. Polymyxin, a peptide antibiotic, was chosen as a model drug for these studies.

In order to determine whether or not the activity of a model drug would be preserved during the PVP/trehalose microneedle formulation process, a number of diffusion experiments were carried out. Well diffusion and disc diffusion experiments based on the Kirby-Bauer Disc method were utilised for these studies. Also referred to as the agar diffusion method or disc diffusion method, the Kirby-Bauer Disc method is used to determine antibiotic susceptibility of a pathogen. The standard procedure involves impregnating a filter disc with an antibiotic and then applying the disc to an agar plate which has been inoculated with the organism to be tested. The plate is then incubated at 37 ºC for 24 to 48 h during which time the antibiotic will diffuse from the filter disc into the agar. The concentration of the antibiotic decreases as a function of the square of the distance of diffusion until the concentration of the antibiotic is too dilute and it no longer inhibits the growth of the microorganism. Where the antibiotic has been effective, clear areas are visible on the agar plate around the antibiotic disc which indicates no pathogen growth. These areas are referred to as zones of inhibition (ZOIs). The diameter of these ZOIs is measured to determine the susceptibility of the organism to the antibiotic in question [214].

Normally, factors such as the rate of diffusion of the antibiotic, the concentration of the antibiotic, viscosity of the culture medium, interaction of the antibiotic with the medium and the sensitivity of the organism to the antibiotic may affect the size of the ZOIs. As such, the disc diffusion method is a simple procedure used to determine antibiotic activity which does not require special equipment and yields easily interpreted results. Interpretation of the ZOIs for the Kirby-Bauer test looks at the diameter of the ZOIs with sizes indicating whether the organism is resistant, intermediate or susceptible to the antibiotic and as such, the results obtained from this method are qualitative [208, 214].

The first experiment examined whether any loss of activity to the drug had occurred during the initial stages of the formulation process. As such, these tests were carried out using liquid formulations, including a control formulation which contained no polymyxin. The results of the control were negative and all the plates tested with the drug infused formulation resulted in ZOIs with an average diameter of 22 ± 2 mm (n=18) indicating that no loss of efficacy to the drug occurred during the initial formulation stages. The next experiment was carried out using drug infused formulation that had been cast into both microneedle arrays and discs (similar to those used in traditional Kirby-Bauer diffusion tests) (Figure 3.18).

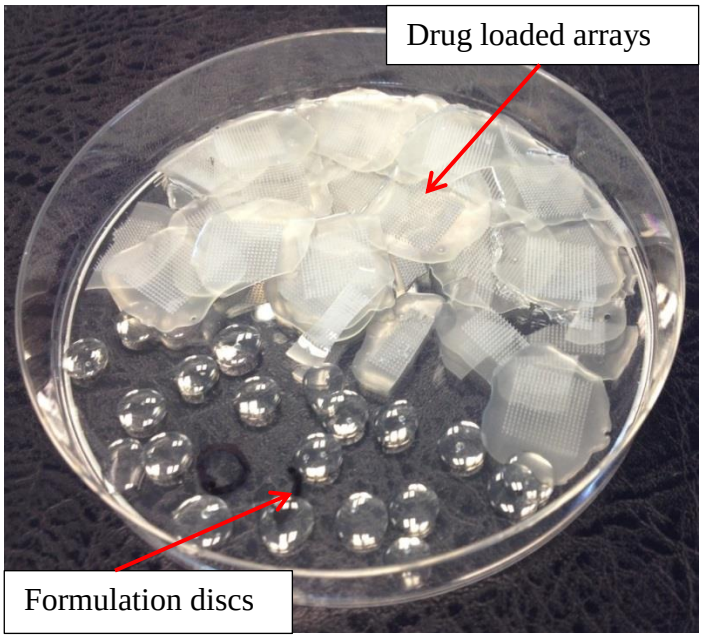

Figure 3.19: Polymyxin loaded formulation discs and microneedles arrays.

Again, the ZOI's on the agar plates with the drug infused discs were on average 21 ± 1 mm in diameter (n=12) which again suggested that the polymyxin peptide was unaffected by this stage of the microneedle fabrication process. In addition to testing the drug infused discs, fully formed microneedle arrays with the encapsulated drug were scraped over the agar plates prior to incubation, scattering the needles over the plate surface. The results indicated that each microneedle formed individual ZOI's equivalent to those formed by the discs (Figure 3.19).

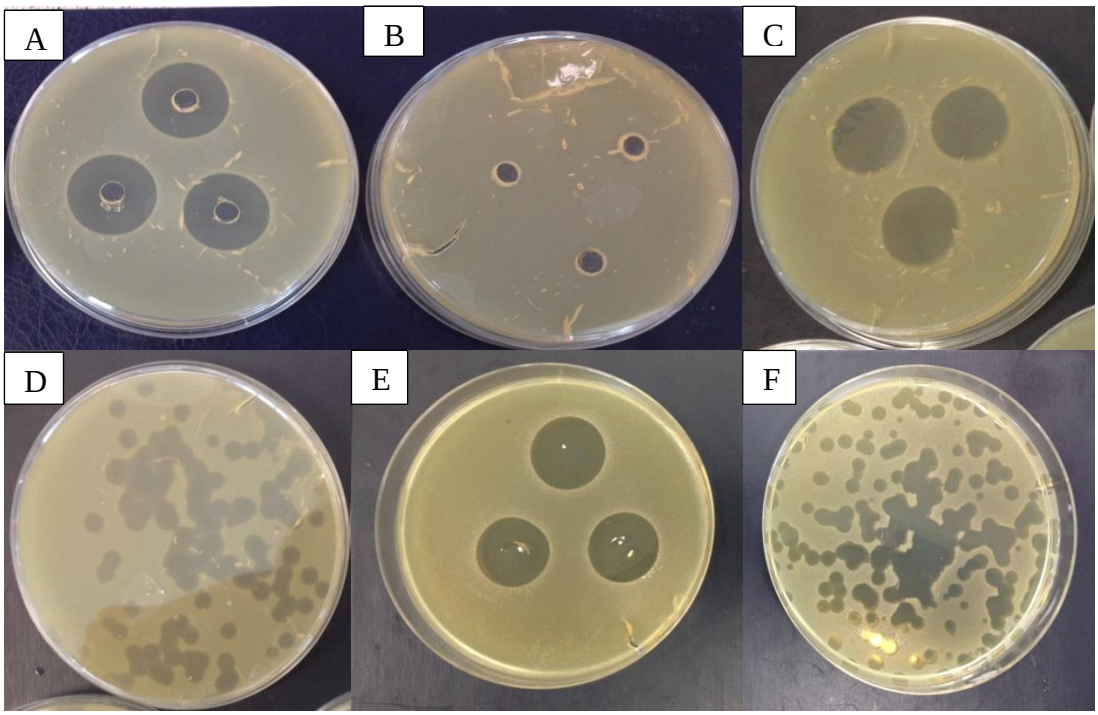

Figure 3.20: Agar plates after diffusion experiments. (A) Agar plate after well diffusion test with polymyxin infused microneedle formulation. (B) Agar plate after well diffusion test with microneedle formulation, no drug. (C) Agar plate after disc diffusion test with polymyxin infused formulation disc. (D) Agar plate after diffusion test with polymyxin infused microneedles. (E) Agar plate after diffusion test with polymyxin infused formulation disc after 70 days storage and (F) Agar plate after diffusion test with polymyxin infused microneedles after 70 days storage.

Finally, the same diffusion tests were carried out on a batch of drug infused discs and microneedle arrays that had been stored in a desiccator for 70 days after fabrication. Once again, the ZOIs formed by the discs were an average of 21 ± 1 mm in diameter (n=10) indicating no loss of drug activity. Similarly, the plates on which the drug loaded needles were scattered showed a multitude of ZOIs comparable to the previous plates. As such, it was determined that no loss of drug activity occurred at any stage of the formulation and fabrication process and additionally, the activity was retained in each individual drug loaded needle. The stability of polymyxin B is given as 6 months in powder form and up to one month in suspension at 4 ºC [215]. As such, the retention of the drugs' activity in the formulation after 70 days at room temperature indicates that the formulation can successfully maintain the drugs' activity over a prolonged period of time.

The amount of drug incorporated into the needles of each microneedle array was calculated as 6.25 µg. Compared with other therapeutic peptides (Table 1.2), the

polymyxin B dose would be sufficient for the delivery of many approved therapeutic peptide drugs with low daily doses such as exenatide (5 µg daily) and teriparatide (20 µg daily).

3.4. Conclusions

The 3:1 PVP/trehalose microneedle formulation was extensively characterised using a wide range of techniques to establish the suitability of the formulation for the systemic delivery of biological pharmaceuticals such as therapeutic peptides and proteins. The results of these experiments indicated that the formulation possessed a sufficiently high T_g for prerequisite physical stability, exhibited moisture sorption behaviour which would facilitate rapid dissolution once applied to the skin (in addition to bolus drug delivery) and arrays cast from this formulation were fully formed and consistently representative of the master moulds.

In addition to the above, further testing was carried out to examine the mechanical strength of the needles to determine the fracture force and skin penetration abilities of the arrays. The effect of elevated RH on the needle tip sharpness was also examined. The results of the above indicated that the PVP/trehalose formulation produced microneedles that were more than adequately robust to penetrate the skin, and that kept a sufficient tip radius after exposure to relatively high RH conditions.

Coupled with the characterisation tests, fluorescence microscopy confirmed that material from the microneedles did not diffuse into the base layer of the array after the casting process. As such, drug material embedded in the microneedle shafts would be expected to remain in the needles only and no loss of the drug payload through diffusion into the base layer would be expected to occur in a system utilising drug loaded needles only.

The skin penetration depths of the PVP/trehalose microneedles were examined using both a novel micro-sectioning technique and non-invasive OCT imaging. Both techniques illustrated that the microneedles were capable of successfully penetrating the SC to an adequate depth to facilitate systemic drug delivery with OCT providing additional data in relation the micro-conduit width and the distance between the microneedle base and the skin surface.

Finally, the formulation was tested to determine if a model peptide drug could be encapsulated in the formulation without any loss of efficacy. A number of well/disc diffusion tests were carried out, the results of which indicated that the polymyxin

model peptide maintained activity during all stages of the formulation process and remained unchanged after 70 days encapsulated in the polymer/sugar microneedle arrays.

This study represents the first use of a tertiary formulation consisting of PVP, trehalose and glycerol for the fabrication of dissolvable microneedles designed to deliver therapeutic peptides transdermally. The characterisation techniques utilised provided comprehensive data on the quality of the formulation in respect to the envisioned application. In addition, this study has employed techniques such as DVS and micro-sectioning in a unique and novel manner to characterise the effectiveness of the polymer/sugar formulation in a rapidly dissolvable microneedle system. The next stage of this study will involve incorporating a model peptide drug into the microneedle formulation and carrying out Franz cell based skin diffusion studies to examine the ability of the microneedles to deliver the drug payload through porcine skin.

CHAPTER 4. PVP AND TREHALOSE BASED MICRONEEDLES FOR THE TRANSDERMAL DELIVERY OF POLYMYXIN B SULPHATE

4.1. Introduction

4.1.1. Transdermal Flux and Occlusion

Permeation of a compound through the SC is generally achieved through passive diffusion with no delivery occurring as a result of active transport or migration due to external forces such gravity, hydrodynamic flow or electrical fields in the case of charged molecules [216, 217]. The routes of permeation are through the intact epidermis and skin appendages, such as hair follicles and sweat glands. Although these appendages have been proposed as routes by which permeation of charged molecules and larger polar compounds (such as peptides) can occur, they account for only 0.1 % of total skin area and contribute little to the overall rate of transdermal flux [218]. Typical transdermal delivery systems utilise the concentration gradient of the drug molecules to traverse the SC and penetrate into the skin. Delivery is via molecular diffusion and is proportional to the magnitude of the concentration gradient and the permeability of the SC to the drug itself. An increase in either of these factors results in an increase in drug flux, which refers to the mass or number of drug molecules passing through a cross sectional area over a certain period of time [217, 219]. Molecular weight also plays a part in skin permeation with penetration occurring only with chemicals having a molecular weight less than approx. 500 Da [216].

Occlusion refers to the process whereby the skin is covered with an impermeable material (e.g. tape, dressing, patch, glove) preventing trans-epidermal water loss and resulting in a decrease in the water gradient across the SC. This then increases the hydration of the SC and ultimately results in an increase in the permeability of the outer layers of the skin. Uptake of water into the skin leads to swelling and structural changes to lipids and corneocytes within the SC. The main lipid components of the SC are long chain ceramides, fatty acids and cholesterol, in contrast to other biological membranes where lipid content contains phospholipids. In hydrated conditions, fractions of these lipids, in addition to some protein components, become fluid leading to increased permeability [220]. Human skin also contains a hygroscopic combination of amino acids, amino acid derivatives and salts collectively termed natural moisturising factor (NMF). The function of NMF is to help maintain tissue pliability through the retention of water within the SC [23].

Studies have shown that the increased permeability arising from occlusion leads to improved drug transport irrespective of lipophilicity [221]. The systemic blood circulation is then eventually reached once the drug material has successfully passed through the skin barrier without degradation [219].

4.1.2. Skin Diffusion Testing

Accurate prediction of the behaviour of a drug *in vivo* through the application of robust and validated *in vitro* models is essential for the development of appropriate formulations for topical transdermal delivery [216]. As part of the increasing interest in the skin as a viable site for drug delivery, diffusion cell systems are routinely used for static *in vitro* transdermal drug delivery testing, providing fundamental information regarding the interaction between the skin, active ingredient and drug formulation. Diffusion cell systems consist of a donor compartment and a receptor compartment, separated by the skin sample, which acts as a barrier between the two. The material being tested is then placed on the surface of the skin in the donor compartment and diffusion through the skin sample is measured by uptake of test material into the receptor phase. By providing this information on the transdermal behaviour of a drug formulation, diffusion testing is instrumental in the development of transdermal products [222].

Diffusion itself is driven by the concentration of the analyte going from high concentration to low. *In vitro* diffusion takes place generally via passive diffusion of the permeant through an artificial or biological membrane from the donor chamber into the receptor chamber. There are many types of diffusion cell systems available including static cell, which may be vertical or 'side-by-side', (Figure 4.1) and continuous flow/flow through systems. A minimum of 3 parallel cells should be run for each formulation being tested however, due the inherent variability encountered with biological samples (including skin), 5 or 6 replicates are often used [223].

Artificial membranes which model biological samples are frequently used in Franz-type diffusion studies and possess some advantages over actual skin samples in that that they are more easily sourced, can be cheaper to obtain and are structurally less complex. One of the main advantages of using artificial membranes is the superior

reproducibility of the permeation data obtained compared with the array of variables associated with real skin such as sample age, race, sex, anatomical site and general individual variabilities [224]. In fact, skin structures can vary between species, different strains of the same species and within the same species (depending on anatomical site). In addition, variations in percutaneous absorption can occur due to skin condition and the level of hydration of the skin [216].

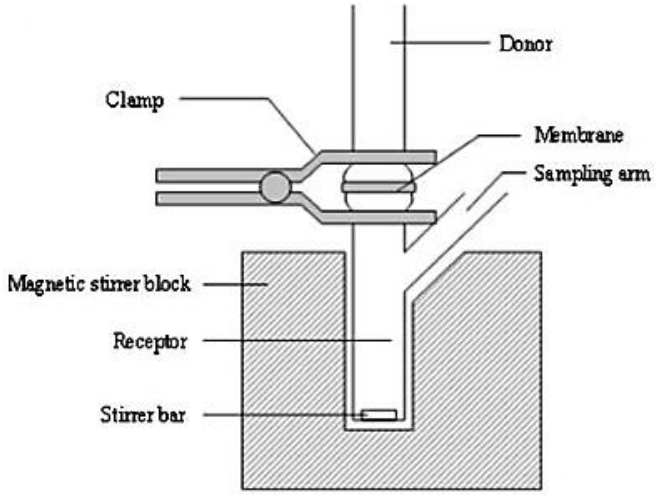

Figure 4.1: Diagram illustrating the typical set up of a static flow, vertical Franz cell system [224].

Franz type diffusion experiments are commonly carried out using synthetic membranes as models for skin which are more easily obtained, cheaper and have less complicated structures than biological samples. As such, synthetic membranes can provide more reproducible data, eliminating such variables as age, race, gender and anatomical site [224, 225]. This holds true for transdermal applications where patches are used and although artificial skin models have been utilised in some microneedle penetration studies [226, 227], human skin or animal skin models are preferable for microneedle based drug diffusion tests. As *in vitro* diffusion tests aim to mimic *in vivo* conditions as much as possible, the receptor medium most commonly utilised is pH 7.4 phosphate buffered saline (PBS) which closely resembles physiological fluids [228].

In addition to the variability inherent in biological skin samples, there are many other factors which must be considered for Franz type diffusion experiments. Tailor made

diffusion cells can exhibit variations in receptor volume and side arm steepness. It is also important that the receptor fluid is in constant contact with the underside of the skin sample throughout the experiment to allow efficient diffusion into the receptor phase to occur. As such, air bubbles in the receptor chamber are to be avoided [222]. This is achieved by degassing the receptor fluid prior to the experiment and by inverting the diffusion cell when filling the receptor chamber with fluid. Temperature control is another factor which must be considered and the temperature of the receptor phase must be maintained throughout the experiment at the *in vivo* skin temperature which is 32 ± 1º C [216]. This is crucial given that temperature directly affects percutaneous flux, typically doubling the rate of flux with each 10 ºC increase [224]. Steady stirring of the receptor fluid is also important to ensure that drug material is distributed uniformly in the receptor fluid and also to maintain temperature equilibrium. The rate of stirring is also crucial to avoid vortex formation which can result in disruption of the static fluid layer directly in contact with the skin sample.

4.1.3. Polymyxin B Sulphate

Polymyxin B sulphate, (Section 3.1), was chosen as the model drug in this study for a variety of reasons. Primarily, its antibiotic properties allowed for the activity of the drug to be evaluated during all stages of the formulation process via a simple Kirby Baur diffusion test. Also, it is a widely available and relatively inexpensive. Polymyxin B is typically formulated as a sulphate salt for both parenteral and inhalation based delivery. It behaves like a detergent and is rapidly bactericidal by targeting the outer cell membrane of the bacteria, increasing the permeability of membrane and leading to cell death through the leakage of cell contents [202]. Polymyxin B has been widely used topically for otic and ophthalmic applications in addition to the treatment of certain skin infections [49] and is often used in conjunction with other drugs such as neomycin, gramicidin and various steroids [229, 230].

4.2. Objectives

Successful delivery of a therapeutic peptide payload is the crux of this dissolving microneedle system. Having demonstrated that the PVP/trehalose microneedles have sufficient mechanical strength and stability to penetrate skin and can adequately protect the activity of a biologically active model peptide within the microneedle matrix, the next stage of this study was to examine the ability of the microneedle system to successfully deliver a model peptide drug, polymyxin B, through porcine skin.

Therefore, the aim of this chapter was to demonstrate the effectiveness of the optimum PVP/trehalose microneedles in delivering the model peptide, polymyxin B, through porcine skin. In addition to monitoring the levels of drug delivered over time, the activity of the polymyxin was monitored at all stages of the formulation and drug delivery process to confirm that no loss of activity occurred. High Performance Liquid Chromatography (HPLC) was used to detect the drug at different time points throughout the diffusion experiment and as such, a HPLC gradient method was developed for the detection of polymyxin in an aqueous PBS solution.

The polymyxin B model peptide was incorporated into the PVP/trehalose formulation and skin diffusion testing carried out to examine the performance of the dissolving microneedles in delivering the model peptide into porcine skin. Franz Diffusion cells were utilised in the drug diffusion studies with the drug loaded microneedles *ex vivo* and analysis carried out using HPLC to quantify both the rate of diffusion and the level of drug delivered to the skin. Although a number of methods have been described using HPLC to analyse polymyxin B samples [206, 231], further optimisation work was needed on the HPLC method as the samples were in a PBS solution containing additional material from the skin sample.

4.3. Experimental

4.3.1. Materials

Polymyxin B sulphate supplied by Sigma Aldrich
PVP average weight 40,000 supplied by Sigma Aldrich
Trehalose D-(+)-trehalose dihydrate (≥98 %) obtained from Fisher Scientific
Glycerol – ACS grade obtained from Reagecon
Brain heart infusion (BHI) obtained from Oxoid Microbiology Products
Salmonella typhimurium (LT2) from Waterford Institute of Technology (WIT) culture collection
Porcine ear skin (untreated) from male and female animals aged 5.5 years – supplied by Dawn Pork and Bacon, Waterford, Ireland
Phosphate buffered saline (PBS) solution obtained from Fischer Scientific

4.3.2. Methods

4.3.2.1. Polymyxin Loaded Microneedles

Polymyxin loaded microneedles were prepared using the same fabrication methods described in Section 2.3.2.3. A 3:1 PVP/trehalose formulation with 2% w/w glycerol was prepared in 10 mL of DI water. 200 mg of polymyxin B sulphate was added to the formulation and mixed thoroughly until the polymyxin was fully dissolved. The loaded formulation was then used to cast microneedle arrays using the vacuum oven method described in Section 2.3.2.4. The dimensions of these arrays were as before: 324 needles with 750 µm length shafts with a base width of 200 µm and inter-needle spacing of 600 µm. Each batch formulated consisted of approx. 20 microneedle arrays.

4.3.2.2. SEM

The instrument used for this experiment was a Hitachi S-2460N SEM with all settings as per Section 2.2.2.7.

4.3.2.3. TGA

The instrument used for this experiment was a TA Instruments Q50 TGA. The experiments were carried out as per Section 2.2.2.8 with no deviation in the settings.

4.3.2.4. DSC

The instrument used for this experiment was a TA Instruments QS 2000 DSC. The experiments were carried out as per Section 2.2.2.9 with no deviation in the settings.

4.3.2.5. DVS

The instrument used for this experiment was a Surface Measurements Systems DVS Intrinsic. The programme settings used were as per Section 2.2.2.10 with no deviation.

4.3.2.6. High Performance Liquid Chromatography (HPLC)

HPLC analysis was carried out using an Agilent 1200 with an Xterra reversed phase C_{18} 5 µm 4.6 x 250 column. A gradient method was developed using two mobile phase components: mobile phase A (water with 0.1 % trifluoroacetic acid (TFA)) and B (acetonitrile with 0.08 % TFA). Starting with 95 % mobile phase A and 5 % B, the gradient changed to 40% B over 30 min and back to 5 % B at 35.10 min, holding then for a total run time of 40 min. The injection volume was 40 µL with a flow rate of 0.5 mL/ min, column temperature of 40 º C and the detection wavelength was set at 214 nm.

4.3.2.7. Liquid Chromatography–Mass Spectrometry (LC-MS)

LC-MS was carried out using an Agilent Technologies 1200 series LC-MSD Trap XCT Ultra. An Agilent Eclipse XDB C_{18} 5 µm 4.6 x 150 mm column was used and the LC settings were as follows: column flow rate was 500 µL/ min, column

temperature was set at 40 ºC and the injection volume was 5 µL. The detector was set at 212, 220, 230 and 280 nm. A gradient method was developed using two mobile phase components: mobile phase A (water with 0.1 % formic acid) and B (acetonitrile with 0.1 % formic acid). Starting with 95 % mobile phase A and 5 % B, the gradient changed to 95 % B over 50 min and back to 5 % B at 55 min, holding then for a total run time of 60 min. The MS system was used in positive mode with electrospray ionisation (ESI). The nebuliser was set at 50 psi, the dry gas at 10 L/ min and the dry temperature used was 350 ºC.

4.3.2.8. Franz Cell Diffusion Test

Prior to the skin diffusion tests, 5 of the polymyxin loaded arrays were taken from the microneedle batch and content uniformity testing carried out with each being tested for weight, total needle weight and drug content. Each array was placed in an amber vial containing 4 mL of PBS and fully dissolved with the aid of a vortex mixer. Each sample was then filtered using a 0.45 µm syringe filter and analysed using HPLC. For each sample of loaded microneedles, 8 Franz cells were used: 6 drug loaded samples and 2 drug loaded formulation discs as controls. Each array was weighed and the drug content calculated using the calibration curve obtained from the content uniformity test.

For the skin diffusion experiments, freshly excised skin (porcine ear), which was obtained prior to steam treatment to preserve SC integrity and stored at -20 ºC, was utilised. After thawing, the skin was then cut into approx. 225 mm^2 pieces and all subjacent cartilage, muscle and adipose tissue was carefully removed with a surgical scalpel and each piece examined for any physical damage or disruption to the SC, discarding any damaged samples. The edges of the receptor cells and donor cells were lightly coated with silicon grease to prevent leakage during receptor cell filling and to seal the cell during the diffusion experiment. Once prepared, the skin samples were washed with PBS buffer and kept on wet tissue at 4 ºC to prevent them from drying out prior to testing. Skin samples were taken from the same general area of the ear to limit variability in skin thickness as much as possible.

Loaded microneedles were then applied to the skin samples with gentle thumb pressure and held for approx. 30 s. Skin samples were then loaded onto the Franz cells and the donor and receptor cells were clamped together. The receptor compartment was then filled with exactly 4 mL of the PBS buffer solution (receptor phase), keeping the cells inverted during the filling process to avoid air bubbles forming between the bottom of the skin sample and receptor phase, thus ensuring contact between the skin sample and the receptor phase. The loaded Franz cells were then placed in a heated water bath (37 ºC) with continuous magnetic stirring. Aliquots of 500 µL were taken at pre-established time intervals (1, 2, 3, 4, 5, 22 h) and replaced with the same volume of fresh, warmed PBS buffer soln. Each 500 µL aliquot was syringe filtered with a 0.45 µm filter and analysed using HPLC.

To determine the levels of drug remaining on the skin surface and contained within the skin itself, the cells were dismantled after the diffusion experiments at 22 h and the SC surface of each skin sample was swabbed with cotton buds which were then placed in amber vials with 2 mL of PBS solution. Each skin sample was then dissected into approx. 20 pieces and placed in amber vials with 2 mL of PBS buffer solution also. Both sets of vials were then placed in an orbital shaker at 200 rpm for 4 h. After this, samples were taken from each vial, syringe filtered and analysed by HPLC.

4.3.2.9. Well Diffusion

Well diffusion tests were carried out as per Section 3.2.2.2, to monitor the activity of the polymyxin after the skin diffusion tests. 2 samples were taken from the receptor phase after 22 h and were applied to inoculated plates as before. 6 plates were used in total with 4 sample plates, 1 standard consisting of a 0.08 mg/ mL polymyxin solution and 1 control consisting of the microneedle formulation with no drug.

4.4. RESULTS & DISCUSSION

4.4.1. HPLC Method Development and Optimisation

Polymyxin is a complex antibiotic consisting of many closely related decapeptide components (mainly B_1, B_2, B_3) and up to 30 additional polypeptides [201, 230]. Although microbiological and chemical methods have been used to determine polymyxin in samples, specificity is limited and these methods cannot provide information on the drug composition. HPLC analysis has been utilised to examine the components of polymyxin and have included both isocratic and gradient methods in addition to a range of mobile phases and buffers [201, 205, 230, 232]. In addition, the low UV absorption and absence of natural fluorescence makes the quantification of polymyxin quite difficult [205] with many studies developing LC analysis methods utilising UV detection wavelengths ranging from 200 – 254 nm [233].

For the purposes of this study, a reverse phase gradient HPLC method was developed utilising two mobile phase components: water (0.1 % TFA) and acetonitrile (0.8 % TFA). The method was optimised by adjusting the experimental parameters including gradient composition, column temperature, injection volume, flow rate and detector wavelength to achieve sufficient separation and resolution of the component peaks in order to effectively quantify the drug at a concentration relevant to the ensuing diffusion testing. The sample of polymyxin B used in this study consisted primarily of the B_1 and B_2 components with B_1 comprising 60-70% of the sample. As such, HPLC analysis resulted in the resolution of two main peaks. Quantitation of polymyxin in the samples was therefore carried out based on the area under the main peak which was attributed to the polymyxin B_1 component of the drug, confirmed by LC-MS analysis.

The HPLC method was developed and validated in accordance with International Conference on Harmonisation (ICH) guidelines [234]. Limits of detection (LOD) and limits of quantitation (LOQ) were determined based on the standard deviation of the response and the slope of the representative calibration curve. The LOD was determined as 3.9 µg/ mL and the LOQ was determined as 11.8 µg/ mL. Calibration curves for the polymyxin standards were linear in the concentration range of 10 µg/ mL to 500 µg/ mL with r^2 value of > 0.99 based on the area under the polymyxin B_1

peak. Blank PBS solutions that had been left overnight with skin samples immersed were analysed to confirm there were no interfering compounds within the skin with the same retention time as the polymyxin peaks.

Initially, a gradient method with a total run time of 60 min was utilised. However, the parameters of the method were optimised with the overall method time reduced to 40 min and elution of the polymyxin peaks obtained at 25 min. Column temperature was initially set at 30 ºC but was increased to 40 ºC as an increase in column temperature corresponded with a decrease in polymyxin retention time. The temperature was subsequently maintained at 40 ºC for this method. The injection volume was initially quite high at 80 µL in order to quantify the polymyxin peaks however, after further optimisation of the method, the injection volume was sufficient at a reduced volume of 40 µL.

The drug content of the 5 microneedle arrays selected for the content uniformity test was calculated using the standard curve obtained from the polymyxin standards. The weight of the 5 arrays ranged from 68.36 mg to 90.39 mg. The calibration curve obtained from these arrays (Figure 4.2) was subsequently utilised to calculate the drug content of each of the diffusion test arrays in addition to the control discs. The estimated drug content of the needles in each array was also calculated using the 5 content uniformity arrays. Each array was weighed before and after the needles were scraped off the base and the mean weight of the needles on each was calculated. The mean weight of needles per array was calculated as 5.27 mg with the weight equivalent drug content of the needles calculated as 0.22 mg.

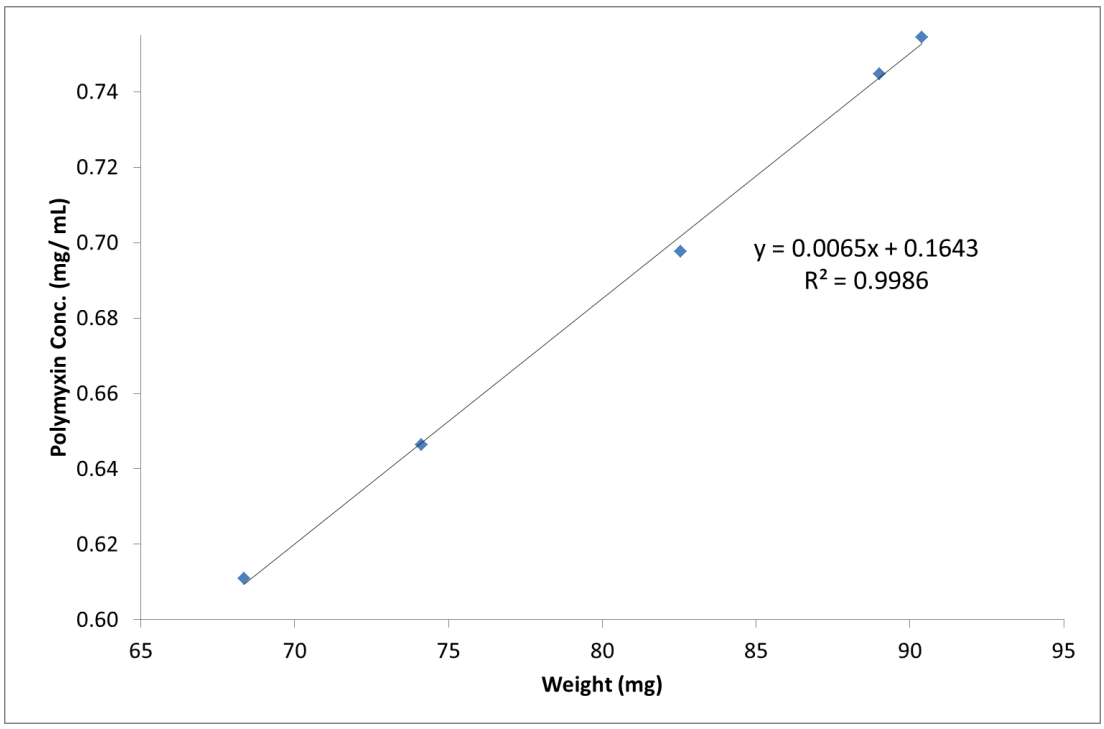

Figure 4.2: Plot of polymyxin concentration vs. array weight. The resulting linear equation was used to calculate the quantity of polymyxin in the arrays used for the Franz diffusion test.

Analysis of the PBS buffer after incorporating skin into solution indicated that none of the unknown skin material peaks eluted at the same retention time as the polymyxin components. However, during the diffusion tests, interference peaks were observed at 7 min and 15 min due to unknown materials most likely originating from the porcine skin sample or part of the microneedle formulation. The gradient method was adequately capable of separating out the various components within the sample to avoid any interference with the polymyxin peaks (Figure 4.3).

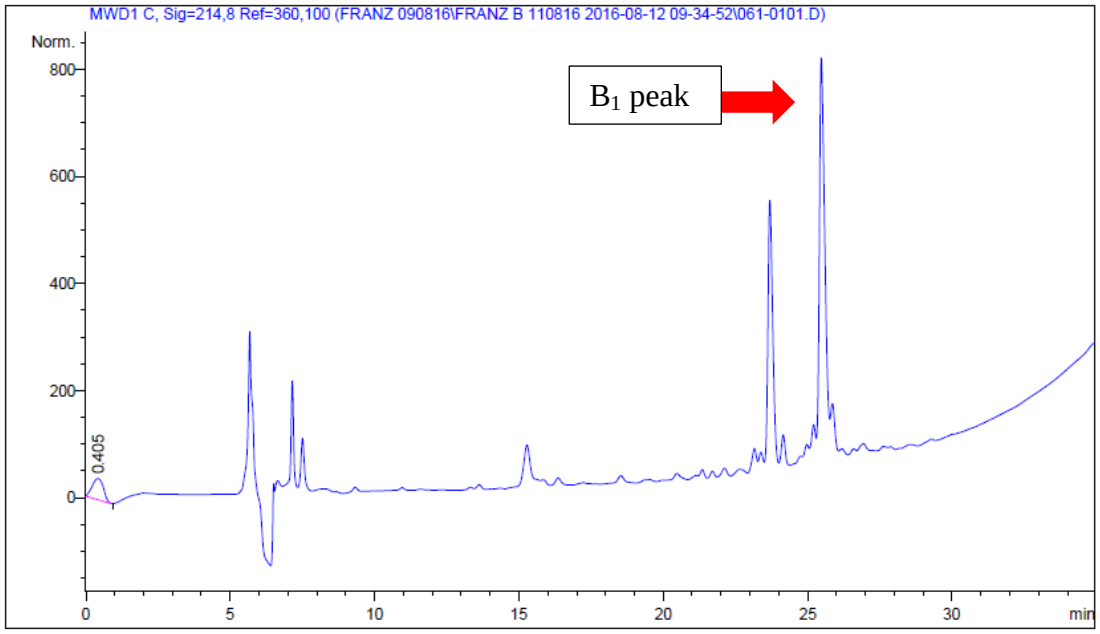

Figure 4.3: Chromatogram detailing polymyxin B_1 peak elution at 25 min from sample taken during skin diffusion test.

The use of polymyxin as a model drug for this study was not completely ideal, however, given that it has a very low UV absorbance and does not fluoresce to any significant degree which makes it difficult to detect at low concentrations [205]. Therefore, higher concentrations of the drug were added to the microneedle formulation to enable detection and as such, this posed the risk of potentially adversely affecting the structural and mechanical integrity of the microneedle shafts and subsequently, their ability to effectively penetrate the skin. Therefore, it was necessary to carry out further characterisation testing on the polymyxin loaded arrays including SEM, DVS and thermal analysis to examine the effect, if any, the high drug content would have on the properties of the arrays, compared with the unloaded formulation (Section 3.3).

4.4.2. LC MS Analysis of Polymyxin Peaks

To confirm the composition of the supplied polymyxin B model drug, LC-MS analysis was carried out (Figure 4.4, Figure 4.5) to determine that the main components of the sample were polymyxin B_1 and B_2. Polymyxin B_1 has a molecular weight of 1203.5 g/mol (exact mass of 1202.8 g/mol) and polymyxin B_2 has a molecular weight of 1189.5 g/mol (exact mass 1188.7 g/mol).

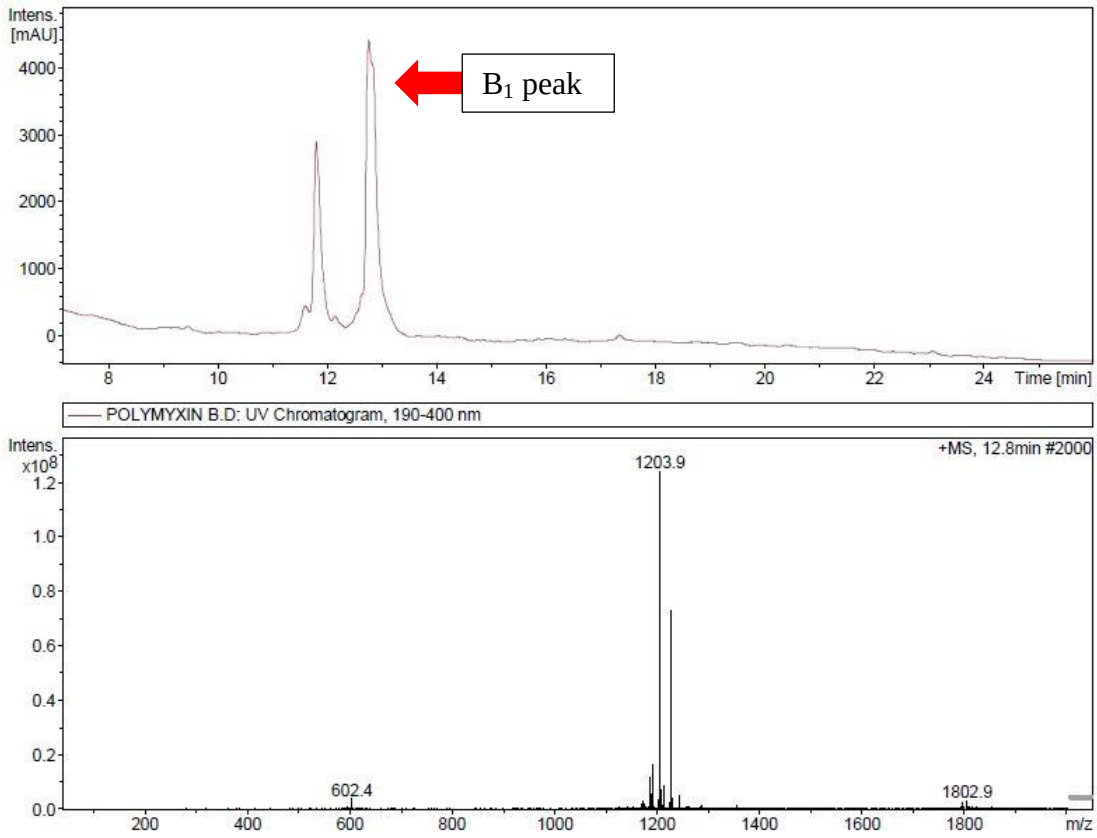

Figure 4.4: LC-UV chromatogram of polymyxin sample showing the polymyxin B_1 peak at 12.8 min (top) with the corresponding mass spectrum of the peak displaying the $[M+H]^+$ ion at m/z = 1204 Da (bottom).

The B_1 composition was given by Sigma Aldrich as between 60 - 70 %. The m/z values obtained for both the B_1 and B_2 peaks were as expected for the B_1 and B_2 components. Analysis of the composition of the polymyxin sample confirmed that the main peak was the B_1 component. Further analysis of the drug after the diffusion experiments would be based on the area under the polymyxin B_1 peak.

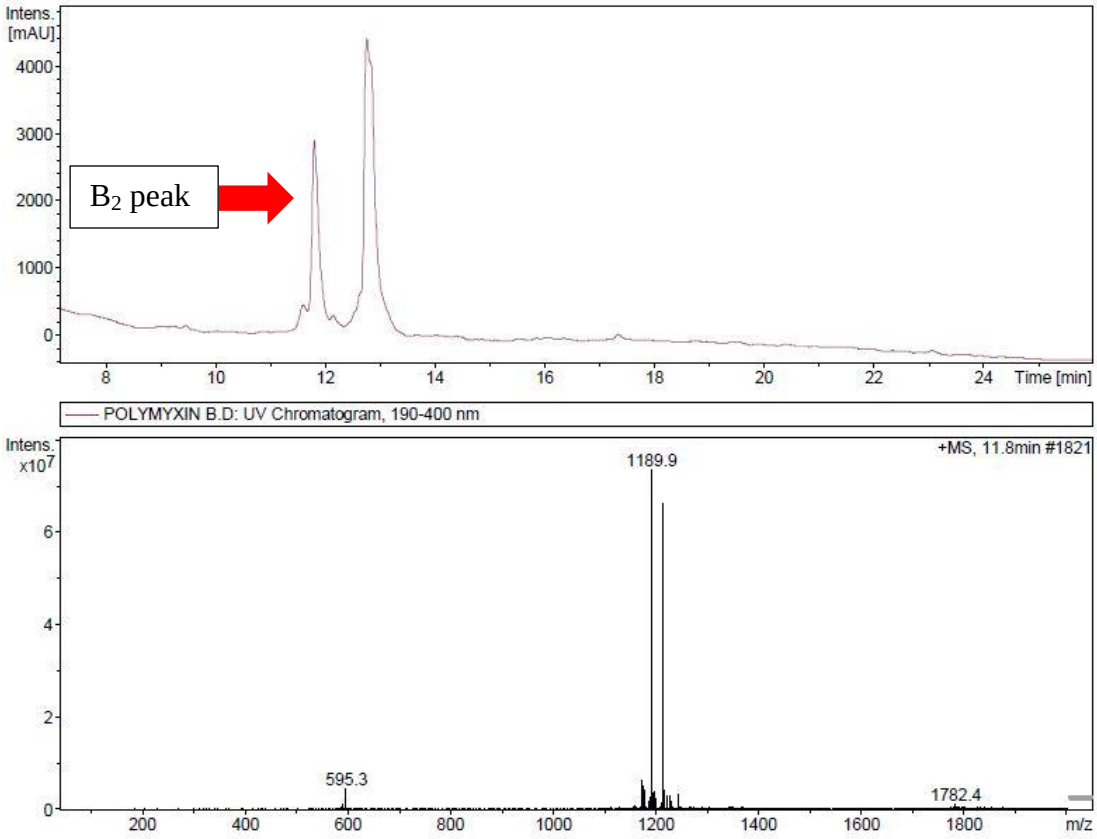

Figure 4.5: LC-UV chromatogram of polymyxin sample showing the polymyxin B_2 peak at 11.9 min (top) with the corresponding mass spectrum of the peak displaying the $[M+H]^+$ ion at m/z = 1190 Da (bottom).

4.4.3. Polymyxin Stability & Well Diffusion

A polymyxin solution (1 mg/ mL) was prepared and then immediately analysed using the developed HPLC gradient method. The solution was then stored at -20 ºC for 5 days after which, the solution was left to thaw at room temperature for a number of hours before being analysed using the same HPLC method. No change in retention time or peak area was observed and no degradation peaks were evident indicating that the polymyxin solution was unaffected by storage at -20 ºC for short periods of time. As such, it was determined that rather than requiring immediate analysis, samples collected during the skin diffusion experiments could be stored at -20 ºC for analysis at a later date.

In addition, samples collected from the receptor phase of the Franz cells during the skin diffusion experiments were incorporated in a well diffusion experiment to

examine the activity of the drug after application and subsequent diffusion through the skin. It was theorised that potential degradation and loss of activity as a result of the possible presence of peptidases in the skin matrix [235-237] may have occurred during the skin diffusion experiment. A standard solution containing 0.08 mg/ mL of polymyxin was used as the equivalent concentration of drug contained in the receptor phase after application. All the samples exhibited ZOI's of approx. 10-11 mm in diameter with the control exhibiting no ZOI's, as expected. As such, it was concluded that the activity of the polymyxin was unaffected by the application and skin diffusion process. This indicated that incorporation of the peptide into the microneedle system and subsequent application would not cause any loss of activity and the efficacy of the loaded dose would be retained

4.4.4. SEM

SEM analysis indicated that the polymyxin loaded microneedles were fully formed and visually free from any structural defects. The needles were solidly formed with very sharp tips (Figure 4.6). As such, it was determined that the addition of the polymyxin drug payload to the microneedle formulation did not adversely affect the casting and formation of the arrays.

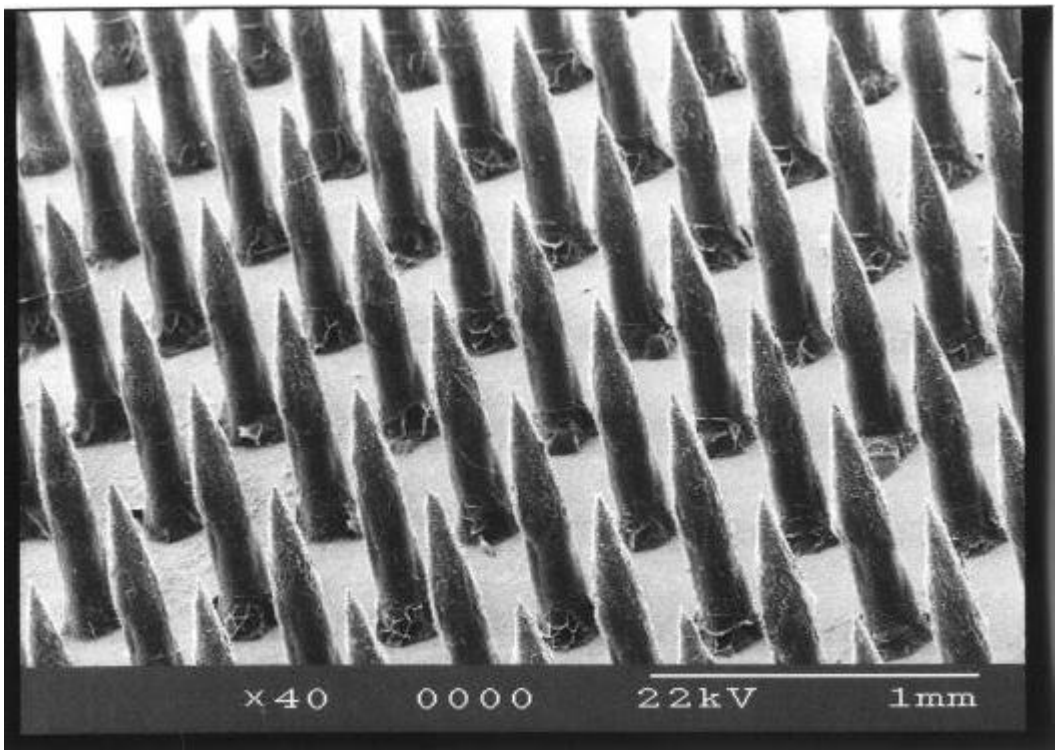

Figure 4.6: SEM image of polymyxin loaded PVP/trehalose microneedles.

4.4.5. Thermal Analysis

Thermal analysis of the drug loaded microneedles indicated that the addition of 20 mg/ mL of polymyxin had little to no effect on the degradation profile of the microneedle formulation. As per Figure 4.7, the degradation profile of the polymyxin loaded microneedle formulation was not significantly different to the unloaded sample (Figure 3.5) which was as expected given that the drug content was a relatively minor component of the formulation (0.05 % w/w).

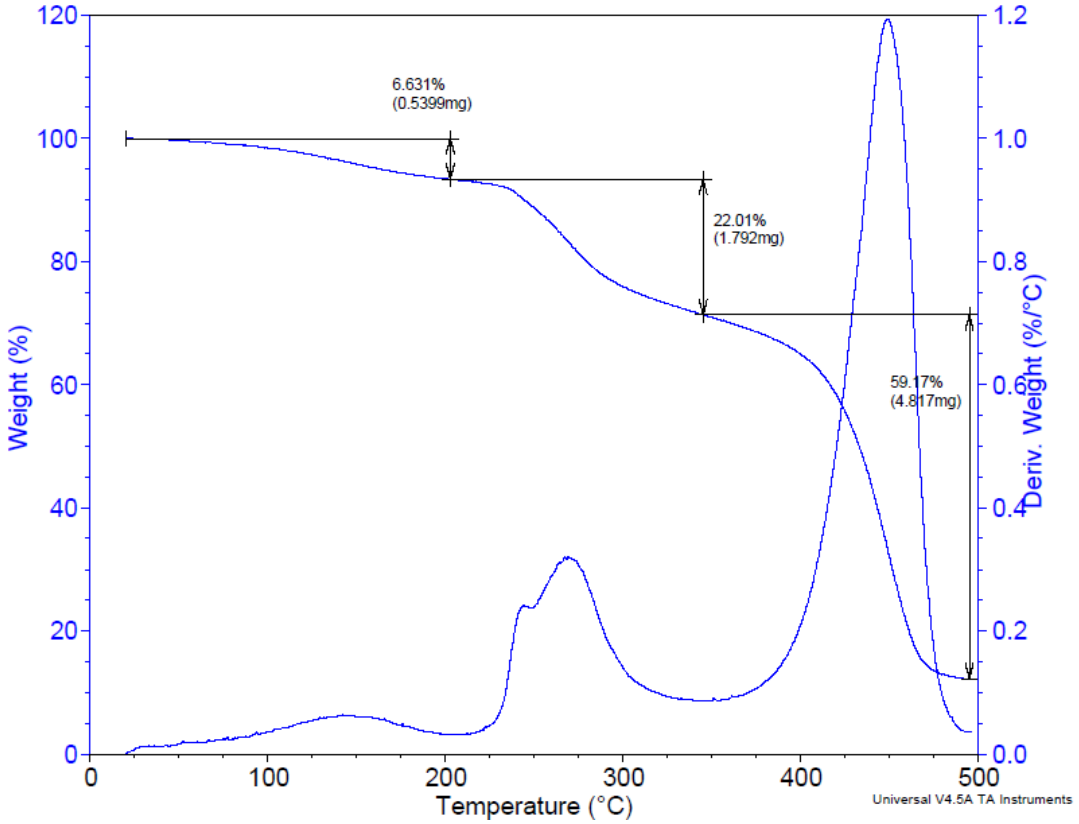

Figure 4.7: TGA thermogram detailing the degradation profile of optimum PVP/trehalose microneedle formulation sample (8.14 mg) incorporating 20 mg/ mL polymyxin.

DSC analysis indicated a reduction in T_g with the polymyxin loaded microneedle arrays compared with unloaded arrays from 111.25º C to 99.31º C (Figure 4.8). Nair *et al* (2001) carried out a study on the influence of a variety of small molecule drug on the T_g of PVP and reported significant lowering of T_g by as much as 40 ºC in PVP blends containing only 10 % w/w drug. The plasticising effect was attributed to hydrogen bonding interactions between the drug and the PVP [238]. Greater interaction between the PVP and the relatively larger polymyxin molecules could therefore potentially account for the observed drop in T_g although further studies would be required in this area. This reduction in T_g however, was not deemed to be detrimental to the functionality of the arrays or to have any significant effect on the structural integrity of the microneedles.

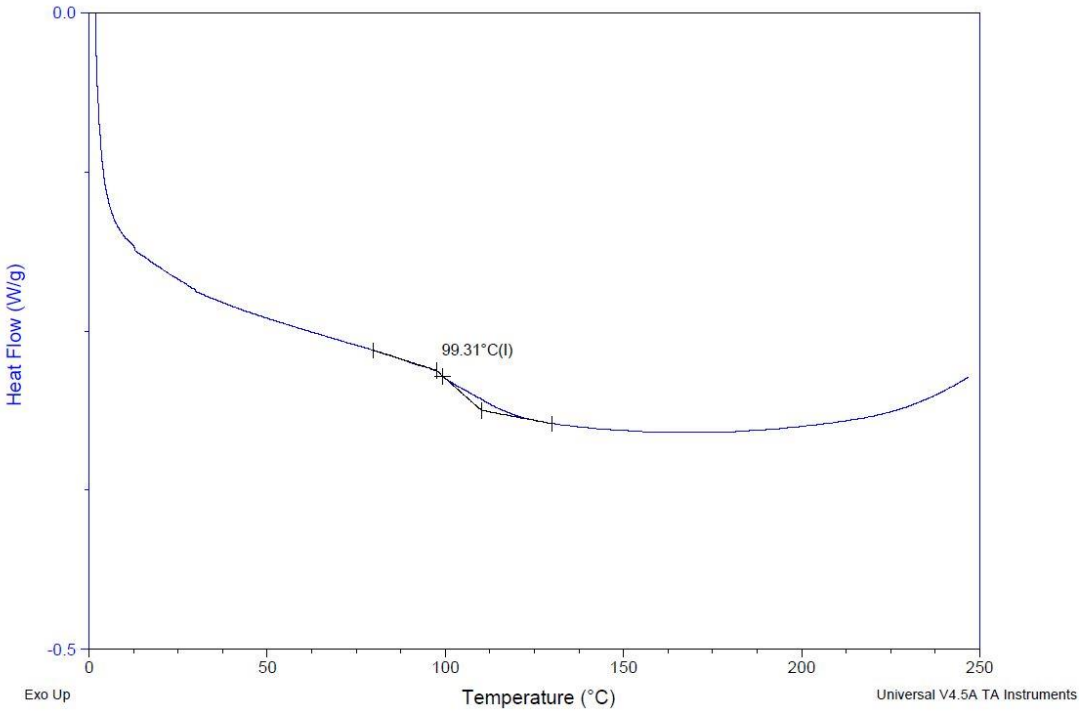

Figure 4.8: DSC thermogram detailing the T_g of the optimum PVP/trehalose microneedle formulation sample incorporating 20 mg/ mL polymyxin.

4.4.6. DVS

DVS analysis of the polymyxin loaded microneedle formulation was utilised to examine the water sorption properties of the PVP/trehalose microneedle formulation. Figure 4.9 illustrated that the mass increase of approx. 25% due to water sorption and the level of hysteresis was similar to that of the unloaded 3:1 PVP/trehalose formulation (Figure 3.6). As such, little effect on the sorption properties of the formulation was observed as a result of the addition of the polymyxin drug payload.

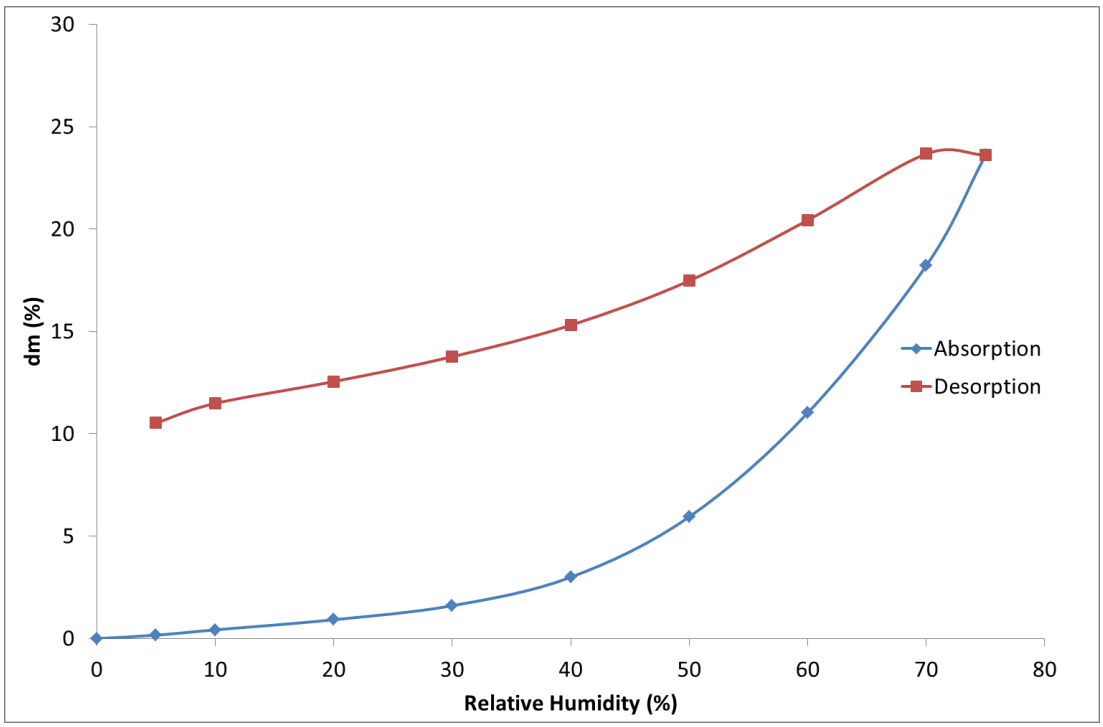

Figure 4.9: Sorption isotherm of polymyxin loaded MN's detailing level of hysteresis.

4.4.7. Skin Diffusion

Often animal skin models are used for *in vitro* penetration studies given that access to human skin can be difficult to obtain [239]. Many animal skin models exist from various mammals, rodents and reptiles, however, porcine skin was chosen for this study for a variety of reasons. Pig skin is generally regarded as a better skin model than most animal models, being closer to human skin based on biochemical properties, morphological and functional data. In addition, porcine ear skin is regarded as particularly suitable for permeation studies, giving results comparable with human skin [240]. Pig skin is also more readily available as waste material from slaughterhouses, which was the source of porcine skin for this study. The skin samples were stored at -20º C for 1-2 months before use, however, this was not expected to affect the permeability of the samples [216, 223].

The Franz cells were set up in a large water bath (Figure 4.10) with the temperature set to 37º C and the diffusion cells sitting in approx. 5 mm of water. The surface temperature of the skin sample was allowed to reach approx. 32º C, as per the

physiological temperature of the skin [241]. Great care was taken to ensure that each cell was placed upright and level to avoid any displacement of the receptor phase or drug material from the skin surface. The donor chambers were not covered to minimise the effects of occlusion where possible and during each sampling stage, the receptor chamber was checked to ensure no bubbles had formed directly beneath the skin sample, which could have adversely affected diffusion into the receptor phase. Care was also taken to avoid introducing air bubbles into the receptor phase when replacing fresh PBS solution during the sampling stages.

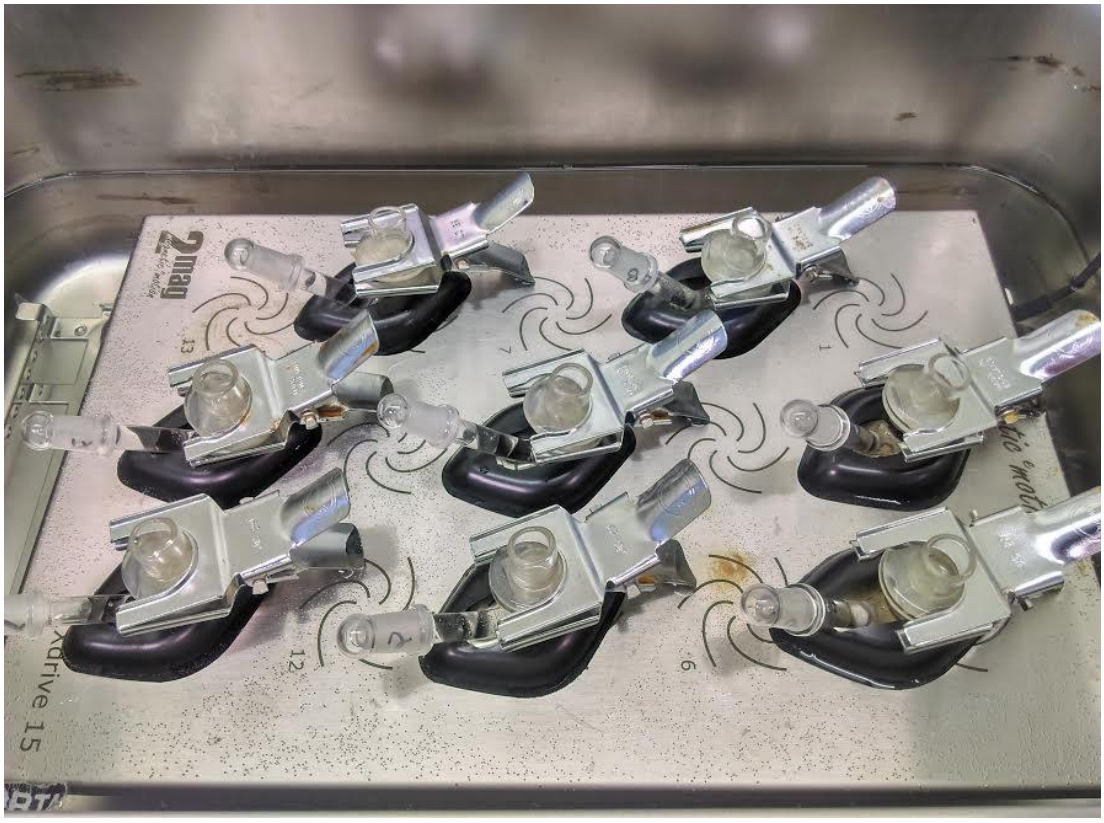

Figure 4.10: Franz diffusion cells set up on a Mixdrive 15 multi-position magnetic stirrer in heated water bath.

The diffusion test results indicated that the drug loaded microneedles initially delivered the polymyxin payload at a relatively rapid rate compared with the control during the first 5 h of the application (Figure 4.11). This suggested that during the initial stages of the application, the micro-channels created by the needles facilitated a rapid uptake of the drug payload. After this initial burst release, the levels of drug diffusion reverted to a rate approx. equivalent to the control disc. The rate of diffusion after this point most likely indicated the effects of occlusion caused by the

arrays covering the skin surface in addition to continuing diffusion through the micro-conduits. The results also indicated that, in addition to the drug contained within the microneedle shafts, drug material within the backing layer continued to diffuse into the skin via a combination of the micro-conduits created by the needles and the onset of occlusion. This diffusion of drug material from the base layer has not to the authors knowledge been previously observed with dissolving microneedle delivery of bioactive macromolecules without additional enhancement techniques [91]. Significantly, the results indicated that the drug payload within the needle shafts (0.22 mg) was rapidly delivered through the skin within 2 h (Table 4.2). Additionally, the rate of delivery from the microneedles was much higher over the initial 3 to 4 h of the experiment.

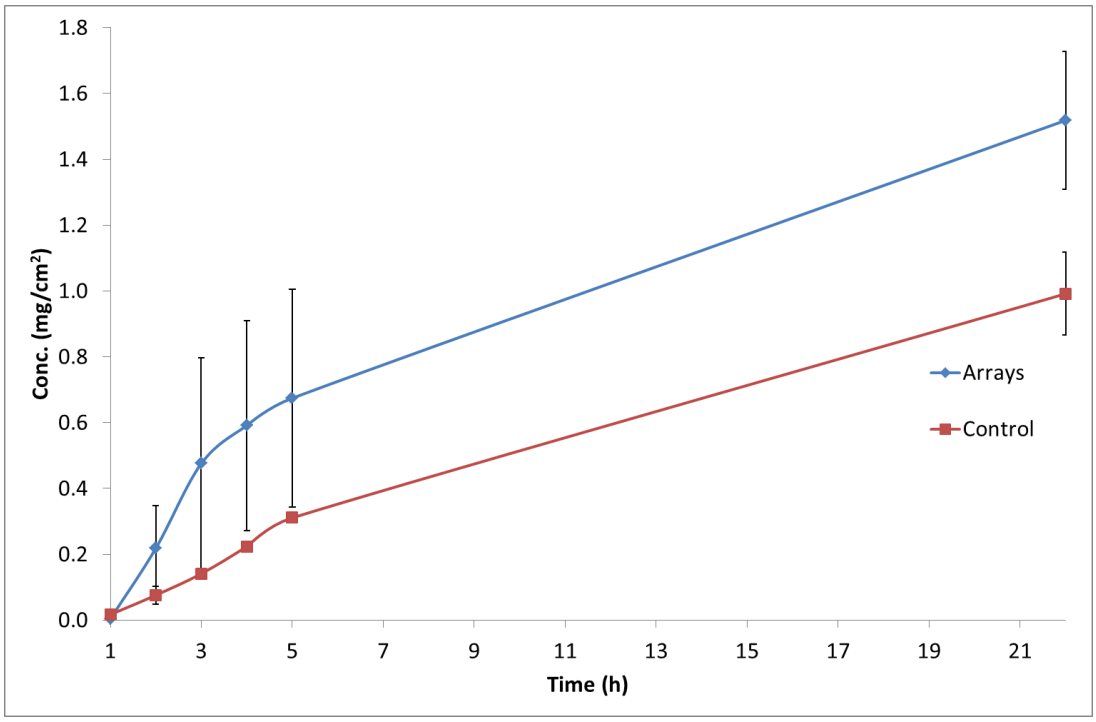

Figure 4.11: Plot of drug concentration delivered over time for microneedle arrays (n=3) and control disc.

As dissolution of PVP based microneedles is quite rapid [242], the microneedle mediated burst release was evident with the arrays. However, the viscosity of the PVP within the microneedle formulation as it began to hydrate may have been responsible for initiating occlusion, resulting in the increased drug diffusion observed in both the arrays and the control discs [23, 243]. A high degree of variability is commonly encountered when carrying out Franz cell diffusion tests on biological

samples and this is evident from the relatively large error bars indicating standard deviation across the samples [219, 222, 224].

Given that the main barrier to skin permeation is the non-viable SC, Fick's diffusion law (Equation 1.1) has been widely utilised to describe the diffusion process [240]. The permeation of molecules through the skin occurs, however, as a result of a number of physical, chemical and biological interactions many of which are nonlinear and as a result, mathematical modelling of percutaneous absorption can be challenging. To determine which kinetic model best described the release rate in each case, the polymyxin release data of the initial 5 h of the experiment for both the arrays and the control were examined using zero order, first order and Higuchi models. When the release rate is constant and independent of the drug concentration, zero order kinetics apply. The basic zero order equation is given as:

$$\boldsymbol{C = C_0 - K_0 t} \qquad \textbf{Equation 4-1}$$

Where:

C = amount of drug released

C_0 = initial amount of drug in solution

K_0 = Zero order rate constant

t = time (h)

To examine the release kinetics in relation to zero order, data is plotted as cumulative drug released as a function of time [244]. Similarly, first order kinetics can be used to describe the release of water soluble drug material in porous and highly permeable materials [217, 244]. The first order equation can be given as:

$$\boldsymbol{Log\ C = Log\ C_0 - Kt/2.303} \qquad \textbf{Equation 4-2}$$

Where:

C_0 = initial drug concentration

K = First order constant

t = time

When first order kinetics apply to a release rate, a straight line is obtained with a slope equal to K/2.303 when log of cumulative remaining drug is plotted against time [244].

The Higuchi equation was initially developed to describe the diffusion of a drug from an ointment and then later applied to solid drug diffusion dispersed in homogenous and granular matrix systems. Based on the principles of diffusion described by Fick's Law, the Higuchi equation describes the release of drug from a variety of topical dosage forms [245, 246]. The basic Higuchi equation is given as:

$$\boldsymbol{C = [D\,(2qt - C_s)C_s t]^{1/2}} \qquad \textbf{Equation 4-3}$$

Where:

C = total drug release per unit area of the matrix (mg/cm^2)

D = diffusion coefficient for the drug in the matrix (cm^2/h)

qt = total drug in a unit volume of the matrix (mg/cm^3)

C_s = dimensional solubility of the drug in the polymer matrix (mg/cm^3)

t = time (h)

Higuchi's model is based on a number of assumptions namely, that the initial drug concentration is higher than the drug solubility, drug diffusion occurs in one dimension, the drug particles are smaller than the thickness of the system, matrix swelling is negligible, perfect sink conditions are maintained and the diffusivity of the drug is constant. To determine whether the release kinetics fit this model, data is plotted as the cumulative percentage of drug release as a function of the square root of time (h) [244].

The data for the drug release from the arrays after 5 h (Table 4.1) most closely fit the Higuchi diffusion model, being linear with an r^2 of 0.9842 and directly proportional to the square root of time. As such, this indicated that the permeation rate was decreasing over the 5 h period in tandem with a decrease in drug concentration delivered.

Table 4.1: Results of model fitting for arrays and control 5 h.

Arrays	Model	SSR	r^2	Slope	Intercept
	Zero order	36.1116	0.956	8.86	-6.24
	First order	0.0007	0.9724	-0.05	2.039
	Higuchi	12.9514	0.9842	29.187	-28.61
Control	**Model**	**SSR**	r^2	**Slope**	**Intercept**
	Zero order	2.2905	0.9926	5.5747	-5.0865
	First order	0.0001	0.9851	-0.0277	2.0276
	Higuchi	12.0956	0.9612	17.782	-18.2

This could be attributed to the initial 'burst' release of polymyxin from the needles after application of the microneedle arrays which then reverted to a more steady release rate, comparable to the control after the same time period. The release of the drug from the control was determined to follow zero order kinetics, indicating that the rate remained constant irrespective of the drug concentration. This typically occurs where an excess of drug is applied to the skin surface and the depletion of drug over time is insignificant [218].

Transport of drug material across the skin typically involves molecular diffusion and is proportional to the drug concentration gradient and permeability of the SC to the drug itself [219]. Many properties of the skin are altered by occlusion including SC permeability, skin hydration, epidermal lipid composition and other cellular and molecular processes. Trapping of moisture, which would normally be lost from the skin surface, occurs leading to increased hydration of the SC and swelling of the corneocytes in addition to increased water uptake in the intercellular skin lipids. The barrier properties of the SC are reduced as a result of increased hydration and, as the SC is extremely hygroscopic, 500 % of its dry weight in moisture can be absorbed in approx. 1 h when immersed in water [25]. The temperature of the skin surface is also increased from 32 to 37 ºC. These factors all contribute to changes in percutaneous absorption [247].

The use of occlusion to improve the skin penetration properties of transdermally applied drugs is common given that water is an effective and safe permeation

enhancer [243], however, its effectiveness is not universal. Increased drug penetration has been observed in the case of lipid-soluble, non-polar molecules with less of an effect seen with more polar molecules. The effect of occlusion can be attributed to a number of factors such as partition coefficient, physico-chemical characteristics and the molecular weight of the drug [25]. In addition to the application of impermeable materials such as dressings or transdermal patches, occlusion can be achieved through the application of highly viscous or lipid based excipients [247]. Experimental requirements of percutaneous penetration such as the avoidance of evaporation from donor cells, loss of analyte and the maintenance of cell thermodynamics results in most studies being carried out under occlusive conditions [216, 247].

The diffusion of the drug which was apparent in both the microneedle treated skin samples and the control indicated that, contrary to expectations for a water soluble peptide drug, permeation through the skin is possible (Table 4.2).

Table 4.2: Drug diffusion at each time point and total drug recovered compared with measured drug content of each array and control.

Time (h)	Arrays (mg) (n=3)	Control (mg) (n=2)
1	0.004 ± 0.001	0.017 ± 0.016
2	0.219 ± 0.128	0.076 ± 0.027
3	0.476 ± 0.321	0.141 ± 0.014
4	0.591 ± 0.319	0.223 ± 0.007
5	0.675 ± 0.33	0.311 ± 0.011
22	1.517 ± 0.209	0.991 ± 0.013
Surface	0.134 ± 0.179	0.056 ± 0.056
Skin	0.281 ± 0.142	0.271 ± 0.026
Total drug recovered (mg)	1.933 ± 0.297	1.319 ± 0.155
Measured drug content (mg)	2.156 ± 0.068	1.689 ± 0.031
% Drug Recovered	89.7 %	78.1 %

In the case of the microneedle treated skin, the creation of micro-conduits by the needles themselves would be expected to facilitate the transportation of drug material through the SC and into the dermal layers. These micro-conduits were expected to remain open and allow drug material from the backing layer to continue to permeate long after initial application, with numerous studies indicating that micro-conduits

can remain open in living tissue for periods up to 72 h after treatment with microneedles [17, 73, 94, 98]. This was indicated by the fact that the concentration of drug contained in the receptor phase after 22 h (1.5 mg) far exceeded the calculated drug content of the needles themselves (0.22 mg). As such, it was clear that drug material from the base of microneedle arrays continued to diffuse into the skin after initial application and after the needles had delivered their drug payload. In contrast, the permeation of drug material through the control sample cannot be attributed to micro-conduits and may have been as a result of occlusion due the application of the PVP/trehalose formulation disc. Softening of the disc on contact with the skin surface would have resulted in the polymer/sugar formulation trapping moisture under the disc and causing the occlusive effect through retained moisture within the SC. This in turn would have affected the barrier properties of the SC and resulted in increased SC permeation [23]. This occlusion would have occurred with both the microneedle samples and the control and as such, may have resulted in steady delivery rate of drug in both sets over the 22 h of the experiment.

The microneedle formulation itself may also have contributed to the permeation of the polymyxin through the skin. The diffusion of drug from the control indicated that either the occlusive effects of the polymer/ sugar formulation or the permeation enhancement abilities of the formulation resulted in penetration of the polymyxin through the SC. Zhang *et al* [248] carried out peptide skin penetration studies, utilising solid microneedles to pre-treat porcine skin prior to application of aqueous peptide formulations. Controls consisted of the application of the peptide formulation to un-treated porcine skin. Drug permeation of the control samples was negligible which indicated that passive permeation across untreated skin was not viable without utilising some form of permeation enhancement. Transdermal patches incorporating PVP have been shown to have favourable drug permeation qualities [249, 250] and may indicate the permeation enhancement qualities of PVP to some extent.

When carrying out skin diffusion experiments, intra laboratory variability refers to variability which occurs due to natural variation in skin samples (inter subject variability), skin preparation techniques and analytical methods [239]. The variability observed between samples in relation to the amount of polymyxin in the receptor, the skin itself or remaining on the surface can be attributed to variations in the

composition of the samples themselves and variations in the thickness of each skin sample given that they were prepared by hand. Extraction of residual drug material from the skin sample was carried out by dissecting the skin after the diffusion experiment into approx. 20 pieces and immersing the skin in 2 mL of PBS and then subjecting it to agitation for approx. 4 h. A homogeniser was trialled as a means of extracting the maximum amount of residual drug at the end of the experiment however, the instrument required a minimum of 10 mL of sample solution in order to effectively homogenise the sample. As immersing the skin sample in 10 mL of PBS would have resulted in the sample being too dilute to analyse, the homogeniser method was not progressed.

Developing an efficient drug extraction procedure for diffusion studies can be challenging as interactions between the analyte and skin matrices, such as lipids and proteins, can result in low drug recovery [251]. Where full thickness skin is used, one potential disadvantage is that certain drugs, particularly lipophilic compounds, can be retained in the dermis instead of diffusing into the receptor fluid [216]. Despite this however, recovery of the drug was high across all arrays (average 90 %) and the control (average 78%) as per Table 4.2, with the majority of drug recovered from the receptor phase indicating that most of the drug payload was delivered through dermal layers of the skin.

4.5. Conclusions

The polymyxin model drug was incorporated into the PVP/trehalose microneedle formulation and successfully delivered through porcine skin. The activity of the model peptide was monitored at all stages of the process using well diffusion tests with no loss of activity observed. A HPLC method was also developed and optimised to separate and quantify the polymyxin from samples taken during the skin diffusion studies.

The fact that the needles were heavily loaded with the polymyxin drug to account for its low detectability and that successful delivery through porcine skin was achieved nonetheless indicated that the microneedle formulation was more than adequately robust to deliver more potent, low dosage peptides without any loss of mechanical strength or skin penetration ability. Delivery of drug through the skin from the control discs also suggested an enhanced permeation effect which could be attributed to the microneedle formulation itself, particularly PVP.

This study represents the first use of a PVP/trehalose based dissolving microneedle system to deliver a therapeutic peptide which has proven to retain the activity of the drug payload through all stages of the formulation process. The successful delivery of the polymyxin model drug exhibited the effectiveness of the microneedle system and as such, the next stage of the study will be to incorporate 2 synthesised therapeutic peptide analogues to examine the effectiveness of the microneedles in delivering peptides with a range of sizes and properties.

CHAPTER 5. DISSOLVING MICRONEEDLE BASED TRANSDERMAL DELIVERY OF SYNTHESISED PEPTIDE ANALOGUES

5.1. Introduction

5.1.1. Peptide Drugs

The chemical diversity of peptides and proteins is unmatched by any other class of biological molecule and the specificity of naturally occurring polypeptides has been refined by millions of years of evolution [43]. They are generally highly selective, efficacious and are effective in low concentrations [46]. Peptides play a crucial role in the regulation of most physiological processes and their therapeutic application has included uses in areas such as neurology, endocrinology and haematology [49]. However, they do have a number of drawbacks (Table 5.1) including relatively high production costs, poor metabolic stability and poor oral bioavailability.

Research is ongoing into developing the potential of a vast array of anti-microbial peptides as alternatives to traditional antibiotics [252]. Similarly, exploring the application of peptides as vaccines is ongoing with advantages over existing vaccines including ease of quality control, chemical stability and the absence of toxic or infectious material [44].

Table 5.1: Advantages and disadvantages of peptide drugs [253].

Advantages	**Disadvantages**
High potency	Poor metabolic stability
High selectivity	Poor membrane permeability
Broad range of targets	Poor oral bioavailability
Potentially lower toxicity than small molecules	High production costs
Low tissue accumulation	Rapid clearance
High chemical and biological diversity	Sometimes poor solubility
Discoverable at peptide and/or nucleic acid levels	

Over 100 peptide pharmaceuticals are currently available on the market in the U.S., Europe and Japan. The peptide drug market is estimated to be worth approx. US$15

billion annually in the U.S. alone with growth expected to result in market value of $23 billion by 2020 [254]. Of the many peptide based drugs available on the market today, the majority are smaller peptides consisting of 5-10 amino acids [253] including synthetic peptide drugs such as Sarenin® (8 aa), Integrilin® (7 aa), Firazyr® (10 aa), Tymtran® (10 aa), Kinevac® (8 aa), Peptavlon® (5 aa) and Zoladex (10 aa) to name a few [53].

5.1.2. Peptide Drug Delivery

The advantages of pharmacological peptides and proteins, which include high specificity and safety, are offset by the limitations in delivery methods available, notably the unsuitability of oral delivery due to gastrointestinal degradation, loss of activity and low intestinal absorption due to their hydrophilicity [47]. However, research continues into developing alternatives to the classic subcutaneous, intramuscular and intravenous delivery routes. These include nasal, pulmonary, sublingual and transdermal as well as studies aiming to make oral delivery viable [44, 255].

Transdermal delivery of peptides and proteins is hampered by the SC which provides an effective barrier to molecules that are charged, hydrophilic and have relatively high molecular weight. Strategies such as chemical or physical permeation enhancers and chemical or formulation modification techniques have been utilised to enhance dermal delivery of peptide and protein drugs [22]. Certain peptides however, have demonstrated permeation enhancement qualities for both transdermal and cell penetration applications. Investigations into the ability of certain peptides to act as skin permeation enhancers for macromolecules have been carried out with hypotheses on modes of action ranging from transient pore formation to interactions with skin lipids or keratin [256-258].

Microneedle mediated delivery of biopharmaceuticals has been explored, particularly the use of coated and dissolvable microneedle systems for the transdermal delivery of biologics such as vaccines [137-140]. The presence of various immunocompetent cells in the skin such as Langerhans cells, keratinocytes, dendritic cells and mast cells make transdermal vaccine delivery an attractive prospect. In addition,

transdermal delivery of insulin using microneedle systems has been widely investigated [135, 136, 143]. The transdermal delivery of therapeutic peptides using microneedle technology has also been explored with studies focussing on coated microneedle systems [259] and utilising pre-treatment of porcine skin with solid microneedles prior to the application of topical peptide formulations [248]. PVP based microneedles have also been investigated in the transdermal delivery of proteins [242].

5.1.3. Peptide Synthesis

Chemical synthesis, in particular solid phase peptide synthesis (SPPS) based on Fluorenylmethyloxycarbonyl (Fmoc) chemistry, is the most widely used method of peptide production (Section 1.4.3.). Chemical methods of peptide synthesis can be traced back over 100 years with the synthesis of the first N-protected dipeptide, benzoyl glycylclycine (Figure 5.1) by Theodor Curtius in 1881 using azide coupling. However, Emil Fischer synthesised the dipeptide glycylglycine (Figure 5.1) by hydrolysis of diketopiperazine in 1901 which is considered the beginning of peptide chemistry [46].

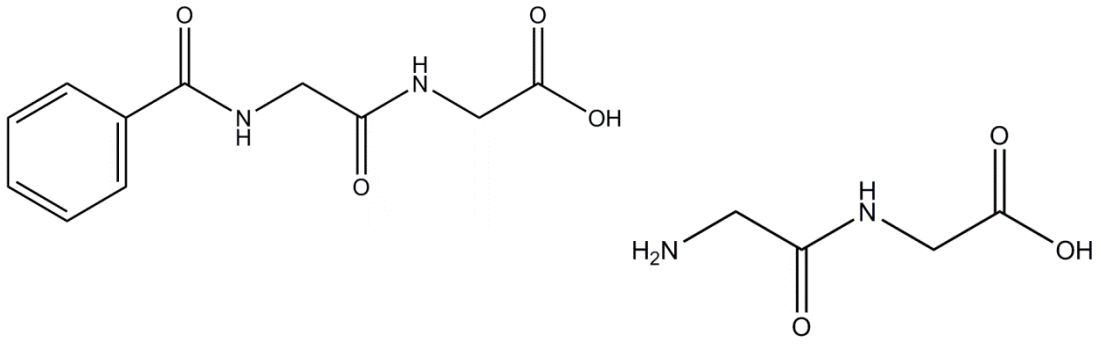

Figure 5.1: Chemical structure of benzoyl glycylglycine (left) [260] and glycylglycine (right) [261].

To overcome synthetic difficulties, further developments such as temporary amino protecting groups (i.e. carbobenzoxy (Cbz) in 1931 and *tert*- butyloxycarbonyl (Boc) in 1957), were introduced, however, a major breakthrough occurred with the discovery of SPPS by Bruce Merrifield in 1963 [46, 262]. Peptide synthesis continued to improve with key developments in automation, protecting groups and

purification techniques (Table 5.2). In general, the process of obtaining synthetic peptides begins with the design of the peptide followed by chemical synthesis, evaluation, purification and finally, application [262].

Table 5.2: Key discoveries in peptide chemistry [46].

Year	Discovery
1901	First published synthesised dipeptide
1957	Boc protecting group
1963	SPPS discovery
1967	Hydrogen Fluoride (HF) cleavage
1968	First automated solid phase synthesiser
1970	Benzhydrylamine (BHA) resin Fmoc protecting group
1973	Wang resin
1976	Preparative HPLC to purify peptides synthesised by SPPS
1977	Orthogonal protection
1987	Rink resin Sieber resin
1992	Fast Boc protocol
1994	Native Chemical Ligation (NCL) for protein and peptide synthesis
1996	Pseudoprolines

SPPS retains the chemistry of solid phase synthesis (SPS) but uses an inert resin as a support where the first amino acid of the peptide sequence is anchored via its C-terminus. Synthesis is then carried out in the C → N direction. Temporary protecting groups are attached to any reactive side chains and the alpha amino group of the amino acid being added. After each addition cycle, the alpha amino protecting group is removed, activating the amino site and allowing coupling with the C-terminus of the next amino acid in the sequence. This process is repeated until the required sequence is obtained and the peptide is then cleaved from the resin. Reactions are driven to completion through the use of excess soluble reagents which are removed

through filtration and washing steps [75]. Many protecting groups are used (e.g. Fmoc, Boc) and various resins can be utilised as solid supports (e.g. polystyrene, Wang, rink amide). Selection of the type of resin is an important step in the SPPS process and characteristics such as swelling properties (mL/g), substitution ratio (mmol/g) and particle size must be taken into consideration as each factor directly affects the purity and final yield of the peptide product [254].

5.1.3.1. Fmoc Synthesis

Fmoc based synthesis was introduced in 1970 by Carpino *et al* [263] and provided a chemically mild alternative to the acid labile Boc group as only moderate base is required in order to remove the alpha amino Fmoc protecting group (Figure 5.2). *T*-butyl based side chain protection was used in addition to hydroxymethylphenoxy based linkers to attach the peptide to the resin support [75]. The finished peptide can be cleaved from the solid support and de-protection of side chain functional groups can be attained under mildly acidic conditions [264]. Some problems associated with Fmoc synthesis included suboptimum solvation of the peptide/resin, slow coupling kinetics and base catalysed side reactions. Improvements in the basic chemistry, in addition to the use of different side chain protecting groups to minimise side reactions, have refined and improved Fmoc synthesis.

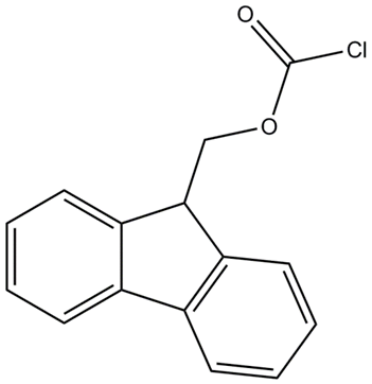

Figure 5.2: Chemical structure of fluorenylmethyloxycarbonyl chloride (Fmoc) group [265].

Cleavage of the peptide from the solid support in addition to removal of side chain protecting groups is typically carried out using trifluoroacetic acid (TFA) which can

also result in the release of reactive species that can cause modifications to susceptible residues such as tryptophan, tyrosine and methionine. These side reactions can be minimised through the use of scavengers such as thioanisole and triisopropylsilane to effectively quench reactive species during TFA cleavage [75].

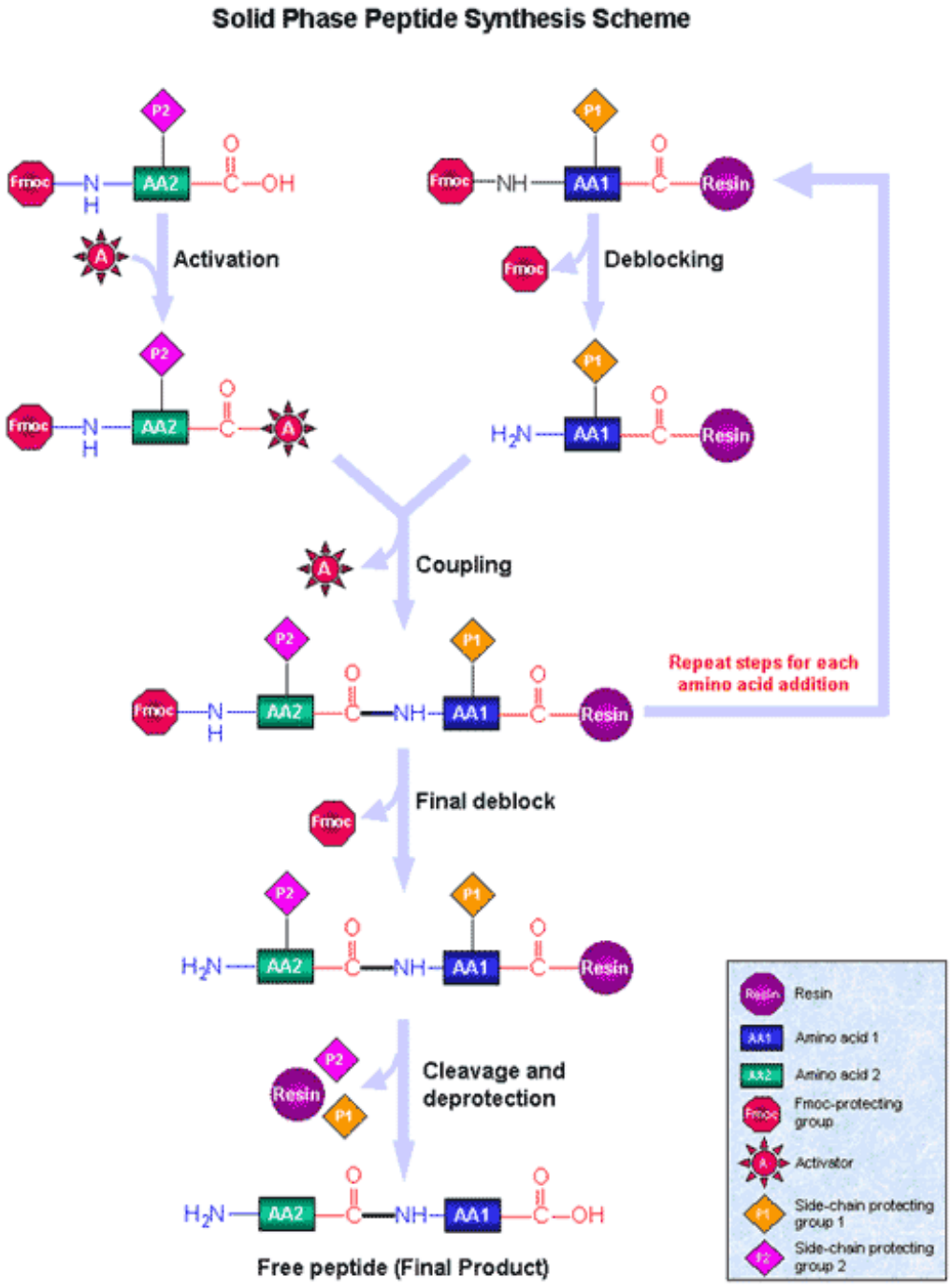

Figure 5.3: Illustration detailing the steps of the Fmoc SPPS [266].

Peptide analysis is commonly carried out using reverse phase HPLC in tandem with MS. Purification using semi-preparative HPLC is also widely utilised [267].

5.2. Objectives

The focus of this chapter was to synthesise analogue versions of 2 existing therapeutic peptides; pentagastrin and sincalide, utilising Fmoc based SPPS chemistry techniques. Once successfully synthesised and purified, the peptide analogues were characterised using LC-MS. The peptide analogues were then incorporated into the optimum PVP/trehalose microneedle formulation as previously described (Section 2.5) and skin diffusion testing carried out to determine the effectiveness of the microneedle system to deliver the peptide analogues through porcine skin. The results of this chapter were then compared with the diffusion results of Section 4.4.7 which used polymyxin B as the peptide drug cargo to evaluate the PVP/trehalose microneedle system's ability to successfully deliver peptides with a range of sizes and properties.

5.2.1. Pentagastrin and Sincalide Synthesis

Pentagastrin is a synthetic 5 amino acid polypeptide (Figure 5.4) which has the same biological effect as gastrin, stimulating the production of gastric acid and pepsin. For this reason, it has been used in oral bioavailability and gastric drug degradation studies [268]. In addition, as it produces flushing, palpitations and increased heartrate when administered parentally, it has been used in diagnostic stimulation tests for medullary thyroid carcinoma (MTC) [269] and panic disorders [270].

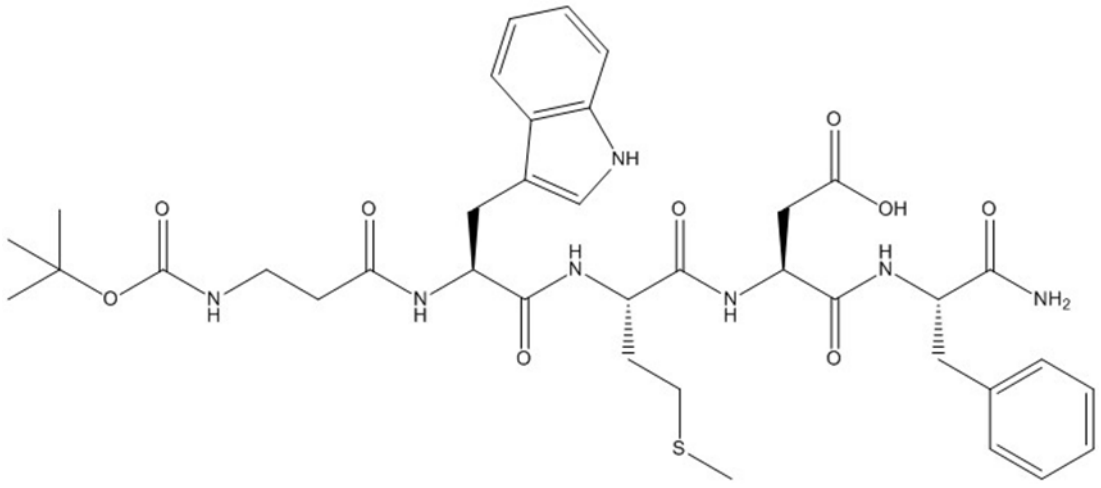

Figure 5.4: Chemical structure of pentagastrin [271].

Sincalide (brand name Kinevac) is an 8 amino acid therapeutic peptide (Figure 5.5) which is used to induce gallbladder and pancreatic secretions, similar to the effects of cholecystokinin. Intravenous bolus administration causes rapid contraction of the gallbladder and its uses include pancreatic function assessment, enzyme activity and the accelerated transit of a barium meal through the small bowel to reduce the level and duration of radiation associated with fluoroscopy and x-ray examination of the small intestine [272].

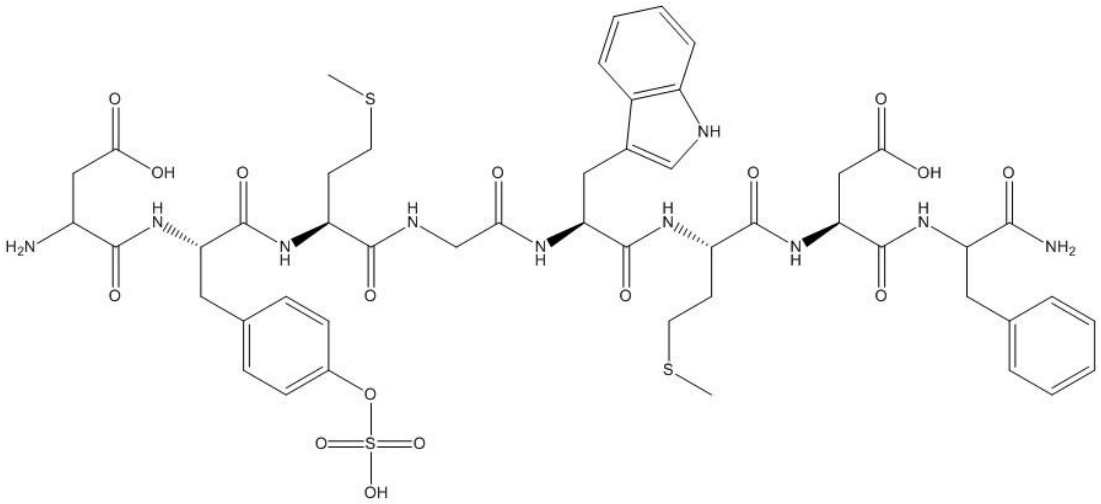

Figure 5.5: Chemical structure of sincalide [273].

5.3. Experimental

5.3.1. Materials

PVP average weight 40,000 Da supplied by Sigma Aldrich
Trehalose D(+)-trehalose dihydrate (≥98 %) obtained from Fisher Scientific
Glycerol – ACS grade obtained from Reagecon
Porcine ear skin (untreated) from male and female animals aged 5.5 years – supplied by Dawn Pork and Bacon, Waterford, Ireland
Phosphate buffered saline (PBS) solution obtained from Fischer Scientific

5.3.1.1. Peptide Synthesis Materials

Rink amide 4-methylbenzhydrylamine (≈1.1 mmol/g loading, 200-400 mesh particle size), polymer-bound purchased from Sigma Aldrich Ireland,
N-N- Dimethylformamide (DMF) supplied by Sigma Aldrich Ireland ,
1-Hydroxybenotriazole hydrate (HOBt) supplied by Lennox Laboratory Supplies,
N,N-Diisopropylethylamine (DIPEA) supplied by Sigma Aldrich Ireland ,
Phenol solution (80%) supplied by Lennox Laboratory Supplies,
Dichloromethane (DCM) supplied by Lennox Laboratory Supplies,
Thioanisole and Triisopylsilane supplied by Lennox Laboratory Supplies,
Trifluoroacetic acid (TFA) supplied by Sigma Aldrich Ireland,
2-(1H-benzotriazole-1-yl)-1,1,3,3-tetramethyluronium hexafluorophosphate (HBTU) supplied by Merck,
1,8-Diazabicyclo(5.4.0)undec-7-ene (DBU), potassium cyanide, ninhydrin, piperidine and diethyl ether supplied by Sigma Aldrich Ireland.

Amino Acids:
Fmoc-L-aspartic acid 4-*tert*-butyl ester (≥98 %), Fmoc-L-phenylalanine (98 %), Fmoc-L-alanine (95 %), Fmoc-L-methionine (≥98 %), Fmoc-O-*tert*-butyl-L-tyrosine (≥98 %), Fmoc-L-tryptophan (Boc) (≥97 %), Fmoc-glycine (≥98 %). All obtained from Sigma Aldrich Ireland.

Kaiser Test Reagents

5 g ninhydrin dissolved in 100 mL EtOH

0.4 mL 0.001 M potassium cyanide dissolved in 20 mL pyridine

40 g of phenol dissolved in EtOH

Cleaving Cocktail (10 mL)

8.8 mL TFA

500 µL DI water

200 µL Phenol (supplied by Lennox Laboratory Supplies),

250 µL Thioanisole (supplied by Sigma Aldrich Ireland)

250 µL Triisopropylsilane (supplied by Sigma Aldrich Ireland)

5.3.2. Methods

5.3.2.1. Fmoc Mediated Solid Phase Peptide Synthesis

1. Rink Amide Resin Preparation

0.25 mmol (0.272 g) of the rink amide resin was weighed out and placed in a glass peptide synthesis vessel. Approx. 20 mL of DCM was added to the vessel which was then capped and placed in a shaker for 30 min to allow the resin to swell. This improved access to the active sites on the resin. After this, the DCM was drained from the vessel using a flow of nitrogen.

2. De-protection of Resin/Amino Acid

25 mL of a de-protection cocktail consisting of 2 % piperidine and 2 % 1,8-Diazabicyclo(5.4.0)undec-7-ene (DBU) in DMF was added to the vessel. The vessel was then agitated for 10 min and the de-protection cocktail was drained using nitrogen flow. Another 25 mL of the de-protection cocktail was added to the resin and agitated for a further 10 min. After this, the de-protection cocktail was drained from the vessel using nitrogen and the resin beads were washed with DCM. The cap and threads of the vessel were carefully wiped to remove any trace of the de-protection cocktail and the beads were washed twice with DMF and then twice more with DCM.

3. Ninhydrin/ Kaiser test

To monitor the de-protection and coupling steps, a Kaiser test (ninhydrin test) for primary amines was carried out after each de-protection and coupling step. 2-3 drops of each Kaiser test reagent were applied to a small sample of the resin beads in a glass culture tube. The tube was then placed in a heated sand bath (110 ºC) for 5 min. An intense blue colour in the resin beads indicated the presence of free/unprotected primary amines.

4. Coupling Step

Once the de-protection step was confirmed, 1 mmol of amino acid was weighed out and placed in a 50 mL centrifuge tube along with 1 mmol HOBt (153 mg) and 0.95 mmol of HBTU (365 mg). 5 mL of DMF and 300 µL of DIPEA were then added to the centrifuge tube and the contents thoroughly mixed using a vortex. Once all components were fully dissolved, the coupling solution was added to the peptide synthesis vessel and agitated for approx. 2-3 h. After this, the coupling solution was drained from the vessel and the resin beads were washed twice with DMF and 3 times with DCM. The Kaiser test was carried out on a small sample of resin beads to confirm the coupling step was successful. No colour change observed indicated that the coupling step had been successful (i.e. absence of free primary amines). After this, the de-protection step was repeated and the coupling process repeated for the next amino acid on the sequence.

5. Cleaving Peptide from Resin

Once the last amino acid was coupled, a final Kaiser test was carried out to confirm the removal of the Fmoc group from this last amino acid in the peptide sequence. 10 mL of the cleaving cocktail was added to the vessel which was then agitated for approx. 1.5 h. The cleaving cocktail (in addition to the cleaved peptide) was then drained from the synthesis vessel with a nitrogen flow and collected in a round bottom flask. The beads were washed twice more with DCM which was also collected in the round bottom flask. Rotary evaporation was then used to remove excess solvent and the remaining solution was added dropwise to cold diethyl ether to precipitate out the peptide product. Prior to use, the diethyl ether was kept in a

cooling bath of sodium chloride and ice. The peptide was then placed in a centrifuge for 10 min at 3000 rpm to form a peptide pellet. Once formed, the diethyl ether was evaporated off leaving the crude peptide product.

6. Peptide Purification

A small sample of the crude peptide was dissolved in 50/50 solution of H_2O/ACN. UV/Vis spectroscopy was carried out on the sample to determine the λ max of the product. The sample was then analysed using Semi-prep HPLC and each main peak in the sample was collected and further analysed using LC-MS to determine the product peak based on the m/z. Once confirmed, the entire crude sample was dissolved in 5 mL of 50/50 solution of H_2O/ACN and purified using semi-prep HPLC. Once all peptide product fractions had been collected, the product was lyophilised and stored at -20 ºC.

5.3.2.2. HPLC Analysis

Pentagastrin Analogue Analysis

HPLC analysis was carried out using an Agilent 1100 with an Xterra reversed phase C_{18} 5 µm 4.6 x 250 column. A gradient method was developed using 2 mobile phase components: mobile phase A (water with 0.1 % TFA) and B (acetonitrile with 0.08 % TFA). Starting with 95 % mobile phase A and 5 % B, the gradient changed to 40% B over 30 min and back to 5 % B at 35.10 min, holding then for a total run time of 40 min. The injection volume was 40 µL with a flow rate of 0.5 mL/ min, column temperature of 40 º C and the detection wavelength was set at 280 nm.

Sincalide Analogue Analysis

HPLC analysis was carried out using an Agilent 1100 with an Xterra reversed phase C_{18} 5 µm 4.6 x 250 column. A gradient method was developed using 2 mobile phase components: mobile phase A (water with 0.1 % TFA) and B (ACN with 0.08 % TFA). Starting with 95 % mobile phase A and 5 % B, the gradient changed to 40% B over 30 min and back to 5 % B at 35.10 min, holding then for a total run time of 40 min. The injection volume was 40 µL with a flow rate of 0.5 mL/ min, column temperature of 40 º C and the detection wavelength was set at 220 nm.

5.3.2.3. Semi-Preparative HPLC

Semi-preparative HPLC was carried out using a Varian Prostar 210 with a Jupiter 10µm C_{18} 300A 250 x 10 mm column supplied by Phenomenex. A gradient run was used for each peptide which was adjusted to optimise peak separation for each sample. Mobile phase A consisted of H_2O with 0.1 % TFA and mobile phase B consisted of ACN with 0.08% TFA. For all samples, the flow rate was 1.8 mL/ min, column temperature was ambient and the injection volume used was 200 µL. The detection wavelength was set at 220 nm.

5.3.2.4. Liquid Chromatography–Mass Spectrometry (LC-MS)

LC-MS was carried out as described in Section 4.3.2.7.

5.3.2.5. Peptide Loaded Microneedles

Peptide loaded microneedles were prepared using the same fabrication methods described in Section 2.3.2. The 3:1 PVP: trehalose formulation with 2% w/w glycerol was prepared in 10 mL of DI water. 5 mg of the peptide analogue was then added to the formulation to give a concentration of 0.5 mg/ mL. Microneedle arrays were then cast with the loaded formulation using the vacuum oven method as per Section 2.3.2.6. Content uniformity studies were also carried out on each batch.

5.3.2.6. Franz Cell Skin Diffusion

Skin diffusion tests were carried out as per Section 4.3.2.8.

5.3.2.7. OCT

OCT analysis was carried out as per Section 3.2.2.13.

5.4. RESULTS & DISCUSSION

5.4.1. Peptide Synthesis

Fmoc synthesis was utilised in this study to synthesise two analogues of current therapeutic peptides, namely pentagastrin and sincalide. As both are simple polypeptides, this was a relatively straightforward synthesis, avoiding any cyclisation steps which were beyond the peptide synthesis techniques available for this study. Given that polymyxin is a cyclic peptide which consists of 10 amino acids, the use of pentagastrin and sincalide analogues provided a good comparison in relation to structure, size and molecular mass. Their use in the skin diffusion study indicated the ability of the microneedle systems to deliver peptides with a range of sizes, structure and properties (Table 5.3).

Table 5.3: Physical and chemical properties of polymyxin B_1, pentagastrin analogue and sincalide analogue

Peptide	MW (g/ mol)	AA Residues	Charge	Structure
Polymyxin B_1	1203.5	10	Cationic	Cyclic, lipid acyl tail
Pentagastrin	667.8	5	Anionic	Linear
Sincalide	1062.4	8	Anionic	Linear

Developing a method to successfully synthesise a peptide through Fmoc SPPS requires the consideration of a wide range of factors. Primarily, the type of peptide required dictates the type of solid support that is used. In addition, the amino acids required dictate the synthesis conditions and reagents that are used. Reaction times and cleavage cocktails are also chosen based on the amino acids in the peptide chain. The Fmoc peptide synthesis of both the pentagastrin and sincalide analogues was carried out using the same synthesis techniques of de-protection, washing, coupling and cleavage. Each synthesis differed only in the amino acids used. All amino acids used were Fmoc protected and did not require side chain protecting groups with the exception of aspartic acid (*tert*-butyl), tyrosine (*tert*-butyl) and tryptophan (Boc).

In solid phase peptide synthesis, the choice of solid support, coupling methodology, de-protection and cleavage steps are key aspects of the process [75]. Treating a peptidyl resin with a cleavage cocktail is not simply initiating the process of cleaving the peptide from the resin but consists of a number of competing reactions which can result in irreversible modification or damage to the peptide unless suitable reagents and conditions are utilised. In addition to cleaving the peptide from the resin, side chain protecting groups need to be removed and scavengers used to protect side chains from these highly reactive protecting groups. Examples of potential side reactions include: alkylation or oxidation of the tryptophan indole ring; alkylation of the tyrosine side chain; oxidation of methionine; and aspartimide formation with aspartic acid [264, 267, 274, 275]. De-protection stages were kept short (2 x 10 min reaction times) to prevent side reactions such as oxidation which can occur with both methionine and tryptophan (tryptophan oxidation was also minimised through the use of Boc protected tryptophan in this synthesis) [267]. In this case, DBU was used in the de-protection steps to remove the Fmoc protecting groups from the resin initially and from each subsequently coupled amino acid. DBU removes Fmoc protecting groups faster than piperidine alone and is unreactive towards the dibenzofulvene intermediary. As such, the use of piperidine in the decoupling solution was primarily to react with the dibenzofulvene by-product [276].

To achieve cleavage of the complete peptide molecule from the solid resin support, a cleavage cocktail containing TFA, DI water, phenol, thioanisole and triisopropylsilane was used. Complete cleavage of the peptide from the resin is usually achieved after 2 h of treatment with TFA, with 1.5 h considered optimal, particularly when methionine or unprotected tryptophan are used, which can be irreversibly modified during prolonged acid treatment [267].

Solvents are another important factor to consider during peptide synthesis. DMF is a widely used solvent in Fmoc-based synthesis, however, it can spontaneously break down over time to produce dimethylamine impurities which are reactive towards the Fmoc protecting groups. Formation of these impurities can be avoided by degassing the DMF prior to use and using freshly opened solvent. DCM is often used as a solvent as it provides good resin swelling and is unreactive towards TFA. It can however, slowly react with piperidine to form crystaline solids and as a result is more

commonly utilised in Boc rather than Fmoc based synthesis [276]. In this case however, de-protection was carried out using piperidine in DMF to minimize such side reactions from occurring. In the washing stages of the synthesis, DMF was used to remove excess reagents whereas DCM was used primarily to remove the residual DMF from the resin.

The pentagastrin analogue synthesised in this study differed from therapeutic pentagastrin in structure only by the absence of the (1,1-dimethylethoxy) carbonyl at the C-terminus. The synthesised peptide consisted of an amide C-terminus due to the use of rink amide as a solid support resin. The synthesised sincalide analogue retained the same amino acid sequence as the therapeutic peptide but without the sulfonyl group attached to the tyrosine residue. In addition, and as per the pentagastrin analogue, as rink amide was used as the solid support resin, this resulted in an amide C-terminus.

Typically, therapeutic peptides are chemically modified through the addition of D – amino acids, pseudo amino acids or cyclisation to improve stability [76] and as such, the stability of these synthesised analogues during the diffusion process needed to be monitored. The presence of trehalose in the microneedle formulation however was expected to contribute to preserving the stability of the peptides in addition to increasing their solubility [44, 277]. After purification, the pentagastrin and sincalide analogues were stored at -20 ºC until standards were prepared and before being incorporated into the microneedle arrays. HPLC analysis of the two peptide analogues after storage showed no indication of any degradation peaks and no degradation peaks were evident from any chromatograms of the peptides during the skin diffusion tests. This suggested that the peptides remained stable throughout the course of the study.

5.4.2. Pentagastrin Analogue

The Fmoc synthesis produced a pentagastrin analogue with the chemical formula $C_{32}H_{41}N_7O_7S$, a molecular weight of 667.78 g/mol and an exact mass of 667.28 g/mol (Figure 5.7).

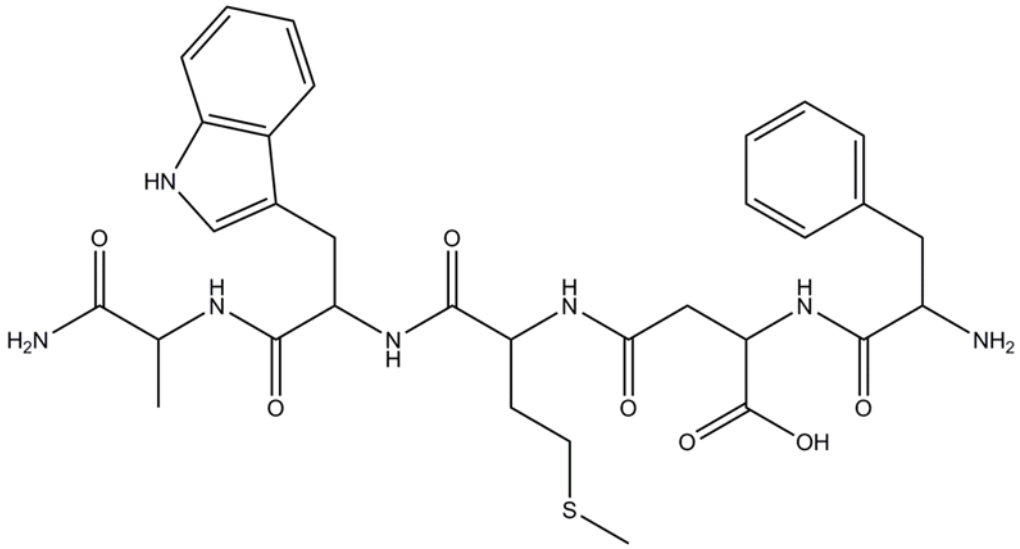

Figure 5.6: Chemical structure of synthesised pentagastrin analogue.

The theoretical yield of peptide was calculated as 199.8 mg using the following equation [276] :

$$\boldsymbol{Theoretical\,Yield\ (mg) = s_{resin} \times m_{resin} \times MW_{peptide}} \qquad \textbf{Equation 5.1}$$

Where: s_{resin} = loading capacity of the resin (mmol/g)
m_{resin} = dry mass of resin used (g)
$MW_{peptide}$ = MW of peptide product (mg)

The final yield of purified peptide was 28.15 mg which equated to only 14 % of the theoretical yield, however, low yields in SPPS (< 20 %) are not uncommon. This is due to the amplifying effects that a decrease in the coupling efficiency of each amino acid addition can have on the final purity of the peptide [254]. The estimated physiochemical properties of the synthesised analogue (Table 5.4) were calculated using the GenScript® online peptide calculator resource [259]. This suggested that the pentagastrin analogue was acidic and anionic with a net charge of -1 at pH 7.

Table 5.4: Peptide properties generated by the GenScript® online peptide calculator resource, as used in previous studies [259].

Peptide Analogue	AA Sequence	Charge	Isoelectric point	pH	Overall % of hydrophobic and hydrophilic residues
Pentagastrin	FDMWA	-1	5.44	Acidic	Hydrophilic: 20% Hydrophobic: 80%
Sincalide	FDMWGMYD	-2	3.90	Acidic	Hydrophilic: 25% Hydrophobic: 62.5% Neutral: 12.5%

5.4.2.1. LC-MS Analysis and Semi Prep HPLC

LC-MS was utilised to determine the peptide peak from the impure sample obtained directly after the synthesis procedure (Figure 5.8). Once identified, the peptide peak was collected using Semi Prep HPLC.

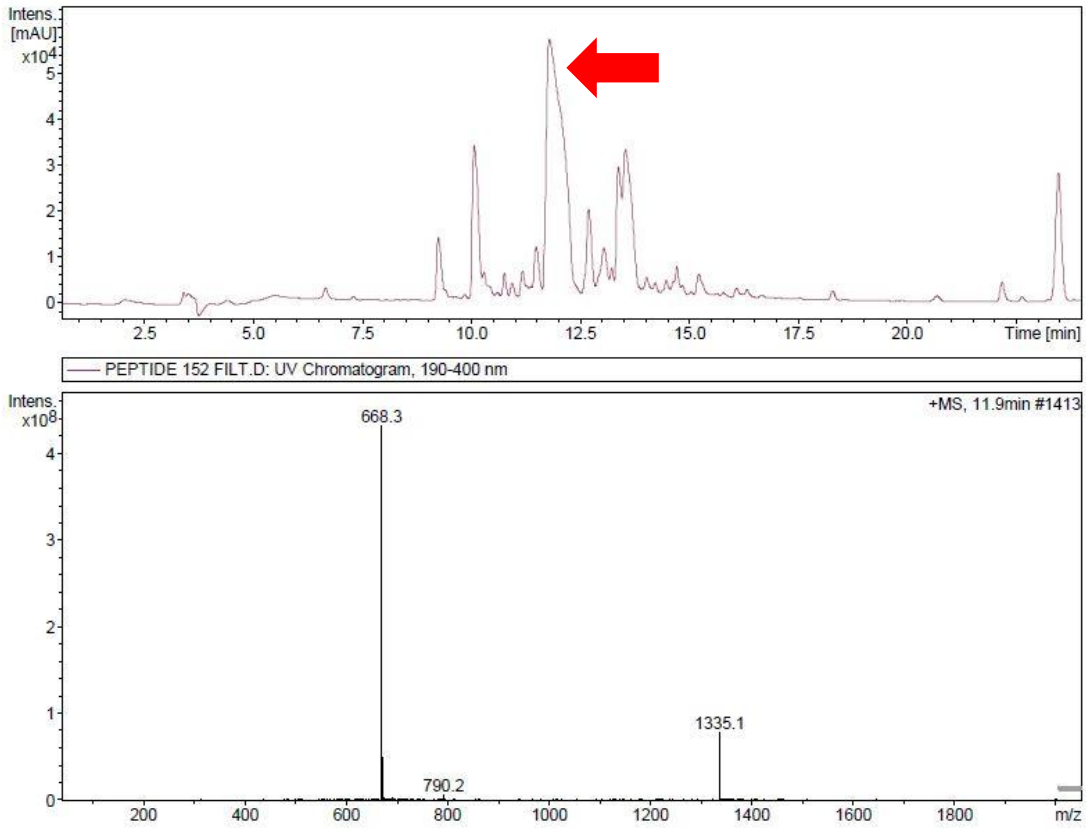

Figure 5.7: LC-UV chromatogram of impure pentagastrin analogue sample showing the pentagastrin peak at 11.9 min (top) with the corresponding mass spectrum of the peak displaying the $[M+H]^+$ ion at m/z = 668.3 Da (bottom).

After all sample fractions had been collected and lyophilised, the purified peptide was analysed once again on LC-MS (Figure 5.9) to confirm collection of the synthesised peptide.

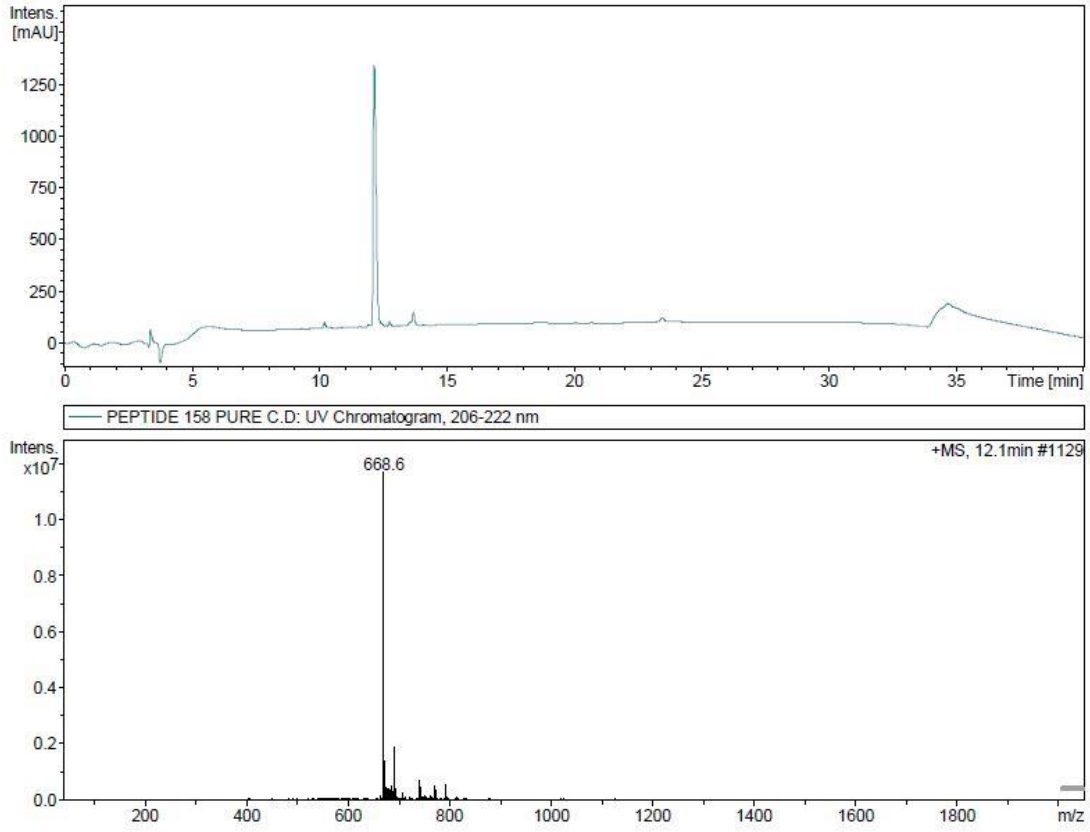

Figure 5.8: LC-UV chromatogram of purified pentagastrin analogue showing the pentagastrin peak at 11.9 min (top) with the corresponding mass spectrum of the peak displaying the $[M+H]^+$ ion at m/z = 668.6 Da (bottom).

5.4.2.2. OCT

The depth of penetration of pentagastrin loaded microneedle arrays was measured using OCT with Figure 5.10 detailing the average penetration depth of 7 individual shafts on the array which was measured as 405 ± 19 µm. The average diameter of the micro-pores formed by the needles was also measured and determined as 237 ± 7 µm which approximately corresponded with the diameter of the needles at the base. This may have indicated that the penetration depth at the point of initial application was deeper than when the image was captured. The elastic resistance of the skin [84] may have resulted in the arrays lifting from the surface of the skin once the pressure of the

initial application was lifted. The distance between the base of the arrays and the skin surface was also measured giving an average distance of 364 ± 10 µm (n=7).

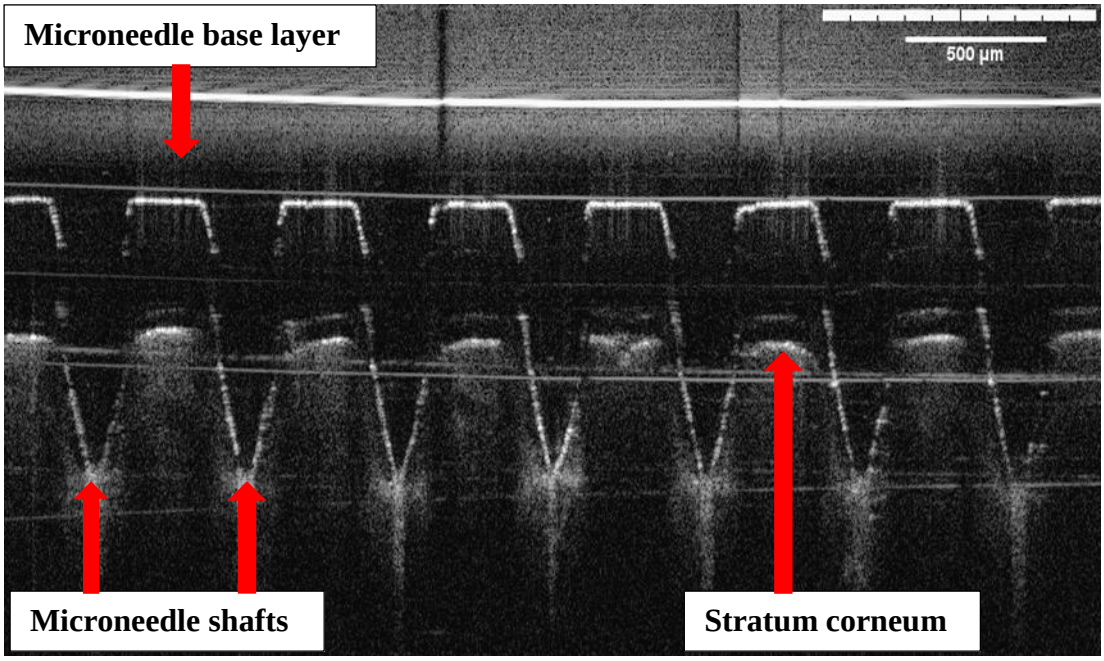

Figure 5.9: OCT image detailing penetration depth of pentagastrin analogue loaded microneedles. This image details needles with an average penetration depth of 405 ± 19 µm (n=7). The dimensions of the arrays used were 750 µm length shafts with a base width of 200 µm and inter-needle spacing of 600 µm.

These results indicated that the pentagastrin needles penetrated the SC and dermal layers to at least a depth equivalent to half the length of the individual needles. The OCT analysis also highlighted the uniform penetration depth across the array with a similar depth achieved by each shaft in the image.

5.4.2.3. Skin Diffusion Study

Skin diffusion testing was carried out on the pentagastrin-loaded microneedles as per the polymyxin loaded arrays (Section 4.3.2.8). No deviation in the Franz cell diffusion procedure was carried out with the exception of the sampling times, which were altered to 30 min intervals for the first 3 h of the experiment in order to obtain a better understanding of the release rate during the initial stages of the diffusion experiment. The HPLC gradient method which was developed for the polymyxin analysis (Section 4.3.2.6) was also utilised to analyse the pentagastrin samples

(Figure 5.11). The method was developed and validated in accordance with ICH guidelines [234]. The LOD and LOQ were determined based on the standard deviation of the response and the slope of the representative calibration curve. The LOD was determined as 0.31 µg/ mL and the LOQ was determined as 1.05 µg/ mL. Calibration curves for the pentagastrin analogue standards were linear in the concentration range of 625 ng / mL to 20 µg/ mL with r^2 values of > 0.99.

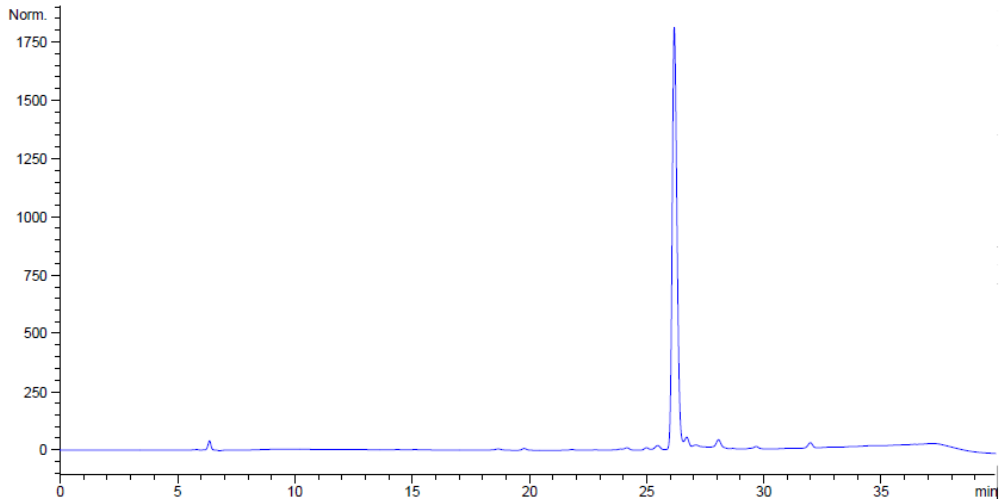

Figure 5.10: Chromatogram of pentagastrin analogue peak with retention time of 26.2 min, using HPLC gradient method developed for polymyxin analysis.

As per the polymyxin skin diffusion tests, the initial release rate of pentagastrin from the microneedle arrays was far higher than that of the control discs during the first hours after application (Figure 5.12). Again, this suggested that the penetration of the SC by the needles facilitated rapid delivery of the drug payload initially from the needles and then, as the arrays began to dissolve, as a result of further diffusion from the backing layer through the micro-pores formed by the needles.

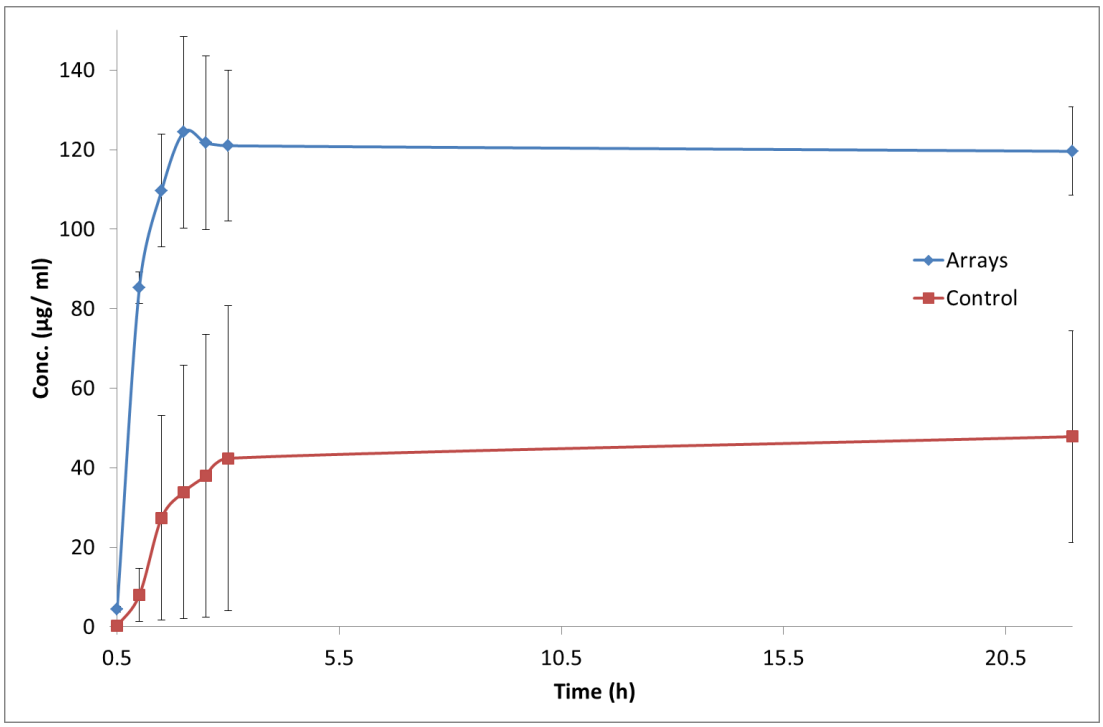

Figure 5.11: Plot detailing the total amount of the pentagastrin analogue content delivered into the receptor phase over time per microneedle arrays (n=3) and control discs (n=2).

Similarly also to the polymyxin arrays (Figure 4.11), the levels of drug diffusion reverted to a rate equivalent to the control discs after approx. 3 h although the data suggests that the rate at this stage for the pentagastrin arrays was almost zero. The concentration of drug delivered from the pentagastrin loaded control discs was far lower than the concentration of drug delivered by the arrays (Table 5.5) which indicated that, although some diffusion occurred as a result of the occlusive effects of the dissolved formulation and possible permeation enhancement of the formulation itself, the pentagastrin peptide did not pass through the SC as readily as polymyxin B. Although pentagastrin is a smaller peptide consisting of only 5 amino acids compared with polymyxin which contains 10, the enhanced penetration of the polymyxin in comparison to pentagastrin may have occurred as a result of the structure and amphipathic properties of the polymyxin [278], particularly its detergent and membrane penetrating qualities in relation to cells with high lipid content [202, 204]. The higher loading of polymyxin in the arrays (20 mg/ mL) may also have resulted in an increased concentration gradient and subsequently, a greater driving force for diffusion compared to the lower pentagastrin concentration (0.5 mg/

mL) [218]. As such, the rapid deposition of drug content from the microneedle shafts after application could explain the initial high delivery rate.

Table 5.5: Drug diffusion at each time point and total pentagastrin recovered compared with measured drug content of each array and control.

Time (h)	Arrays (µg) (n=3)	Control (µg) (n=2)
0.5	4.49 ± 0.67	0.20 ± 0.05
1	85.29 ± 8.04	8.04 ± 6.61
1.5	109.67 ± 14.15	27.42 ± 25.75
2	124.38 ± 24.08	33.92 ± 31.91
2.5	121.67 ± 21.83	37.99 ± 35.61
3	120.99 ± 18.99	42.39 ± 38.34
22	119.58 ± 11.09	47.83 ± 26.61
Surface	1.37 ± 1.01	11.17 ± 10.20
Skin	8.44 ± 0.99	12.41 ± 12.17
Total drug recovered (µg)	129.39 ± 10.99	71.41 ± 4.23
Measured drug content (µg)	144.70 ± 14.35	126.56 ± 13.29
% Drug Recovered	89.4 %	56.4 %

Drug recovery from the arrays was high at ≈90 % however, only 56 % of the initial drug load was recovered from the controls (Table 5.5). The absence of degradation peaks on the HPLC chromatograms suggested that the pentagastrin remained stable during the diffusion study and as such, discounted peptide instability as a cause of the low recovery. A possible explanation may have been that the hydrophobic nature of the phenylalanine and tryptophan residues of the peptide may have resulted in high levels of drug retention in the lipid layers of the SC. As such, the skin surface swabbing and drug recovery steps carried out in PBS solution after the diffusion test may have been inefficient at removing any residual drug retained in the skin layers.

The release rate of the pentagastrin from the microneedle arrays during the first 2 h of the study most closely fit a first order release rate with an r^2 of 0.98 (Table 5.6). Model fitting of the control disc drug release indicated that the rate correlated with both zero and first order rates with r^2 values of 0.96. This suggested that, unlike polymyxin, the pentagastrin permeation from the control disc was more passive and most likely due to the occlusive effects of the formulation. The first order nature of

the pentagastrin release from the arrays in the first 2 h can be attributed to the initial deposition of drug from the needles combined with the subsequent increase in permeability due to the micro-channels formed by the arrays. In addition, the onset of occlusion from the formulation would have contributed to the drug release rate.

Table 5.6: Results of model fitting for pentagastrin loaded arrays and control after 2 h of the diffusion study.

Arrays	Model	SSR	r^2	Slope	Intercept
	Zero order	0.058	0.86	0.531	-0.105
	First order	0.006	0.98	0.549	0.22
	Higuchi	0.033	0.92	1.165	-0.707
Control	**Model**	**SSR**	**r^2**	**Slope**	**Intercept**
	Zero order	0.002	0.96	0.19	-0.101
	First order	0.001	0.96	0.096	0.053
	Higuchi	0.002	0.95	0.402	-0.299

5.4.3. Sincalide Analogue

Synthesis produced a sincalide analogue $C_{49}H_{62}N_{10}O_{13}S_2$ with a molecular weight of 1063.21 g/mol and exact mass of 1062.39 g/mol (Figure 5.13). The theoretical yield was calculated using Equation 7 and determined as 318 mg. The final yield of purified peptide was 26 mg which represented a % yield of 8.2 %. This low yield may have been as a result of the additional coupling steps in the sincalide synthesis compared with that of pentagastrin.

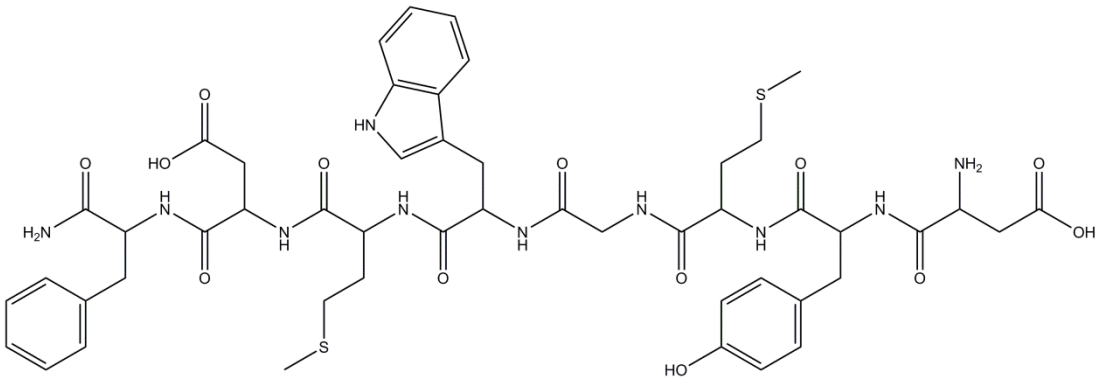

Figure 5.12: Chemical structure of the synthesised sincalide analogue.

The amplifying effects of coupling inefficiency on the final purity of the peptide, as described with pentagastrin, could potentially have a greater effect on the sincalide synthesis due to its longer chain length. [254]. The estimated physiochemical properties of the synthesised analogue were calculated using the GenScript® online peptide calculator resource (Table 5.4) [259]. This suggested that the sincalide analogue was acidic and anionic with a net charge of -2 at pH 7.

5.4.3.1. LC-MS analysis and Semi Prep HPLC

As with the pentagastrin analogue, LC-MS was utilised to determine the peptide peak from the impure sample obtained directly after the synthesis procedure (Figure 5.14). Semi Prep HPLC was then utilised to isolate the pure peptide from the crude sample. After all sample fractions had been collected and lyophilised, the purified peptide was analysed once again on LC-MS (Figure 5.15) to confirm that collection of the synthesised peptide was successful

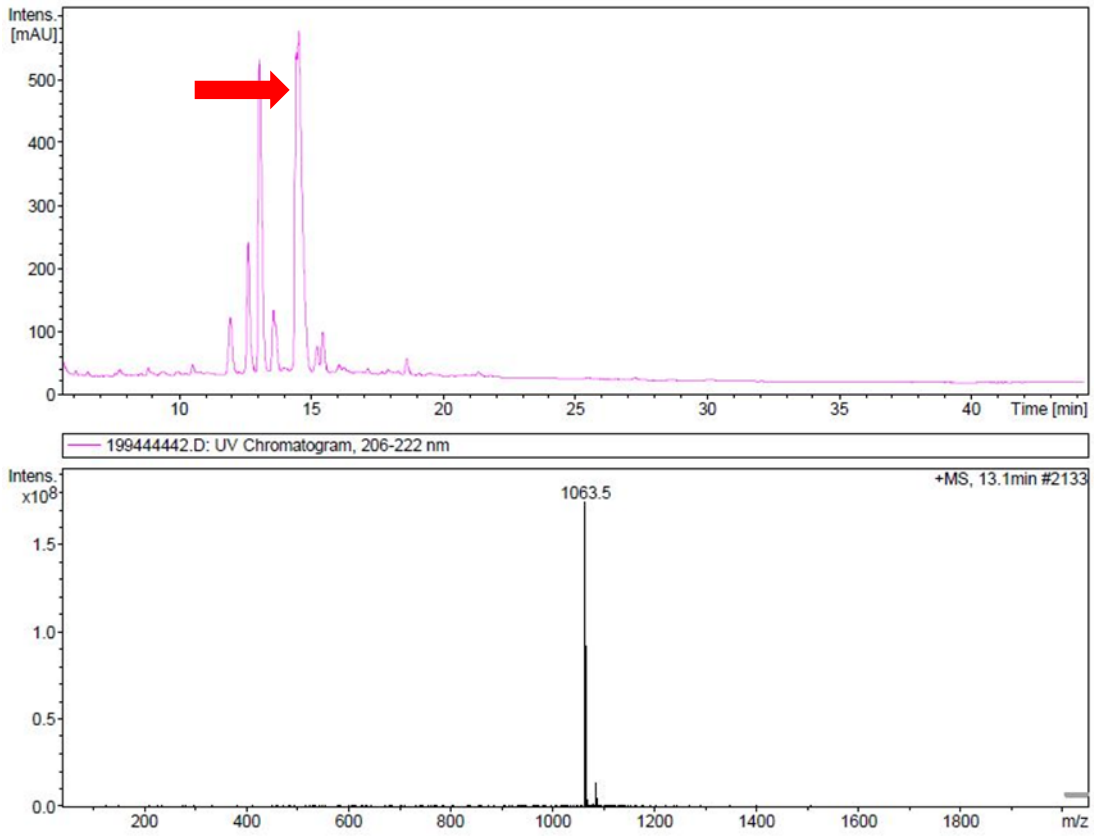

Figure 5.13: LC-UV chromatogram of impure sincalide analogue sample showing the sincalide peak at 14.4 min (top) with the corresponding mass spectrum of the peak displaying the $[M+H]^+$ ion at m/z = 1063.5 Da (bottom).

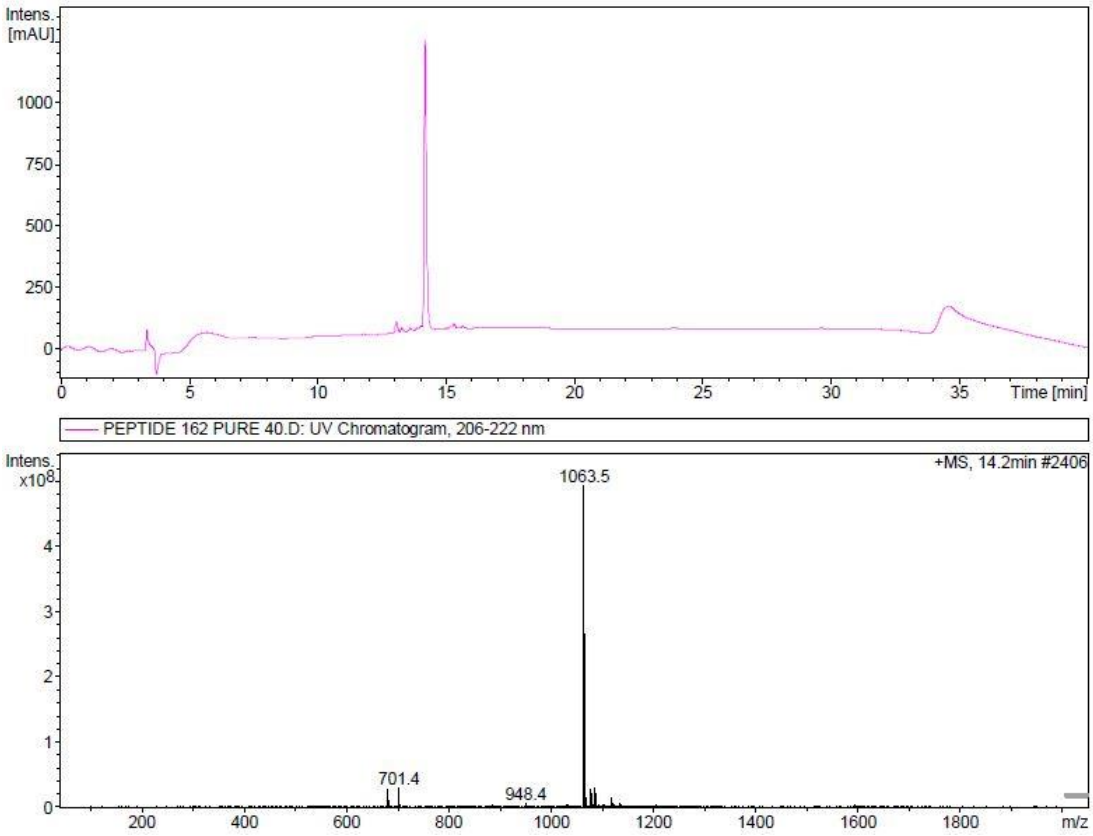

Figure 5.14: LC-UV chromatogram of purified sincalide analogue showing the sincalide peak at 14.4 min (top) with the corresponding mass spectrum of the peak displaying the $[M+H]^+$ ion at m/z = 1063.5 Da (bottom).

5.4.3.2. OCT

The skin penetration of the sincalide loaded microneedle arrays was imaged using OCT with the penetration of 7 individual shafts detailed as per Figure 5.16. The average penetration depth of the 7 needles was measured as 284 ± 19 µm. The average diameter of the micro-pores formed by the needles was also measured and determined as 225 ± 14 µm and the distance between the base of the arrays and the skin surface was measured with an average distance of 341 ± 23 µm. Contrast in the image between the array and the skin was not as clear as the image obtained with the pentagastrin arrays. This was attributed to a higher level of hydration of the skin site used for the sincalide array application which resulted in a more rapid dissolution time and subsequently, a less defined image. Despite this, the penetration qualities of the array were evident and the penetration depths achieved indicated that the arrays could successfully deliver the drug payload.

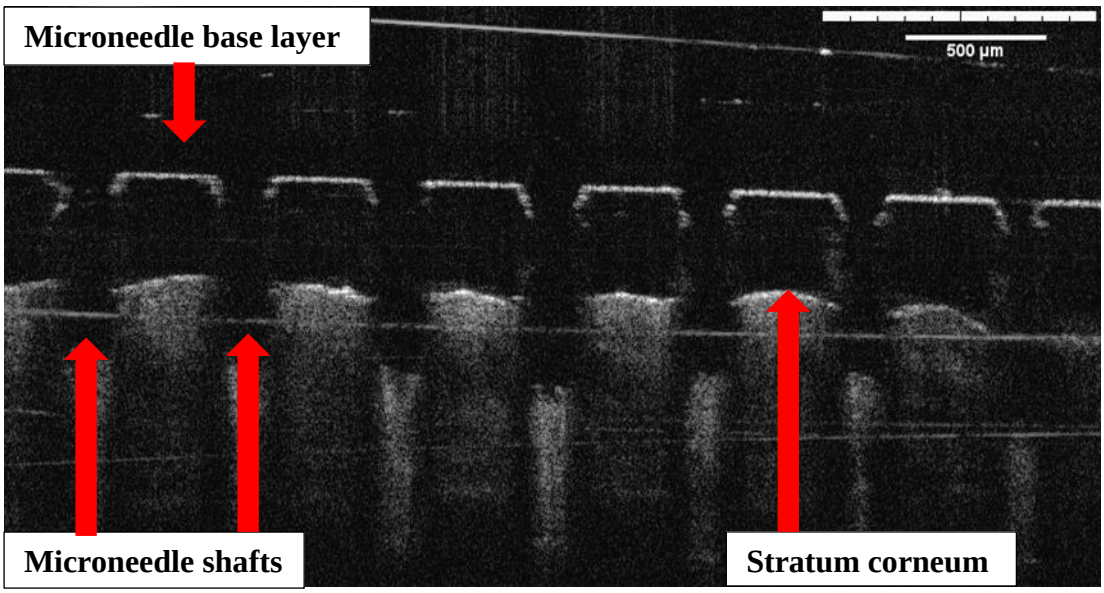

Figure 5.15: OCT image detailing penetration depth of sincalide analogue loaded microneedles. This image details needles with an average penetration depth of 284 ± 19 µm (n=7).

5.4.3.3. Solubility Study

Initial diffusion experiments with the sincalide analogue resulted in poor drug recovery which was attributed to the poor solubility of the peptide and as such, a solubility study was carried out. The study found that the addition of 20 mg of Tween® 80 to a 10 mL PBS solution containing 1 mg of the sincalide analogue resulted in a 30 % increase in saturation solubility (0.07 mg/ mL) compared with the addition of 10 mg of Tween® 80 (0.05 mg/ mL) or PBS solution alone (0.06 mg/ mL) (Figure 5.17). Given these results, subsequent skin diffusion studies utilised the addition of 2 mg/ mL Tween® 80 to the PBS based receptor phase. Due to the low yield of sincalide obtained from the synthesis, and therefore limited supply of the peptide, this study was carried out once with n=1.

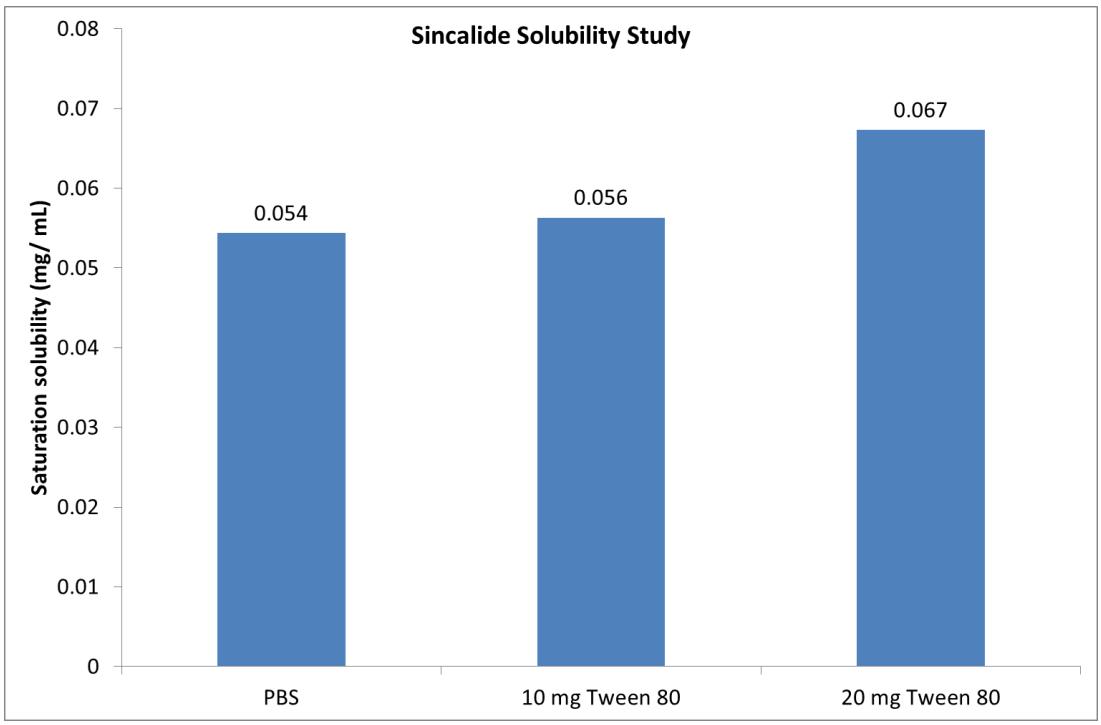

Figure 5.16: Chart detailing the saturation solubility of 3 sincalide solutions (n=1).

5.4.3.4. Skin Diffusion Study

Skin diffusion testing was carried out as per the pentagastrin loaded arrays (Section 5.4.2.3). The HPLC gradient method developed for the polymyxin analysis (Section 4.3.2.6) was also utilised to analyse the sincalide samples (Figure 5.18). The method was developed and validated in accordance with ICH guidelines [234]. The LOD and LOQ were determined based on the standard deviation of the response and the slope of the representative calibration curve. The LOD was determined as 0.43 µg/ mL and the LOQ was determined as 1.42 µg/ mL. Calibration curves for the sincalide analogue standards were linear in the concentration range of 625 ng/ mL to 20 µg/ mL with r^2 values of > 0.99.

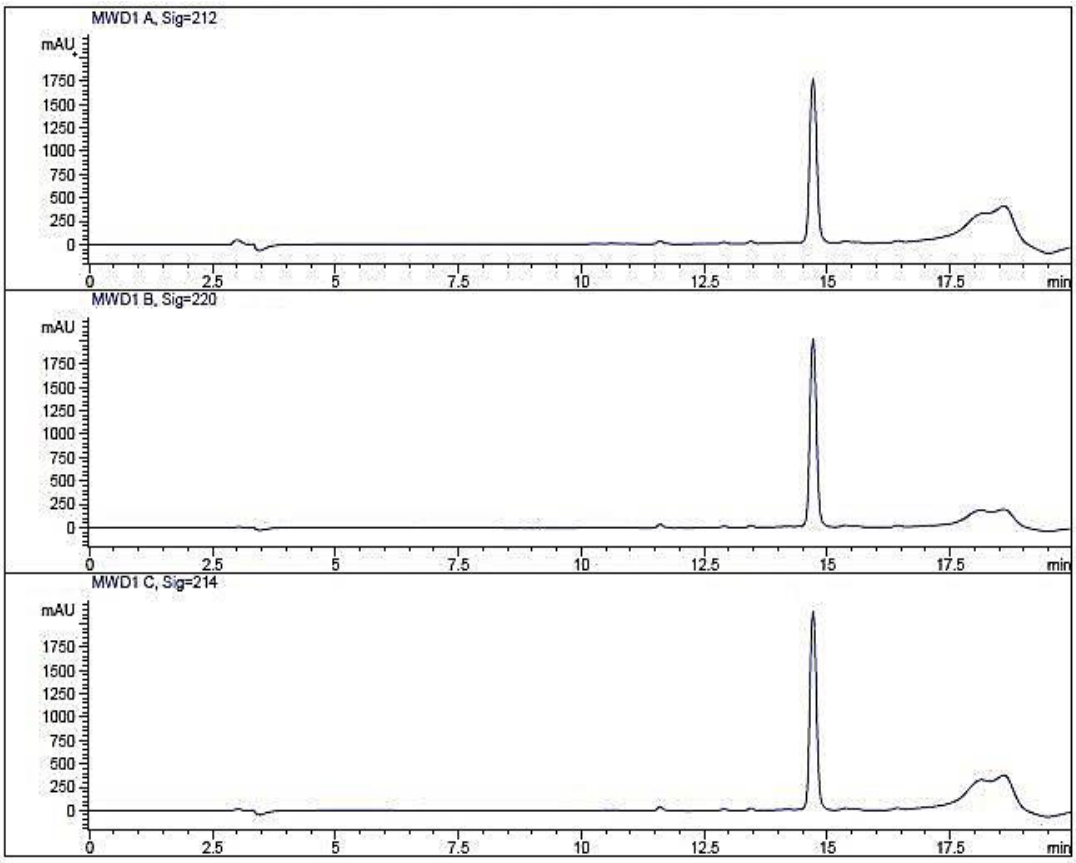

Figure 5.17: Chromatograms of sincalide analogue during HPLC method development detailing analysis at 3 wavelengths: 212 nm, 214 nm and 220 nm. Retention time = 14.5 min.

The drug concentration delivered by the sincalide loaded arrays was initially higher than the control discs although the release rate for both appeared similar (Figure 5.19). Interestingly, however, a sharp drop in the release rate was observed with the arrays between 1 – 2 h of the diffusion test. This trend was observed across all 3 arrays and may have been as a result of degradation of the drug in the skin. However, HPLC analysis of the samples taken throughout the experiment failed to indicate any degradation peaks which would have been expected if the drug had destabilised.

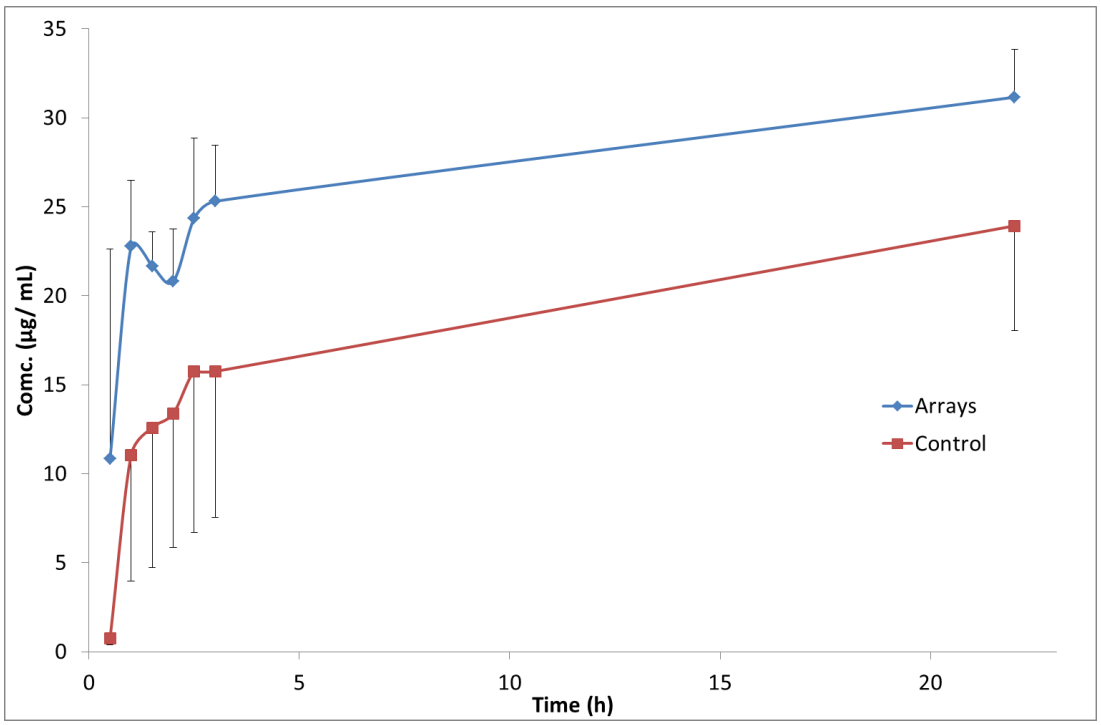

Figure 5.18: Plot detailing the total amount of the sincalide analogue content delivered into the receptor phase over time per microneedle arrays (n=3) and control discs (n=2).

As the drug loaded arrays were formulated without the addition of Tween® 80, the lower solubility of the sincalide may have resulted in non-homogeneous distribution of drug in the microneedle arrays. This may have caused drug particulates to collect in the needles during the casting stage and this would have resulted in a high burst release during the initial stage of the diffusion study. In addition, the average measured drug content per array was low at only approx. 53 µg compared with the pentagastrin arrays which contained an average of 145 µg. Considering both batches were formulated with 0.5 mg/ mL of drug, the lower measured drug content of the sincalide arrays suggested solubility issues which may have caused loss of drug material during the filtering process prior to HPLC analysis.

As with the pentagastrin samples, drug recovery from the measured content in the arrays was high at 86 % with drug recovery from the control samples also high at 90 % (Table 5.7). The addition of Tween® 80 to the receptor phase, which was shown to increase the solubility of the sincalide (Section 5.4.3.3), possibly contributed to the higher drug recovery in addition to its use in the PBS solution used to swab the SC surface and extract drug from the dissected skin at the end of the experiment.

Table 5.7: Drug diffusion at each time point and total sincalide analogue recovered compared with measured drug content of each array and control.

Time (h)	Arrays (µg) (n=3)	Control (µg) (n=2)
0.5	10.85 ± 11.79	0.76 ± 0.36
1	22.78 ± 3.70	11.05 ± 7.08
1.5	21.67 ± 1.93	12.58 ± 7.85
2	20.80 ± 2.93	13.39 ± 7.53
2.5	24.35 ± 4.49	15.74 ± 9.06
3	25.31 ± 3.15	15.75 ± 8.19
22	31.16 ± 2.68	23.93 ± 5.91
Surface	4.33 ± 1.83	4.43 ± 1.58
Skin	9.91 ± 0.36	6.21 ± 0.12
Total drug recovered (µg)	45.39 ± 4.13	34.57 ± 4.44
Measured drug content (µg)	52.99 ± 4.34	38.19 ± 1.67
% Drug Recovered	85.7 %	91 %

The apparent drop in drug concentration observed during the initial hours of the experiment resulted in low r^2 values when the data was applied to the release rate model fitting (Table 5.8). Therefore, although the results indicated that the arrays fitted the Higuchi model with the control disc also fitting this model most closely, the poor fit in all cases suggested that the release rates could not be confidently assigned to any particular model.

Table 5.8: Results of model fitting for sincalide analogue loaded arrays and control.

Arrays	Model	SSR	r^2	Slope	Intercept
	Zero order	0.019083	0.6073	0.0821	0.2518
	First order	0.007745	0.6347	-0.0555	-0.1258
	Higuchi	0.015369	0.6837	0.2144	0.1218
Control	**Model**	**SSR**	**r^2**	**Slope**	**Intercept**
	Zero order	0.028118	0.7375	0.1344	0.0671
	First order	0.007026	0.7928	-0.0784	-0.0261
	Higuchi	0.018407	0.8282	0.3504	-0.145

It was clear when comparing the diffusion results for all 3 model peptides that the microneedle arrays delivered higher concentrations of drug than the control discs. However, there was a marked difference in the release rates for each peptide. This could be attributed to the differences in MW and chemical properties of each drug, most notably that polymyxin is cationic and basic and both peptide analogues are acidic and anionic (Table 5.3). Drug release from the control discs which occurred with all 3 peptide loaded samples again indicated that the PVP/trehalose formulation facilitated diffusion through the SC of the skin sample as a result of occlusion and also potentially, of permeation enhancement qualities of the formulation itself [249, 250].

Rocco *et al* (2016) reported improved transdermal permeation of a tetrapeptide, AAPV, by utilising direct coupling of a C_7 acyl lipid group to either the N-terminal or C-terminal to the peptide [279]. Similarly, Namjoshi *et al* (2014) utilised short chain lipoamino acids ($C_6 - C_{10}$) to improve permeability of the same tetrapeptide utilising solid phase peptide synthesis to couple the conjugate to the peptide [280]. The increased permeability of these lipid conjugated peptides suggests that the lipid acyl tail of the polymyxin resulted in greater passive permeability qualities compared with the 2 synthesised peptides. Figure 5.20 illustrates % drug delivered from each array and, although the initial amount of drug delivered by the pentagastrin and sincalide loaded arrays is higher, the delivery rates revert to almost zero after the first ≈3 h of the study. The polymyxin loaded arrays however, continued to deliver drug at a steady rate following the initial burst release from the needles after 3-4 h. This may have been due to the onset of occlusion coupled with the permeation qualities of the polymyxin.

One trend which was evident from Figure 5.20 was the amount of drug delivered during the initial stages of the experiments for each peptide. Approx. 85 % of the lowest MW peptide, pentagastrin, was delivered during the first 2 h after application. In contrast, only ≈20 % of the highest MW peptide, polymyxin, was delivered at this time-point. Zhang *et al* (2014) utilised solid microneedles with shaft lengths of 150 µm to pre-treat porcine skin in order to enhance the transdermal delivery of a range of hydrophilic peptides. They concluded that the transdermal permeation rate of the peptides was dependent on the MW and reported a decrease in permeation for higher

MW peptides [248]. This hypothesis could explain the rapid delivery of the pentagastrin (MW 667.78 g/mol) during the initial 2 h of the experiment and, to an extent, the initially rapid delivery of sincalide (1062.39 g/mol) during the same time period. After application of the microneedle arrays, the pentagastrin was delivered extremely rapidly at a rate whereby almost 90 % of the drug load permeated into the receptor phase within 2 h. In contrast, the higher MW sincalide, although initially delivered at a comparable rate to the pentagastrin in the first hour (≈40 % of drug load), displayed a reduced delivery rate for the remainder of the experiment. This suggested that, after the initial microneedle mediated delivery, permeation of the higher MW sincalide was lower. The reduction in release rate after this point in both cases however, most likely occurred for different reasons. In the case of the pentagastrin, as most of the drug content had been delivered, the concentration of drug remaining on the skin surface or within the skin was potentially too low to drive diffusion into the receptor phase.

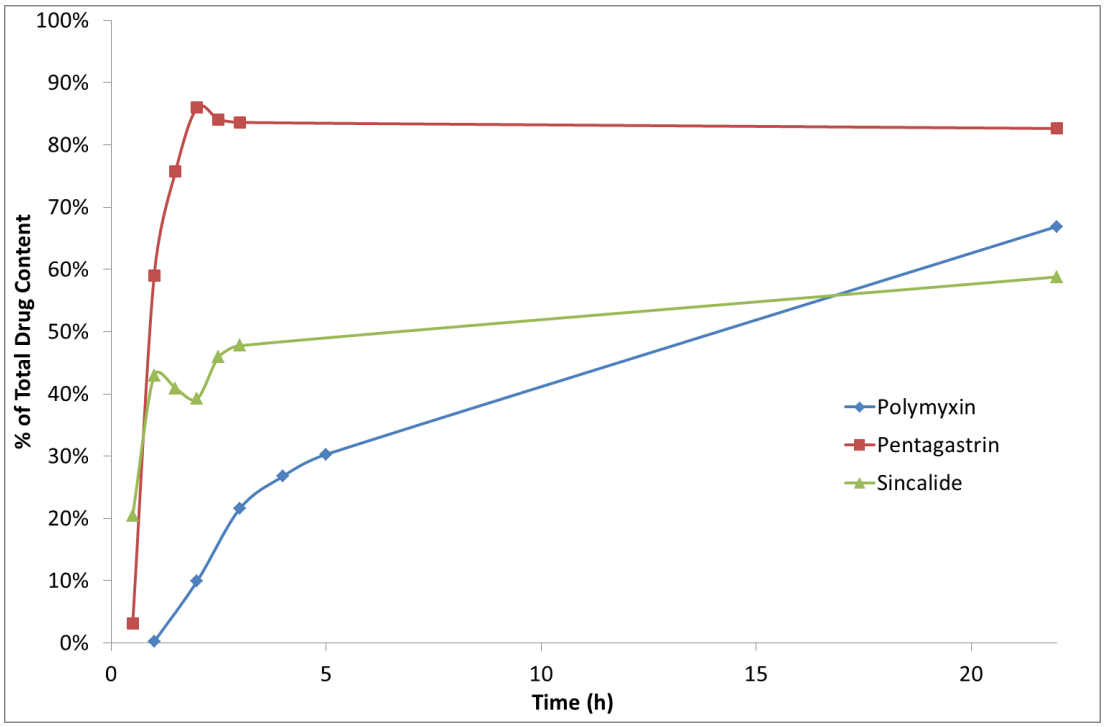

Figure 5.19: Plot of % of total drug from the microneedle arrays released across all 3 peptide studies.

As suggested above, in addition to the higher MW of sincalide, solubility issues with the sincalide analogue appeared to have resulted in retention of the peptide in the skin as approx. 32 % of the total recovered drug was retrieved from the skin sample

and skin surface. Significantly, these results suggested that, for lower MW peptides, the microneedle system could potentially deliver almost the entire drug cargo (including any drug reservoir in the backing layer) within 2-3 h after application.

Examination of the % drug released from the control discs (Figure 5.21) indicated that the polymyxin permeated at a relatively constant rate throughout the study. This suggested that, in tandem with occlusion, the permeation qualities of polymyxin facilitated steady transdermal delivery. The delivery of pentagastrin from the control discs was initially rapid but declined after approx. 3 h. This suggested that, without microneedle assisted delivery, transdermal penetration of pentagastrin does still occur albeit at a lower rate. This may have been due to permeation through skin appendages such as hair follicles and sweat glands in conjunction with the onset of occlusion caused by the polymer disc formulation. This was likely given that some absorption of drug material via these appendages can occur in the case peptide based drugs [218].

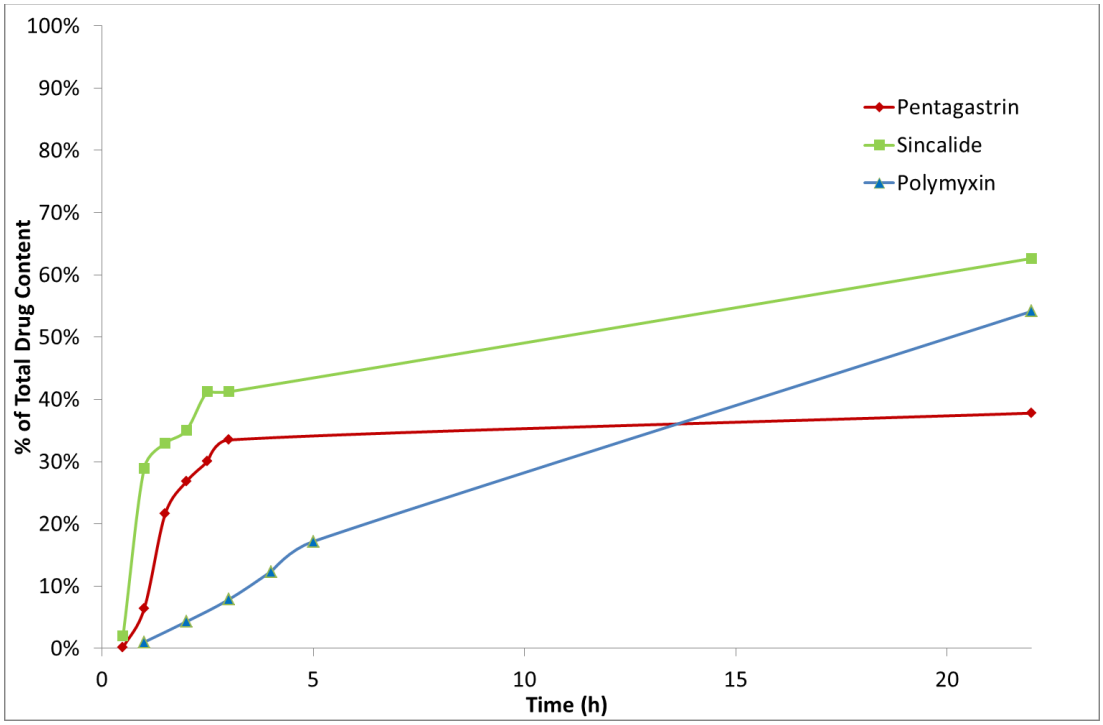

Figure 5.20: Plot of % of total drug in the control discs released across all 3 peptide studies.

A similar release was observed with the sincalide loaded control disc with rapid drug uptake occurring during the initial 2 h of the study also possibly due to skin appendage delivery. However, the control disc continued to deliver the sincalide at a steadily increasing rate throughout the experiment most likely due to the reduced barrier properties of the SC as a result occlusion.

Numerous studies have examined the feasibility of dissolving microneedles as delivery systems for bioactive therapeutics with a large number focussing on the intradermal delivery of vaccines [94, 137] or insulin [131, 135, 136]. Some studies have proposed dissolving microneedle systems intended for the delivery of biomolecules but have examined the drug delivery properties of the microneedles utilising non-biological model drugs such as sulforhodamine [129, 200]. To the author's knowledge, this is the first reported study of a dissolving microneedle system specifically designed for the delivery of therapeutic peptides in which the microneedle system has been extensively characterised and tested. Utilising a range of peptides, the physical and mechanical properties of the microneedle system were examined in addition to drug release studies focussing on the effectiveness of the system to deliver peptides with a range of properties and sizes.

5.5. Conclusions

Rink amide resin mediated solid phase peptide synthesis techniques were successfully utilised to synthesise analogues of two current therapeutic peptides; pentagastrin and sincalide. These peptides were purified and characterised using Semi Prep HPLC and LC-MS and incorporated into the PVP/trehalose based dissolving microneedle formulation. Skin penetration studies were carried out on the drug loaded microneedles using OCT which indicated that the arrays retained their ability to penetrate the SC of porcine skin to a depth adequate to facilitate the release of the drug payload. Franz cell based skin diffusion studies were then carried out to examine the quantity of drug delivered through porcine skin in addition to the drug release rate for each drug loaded array.

The results of the skin diffusion experiments indicated that the dissolving microneedles were capable of delivering all three peptides through porcine skin however, release rates varied in each case. These variations were attributed to the physical and chemical properties of each peptide with MW appearing to be a major factor. Almost the entire dose of the lowest MW peptide, pentagastrin, was delivered by the microneedles within the first 2 h after application. The higher MW sincalide peptide was initially delivered rapidly however, the rate of permeation was slow after the apparent microneedle-mediated burst release. Subsequent drug recovery examination of the skin samples suggested retention of the sincalide in the skin which resulted in lower concentrations of drug being delivered into the receptor phase of the diffusion cells. This was in contrast to the polymyxin diffusion studies which indicated an initially rapid delivery rate from the microneedle arrays followed by a steady release rate over a 22 h period.

CHAPTER 6. DISSOLVING MICRONEEDLES FOR THE TRANSDERMAL DELIVERY OF SUSTAINED RELEASE POLYMYXIN B LOADED MICRO-PARTICLES

6.1. Introduction

6.1.1. Micro-particle and Nanoparticle Based Drug Delivery

Biopharmaceuticals such as therapeutic peptides and proteins are highly specific which makes them ideal for the treatment of a wide variety of conditions. Their structural complexity, which is the key to their specificity is however, also the reason that formulation and delivery of these therapeutics is so challenging. The intrinsic physicochemical instability, short plasma half-lives and poor membrane permeability due to relatively high molecular weight and polar nature of bioactive drugs limits them to needle based delivery which also requires frequent dosing [281].

Polymer based sustained release systems have been investigated to enhance delivery of therapeutic peptides and proteins with the aim of both improving patient compliance and reducing the frequency of administration [282]. The use of nano-emulsions and particulate delivery systems, which have been shown to stimulate strong immune responses, have been extensively studied for the delivery of synthetic long peptide (SLP) based vaccines [283]. One such particulate based technique is micro or nano-encapsulation whereby the bioactive drug is enveloped in a polymeric particle which subsequently protects the drug from chemical or enzyme mediated degradation, improves bioavailability and facilitates slow, controlled release rates [284, 285]. When formulated for delivery via injection, the encapsulation of bioactive agents into biocompatible and biodegradable polymers can extend the duration of action of the drugs, reducing peak and valley blood level fluctuations. These long-acting release systems also reduce the frequency of injection, subsequently improving patient compliance.

The controlled release of drug material can be achieved through formulating the polymer to degrade in response to environmental conditions or chemical degradation, causing diffusion of the drug through the polymer matrix [286]. In addition to parenteral formulations, the use of polymeric encapsulation has also been investigated in a number of non-invasive systems such as oral, nasal, pulmonary and transdermal [287]. Topical formulations consisting of polymeric nanoparticles, solid lipid nanoparticles, liposomes and nano-emulsions have been utilised to enhance cutaneous drug delivery. Advantages of employing such nanoparticle based systems

for the treatment of skin diseases include improved drug stability and skin permeation, reduced side effects and targeted delivery to the disease site with minimal systemic exposure [288].

The use of microencapsulation can be particularly suited to the delivery of peptide and protein drugs in that the encapsulated drug is protected within the particles from enzymatic degradation and slow, controlled release can result in higher blood concentrations over prolonged periods of time [284]. The effective use of polymeric nanoparticles and micro-particles to deliver biopharmaceuticals depends however, upon a number of key requirements. The particle delivery system must include sufficiently high drug loading, high encapsulation efficiency and a release profile appropriate for the drug being delivered. Additionally, the structural and chemical integrity of the drug must be maintained. A wide range of materials have been utilised for such delivery systems including hydrophilic polymer scaffolds such as hydrogels, and hydrophobic scaffolds including non-degradable and degradable polymers. Of these, biodegradable polymers are the preferred choice given that they do not need to be surgically removed after drug release [281]. In addition, synthetic polymers are most widely used for particle formulation given that natural polymers such as proteins or polysaccharides can vary in purity and may also require crosslinking which can inactivate the embedded drug material [289].

6.1.2. Poly(lactic acid-co-glycolic acid) (PLGA)

Many biocompatible polymers including polylactic acid, dextran and chitosan have been investigated in drug delivery systems with poly(lactic acid-co-glycolic acid) (PLGA) the most widely used. PLGA is a biodegradable polymer and is approved by both the Food and Drug Administration (FDA) and the European Medicines Agency (EMA) for use as an excipient in parenteral formulations [290]. In addition to its biocompatibility and mechanical strength, the degradation rate of PLGA can be controlled through the monomer ratio and the polymer molecular weight. Higher lactic acid per glycolic acid ratio results in polymer which is more hydrophobic and less susceptible to hydrolytic cleavage. Similarly, increasing the molecular weight also increases hydrophobicity and rate of degradation. As such, adjustment of these variables allows the degradation rate to be tailored as required with drug release rates

correlating with the rate of polymer degradation [281]. The monomer units formed after degradation are water soluble, easily metabolised into carbon dioxide and water and are cleared from the body by respiration [286]. A potential limitation of using PLGA for delivery of bio-actives however, is the acidic microenvironment which results from the degradation of PLGA which can cause stability issues for certain biomolecules [281]. Immediately on application, the polymer begins to react with water in the body and degradation is initiated through hydrolytic cleavage of the ester bonds between lactic acid and glycolic acid (Figure 6.1) [286]. Physical or chemical interaction that can occur between the acid end-groups and the bioactive material may result in drug deactivation. Interaction between certain cationic peptides and the polymer phase of lower molecular weight PLGAs has also been reported [287]. Despite this potential drawback, PLGA has been utilised for particle encapsulation of a number of therapeutic peptides including LL37 for improved wound healing [290] and the antimicrobial plectasin for delivery to infected epithelia in the airways [291].

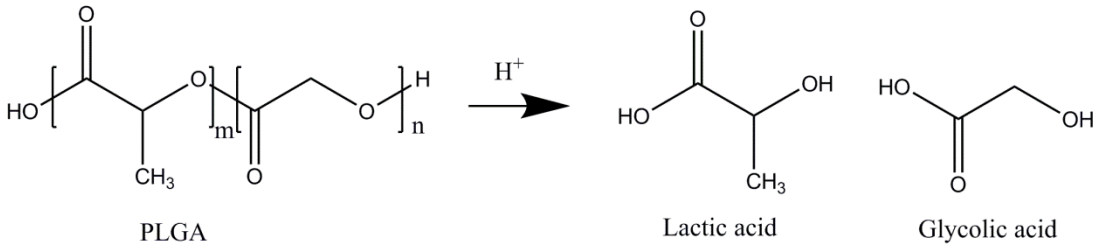

Figure 6.1: Degradation of PLGA into lactic acid and glycolic acid [286].

Drug release from PLGA systems typically includes 3 phases namely initial burst release, a lag phase and an active erosion phase. In addition, upon hydration of the polymer, there are 3 separate areas where drug material is found which are: dissolved in the polymer phase; dispersed in a non-polymer drug state; and dissolved within aqueous pores in the polymer [287]. PLGA has been utilised in a wide variety of drug delivery systems including microspheres, microcapsules, nanoparticles, pellets, implants and films carrying an array of bioactive ingredients including vaccines, peptides, proteins and micro-molecules [286].

6.1.3. Drug Loading PLGA Micro/nanoparticles

Successful encapsulation of therapeutic peptides and proteins utilising PLGA is commonly carried out using the emulsion/solvent evaporation technique. This method involves dissolving the polymer in a water immiscible, volatile organic solvent and then adding the drug, either dispersing or dissolving, to the polymeric solution. This solution is then emulsified in an aqueous phase to produce polymeric droplets which can be formed through sonication, homogenisation or simple mixing [281]. The organic solvent is then evaporated which subsequently hardens the polymeric nano/micro-particles which also contain the drug material. Many factors affect the properties of the nano/micro-particles including the solubility of the drug, solvent type, temperature, sonication settings, polymer composition and viscosity to name a few [292]. A double emulsion technique (Figure 6.2) can also be utilised where the primary water/oil (W/O) emulsion is added to an aqueous solution containing a surfactant, such as polyvinyl alcohol (PVA), and sonicated to obtain a water/oil/water (W/O/W) double emulsion [293]. Double emulsions can however, be challenging to formulate and stabilise. Internal aqueous droplets have the potential to coalesce, forming a core-shell structure. Additionally, the internal aqueous phase can be released into the external aqueous phase through coalescence with the surface and the oil droplets can also potentially coalesce. These issues can be minimised however by utilising polymeric stabilisers such as PVA [281]. For the encapsulation of water-soluble drugs such as peptides and proteins, the double emulsion method can avoid partitioning of the drug material into the aqueous phase and subsequent loss of drug loading efficiency which can occur when the conventional W/O solvent evaporation technique is employed [292].

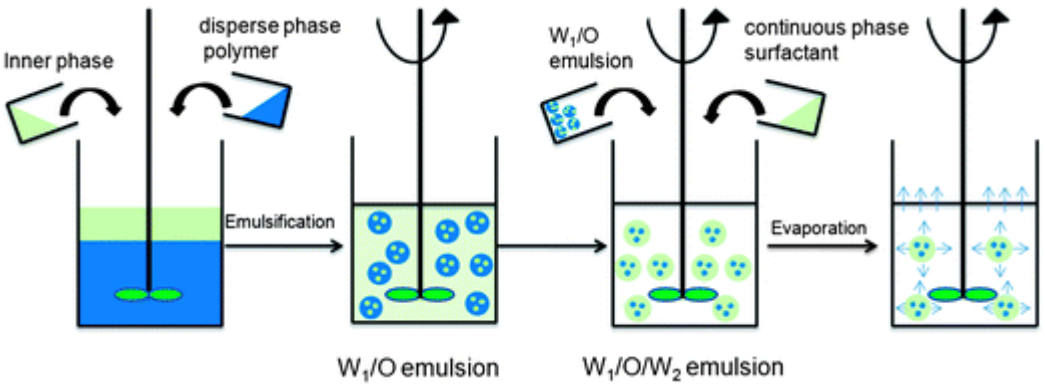

Figure 6.2: Diagram illustrating the double emulsion solvent evaporation method of polymer based particle formulation [294].

After the particles have been formulated, freeze drying/lyophilisation, is often carried out to preserve the stability and activity of the pharmaceutical product allowing for long term storage. Lyophilisation involves 3 steps namely: solidification of the sample by freezing; primary drying corresponding with ice sublimation; and secondary drying which involves desorption of unfrozen water in the sample. Issues related to freeze drying of polymer particles include mechanical stress due to crystallisation which can destabilise the particles and aggregation or irreversible coalescence due to the high concentration of particles in the dried sample. The addition of cryo-protectants such as trehalose, sucrose, glucose and other sugars can improve the resistance of the particles to these effects and improve stability [295].

6.1.4. Transdermal Delivery of Micro/nanoparticles

The ability of topically applied micro/nanoparticles to effectively penetrate the SC relies upon a range of complex elements such as the material properties of the particles, the size and shape of individual particles and other physicochemical factors [104]. Passive permeation of particles ranging in size from 50 to 500 nm through epithelial barriers has been reported [285] however, the role of hair follicles and other skin appendages has not yet been fully determined. Penetration of nanoparticles through hair follicles has been demonstrated, however, with penetration depth depending largely on particle size which indicates a mechanical element to the penetration process [296]. Microneedle mediated skin pre-treatment prior to nanoparticle application has been utilised in a number of studies [103, 104, 297] and enhanced transdermal delivery of nanoparticles by utilising microneedles to pre-treat the skin and allow delivery to deeper dermal layers has been reported [103]. This pre-treatment approach could allow targeted delivery to mast cells and lymphocytes for the treatment of inflammatory and allergic skin diseases as well as offering access to Langerhans and dendritic cells in the case of vaccine delivery [288].

6.2. Objectives

The effectiveness of the PVP/trehalose microneedle system has been demonstrated following the successful delivery of the polymyxin b model drug and subsequent delivery of two synthetic peptide analogues. The rapid dissolution of the microneedle formulation facilitated the burst release of the peptides with relatively rapid rates of release evident within the first 3-4 h of application. Maintaining the focus of this project on systemic transdermal drug delivery, the final stage of this research focussed on exploring a controlled and sustained release delivery system comprising of the PVP/trehalose formulation incorporating a payload of biodegradable, peptide-loaded PLGA particles. The dissolving microneedle system was utilised to rapidly deposit the payload of PLGA particles which slowly degrade and release the peptide systemically over time. Characterisation of these microneedles was carried out as before to examine the mechanical strength and stability of the particle loaded arrays.

As before, the focus of this chapter was to maintain the use of mild formulation conditions, avoiding elevated temperatures and extremes of pH which may adversely affect the activity of the peptide drug. Park *et al.* (2006) [128] investigated PLA and CMC micro-particles encapsulated in PLGA microneedles for the controlled release of BSA. Exposure of the drug to temperatures of 135 ºC, as used in the fabrication of the PLGA microneedles, resulted in total denaturation after 1 h. As such, the aim of this study was to protect the activity of the peptide drug by utilising the PLGA to formulate the particles, using a double emulsion solvent evaporation method without utilising elevated temperatures, pH or harsh organic solvents. With the exception of the use of DCM, all solutions utilised were aqueous in nature. The release of the drug from the particles was monitored over time and the ability of the dissolving microneedle system to successfully deliver the particles transdermally *in vitro* was also investigated.

6.3. Experimental

6.3.1. Materials

PLGA ester terminated lactide:glycolide 50:50 MW 38,000- 54,000, PLGA ester terminated lactide:glycolide 75:25 MW 76,000-115,000, PLGA acid terminated MW 7,000-17,000.

Polymyxin b sulphate supplied by Sigma Aldrich Ireland

PVP average weight 40,000 supplied by Sigma Aldrich

Trehalose D(+)- trehalose dihydrate (≥98 %) obtained from Fisher Scientific

Glycerol – ACS grade obtained from Reagecon

Coumarin 6 (≥99 %) supplied by Sigma Aldrich Ireland

PVA hydrolysed (87 – 89%) supplied by Sigma Aldrich

Brain heart infusion obtained from Oxoid Microbiology Products

Salmonella typhimurium (LT2) from WIT culture collection

Tween ® 80 obtained from Sigma Aldrich Ireland

6.3.2. Methods

6.3.2.1. Preparation of the PLGA Micro/ nanoparticles

200 mg of the PLGA polymer was dissolved in 2 mL dichloromethane (DCM). 50 µL of water (for unloaded particles) or aqueous drug solution (for loaded particles) was then added to the PLGA solution. The aqueous drug solution used was a 50 mg/ mL solution of polymyxin (representing the maximum concentration of polymyxin soluble in water). The mixture was then sonicated by probe-sonication (Sonics vibracell, model CV188) at its maximum amplitude, to form the primary water/oil (W/O) emulsion. This sonication was carried out while the mixture was standing on ice. The W/O emulsion was then added to 4 mL of 1% w/v PVA solution and a water/oil/water (W/O/W) emulsion was then formed by another 1 min of probe sonication on ice. The W/O/W emulsion was then transferred to 100 mL of 0.3% w/v PVA solution on a stirring plate at a mild stirring rate. The solution was stirred for 3 h, allowing the DCM to evaporate, and the particles to harden. The particle dispersion was then centrifuged at 4000 rpm for 20 min and the supernatant decanted. The particles were re-dispersed in fresh DI water using a vortex mixer and

centrifuged for another 20 min at 4000 rpm. This procedure was repeated 3 times to wash excess residual PVA from the particles. Once thoroughly washed, the particles were dried and characterised using SEM and DLS.

For coumarin 6 loaded particles, 1 mg of coumarin 6 was added with 200 mg of PLGA to 2 mL of DCM which was then emulsified with 50 µL of H_2O to form the primary W/O emulsion. The W/O/W emulsion was then obtained utilising the procedure as before.

6.3.2.2. Particle Yield, Drug Content and Drug Encapsulation

The mean values of 3 nano/micro-particle batches were used to calculate particle yield, drug content and drug encapsulation. After formulating the particles and obtaining the yield (mg), each batch was dissolved in 10 mL of 50:50 H_2O/ACN and the dissolved particles analysed using HPLC to determine the drug content.

The particle yield was calculated using Equation 6.1:

$$\frac{\textbf{mass of particles recovered} \times \mathbf{100}}{\textbf{mass of polymeric material and drug}} \qquad \textbf{Equation 6.1 [298]}$$

Drug content (% w/w) was calculated using Equation 6.2:

$$\frac{\textbf{mass of drug in particles} \times \mathbf{100}}{\textbf{mass of particles recovered}} \qquad \textbf{Equation 6.2 [298]}$$

Drug encapsulation (%) was calculated using Equation 6.3:

$$\frac{\textbf{mass of drug in particles} \times \mathbf{100}}{\textbf{mass of drug in formulation}} \qquad \textbf{Equation 6.3 [298]}$$

6.3.2.3. SEM

SEM analysis was carried out as per Chapter 2, Section 2.2.2.7.

6.3.2.4. OCT

OCT was carried out as per Chapter 3, Section 3.2.2.13.

6.3.2.5. Fluorescence Microscopy

The instrument used for this analysis was an Olympus BX51 Fluorescence Microscope and the samples were viewed using a fluorescein isothiocyanate (FTIC) filter cube.

6.3.2.6. Dynamic Light Scattering (DLS)

DLS was carried out on the micro-particles to determine the average particle size per batch. Analysis was carried out using a Microtac Nanotrac Wave II particle analyser. Each sample was analysed in an aqueous dispersion medium with the instrument carrying out 3 analyses of each sample.

6.3.2.7. HPLC

UV HPLC analysis was carried out using an Agilent Technologies 1200 with an Xterra reversed phase C_{18} 5 µm 4.6 x 250 column. A gradient method was developed with mobile phase A (water with 0.1 % trifluoroacetic acid (TFA)) and B (acetonitrile with 0.08 % TFA). Starting with 95 % mobile phase A and 5 % B, the composition changed to 40% B over 30 min and back to 5 % B at 35.10 min to the end of the run time of 40 min. The injection volume was 40 µL with a flow rate of 0.5 mL/ min, column temperature of 40 º C and the detection wavelength was set at 214 nm.

Fluorescence detection (FLD) HPLC was carried out on the coumarin 6 standards and fluorescent particle loaded microneedles using Agilent Technologies 1200 fitted with a standard Agilent FLD detector and a Waters Symmetry Shield reverse phase C_{18} 5 µm 3.9 x 150 mm column. A dual mobile phase isocratic method was used consisting of 20 % H_2O with 0.1 % TFA) and 80 % MeOH. The flow rate was set at 1 mL/ min, the injection volume was 5 µL and total run time was 10 min with no column temperature control. The absorption wavelength was set at 458 nm and the fluorescence emission wavelength was set at 512 nm [103, 299]. LOD and LOQ were determined based on the standard deviation of the response and the slope of the representative calibration curve. The LOD was determined as 35 ng/ mL and the LOQ was determined as 105 ng/ mL. Calibration curves for the coumarin 6 standards were linear in the concentration range of 0.3 µg/ mL to 10 µg/ mL with r^2 value of 1 based on the area under the sample peak.

6.3.2.8. TGA

TGA analysis was carried out as per Chapter 2, Section 2.2.2.8.

6.3.2.9. DSC

DSC analysis was carried out as per Chapter 2 Section 2.2.2.9.

6.3.2.10. DVS

DVS analysis was carried out as per Chapter 2, Section 2.2.2.10.

6.3.2.11. Franz Cell Skin Diffusion

Skin diffusion tests were carried out as per Chapter 4, Section 4.3.2.8.

6.3.2.12. Well Diffusion Tests

The well diffusion tests were carried out as per Section 3.2.2.2 with 8 petri dishes prepared with inoculated media and 3 wells on each plate. For these tests, a batch of polymyxin loaded particles, prepared as per Section 6.3.2.1 were dissolved in an 8 mL solution of 50:50 H_2O/ACN and 50 µL of this solution was applied to each well on the 6 sample plates. A control sample consisting of unloaded PLGA particles dissolved in 50:50 H_2O/ACN was also prepared and 50 µL of this solution was applied to each well in the 2 control plates. Additionally, well diffusion testing was carried out on samples taken at the end of the drug release study to determine whether the activity of the polymyxin was affected by the degradation of the PLGA particles.

6.3.2.13. Drug Release Studies

To determine the release of polymyxin from drug loaded particles over time, 3 batches of drug loaded particles were prepared as per Section 6.3.2.1. Once formulated, 120 mg of each nano/micro-particle batch was placed in a 15 mL centrifuge tube and 2 mL of PBS pH 7.4 solution was added to the tube. The tubes were vortexed to fully disperse the particles in the PBS solution and the centrifuge tubes were then placed in a heated orbital shaker set at 37 ºC and 250 rpm for 24 h. After this, the tubes were transferred to a centrifuge for 5 min at 5000 rpm to compact the particles. Once completed, the PBS solution was removed, filtered with a 0.45 µm syringe filter and analysed using HPLC. Another 2 mL of fresh PBS solution was added to the centrifuge tubes and each was vortexed to break up the particle pellet and re-disperse the particles in the solution. Once fully dispersed, the centrifuge tubes were returned to the orbital shaker for another 24 h and the process was repeated over a period of 2 weeks.

6.4. RESULTS & DISCUSSION

6.4.1. Preparation of the PLGA Micro/ nanoparticles

The double emulsion solvent evaporation method utilised in the formulation of the PLGA particles consistently produced particles that were relatively uniform in size and fully formed without any visible defects in the spherical structure. The well diffusion tests carried out on the polymyxin loaded particles dissolved in H_2O/ACN resulted in Zones of Inhibition (ZOI's) with an average diameter of 14.5 mm (± 0.7) for all of the polymyxin loaded particle solutions with no ZOI's visible on the control plates (Figure 6.3). This indicated that polymyxin was successfully encapsulated into the PLGA particles and also that the encapsulation process, including the use of DCM, did not result in any loss of polymyxin activity.

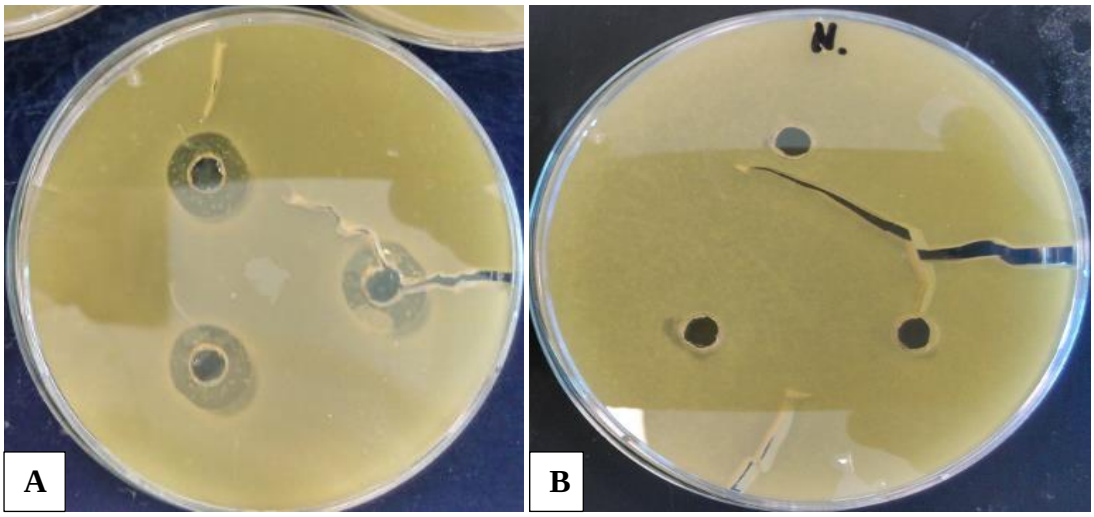

Figure 6.3: Well diffusion plates: (A) illustrating ZOI's after application of polymyxin loaded PLGA MP solution and (B) illustrating control plate after application of MP solution, no drug.

The development of a successful particle based drug delivery system however, is dependent on three key requirements namely high drug loading, high encapsulation efficiency and a suitable release rate [281]. The average nano/micro-particle yield was calculated as 43.8 ± 2.9 % across 3 drug loaded batches and similarly, the same batches had a mean drug content (% w/w) calculated as 0.5 ± 0.1 %. The average drug encapsulation efficiency of the 3 batches was calculated as 21.5 ± 3.4 % which was quite low, indicating that the majority of the polymyxin solution failed to be

encapsulated into the particles and was subsequently lost in the particle formulation process.

Issues associated with double emulsions which may have contributed to the low encapsulation of drug include the potential for the internal aqueous droplets to coalesce and subsequently get released into the external phase as a result of instability of the primary W/O emulsion. Loss of some of the internal aqueous phase typically occurs during the second emulsification step due to oil drop breakup, but the addition of surfactant to the primary emulsion can stabilise the droplets, reducing the risk of coalescence with the external aqueous phase. A drop in encapsulation efficiency can also occur due to increased biologics concentration in the primary emulsion [281]. Low drug encapsulation can also be attributed to the water soluble nature of the drug which can lead to rapid partitioning into the aqueous phase and decreased entrapment in the polymer particles. Increasing the theoretical drug loading has also been shown to reduce the overall drug encapsulation which may be as a result of drug leakage into the aqueous phase at high loadings [291, 298]. These parameters may have affected the final encapsulation efficiency given the water soluble nature of polymyxin coupled with the high concentration of polymyxin used in the formulation process.

Other parameters that can affect the encapsulation efficiency include the type of PLGA utilised, with lower encapsulation efficiency resulting from the use of low molecular weight PLGA containing a higher lactide to glycolide ratio. In addition, longer sonication times tend to lower encapsulation efficiency by not only reducing particle size but by also causing the PLGA to degrade prematurely. This polymer degradation can lead to drug loss during the washing stages as a result of the increased permeability of the particles [300]. Loss of encapsulated biologics has also been reported during long solvent evaporation steps [293] and as such, reducing the evaporation time would potentially increase the particle drug loading efficiency.

6.4.2. SEM

SEM was used to examine the size and morphology of the particles in each batch. The molecular weight of PLGA used did not seem to affect the particle size with

low, medium and large molecular weight PLGA producing particles which appeared to be relatively uniform in size for each batch, ranging from 500 nm to 5 µm (Figure 6.4). The particles were spherical in shape with no visible pores or pitting on the surface, which can have negative effects on the durability and structural integrity potentially causing accelerated degradation [300]. Furthermore, the particles appeared evenly distributed throughout the sample with no indication of aggregation or clustering. Lyophilisation of the particles was carried out at the end of the formulation process for initial particle batches. However, this resulted in flocculation and aggregation of the particles. For this reason, subsequent batches of particles were formulated without lyophilisation, with the drying step carried out in a fume hood. This process did not appear to adversely affect the particle structure or dispersion.

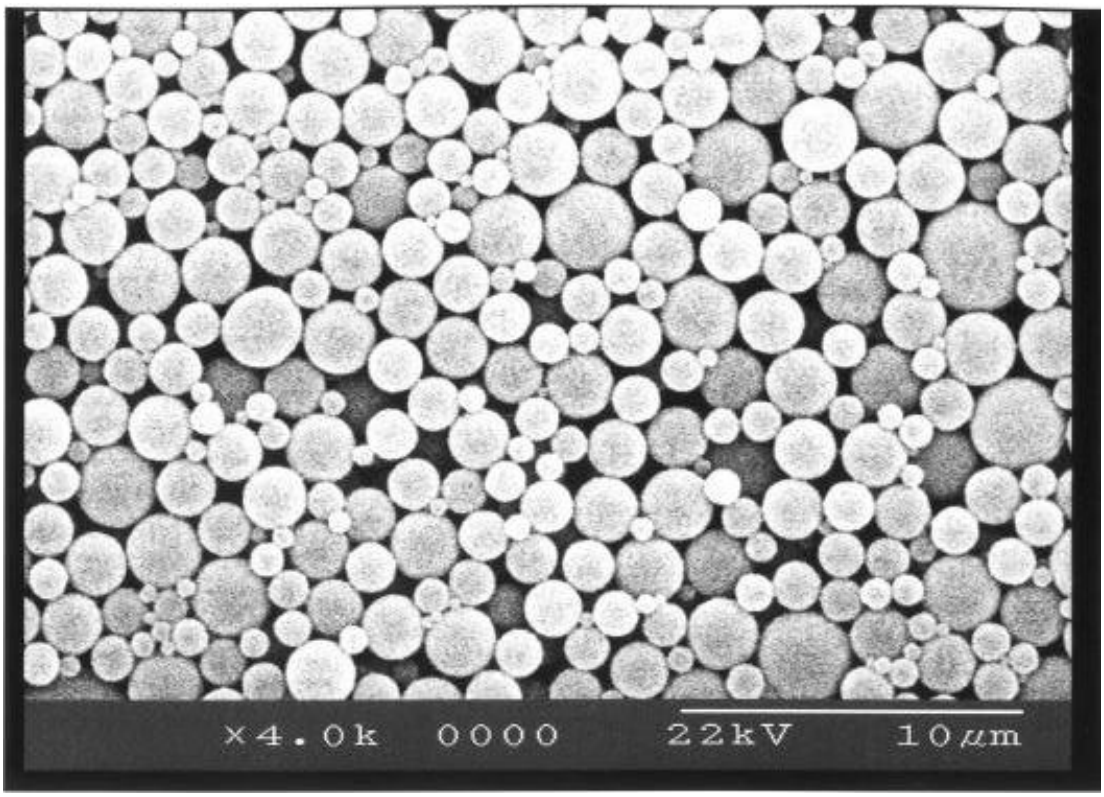

Figure 6.4: SEM image of high MW PLGA micro-particles.

In addition to examining the morphology of the PLGA particles, SEM was also utilised to examine particle loaded microneedles with Figure 6.5 illustrating the tip of an individual needle shaft with PLGA particles clearly visible embedded in the needle structure. The SEM images also indicated that no loss of tip sharpness was

apparent due to the presence of the particles in the formulation, which may have settled in the tips of the needles during the casting and drying process.

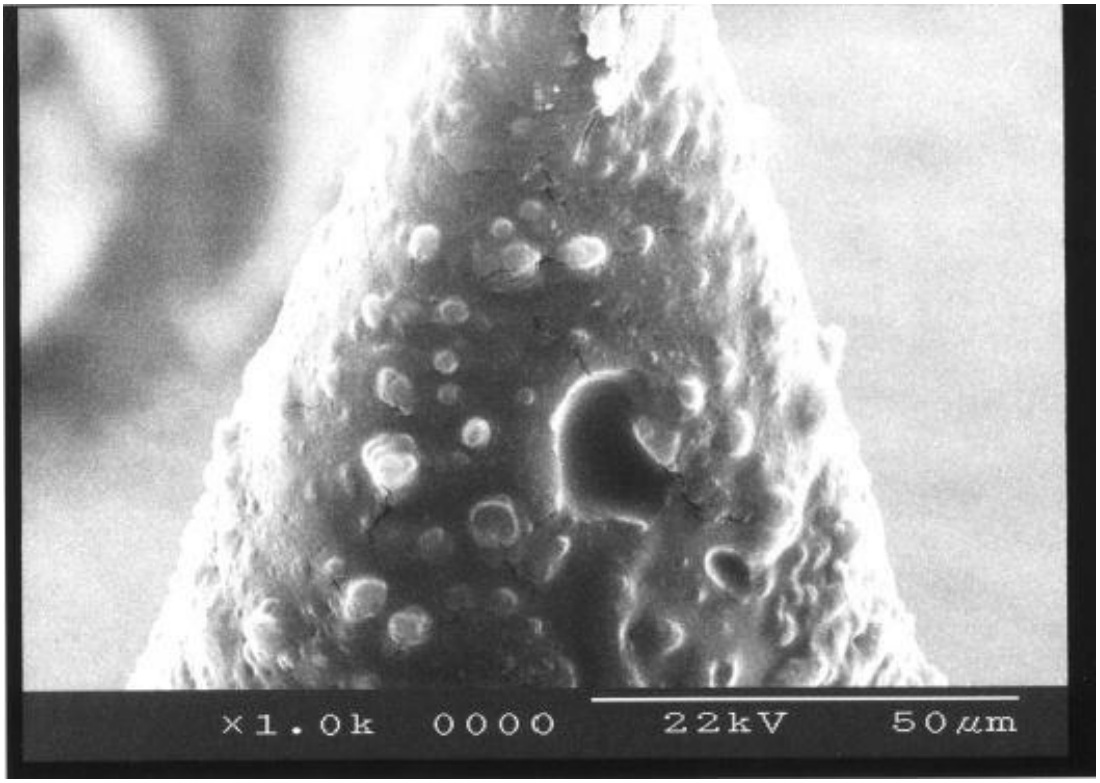

Figure 6.5: SEM image of micro-particle loaded microneedle with visible micro-particles embedded in the needle shaft.

6.4.3. DLS

DLS analysis provided data relating to the mean diameter and the polydispersity index (PI) of each batch of particles. As per the SEM analysis, DLS indicated no apparent correlation between particle size and the molecular weight or feed ratio of the PLGA used (Table 6.1). Similarly, as per the results obtained for sample D (Table 6.1), drug loading did not appear to have any major effect on the particle size. The main factors affecting the mean particle size, standard deviation and heterogeneity of each batch were not immediately apparent based on the DLS data. A probe sonicator was utilised for samples A, B, C and D however, due to the unavailability of the probe sonicator at the time, a bath sonicator set up was utilised for sample E.

Table 6.1: Results of DLS analysis on 5 nano/ micro-particle batches detailing MW, feed ratio, mean diameter (MV) and polydispersity index (PI).

	PLGA MW (g/ mol) (n=3)	Feed Ratio (lactide:glycolide)	Mean Diameter (MV) (nm)	Polydispersity Index (PI)
A	7,000 – 17,000 (low)	50:50	1107 ± 862	6.6
B	38,000 – 54,000 (med)	50:50	446 ± 149.6	1.04
C	76,000 – 115,000 (high)	75:25	907 ± 161.3	0.004
D	Polymyxin loaded (low)	50:50	474 ± 185.6	1.91
E	Coumarin loaded (high)	75:25	4610 ± 1757	0.14

The larger mean particle diameter of the coumarin loaded particles in sample E may have been due to the lower energy of the bath sonicator however, the PI was relatively low indicating relatively uniform dispersion. Samples B, C and D exhibited smaller mean particle sizes and low PI indicating relatively uniform dispersion of particles in each sample. The mean particle size in sample A was larger however and, with a PI of 6.6, indicated a much less homogenous dispersion than B, C and D. As sample A represented one of earlier batches in this study, the improved results seen with samples B, C and D, which were formulated later, could have been attributed to improved operator technique.

6.4.4. DSC and TGA

Thermal analysis of the MP loaded microneedle formulation (Figure 6.6) indicated that the degradation profile remained relatively unchanged compared to the unloaded 3:1 PVP/trehalose formulation.

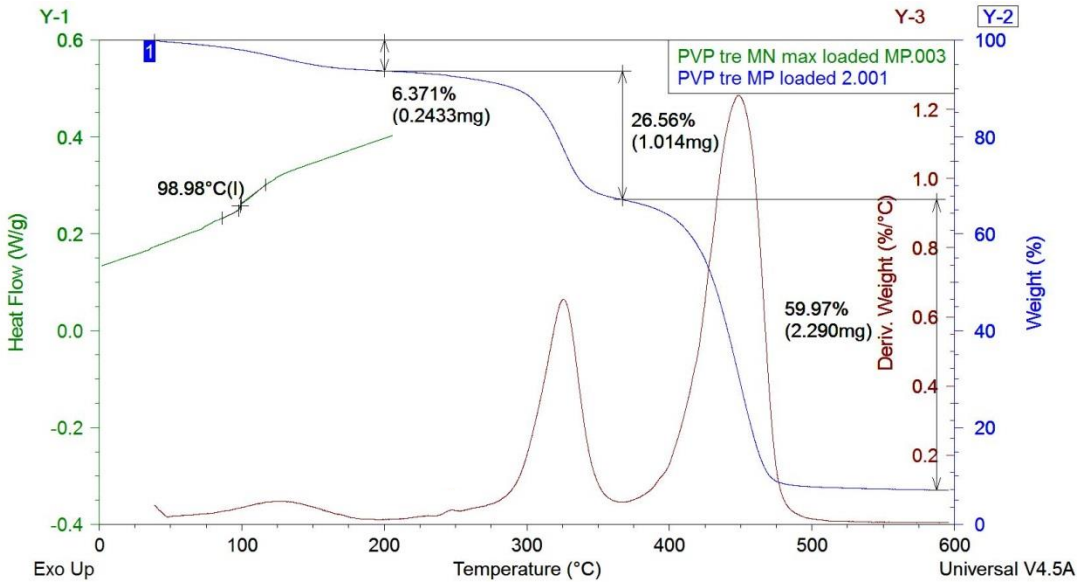

Figure 6.6: Overlaid TGA and DSC thermograms for medium MW PLGA particle loaded microneedle formulation illustrating thermal degradation profile and T_g.

The most notable exception was the drop in T_g with the particle loaded formulation to 98.81 ± 0.05 ºC (n=3) from 112.4 ± 1.4 ºC (n=3) for the unloaded formulation (Section 3.3.1.2). Although this represented a drop in T_g of approx. 10 ºC, it was not expected to result in a significant reduction in the mechanical strength of the needles.

6.4.5. DVS

DVS analysis of the particle loaded microneedle formulation indicated that the water sorption properties of the microneedles remained relatively unchanged as a result of the incorporation of particles into the microneedle matrix. Figure 6.7 illustrated that the mass increase of approx. 25% due to water sorption and the level of hysteresis was similar to that of the unloaded 3:1 PVP/trehalose formulation (Figure 3.6) and as such, it was concluded that the addition of the particles had little effect on the sorption properties of the formulation. Consequently, it was expected that the particle loaded microneedles would display similar moisture uptake and subsequent dissolution properties as the unloaded microneedles.

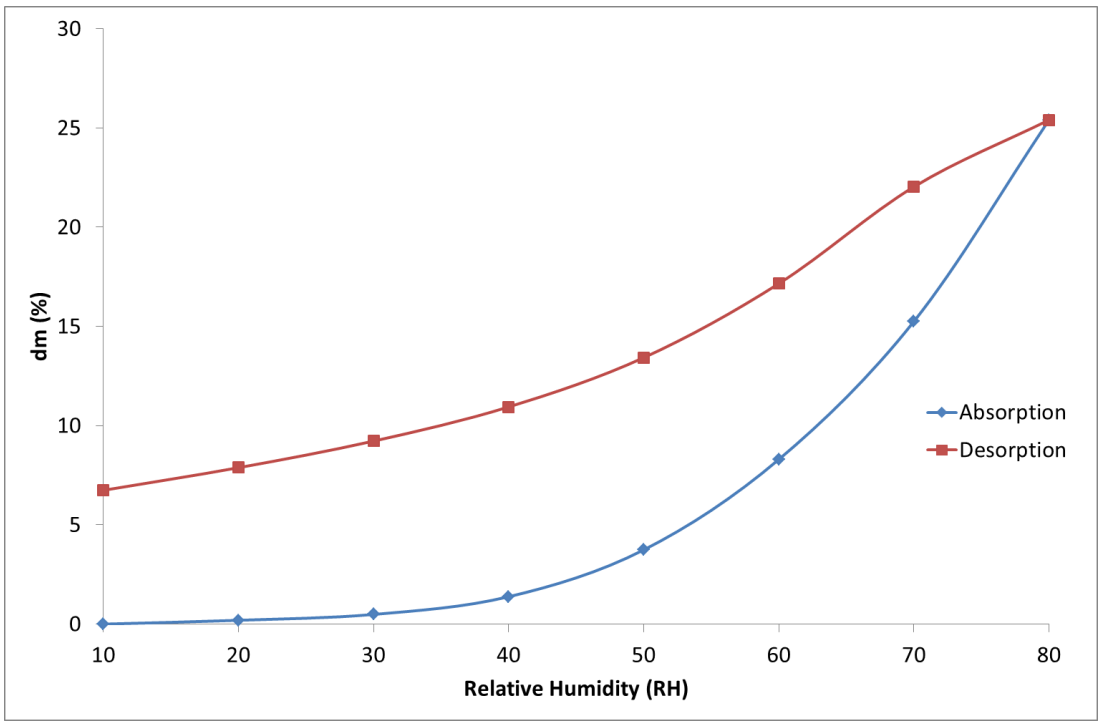

Figure 6.7: Plot of water sorption isotherm from micro-particle loaded PVP/trehalose microneedle formulation.

6.4.6. OCT

OCT analysis indicated that the particle-loaded microneedles were capable of penetrating the SC and dermal layers to an average depth of 325 ± 24µm (n=5) (Figure 6.8). The average micro-pore size was also determined as 246 ± 12 µm and the average space between the skin surface and the base of the arrays was calculated as 384 ± 31µm. As per the peptide loaded arrays, the PLGA particle loaded microneedles were capable of penetrating the SC to a depth sufficient to deposit the particles deep within the dermis. Coupled with the expected onset of occlusion as a result of the hydration of the PVP/trehalose formulation, this was expected to facilitate continued diffusion of particles contained within the backing layer of the arrays. In addition, the OCT image illustrated the dispersion of particles within the microneedle matrix, with PLGA particles visible in the backing layer and the needles themselves.

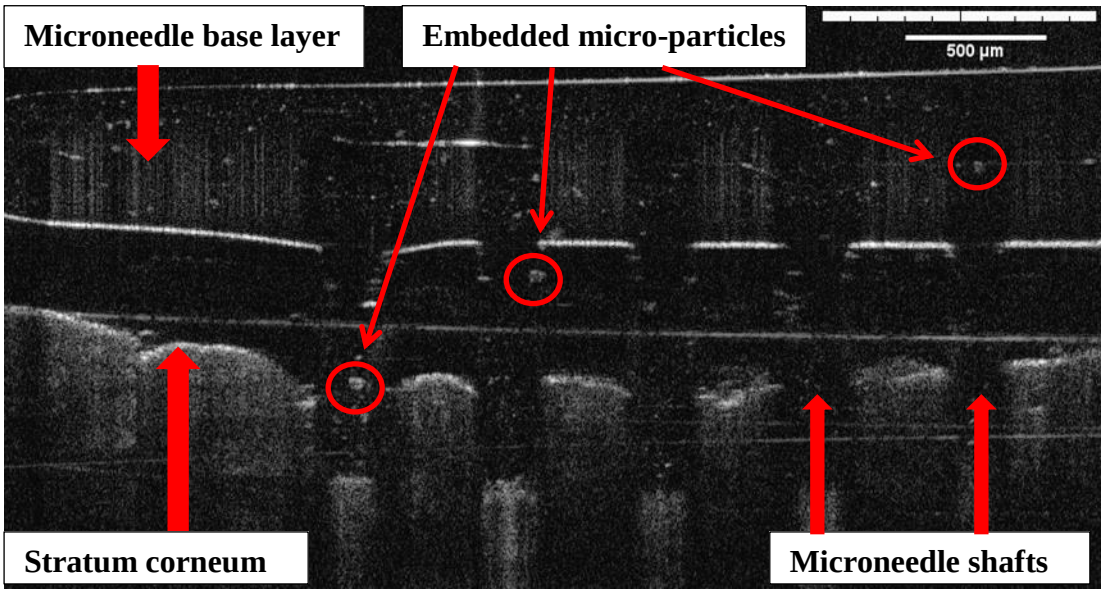

Figure 6.8: OCT image illustrating the penetration depth of particle loaded microneedles with visible particles embedded within the microneedle matrix. Variation in particle sizes due to emulsification step utilising bath sonicator and heterogeneous distribution within the arrays.

6.4.7. Drug Release Studies

After daily analysis of the drug loaded particles over a period of 2 weeks, no trace of polymyxin was found in any of the PBS solution samples analysed. SEM images taken at the end of the study indicated though that degradation of the particles was occurring (Figure 6.9) and as such, it was expected that drug material would be released. The calculated drug encapsulation efficiency of the particle formulation procedure however, was relatively low at only 18.8% and, as such, coupled with the slow degradation rate of the PLGA particles, the amount of actual polymyxin released was determined to be extremely low and most likely lower than the limit of detection of the HPLC analysis method.

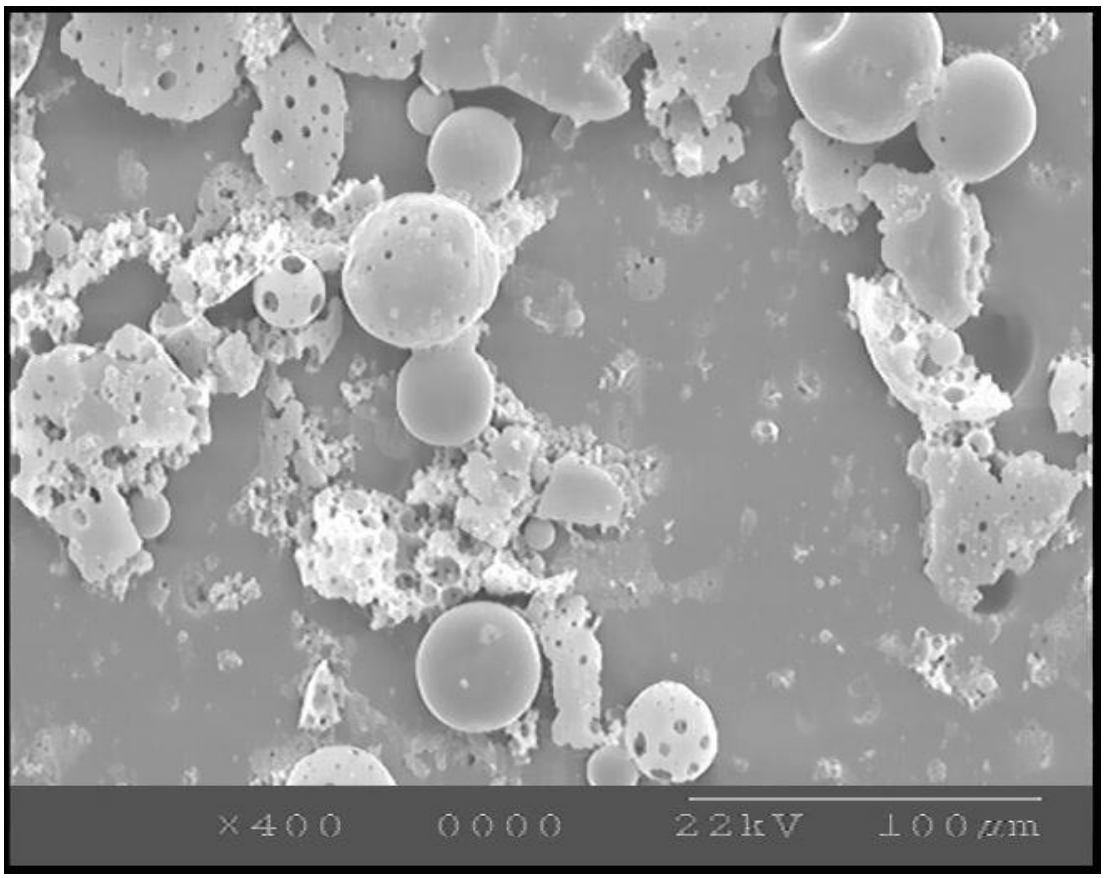

Figure 6.9: SEM image detailing degradation of polymyxin loaded PLGA micro-particle after 15 days.

The fact that the particles, although displaying signs of degradation, were still quite intact and retaining the drug payload, was further indication of their slow drug release properties. This was confirmed by the well diffusion test (Figure 6.10), carried out at the end of the drug release study which indicated the presence of polymyxin still within the PLGA particles.

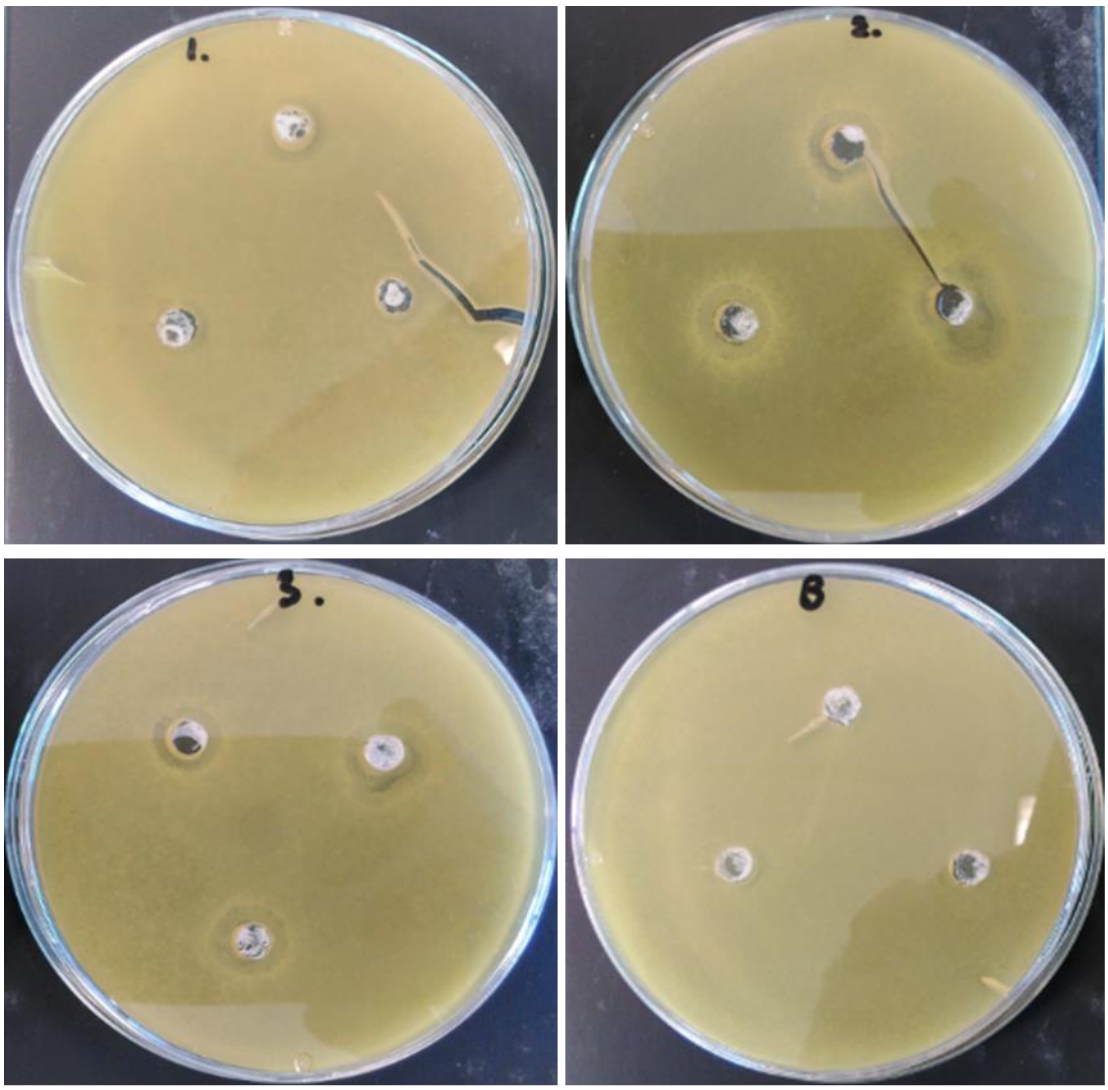

Figure 6.10: Well diffusion plates illustrating activity of polymyxin loaded PLGA particle solution to determine the presence of drug after 2 week release study. Plates 1, 2, 3 contain dissolved drug loaded PLGA particle solution, plate B contains MP solution with no drug.

ZOI's with an average diameter of 6 mm were visible on all the drug loaded sample plates with no ZOI's visible on the control. The pH of the PBS solution was also monitored throughout the experiment and remained at pH 7 with no apparent increase in acidity due to degradation of the PLGA. Additionally, after dissolving the particles in H_2O and ACN at the end of the study, the pH was again measured as pH 7. This indicated that the degradation of the PLGA particles had little to no effect on the local pH. This was not expected to negatively affect the activity of the polymyxin as decomposition of polymyxins in aqueous solution is not adversely affected at pH ≤ 7 [206, 232].

6.4.8. Skin Diffusion Testing of Microneedle Loaded Coumarin 6 Micro-particles

Coumarin 6 (Figure 6.11) is a highly fluorescent compound which has been widely utilised as a fluorescent marker, particularly in the detection of polymeric nanoparticles delivered into cells and as a probe in protein microenvironment determination [301]. As it is lipophilic and does not dissolve in aqueous solutions, the use of coumarin 6 was particularly well suited as a marker for transdermal delivery of the polymeric particles given that its detection in skin tissues could be attributed solely to the presence of coumarin loaded particles as opposed to free coumarin 6 released into the tissues [103].

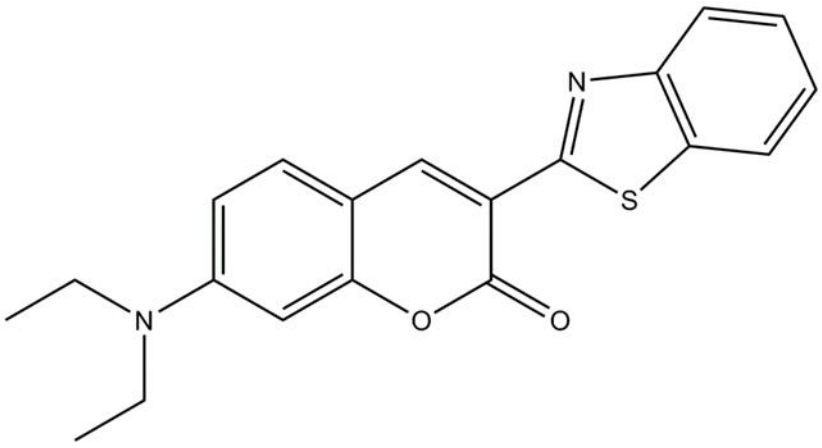

Figure 6.11: Chemical structure of coumarin 6 [302].

Examination of the microneedle arrays loaded with the fluorescent particles using fluorescence microscopy illustrated the dispersion and concentration of the particles in the microneedle matrix. In Figure 6.12, the concentration of particles in the microneedle shafts was evident due to the high level of fluorescence in comparison to the surrounding array. This is most likely due to gravity-induced pooling of the micro-particles in the needle moulds during the casting process. This may have resulted in a higher concentration of particles in the needles as opposed to the back layer. Individual particles can also be clearly seen embedded in the backing layer although these images do illustrate the poly-dispersion of particles within the arrays, with some areas clearly devoid of particles and others containing higher concentrations.

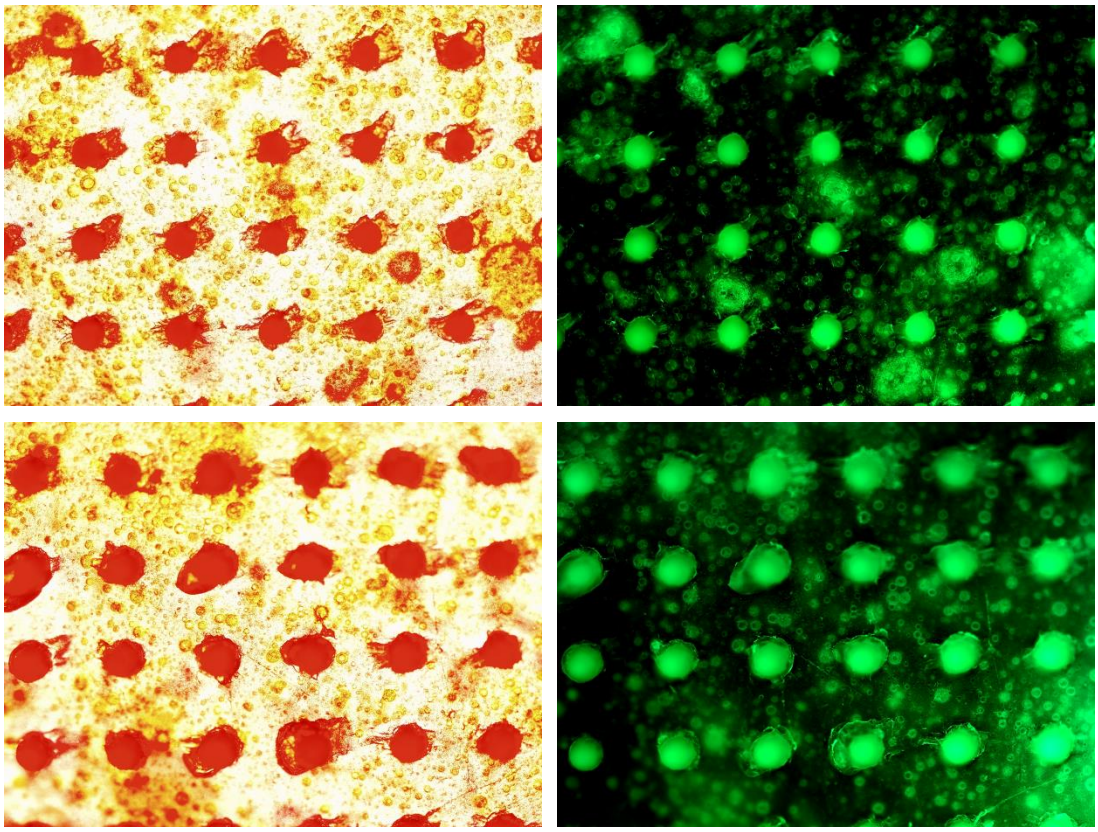

Figure 6.12: Standard optical (left) and fluorescence (right) microscopy images of coumarin 6 micro-particle loaded microneedle arrays illustrating the micro-particles embedded in the microneedle shafts.

Fluorescence microscopy images taken of skin samples after the diffusion studies clearly illustrated the deposition of the PLGA particles on the skin surface and in the micro-channels formed by the microneedles themselves (Figure 6.13). Zhang *et al.* (2010) carried out a study into the transdermal delivery of coumarin 6 loaded polystyrene nanoparticles through microneedle pre-treated porcine skin. With results mirroring those of this study, they observed high levels of fluorescence in the micro-conduits as opposed to the surrounding tissue. This was indicated that the SC was the main barrier to particle penetration although they did report penetration of particles through skin appendages [103].

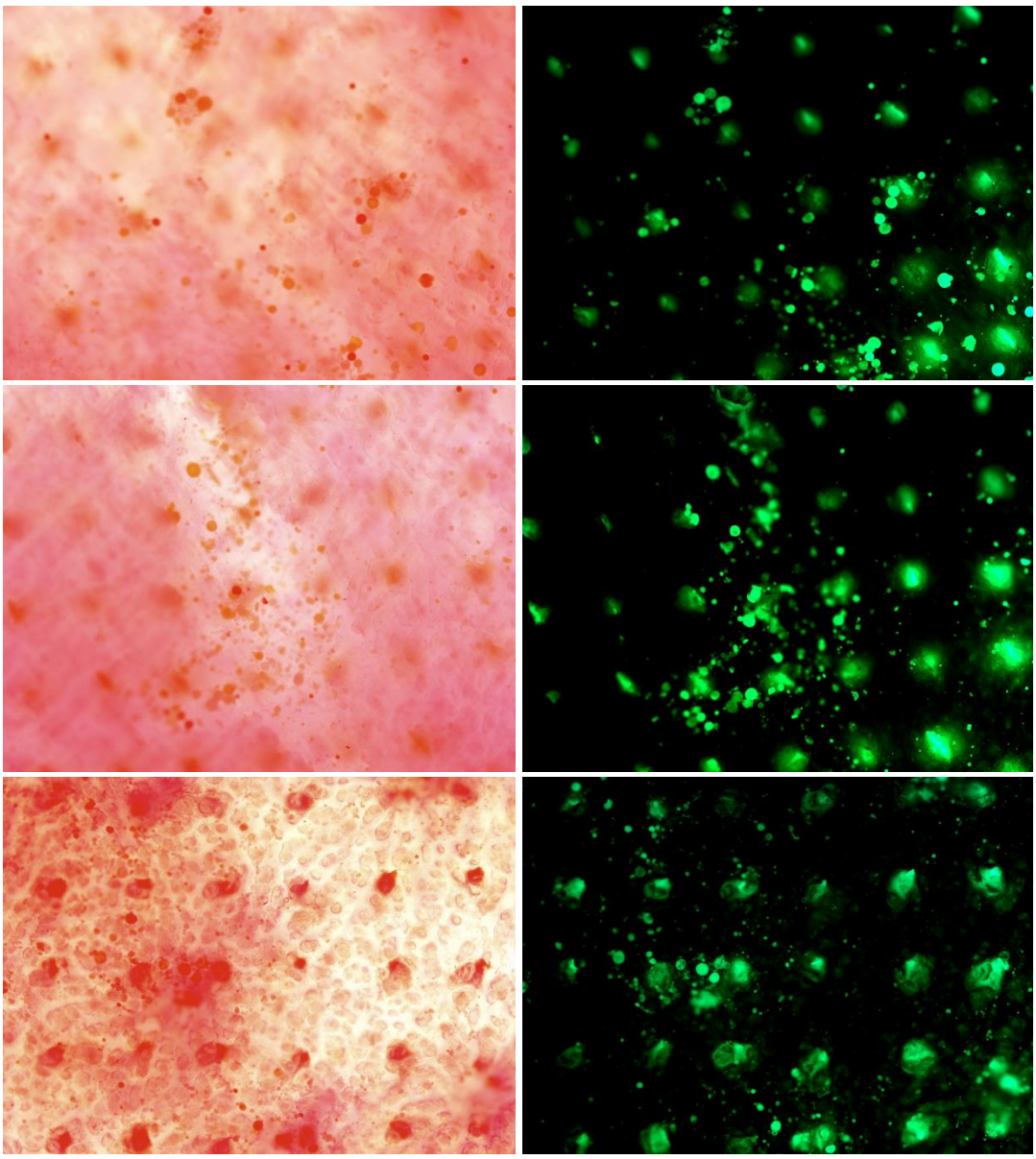

Figure 6.13: Standard optical (left) and fluorescence microscopy (right) images of post microneedle array application skin after 20 h diffusion testing illustrating microneedle micro-conduits and deposition of coumarin 6 loaded micro-particles.

Additionally, fluorescence microscopy images of the PBS receptor phase after 20 h of microneedle array application (Figure 6.14) clearly showed the presence of fluorescent micro-particles which indicated that, after being deposited within the tissue layers of the skin, the particles were capable of penetrating through the skin into the receptor phase. In addition, no particles were detected in the receptor phase after application of the aqueous dispersion control solution. Coulman *et al.* (2009) reported that polystyrene nanoparticles delivered through microneedle treated skin failed to permeate beyond the epidermal layer and exhibited progressive transdermal

retardation which would limit the application for systemic delivery [104]. Similarly, Zhang *et al.* (2010) reported high levels of particle accumulation in the epidermis with little penetration into the dermis [103]. This indicated that depositing the particles deep into the skin with the dissolving microneedles facilitated further penetration of the particles into the dermal layers as opposed to retention in the epidermis.

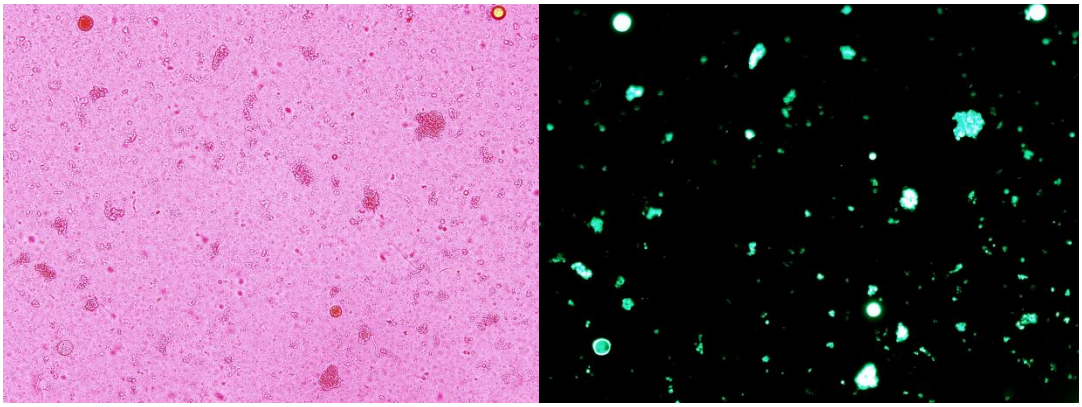

Figure 6.14: Standard optical microscope image (left) of receptor phase droplet after 20 h diffusion and same image (right) viewed using fluorescent filter highlighting coumarin 6 loaded micro-particles.

Fluorescence microscopy imaging was also taken of cross sections of post diffusion test skin samples to examine the penetration of the microneedles into the skin. Figure 6.15 illustrated the penetration depth of the microneedle shafts into the skin and highlighted the high concentration of particles that were encapsulated within the microneedle matrix, particularly the needle shafts. In addition, micro-particles can be seen embedded in the surrounding skin tissue.

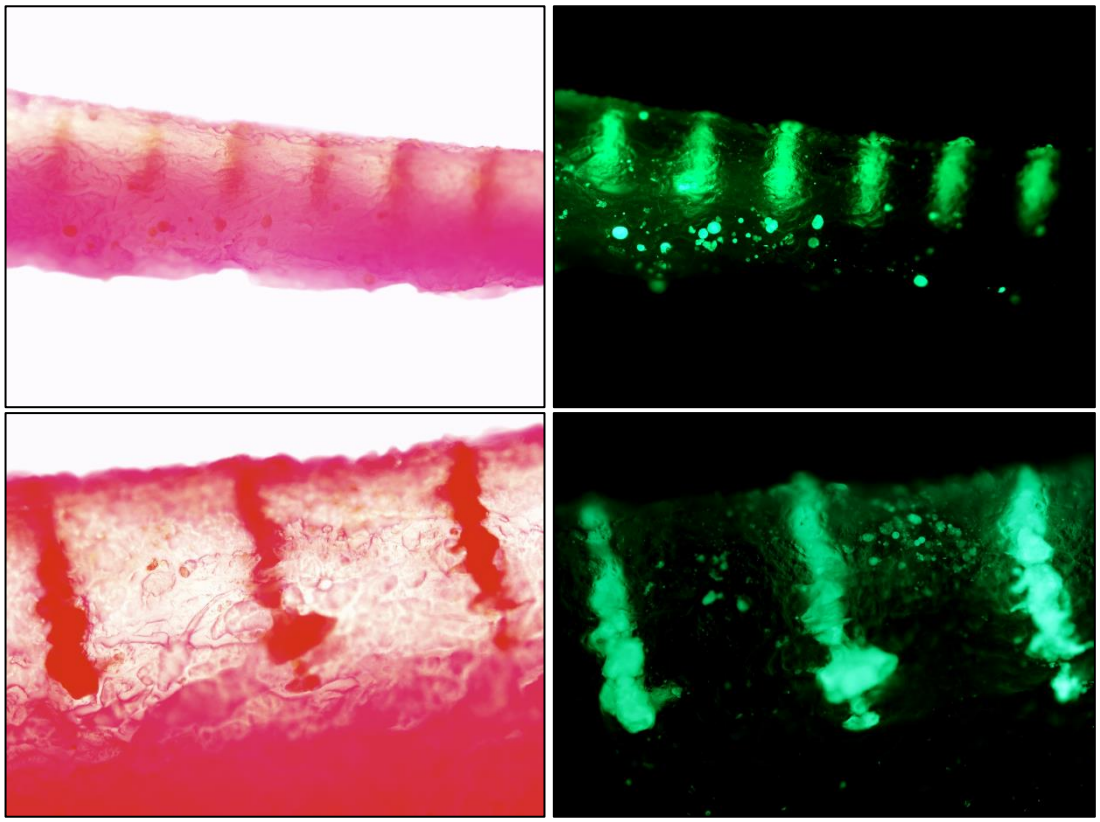

Figure 6.15: Cross section of post diffusion test skin after microneedle application. Images on the left show standard optical microscopy image, illustrating penetration depth of microneedles. Images on the right taken using FITC filter equipped fluorescence microscope illustrate fluorescence of the coumarin 6 loaded microneedles and deposited micro-particles.

As discussed above, dispersion of the micro-particles was not uniform in the formulation and as such, content uniformity testing could not be carried out on the formulation prior to the diffusion study. This was most likely as a result of the wide range of particle sizes in each batch with particles ranging from < 500 nm to > 100 µm. In order to ensure more uniform dispersion, further optimisation of this process would be required. Optimising particle formulation would ensure consistent particle sizes, particularly the formation of nanoparticles which would potentially be easier to suspend in the microneedle formulation more homogenously, as opposed to micro-particles.

Despite the fact that dispersion of particles in the microneedle matrix was not uniform, the release profile mirrored that of the previous studies into peptide release from the microneedle arrays (Section 4.4.7, Section 5.4.3.4). The microneedles delivered the particles at a faster initial rate than the control discs over the first 3-4 h

of the experiment before reverting to a rate comparable with the control discs (Figure 6.16). Two control types were utilised in the skin diffusion study namely a control disc of the microneedle formulation incorporating the fluorescent particles and an aqueous dispersion of the fluorescent particles (control).

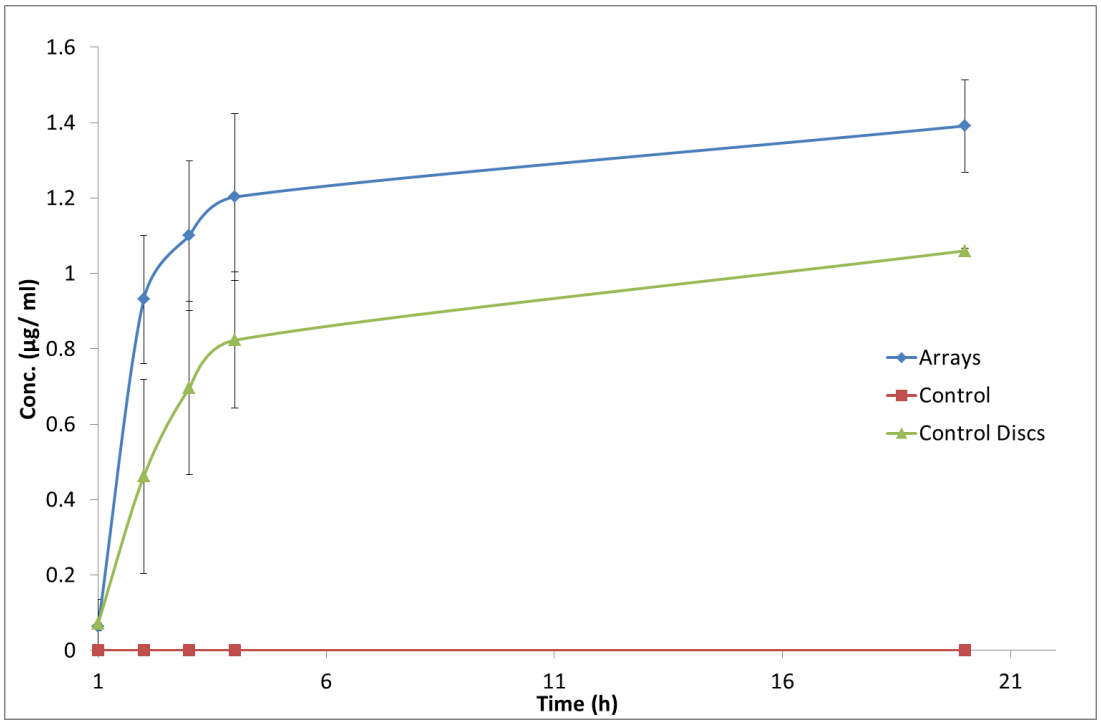

Figure 6.16: Coumarin 6 loaded micro-particle release profile from microneedle arrays, control discs and aqueous control solution.

In the case of the aqueous micro-particle dispersion, no particles were evident in the receptor phase at any stage of the experiment. This would suggest that the microneedle formulation itself contributed to the enhanced permeation of the particles through the skin, possible due to enhanced occlusion as a result of the formulation and the potential permeation enhancement properties of the PVP as described in Section 4.4.7.

Although scope remains for further optimisation, this system illustrated the successful transdermal delivery of PLGA particles by utilising the PVP/trehalose dissolving microneedle system. Compared with other studies which have utilised microneedles in a pre-treatment capacity [103, 104, 297], this system has illustrated suitability for systemic as opposed to intradermal drug delivery. There are a number of studies which have been carried out on dissolving microneedles to deliver drug

loaded particles. Ali *et al.* (2017) investigated the delivery of a peptide mediated DNA vaccine for the treatment of cervical cancer and reported a high antigen specific immune response however, the use of high MW PVP (360 kDa) in the study introduces the risk of polymer accumulation and renal clearance issues [166]. DeMuth *et al.* incorporated PLGA micro-particles into the tips of PAA microneedles and reported deposition of particles in murine skin up to a depth of 400 μm however, as the particles were confined to the tips of the needles, this potentially limited the amount of drug capable of being delivered via this system [303].

6.5. Conclusions

A double emulsion solvent evaporation technique was successfully employed to produce PLGA nano/micro-particles with relatively uniform size and shape. Polymyxin B was successfully loaded into the particles, however, the encapsulation efficiency was low at only 21.5 ± 3.4 %. The particles were incorporated in the PVP/trehalose microneedle formulation and microneedle arrays were cast as before. The addition of the particles to the arrays was determined to have little effect on the characteristics of the microneedles through thermal analysis, sorption profile analysis and SEM. The addition of the particles was not expected to affect the ability of the arrays to penetrate the skin and deliver the drug loaded particle payload. This was confirmed by OCT analysis which illustrated that the particle loaded needles were capable of penetrating the SC barrier to a sufficient depth (≈325 μm) to enable deposition of the particles within the dermal layers.

The polymyxin loaded particles were analysed to determine the drug release profile over time as a result of PLGA degradation. Although degradation of the particles was visible from SEM analysis, no drug release was detected in the samples analysed using HPLC. This was determined to be as a result of the slow degradation of the particles and subsequent low levels of drug released as a result. Additionally, poor drug encapsulation efficiency resulted in low levels of polymyxin within the particles. Well diffusion studies, however, indicated the presence of polymyxin within the particles after drug release study. This suggested that formulating faster degrading PLGA should result in detectable drug release over the same time period.

It was determined that optimisation of the particle drug loading would be required in order to develop this microneedle based sustained release system into an effective drug delivery method. A number of factors would need to be considered in order to achieve this including drug loading and type of drug utilised. By reducing the concentration of polymyxin incorporated into the formulation at the primary emulsion phase, the encapsulation efficiency of the particles may be increased. Less water soluble peptides may also be more successfully encapsulated in the PLGA particles and as such, may be more suitable drug candidates for this delivery system. Controlling the particle size to ensure nanoparticle yields which may result in more homogenous distribution within the microneedle matrix would also be required.

Increasing the sonication time can also reduce particle size by increasing shear stress which results in the breakdown of the primary emulsion droplets [300].

The dissolving microneedle based PLGA nano/micro-particle delivery system presented here exhibits vast potential as an effective sustained release transdermal peptide drug delivery system. To the author's knowledge, this is the first use of a PVP/trehalose dissolving microneedle system as a vehicle for PLGA particle delivery designed specifically for the sustained, systemic delivery of therapeutic biomolecules. However, further studies into the optimisation of the double emulsion particle formulation method are needed to improve particle size consistency and drug encapsulation efficiency. In addition, utilising a range of PLGA compositions would be required in order to achieve a better drug release profile.

CHAPTER 7. CONCLUSIONS & FUTURE WORK

7.1. Conclusions

The results obtained from the characterisation testing of the various PVP/trehalose formulations and subsequent statistical analysis has shown the effects each component has on the physical properties of each of the formulations. In addition to the morphological examination of the moulded microneedle arrays using SEM, the parameters of the various formulations investigated included disintegration time, T_g and water sorption behaviour. By examining each parameter, the effects of the polymer, sugar and plasticiser content was determined and statistical analysis also indicated the statistically significant factors for each property. From this analysis, a combination of 3:1 PVP/trehalose with 2% w/w glycerol was determined as the optimum formulation to proceed with the microneedle study.

The 3:1 PVP/trehalose microneedle formulation was extensively characterised using a wide range of techniques to establish the suitability of the formulation for the systemic delivery of biological pharmaceuticals such as therapeutic peptides and proteins. The results of these experiments indicated that the formulation possessed a sufficiently high T_g for prerequisite physical stability, exhibited moisture sorption behaviour which would facilitate rapid dissolution once applied to the skin (in addition to bolus drug delivery) and arrays cast from this formulation were fully formed and consistently representative of the master moulds. In addition, further testing was carried out to examine the mechanical strength of the needles to determine the fracture force and skin penetration abilities of the arrays. The effect of elevated RH on the needle tip sharpness was also examined. The results of the above indicated that the PVP/trehalose formulation produced microneedles that were more than adequately robust to penetrate the skin, and that kept a sufficient tip radius after exposure to relatively high RH conditions.

Coupled with the characterisation tests, fluorescence microscopy confirmed that material from the microneedles did not diffuse into the base layer of the array after the casting process. As such, drug material embedded in the microneedle shafts would be expected to remain in the needles only and no loss of the drug payload through diffusion into the base layer would be expected to occur if this was required in the drug delivery system.

The formulation was tested to determine if a model peptide drug, polymyxin B, could be encapsulated in the formulation without any loss of efficacy. A number of well/disc diffusion tests were carried out, the results of which indicated that the peptide maintained activity during all stages of the formulation process and remained unchanged after 70 days encapsulated in the polymer/sugar microneedle arrays. Following this, skin diffusion tests were carried out on microneedle arrays loaded with polymyxin B to determine the ability of the microneedles to successfully deliver the drug payload through porcine skin.

After successfully delivering the polymyxin B peptide, the microneedle arrays were loaded with two synthesised peptide analogues of existing therapeutic peptides. Fmoc based solid phase peptide synthesis was used to synthesise analogues of pentagastrin and sincalide which were then loaded into the microneedle arrays and delivered through porcine skin. The dissolving microneedle system successfully delivered all three peptides through porcine skin, delivering a greater concentration of drug at a higher rate than drug loaded control discs.

The final stage of the research aimed to develop a sustained release peptide drug delivery system utilising PLGA particles embedded in the PVP/trehalose dissolving microneedles. PLGA particles loaded with polymyxin were successfully formulated and incorporated into the microneedle arrays. Although the release profile of the drug from the particles over time could not be determined, the activity of the polymyxin in the particles was monitored and determined to have been unaffected by the formulation process and degradation over time of the PLGA particles. Coumarin 6 loaded PLGA particles were then utilised in skin diffusion studies to determine the ability of the microneedles to successfully deliver particles through the SC and into the dermal layers. Fluorescent microscopy and FLD HPLC was utilised to confirm that the coumarin 6 particles were successfully administered through the skin by the microneedles. In addition, the results indicated that the PVP/trehalose formulation itself may also have skin permeation enhancement qualities as particle delivery was observed from PVP/trehalose formulation control discs and not from aqueous based fluorescent particle dispersion.

7.2. Future Work

This study represents the first use of a tertiary formulation consisting of PVP, trehalose and glycerol for the fabrication of dissolvable microneedles designed to deliver therapeutic peptides transdermally. The characterisation techniques utilised provided comprehensive data on the quality of the formulation in respect of the envisioned application.

In combination with the characterisation techniques utilised in this study, additional studies may also be carried out on the PVP/trehalose formulations utilising Fourier transform infrared (FTIR) spectroscopy and solid state nuclear magnetic resonance (NMR) spectroscopy to further examine the bonding interactions between the polymer, sugar and plasticiser. Studies have been conducted into the characteristics of hydrogen bonding between PVP and trehalose [188, 189] and between PVP and plasticisers (glycerol and PEG 400) [171, 172, 190] and the effect these interactions have on the T_g of the amorphous mixtures. Given the influence that the T_g has on the physical stability and stabilising properties of the microneedle formulation [160, 183], developing a thorough understanding of the molecular interactions within the microneedle formulation would help to further develop and optimise the dissolving microneedle system. Similarly, further studies utilising DVS to develop a method of correlating moisture sorption data with dissolution profile for polymer/sugar dissolving microneedles would allow a comprehensive system of tailoring the dissolving microneedle for application with a number of therapeutic peptides or proteins. Combining these characterisation techniques with statistical analysis would allow for the prediction of the properties of various polymer/sugar/plasticiser combinations. Such characterisation techniques could potentially be utilised to modify and optimise the formulation for the delivery of other biologics and macromolecules such as larger peptides and therapeutic proteins.

The results of the drug diffusion studies indicated that the microneedle system was especially effective at rapidly delivering lower MW peptides. Further studies incorporating smaller peptides (2/3/4 amino acid residues) could be carried out to examine if this delivery profile is maintained where smaller peptides with a variety of amino acid residues are utilised.

Further optimisation of the microneedle mediated PLGA particle based sustained release system would be required to increase the encapsulation efficiency and facilitate controlled drug release of the particles. Investigating different combinations of PLGA in relation to molecular weight and feed ratio in conjunction with optimisation of the particle formulation process would allow for more controlled and predictable drug release due to PLGA degradation and more uniform particle size. The factors affecting PLGA particle formulation and subsequent drug loading are many and varied and as such, extensive research into this area would be required. In addition to the experimental factors (such as the PLGA used, emulsification parameters, sonication times, drug loading concentrations and evaporation conditions), interactions between the peptides and the PLGA could be examined to determine the effects on adsorption of the drug into the particles and subsequent release profiles.

The relatively low encapsulation efficiency associated with emulsion methods of particle formulation may be overcome through the investigation of other methods such as phase separation, spray drying, spray freeze drying, electrospray and supercritical fluid technologies. Further investigation into the use of such techniques may result in higher drug encapsulation but may need to be weighed against potential drawbacks such as residual solvents, particle aggregation, fragile particles and extended formulation times to name a few [282].

It is evident from the literature that microneedle technology has a wide range of potential drug and vaccine delivery applications. A recurring issue which is associated with these systems, however, is that reproducible manufacture at commercial scale can be challenging. Utilising high-precision materials deposition technologies, such as 3-D printing, is one promising route which could be used to overcome these issues. At the forefront of this area of research is the deposition of biomolecules without any loss of activity. The effective PVP/trehalose based dissolving microneedle formulation developed in this study, which has been designed specifically for the encapsulation and delivery of biomolecules could be readily utilised in such strategy and could lead to a viable commercial application of this exciting, new drug delivery technology.

APPENDIX I

LIST OF OUTPUTS

Dillon, C., Hughes, H., O'Reilly, N., McLoughlin, P., Development of Novel Drug Delivery Technologies for the Transdermal Delivery of Therapeutic Peptides. Poster presentation, 3rd International Conference on Microneedles 19th - 21st May 2014, University of Maryland School of Pharmacy, Baltimore, MD.

Dillon, C., Development of Microneedles for the Transdermal Delivery of Therapeutic Peptides. Oral presentation given at HIPODERM Seminar: Challenges in Dermal Formulation and Analysis, 5th February 2015, Waterford Institute of Technology.

Dillon, C., Hughes, H., O'Reilly, N., McLoughlin, P., Development of Novel Drug Delivery Technologies for the Transdermal Delivery of Therapeutic Peptides. Poster presentation, Waterford Institute of Technology Research Day 28th April 2015.

Dillon, C., Hughes, H., O'Reilly, N., McLoughlin, P., Development of Novel Drug Delivery Technologies for the Transdermal Delivery of Therapeutic Peptides. Poster presentation, 15th International Perspectives in Percutaneous Penetration Conference 30th March -1st April 2016. La Grande Motte, Montpelier, France.

Dillon, C., Hughes, H., O'Reilly, N., McLoughlin, P., Development of Novel Drug Delivery Technologies for the Transdermal Delivery of Therapeutic Peptides. Poster presentation & 3 Minute Thesis Talk, Waterford Institute of Technology Research Day 4th May 2016.

Dillon, C., Hughes, H., O'Reilly, N., McLoughlin, P., Development of Novel Drug Delivery Technologies for the Transdermal Delivery of Therapeutic Peptides. Poster presentation, 4th International Conference on Microneedles, 23rd – 25th May 2016. Brentwood, London.

Dillon, C., Hughes, H., O'Reilly, N., McLoughlin, P., Development of Novel Drug Delivery Technologies for the Transdermal Delivery of Therapeutic Peptides. Flash Oral and Poster presentation, 69th Irish Universities Chemistry Research Colloquium, 22nd -23rd June 2017. Dublin City University, Dublin.

APPENDIX II

PUBLICATIONS

Dillon, C., Hughes, H., O'Reilly, N.J., McLoughlin, P., 'Formulation and characterisation of dissolving microneedles for the transdermal delivery of therapeutic peptides'. Published in the International Journal of Pharmaceutics, June 2017.

REFERENCES:

1. Benson HAE, Watkinson AC. Topical and Transdermal Drug Delivery : Principles and Practice. Hoboken, NJ, USA: Wiley; 2011.
2. Prausnitz MR, Langer R. Transdermal drug delivery. Nature biotechnology. 2008;26(11):1261-8.
3. Gill HS, Prausnitz MR. Coated microneedles for transdermal delivery. Journal of Controlled Release. 2007;117(2):227-37.
4. Kim YC, Park JH, Prausnitz MR. Microneedles for drug and vaccine delivery. Advanced Drug Delivery Reviews. 2012;64(14):1547-68.
5. Menon GK. New insights into skin structure: scratching the surface. Advanced Drug Delivery Reviews. 2002;54, Supplement(0):S3-S17.
6. Kolarsick PAJ, Kolarsick, M. A., Goodwin, C. Anatomy and physiology of the skin. J Dermatol Nurses' Assoc. 2011;3:203-13.
7. Draelos Z, Pugliese PT. Physiology of the Skin (3rd Edition). Carol Stream, IL, USA: Allured Business Media; 2011.
8. Jun J-I, Lau LF. The Matricellular Protein CCN1/CYR61 Induces Fibroblast Senescence and Restricts Fibrosis in Cutaneous Wound Healing. Nature cell biology. 2010;12(7):676-85.
9. Ratna M. Topical and transdermal drug delivery: what a pharmacist needs to know College of Pharmacy, Glendale Midwestern University, Arizona2004 [cited 2015 03/06/2015]. Available from: http://www.inetce.com/articles/pdf/221-146-04-054-h01.pdf.
10. Graham-Brown R, Burns T. Lecture Notes : Dermatology (10th Edition). Hoboken, NJ, USA: Wiley-Blackwell; 2011.
11. Jablonski NG. Skin : A Natural History. Berkeley, CA, USA: University of California Press; 2013.
12. Haas ML. Principles of Skin Care and the Oncology Patient. Pittsburgh, PA, USA: Oncology Nursing Society; 2010.
13. Current Technologies to Increase the Transdermal Delivery of Drugs. Sharjah, UAE: Bentham Science Publishers; 2010.
14. Venus M, Waterman J, McNab I. Basic physiology of the skin. Surgery (Oxford). 2010;28(10):469-72.
15. Dermatological Treatments. SAIF Zone, Sharjah, UAE: Bentham Science Publishers; 2012.
16. Walter JR, Xu S. Therapeutic transdermal drug innovation from 2000 to 2014: current status and outlook. Drug Discov Today. 2015.
17. Wermeling DP, Banks SL, Hudson DA, Gill HS, Gupta J, Prausnitz MR, et al. Microneedles permit transdermal delivery of a skin-impermeant medication to humans. Proc Natl Acad Sci U S A. 2008;105(6):2058-63.
18. Park JH, Allen MG, Prausnitz MR. Biodegradable polymer microneedles: Fabrication, mechanics and transdermal drug delivery. Journal of Controlled Release. 2005;104(1):51-66.
19. Davidson A, Al-Qallaf B, Das DB. Transdermal drug delivery by coated microneedles: Geometry effects on effective skin thickness and drug permeability. Chemical Engineering Research & Design. 2008;86(11A):1196-206.
20. Index RLTID. Belladonna and Opium 2004 [01/07/15]. Available from: http://www.rxlist.com/belladonna-and-opium-drug.htm.
21. Partidos CD, Beignon AS, Mawas F, Belliard G, Briand JP, Muller S. Immunity under the skin: potential application for topical delivery of vaccines. Vaccine. 2003;21(7–8):776-80.

22. Badenhorst T, Svirskis, D., Wu, Z. Pharmaceutical strategies for the topical dermal delivery of peptides/proteins for cosmetic and therapeautic applications. Austin J Pharmacol Ther. 2014;2(6):1 - 10.
23. Williams AC, Barry BW. Penetration enhancers. Advanced Drug Delivery Reviews. 2012;64, Supplement(0):128-37.
24. Escobar-Chávez J. J, Rodríguez-Cruz, I., M., Domínguez-Delgado C., L.,. Chemical and physical enhancers for transdermal drug delivery 2012 [05/06/2015]. Available from: http://www.intechopen.com/books/pharmacology/chemical-and-physical-enhancers-for-transdermal-drug-delivery.
25. Zhai H, Maibach HI. Occlusion vs. skin barrier function. Skin Research and Technology. 2002;8(1):1-6.
26. Lane ME. Skin penetration enhancers. International Journal of Pharmaceutics. 2013;447(1–2):12-21.
27. Index RLTID. Liposyne II 2009 [01/07/15]. Available from: http://www.rxlist.com/liposyn-drug.htm.
28. Shin S-C, Cho C-W, Oh I-J. Effects of non-ionic surfactants as permeation enhancers towards piroxicam from the poloxamer gel through rat skins. International Journal of Pharmaceutics. 2001;222(2):199-203.
29. Information NCfB. Tween 80 [01/07/15]. Available from: https://pubchem.ncbi.nlm.nih.gov/compound/5281955.
30. Ciriminna R, Lomeli-Rodriguez M, Demma Cara P, Lopez-Sanchez JA, Pagliaro M. Limonene: a versatile chemical of the bioeconomy. Chemical Communications. 2014;50(97):15288-96.
31. Ching CTS, Camilleri I, Connolly P. A low-cost, programmable device for versatile current delivery in iontophoresis applications. Sensors and Actuators B: Chemical. 2005;106(2):534-40.
32. Mitragotri S. Devices for overcoming biological barriers: The use of physical forces to disrupt the barriers. Advanced Drug Delivery Reviews. 2013;65(1):100-3.
33. Kanikkannan N, Singh J, Ramarao P. Transdermal iontophoretic delivery of timolol maleate in albino rabbits. International Journal of Pharmaceutics. 2000;197(1–2):69-76.
34. Kumar V, Banga AK. Modulated iontophoretic delivery of small and large molecules through microchannels. International Journal of Pharmaceutics. 2012;434(1–2):106-14.
35. Katikaneni S, Li G, Badkar A, Banga AK. Transdermal delivery of a ~13 kDa protein—an in vivo comparison of physical enhancement methods. Journal of Drug Targeting. 2010;18(2):141-7.
36. Denet AR, Vanbever R, Preat V. Skin electroporation for transdermal and topical delivery. Advanced Drug Delivery Reviews. 2004;56(5):659-74.
37. Gratieri T, Alberti I, Lapteva M, Kalia YN. Next generation intra- and transdermal therapeutic systems: Using non- and minimally-invasive technologies to increase drug delivery into and across the skin. European Journal of Pharmaceutical Sciences. 2013;50(5):609-22.
38. Shahzad Y, Louw R, Gerber M, du Plessis J. Breaching the skin barrier through temperature modulations. Journal of Controlled Release. 2015;202(0):1-13.
39. Pharmaceutical Formulation Development of Peptides and Proteins. London, GBR: CRC Press; 1999.

40. Barrett GC, Elmore DT. Amino Acids and Peptides. West Nyack, NY, USA: Cambridge University Press; 1998.
41. Synthetic Peptides : A User's Guide. Cary, NC, USA: Oxford University Press, USA; 2002.
42. Inc. NEB. Amino acid structures 2015. Available from: https://www.neb.com/tools-and-resources/usage-guidelines/amino-acid-structures.
43. Lax RL. The future of peptide development in the pharmacetutical industry: Polypeptide Group; 2012. Available from: http://www.polypeptide.com/web/upload/medias/1401702726538c49464a6f5.pdf.
44. Uhlig T, Kyprianou T, Martinelli FG, Oppici CA, Heiligers D, Hills D, et al. The emergence of peptides in the pharmaceutical business: From exploration to exploitation. EuPA Open Proteomics. 2014;4(0):58-69.
45. Renukuntla J, Vadlapudi AD, Patel A, Boddu SHS, Mitra AK. Approaches for enhancing oral bioavailability of peptides and proteins. International Journal of Pharmaceutics. 2013;447(1–2):75-93.
46. Chandrudu S, Simerska P, Toth I. Chemical methods for peptide and protein production. Molecules. 2013;18(4):4373-88.
47. Castro PM, Fonte P, Sousa F, Madureira AR, Sarmento B, Pintado ME. Oral films as breakthrough tools for oral delivery of proteins/peptides. Journal of Controlled Release. 2015;211(0):63-73.
48. Tsomaia N. Peptide therapeutics: Targeting the undruggable space. European Journal of Medicinal Chemistry. 2015;94:459-70.
49. Edwards CMB, Cohen MA, Bloom SR. Peptides as drugs 1999. 92 p1-4.
50. Brange J, Langkjoer L. Insulin structure and stability. Pharm Biotechnol. 1993;5:315-50.
51. Mohammed YH, Yamada M, Lin LL, Grice JE, Roberts MS, Raphael AP, et al. Microneedle Enhanced Delivery of Cosmeceutically Relevant Peptides in Human Skin. PLoS ONE. 2014;9(7):e101956.
52. Chemicals F. The insulin peptide family 2012 [26/06/15]. Available from: http://www.fefchemicals.com/biopharm/scientific-information/articles/the-insulin-peptide-family/.
53. Vlieghe P, Lisowski V, Martinez J, Khrestchatisky M. Synthetic therapeutic peptides: science and market. Drug Discovery Today. 2010;15(1–2):40-56.
54. Edwards CMB, Cohen MA, Bloom SR. Peptides as drugs. Qjm-Monthly Journal of the Association of Physicians. 1999;92(1):1-4.
55. Reichert J. Development trends for peptide therapeutics. In: Pechon P, Tartar, A., Dunn, M.R., editor. A comprehensive quantitative analysis of peptide therapeutics in clinical development: Peptide Therapeutics Foundation; 2010.
56. Sun L. Peptide-based drug development. Mod Chem Appl. 2013;1(1).
57. Fosgerau K, Hoffmann T. Peptide therapeutics: current status and future directions. Drug Discovery Today. 2015;20(1):122-8.
58. FDA. Copaxone 2009 [26/06/15]. Available from: http://www.accessdata.fda.gov/drugsatfda_docs/label/2009/020622s057lbl.pdf.
59. FDA. Byetta 2009 [26/06/15]. Available from: http://www.accessdata.fda.gov/drugsatfda_docs/label/2009/021773s9s11s18s22s25lbl.pdf.
60. FDA. Forsteo 2002 [26/06/15]. Available from: http://www.accessdata.fda.gov/drugsatfda_docs/label/2009/021318s012lbl.pdf.

61. FDA. Miacalcin 2012 [26/06/15]. Available from: http://www.accessdata.fda.gov/drugsatfda_docs/label/2012/017808s034lbl.pdf.
62. FDA. Sandostatin LAR 2008 [26/06/15]. Available from: http://www.accessdata.fda.gov/drugsatfda_docs/label/2008/021008s021lbl.pdf.
63. FDA. Leuprorelin 2001 [26/06/15]. Available from: http://www.accessdata.fda.gov/drugsatfda_docs/nda/2001/20-708S011_Lupron_admincorres_P1.pdf.
64. FDA. Zoladex 2009 [26/06/15]. Available from: http://www.accessdata.fda.gov/drugsatfda_docs/label/2009/020578s028s029s030lbl.pdf.
65. Pauletti GM, Gangwar S, Siahaan TJ, Aube J, Borchardt RT. Improvement of oral peptide bioavailability: Peptidomimetics and prodrug strategies. Advanced Drug Delivery Reviews. 1997;27(2-3):235-56.
66. Castanho M, Santos NC, ebrary Inc. Peptide drug discovery and development translational research in academia and industry. Available from: http://libproxy.sdsu.edu/login?url=http://site.ebrary.com/lib/sdsulib/Doc?id=10504127 View Electronic Book (SDSU users only).
67. Leonard TW, Lynch J, McKenna MJ, Brayden DJ. Promoting absorption of drugs in humans using medium-chain fatty acid-based solid dosage forms: GIPET. Expert Opin Drug Deliv. 2006;3(5):685-92.
68. Book C. Cyclosporine A 2010. Available from: http://www.chemicalbook.com/ChemicalProductProperty_EN_CB5163816.htm.
69. Christophersen PC, Zhang L, Yang M, Nielsen HM, Müllertz A, Mu H. Solid lipid particles for oral delivery of peptide and protein drugs I – Elucidating the release mechanism of lysozyme during lipolysis. European Journal of Pharmaceutics and Biopharmaceutics. 2013;85(3, Part A):473-80.
70. Parmentier J, Thewes B, Gropp F, Fricker G. Oral peptide delivery by tetraether lipid liposomes. International Journal of Pharmaceutics. 2011;415(1–2):150-7.
71. Livingstone C. Peptide and protein drug delivery and the academic-industry interface. Pharmaceutical Science & Technology Today. 1998;1(8):324-5.
72. Aldrich S. L-Aspartic Acid 2015 [02/07/15]. Available from: http://www.sigmaaldrich.com/catalog/product/sigma/a9256?lang=en&region=IE.
73. Li GH, Badkar A, Nema S, Kolli CS, Banga AK. In vitro transdermal delivery of therapeutic antibodies using maltose microneedles. International Journal of Pharmaceutics. 2009;368(1-2):109-15.
74. Lin WQ, Cormier M, Samiee A, Griffin A, Johnson B, Teng CL, et al. Transdermal delivery of antisense oligonucleotides with microprojection patch (Macroflux (R)) technology. Pharmaceutical Research. 2001;18(12):1789-93.
75. Stawikowski M, Fields GB. Introduction to peptide synthesis. Curr Protoc Protein Sci. 2012;Chapter 18:Unit 18 1.
76. Shadidi M, Sioud M. Selective targeting of cancer cells using synthetic peptides. Drug Resistance Updates. 2003;6(6):363-71.
77. Chemblink. Glatiramer acetate 2015 [02/07/15]. Available from: http://www.chemblink.com/products/147245-92-9.htm.
78. Networks M. Oxytocin 2014 [02/07/2015]. Available from: http://www.molecular-networks.com/biopath3/biopath/mols/Oxytocin.
79. Albericio F. Developments in peptide and amide synthesis. Current Opinion in Chemical Biology. 2004;8(3):211-21.

80. McAllister DV, Allen MG, Prausnitz MR. Microfabricated Microneedles for Gene and Drug Delivery. Annual Review of Biomedical Engineering. 2000;2(1):289-313.
81. Gupta J, Gill HS, Andrews SN, Prausnitz MR. Kinetics of skin resealing after insertion of microneedles in human subjects. Journal of Controlled Release. 2011;154(2):148-55.
82. Gill HS, Prausnitz MR. Pocketed microneedles for drug delivery to the skin. Journal of Physics and Chemistry of Solids. 2008;69(5–6):1537-41.
83. Cormier M, Johnson B, Ameri M, Nyam K, Libiran L, Zhang DD, et al. Transdermal delivery of desmopressin using a coated microneedle array patch system. Journal of Controlled Release. 2004;97(3):503-11.
84. Donnelly RF, Garland MJ, Morrow DIJ, Migalska K, Singh TRR, Majithiya R, et al. Optical coherence tomography is a valuable tool in the study of the effects of microneedle geometry on skin penetration characteristics and in-skin dissolution. Journal of Controlled Release. 2010;147(3):333-41.
85. Yan GA, Warner KS, Zhang J, Sharma S, Gale BK. Evaluation needle length and density of microneedle arrays in the pretreatment of skin for transdermal drug delivery. International Journal of Pharmaceutics. 2010;391(1-2):7-12.
86. Bal SM, Kruithof AC, Zwier R, Dietz E, Bouwstra JA, Lademann J, et al. Influence of microneedle shape on the transport of a fluorescent dye into human skin in vivo. Journal of Controlled Release. 2010;147(2):218-24.
87. Martin CJ, Allender CJ, Brain KR, Morrissey A, Birchall JC. Low temperature fabrication of biodegradable sugar glass microneedles for transdermal drug delivery applications. Journal of Controlled Release. 2012;158(1):93-101.
88. Kaushik S, Hord AH, Denson DD, McAllister DV, Smitra S, Allen MG, et al. Lack of pain associated with microfabricated microneedles. Anesth Analg. 2001;92(2):502-4.
89. Kaur M, Ita KB, Popova IE, Parikh SJ, Bair DA. Microneedle-assisted delivery of verapamil hydrochloride and amlodipine besylate. European Journal of Pharmaceutics and Biopharmaceutics. 2014;86(2):284-91.
90. van der Maaden K, Varypataki EM, Yu H, Romeijn S, Jiskoot W, Bouwstra J. Parameter optimization toward optimal microneedle-based dermal vaccination. European Journal of Pharmaceutical Sciences. 2014;64(0):18-25.
91. Garland MJ, Caffarel-Salvador E, Migalska K, Woolfson AD, Donnelly RF. Dissolving polymeric microneedle arrays for electrically assisted transdermal drug delivery. Journal of Controlled Release. 2012;159(1):52-9.
92. Tuan-Mahmood T-M, McCrudden MTC, Torrisi BM, McAlister E, Garland MJ, Singh TRR, et al. Microneedles for intradermal and transdermal drug delivery. Eur J Pharm Sci. 2013;50(5):623-37.
93. Guo L, Chen J, Qiu Y, Zhang S, Xu B, Gao Y. Enhanced transcutaneous immunization via dissolving microneedle array loaded with liposome encapsulated antigen and adjuvant. International Journal of Pharmaceutics. 2013;447(1–2):22-30.
94. Chen M-C, Huang S-F, Lai K-Y, Ling M-H. Fully embeddable chitosan microneedles as a sustained release depot for intradermal vaccination. Biomaterials. 2013;34(12):3077-86.
95. Nayak A, Das DB. Potential of biodegradable microneedles as a transdermal delivery vehicle for lidocaine. Biotechnology Letters. 2013;35(9):1351-63.
96. Norman JJ, Arya JM, McClain MA, Frew PM, Meltzer MI, Prausnitz MR. Microneedle patches: Usability and acceptability for self-vaccination against influenza. Vaccine. 2014;32(16):1856-62.

97. Cleary G. Microneedles for Drug Delivery. Pharmaceutical Research. 2011;28(1):1-6.
98. van der Maaden K, Jiskoot W, Bouwstra J. Microneedle technologies for (trans)dermal drug and vaccine delivery. Journal of Controlled Release. 2012;161(2):645-55.
99. Zhou C-P, Liu Y-L, Wang H-L, Zhang P-X, Zhang J-L. Transdermal delivery of insulin using microneedle rollers in vivo. International Journal of Pharmaceutics. 2010;392(1–2):127-33.
100. Park JH, Choi SO, Seo S, Bin Choy Y, Prausnitz MR. A microneedle roller for transdermal drug delivery. European Journal of Pharmaceutics and Biopharmaceutics. 2010;76(2):282-9.
101. Henry S, McAllister DV, Allen MG, Prausnitz MR. Microfabricated microneedles: A novel approach to transdermal drug delivery Journal of Pharmaceutical Sciences. 1999;88(9):948-.
102. Banks SL, Paudel KS, Brogden NK, Loftin CD, Stinchcomb AL. Diclofenac Enables Prolonged Delivery of Naltrexone Through Microneedle-Treated Skin. Pharmaceutical Research. 2011;28(5):1211-9.
103. Zhang W, Gao J, Zhu QG, Zhang M, Ding XY, Wang XY, et al. Penetration and distribution of PLGA nanoparticles in the human skin treated with microneedles. International Journal of Pharmaceutics. 2010;402(1-2):205-12.
104. Coulman SA, Anstey A, Gateley C, Morrissey A, McLoughlin P, Allender C, et al. Microneedle mediated delivery of nanoparticles into human skin. International Journal of Pharmaceutics. 2009;366(1–2):190-200.
105. Teo AL, Shearwood C, Ng KC, Lu J, Moochhala S. Transdermal microneedles for drug delivery applications. Materials Science and Engineering B-Solid State Materials for Advanced Technology. 2006;132(1-2):151-4.
106. Rattanapak T, Birchall J, Young K, Ishii M, Meglinski I, Rades T, et al. Transcutaneous immunization using microneedles and cubosomes: Mechanistic investigations using Optical Coherence Tomography and Two-Photon Microscopy. Journal of Controlled Release. 2013;172(3):894-903.
107. Information NCfB. Melanostatin 2015 [02/07/15]. Available from: https://pubchem.ncbi.nlm.nih.gov/compound/92910.
108. Co. SAsC. PAL-KTTKS 2011 [02/07/15]. Available from: http://www.apischemical.com/APIsproducts2/214047-00-4,PAL-KTTKS.htm.
109. Kelchen MN, Siefers KJ, Converse CC, Farley MJ, Holdren GO, Brogden NK. Micropore closure kinetics are delayed following microneedle insertion in elderly subjects. Journal of Controlled Release. 2016;225:294-300.
110. van der Maaden K, Varypataki EM, Romeijn S, Ossendorp F, Jiskoot W, Bouwstra J. Ovalbumin-coated pH-sensitive microneedle arrays effectively induce ovalbumin-specific antibody and T-cell responses in mice. European Journal of Pharmaceutics and Biopharmaceutics. 2014;88(2):310-5.
111. Uddin MJ, Scoutaris N, Klepetsanis P, Chowdry B, Prausnitz MR, Douroumis D. Inkjet printing of transdermal microneedles for the delivery of anticancer agents. International Journal of Pharmaceutics. 2015;494(2):593-602.
112. BASF. Soluplus [02/07/15]. Available from: http://www.pharma-ingredients.basf.com/Products.aspx?PRD=30446233.
113. Khandan O, Kahook MY, Rao MP. Fenestrated microneedles for ocular drug delivery. Sensors and Actuators B: Chemical. 2016;223:15-23.
114. Xie Y, Xu B, Gao Y. Controlled transdermal delivery of model drug compounds by MEMS microneedle array. Nanomedicine: Nanotechnology, Biology and Medicine. 2005;1(2):184-90.

115. Witting M, Obst K, Pietzsch M, Friess W, Hedtrich S. Feasibility study for intraepidermal delivery of proteins using a solid microneedle array. International Journal of Pharmaceutics. 2015;486(1–2):52-8.
116. Information NCfB. Desmopressin 2015 [02/07/15]. Available from: https://pubchem.ncbi.nlm.nih.gov/compound/5311065.
117. Martanto W, Moore JS, Kashlan O, Kamath R, Wang PM, O'Neal JM, et al. Microinfusion using hollow microneedles. Pharmaceutical Research. 2006;23(1):104-13.
118. Lhernould MS, Deleers M, Delchambre A. Hollow polymer microneedles array resistance and insertion tests. International Journal of Pharmaceutics. 2015;480(1-2):152-7.
119. Vecchione R, Coppola S, Esposito E, Casale C, Vespini V, Grilli S, et al. Electro-Drawn Drug-Loaded Biodegradable Polymer Microneedles as a Viable Route to Hypodermic Injection. Advanced Functional Materials. 2014;24(23):3515-23.
120. Norman JJ, Choi SO, Tong NT, Aiyar AR, Patel SR, Prausnitz MR, et al. Hollow microneedles for intradermal injection fabricated by sacrificial micromolding and selective electrodeposition. Biomedical Microdevices. 2013;15(2):203-10.
121. Vinayakumar KB, Hegde GM, Nayak MM, Dinesh NS, Rajanna K. Fabrication and characterization of gold coated hollow silicon microneedle array for drug delivery. Microelectronic Engineering. 2014;128(0):12-8.
122. Kim M, Jung B, Park JH. Hydrogel swelling as a trigger to release biodegradable polymer microneedles in skin. Biomaterials. 2012;33(2):668-78.
123. Nuxoll E. BioMEMS in drug delivery. Advanced Drug Delivery Reviews. 2013;65(11–12):1611-25.
124. Kochhar JS, Zou S, Chan SY, Kang L. Protein encapsulation in polymeric microneedles by photolithography. International Journal of Nanomedicine. 2012;7:3143-54.
125. McGrath MG, Vucen S, Vrdoljak A, Kelly A, O'Mahony C, Crean AM, et al. Production of dissolvable microneedles using an atomised spray process: Effect of microneedle composition on skin penetration. European Journal of Pharmaceutics and Biopharmaceutics. 2014;86(2):200-11.
126. Biodegradable Polymers in Clinical Use and Clinical Development. Hoboken, NJ, USA: John Wiley & Sons; 2011.
127. Julinova M, Kupec J, Slavik R, Vaskova M. Initiating Biodegradation of Polyvinylpyrrolidone in an Aqueous Aerobic Environment: Technical Note. Ecological Chemistry and Engineering S-Chemia I Inzynieria Ekologiczna S. 2013;20(1):199-208.
128. Park JH, Allen MG, Prausnitz MR. Polymer microneedles for controlled-release drug delivery. Pharm Res. 2006;23(5):1008-19.
129. Chu LY, Prausnitz MR. Separable arrowhead microneedles. Journal of Controlled Release. 2011;149(3):242-9.
130. Moga KA, Bickford LR, Geil RD, Dunn SS, Pandya AA, Wang Y, et al. Rapidly–Dissolvable Microneedle Patches Via a Highly Scalable and Reproducible Soft Lithography Approach. Advanced Materials. 2013;25(36):5060-6.
131. Zhu DD, Chen BZ, He MC, Guo XD. Structural optimization of rapidly separating microneedles for efficient drug delivery. Journal of Industrial and Engineering Chemistry. 2017;51:178-84.

132. Modepalli N, Shivakumar HN, McCrudden MTC, Donnelly RF, Banga A, Murthy SN. Transdermal Delivery of Iron Using Soluble Microneedles: Dermal Kinetics and Safety. Journal of Pharmaceutical Sciences. 2016;105(3):1196-200.
133. Quinn HL, Bonham L, Hughes CM, Donnelly RF. Design of a Dissolving Microneedle Platform for Transdermal Delivery of a Fixed-Dose Combination of Cardiovascular Drugs. Journal of Pharmaceutical Sciences. 2015;104(10):3490-500.
134. Liu S, Jin MN, Quan YS, Kamiyama F, Katsumi H, Sakane T, et al. The development and characteristics of novel microneedle arrays fabricated from hyaluronic acid, and their application in the transdermal delivery of insulin. Journal of Controlled Release. 2012;161(3):933-41.
135. Chen M-C, Ling M-H, Kusuma SJ. Poly-γ-glutamic acid microneedles with a supporting structure design as a potential tool for transdermal delivery of insulin. Acta Biomaterialia. 2015;24:106-16.
136. Yu W, Jiang G, Liu D, Li L, Chen H, Liu Y, et al. Fabrication of biodegradable composite microneedles based on calcium sulfate and gelatin for transdermal delivery of insulin. Materials Science and Engineering: C. 2017;71:725-34.
137. Vrdoljak A, Allen EA, Ferrara F, Temperton NJ, Crean AM, Moore AC. Induction of broad immunity by thermostabilised vaccines incorporated in dissolvable microneedles using novel fabrication methods. Journal of Controlled Release. 2016;225:192-204.
138. Raphael AP, Crichton ML, Falconer RJ, Meliga S, Chen X, Fernando GJP, et al. Formulations for microprojection/microneedle vaccine delivery: Structure, strength and release profiles. Journal of Controlled Release. 2016;225:40-52.
139. Hsueh K-J, Chen M-C, Cheng L-T, Lee J-W, Chung W-B, Chu C-Y. Transcutaneous immunization of Streptococcus suis bacterin using dissolving microneedles. Comparative Immunology, Microbiology and Infectious Diseases. 2017;50:78-87.
140. Nakatsukasa A, Kuruma K, Okamatsu M, Hiono T, Suzuki M, Matsuno K, et al. Potency of whole virus particle and split virion vaccines using dissolving microneedle against challenges of H1N1 and H5N1 influenza viruses in mice. Vaccine. 2017;35(21):2855-61.
141. Arya JM, Dewitt K, Scott-Garrard M, Chiang Y-W, Prausnitz MR. Rabies vaccination in dogs using a dissolving microneedle patch. Journal of Controlled Release. 2016;239:19-26.
142. Rouphael NG, Paine M, Mosley R, Henry S, McAllister DV, Kalluri H, et al. The safety, immunogenicity, and acceptability of inactivated influenza vaccine delivered by microneedle patch (TIV-MNP 2015): a randomised, partly blinded, placebo-controlled, phase 1 trial. The Lancet. 2017;390(10095):649-58.
143. Seong K-Y, Seo M-S, Hwang DY, O'Cearbhaill ED, Sreenan S, Karp JM, et al. A self-adherent, bullet-shaped microneedle patch for controlled transdermal delivery of insulin. Journal of Controlled Release. 2017.
144. Kearney M-C, Caffarel-Salvador E, Fallows SJ, McCarthy HO, Donnelly RF. Microneedle-mediated delivery of donepezil: Potential for improved treatment options in Alzheimer's disease. European Journal of Pharmaceutics and Biopharmaceutics. 2016;103:43-50.
145. Cai B, Xia W, Bredenberg S, Li H, Engqvist H. Bioceramic microneedles with flexible and self-swelling substrate. European Journal of Pharmaceutics and Biopharmaceutics. 2015;94:404-10.

146. Donnelly RF, Morrow DIJ, Singh TRR. Microneedle-mediated Transdermal and Intradermal Drug Delivery (2nd Edition). Somerset, NJ, USA: Wiley-Blackwell; 2012.
147. Patist A, Zoerb H. Preservation mechanisms of trehalose in food and biosystems. Colloids and Surfaces B: Biointerfaces. 2005;40(2):107-13.
148. Demir YK, Akan Z, Kerimoglu O. Characterization of polymeric microneedle arrays for transdermal drug delivery. PLoS ONE. 2013.
149. Li G, Badkar A, Kalluri H, Banga AK. Microchannels created by sugar and metal microneedles: Characterization by microscopy, macromolecular flux and other techniques. Journal of Pharmaceutical Sciences. 2010;99(4):1931-41.
150. Donnelly RF, Morrow DIJ, Singh TRR, Migalska K, McCarron PA, O'Mahony C, et al. Processing difficulties and instability of carbohydrate microneedle arrays. Drug Development and Industrial Pharmacy. 2009;35(10):1242-54.
151. Loizidou EZ, Williams NA, Barrow DA, Eaton MJ, McCrory J, Evans SL, et al. Structural characterisation and transdermal delivery studies on sugar microneedles: Experimental and finite element modelling analyses. European Journal of Pharmaceutics and Biopharmaceutics. 2015;89:224-31.
152. Biomedicals M. Propranolol Hydrochloride 2014 [18/05/15]. Available from: http://www.mpbio.com/product.php?pid=02190088&country=103.
153. Simperler A, Kornherr A, Chopra R, Bonnet PA, Jones W, Motherwell WDS, et al. Glass transition temperature of glucose, sucrose, and trehalose: An experimental and in silico study. Journal of Physical Chemistry B. 2006;110(39):19678-84.
154. Simperler A, Kornherr A, Chopra R, Jones W, Motherwell WDS, Zifferer G. The glass transition temperatures of amorphous trehalose–water mixtures and the mobility of water: an experimental and in silico study. Carbohydrate Research. 2007;342(11):1470-9.
155. Teramoto N, Sachinvala ND, Shibata M. Trehalose and trehalose-based polymers for environmentally benign, biocompatible and bioactive materials. Molecules. 2008;13(8):1773-816.
156. Higashiyama T. Novel functions and applications of trehalose. Pure and Applied Chemistry. 2002;74(7):1263-9.
157. Jain NK, Roy I. Effect of trehalose on protein structure. Protein Sci. 2009;18(1):24-36.
158. Ogain ON, Li JH, Tajber L, Corrigan OI, Healy AM. Particle engineering of materials for oral inhalation by dry powder inhalers. I-Particles of sugar excipients (trehalose and raffinose) for protein delivery. International Journal of Pharmaceutics. 2011;405(1-2):23-35.
159. Barreca D, Laganà G, Magazù S, Migliardo F, Bellocco E. Glycerol, trehalose and glycerol–trehalose mixture effects on thermal stabilization of OCT. Chemical Physics. 2013;424(0):100-4.
160. Cicerone MT, Soles CL. Fast dynamics and stabilization of proteins: binary glasses of trehalose and glycerol. Biophys J. 2004;86(6):3836-45.
161. Dirama TE, Carri GA, Sokolov AP. Role of hydrogen bonds in the fast dynamics of binary glasses of trehalose and glycerol: a molecular dynamics simulation study. J Chem Phys. 2005;122(11):114505.
162. Pritchard HW. Desiccation and Plant Survival. Cary, NC, USA: CABI Publishing; 2002.
163. Sinnott M. Carbohydrate Chemistry and Biochemistry : Structure and Mechanism. Cambridge, GBR: Royal Society of Chemistry; 2007.

164. Haaf F, Sanner A, Straub F. Polymers of N-Vinylpyrrolidone - Synthesis, Characterization and Uses. Polymer Journal. 1985;17(1):143-52.
165. Folttmann H. Polyvinylpyrrolidone (PVP) - one of the most widely used excipients in pharmaceuticals: an overview. Drug Delivery Technology. 2008;8(6):22-7.
166. Bader RA, Putnam DA. Engineering Polymer Systems for Improved Drug Delivery. Somerset, NJ, USA: John Wiley & Sons, Incorporated; 2014.
167. Höhne G, Hemminger W, Flammersheim HJ. Differential scanning calorimetry. 2nd rev. and enl. ed. Berlin ; New York: Springer; 2003. xii, 298 p. p.
168. Ke C-J, Lin Y-J, Hu Y-C, Chiang W-L, Chen K-J, Yang W-C, et al. Multidrug release based on microneedle arrays filled with pH-responsive PLGA hollow microspheres. Biomaterials. 2012;33(20):5156-65.
169. Sullivan SP, Murthy N, Prausnitz MR. Minimally Invasive Protein Delivery with Rapidly Dissolving Polymer Microneedles. Advanced Materials. 2008;20(5):933-8.
170. Chen T, Fowler A, Toner M. Literature Review: Supplemented Phase Diagram of the Trehalose–Water Binary Mixture. Cryobiology. 2000;40(3):277-82.
171. Feldstein MM, Shandryuk GA, Platé NA. Relation of glass transition temperature to the hydrogen-bonding degree and energy in poly(N-vinyl pyrrolidone) blends with hydroxyl-containing plasticizers. Part 1. Effects of hydroxyl group number in plasticizer molecule. Polymer. 2001;42(3):971-9.
172. Feldstein MM, Roos A, Chevallier C, Creton C, Dormidontova EE. Relation of glass transition temperature to the hydrogen bonding degree and energy in poly(N-vinyl pyrrolidone) blends with hydroxyl-containing plasticizers: 3. Analysis of two glass transition temperatures featured for PVP solutions in liquid poly(ethylene glycol). Polymer. 2003;44(6):1819-34.
173. Brown ME. Introduction to Thermal Analysis, Volume 2 : Techniques and Applications (2nd Edition). Secaucus, NJ, USA: Kluwer Academic Publishers; 2001.
174. Method for preparing trehalose crystals. Google Patents; 2013.
175. Belfiore LA. Physical Properties of Macromolecules. Hoboken, NJ, USA: John Wiley & Sons; 2010.
176. Gupta A. Polymer Chemistry. Meerut, IND: Pragati Prakashan; 2010.
177. Brostow W, Chiu R, Kalogeras IM, Vassilikou-Dova A. Prediction of glass transition temperatures: Binary blends and copolymers. Materials Letters. 2008;62(17–18):3152-5.
178. Lai MC, Hageman MJ, Schowen RL, Borchardt RT, Topp EM. Chemical stability of peptides in polymers. 1. Effect of water on peptide deamidation in poly(vinyl alcohol) and poly(vinyl pyrrolidone) matrixes. Journal of Pharmaceutical Sciences. 1999;88(10):1073-80.
179. Inc. A. Polyvinylpyrrolidone polymers 2013 [30/07/15]. Available from: http://www.brenntagspecialties.com/en/downloads/Products/Multi_Market_Principals/Ashland/PVP_-_PVP_VA/PVP_Brochure.pdf.
180. Aldrich S. Glycerol 2017 [cited 2014 10/09/14]. Available from: http://www.sigmaaldrich.com/catalog/product/sigma/g5516?lang=en&region=IE.
181. Aldrich S. Poly(ethlyene glycol) 2017 [cited 2014 10/09/14]. Available from: http://www.sigmaaldrich.com/catalog/product/sial/p3015?lang=en&region=IE.
182. Nicholson JW. Chemistry of Polymers (3rd Edition). Cambridge, GBR: Royal Society of Chemistry; 2006.

183. Cicerone MT, Tellington A, Trost L, Sokolov A. Substantially Improved Stability. BioProcess International. 2003.
184. Franks F. Freeze-drying of Pharmaceuticals and Biopharmaceuticals : Principles and Practice. Cambridge, GBR: Royal Society of Chemistry; 2007.
185. Pinal R. Entropy of Mixing and the Glass Transition of Amorphous Mixtures. Entropy. 2008;10(3):207-23.
186. Zhang J, Zografi G. Water vapor absorption into amorphous sucrose-poly(vinyl pyrrolidone) and trehalose–poly(vinyl pyrrolidone) mixtures. Journal of Pharmaceutical Sciences. 2001;90(9):1375-85.
187. Royall P. Solid State Characterization of Pharmaceuticals (3rd Edition). Hoboken, NJ, USA: Wiley-Blackwell; 2011.
188. Imamura K, Asano Y, Maruyama Y, Yokoyama T, Nomura M, Ogawa S, et al. Characteristics of hydrogen bond formation between sugar and polymer in freeze-dried mixtures under different rehumidification conditions and its impact on the glass transition temperature. Journal of Pharmaceutical Sciences. 2008;97(3):1301-12.
189. Imamura K, Ohyama KI, Yokoyama T, Maruyama Y, Imanaka H, Nakanishi K. Temperature scanning FTIR analysis of interactions between sugar and polymer additive in amorphous sugar-polymer mixtures. Journal of Pharmaceutical Sciences. 2008;97(1):519-28.
190. Feldstein MM, Kuptsov SA, Shandryuk GA, Platé NA. Relation of glass transition temperature to the hydrogen-bonding degree and energy in poly(N-vinyl pyrrolidone) blends with hydroxyl-containing plasticizers. Part 2. Effects of poly(ethylene glycol) chain length. Polymer. 2001;42(3):981-90.
191. Wang Q, Yao G, Dong P, Gong Z, Li G, Zhang K, et al. Investigation on fabrication process of dissolving microneedle arrays to improve effective needle drug distribution. European Journal of Pharmaceutical Sciences. 2015;66(0):148-56.
192. Ko P-T, Lee IC, Chen M-C, Tsai S-W. Polymer microneedles fabricated from PCL and PCL/PEG blends for transdermal delivery of hydrophilic compounds. Journal of the Taiwan Institute of Chemical Engineers. 2015;51:1-8.
193. Khanna P, Flam BR, Osborn B, Strom JA, Bhansali S. Skin penetration and fracture strength testing of silicon dioxide microneedles. Sensors and Actuators A: Physical. 2011;170(1–2):180-6.
194. Donnelly RF, Majithiya R, Singh TRR, Morrow DIJ, Garland MJ, Demir YK, et al. Design, Optimization and Characterisation of Polymeric Microneedle Arrays Prepared by a Novel Laser-Based Micromoulding Technique. Pharmaceutical Research. 2011;28(1):41-57.
195. Römgens AM, Bader DL, Bouwstra JA, Baaijens FPT, Oomens CWJ. Monitoring the penetration process of single microneedles with varying tip diameters. Journal of the Mechanical Behavior of Biomedical Materials. 2014;40(0):397-405.
196. You XQ, Chang JH, Ju BK, Pak JJ. Rapidly dissolving fibroin microneedles for transdermal drug delivery. Materials Science & Engineering C-Materials for Biological Applications. 2011;31(8):1632-6.
197. Davis SP, Landis BJ, Adams ZH, Allen MG, Prausnitz MR. Insertion of microneedles into skin: measurement and prediction of insertion force and needle fracture force. Journal of Biomechanics. 2004;37(8):1155-63.
198. Roxhed N, Gasser TC, Griss P, Holzapfel GA, Stemme G. Penetration-enhanced ultrasharp microneedles and prediction on skin interaction for

efficient transdermal drug delivery. Journal of Microelectromechanical Systems. 2007;16(6):1429-40.
199. Gill HS, Denson DD, Burris BA, Prausnitz MR. Effect of microneedle design on pain in human volunteers. Clin J Pain. 2008;24(7):585-94.
200. Lee JW, Park JH, Prausnitz MR. Dissolving microneedles for transdermal drug delivery. Biomaterials. 2008;29(13):2113-24.
201. Thomas TA, Broun EC, Abildskov KM, Kubin CJ, Horan J, Yin MT, et al. High performance liquid chromatography-mass spectrometry assay for polymyxin B1 and B2 in human plasma. Ther Drug Monit. 2012;34(4):398-405.
202. Kwa AL, Tam VH, Falagas ME. Polymyxins: a review of the current status including recent developments. Ann Acad Med Singapore. 2008;37(10):870-83.
203. Kubin CJ, Ellman TM, Phadke V, Haynes LJ, Calfee DP, Yin MT. Incidence and predictors of acute kidney injury associated with intravenous polymyxin B therapy. Journal of Infection. 2012;65(1):80-7.
204. Falagas ME, Kasiakou SK. Toxicity of polymyxins: a systematic review of the evidence from old and recent studies. Critical Care. 2006;10(1).
205. Cheah SE, Bulitta JB, Li J, Nation RL. Development and validation of a liquid chromatography-mass spectrometry assay for polymyxin B in bacterial growth media. J Pharm Biomed Anal. 2014;92:177-82.
206. Taylor RB, Richards RME, Low AS, Hardie L. Chemical stability of polymyxin B in aqueous solution. International Journal of Pharmaceutics. 1994;102(1–3):201-6.
207. Information NCfB. Polymyxin B 2015 [02/07/15]. Available from: https://pubchem.ncbi.nlm.nih.gov/compound/9833652.
208. Bassiri E. Antibiotic Sensitivity Testing University of Pennsylvania School of Arts and Sciences. Available from: http://www.sas.upenn.edu/LabManuals/biol275/Table_of_Contents_files/10-Antibiotics-New.pdf.
209. Rockland LB. Saturated salt solutions for static control of relative humidity between 5 degrees C and 40 degrees C. Analytical Chemistry. 1960;32(10):1375-6.
210. Aldrich S. Sodium Fluorescein Salt 2015 [28/08/15]. Available from: http://www.sigmaaldrich.com/catalog/product/sial/f6377?lang=en&region=IE.
211. Yang S, Feng Y, Zhang L, Chen N, Yuan W, Jin T. A scalable fabrication process of polymer microneedles. International Journal of Nanomedicine. 2012;7:1415-22.
212. Liu S, Jin M-n, Quan Y-s, Kamiyama F, Kusamori K, Katsumi H, et al. Transdermal delivery of relatively high molecular weight drugs using novel self-dissolving microneedle arrays fabricated from hyaluronic acid and their characteristics and safety after application to the skin. European Journal of Pharmaceutics and Biopharmaceutics. 2014;86(2):267-76.
213. Lee M-T, Lee IC, Tsai S-W, Chen C-H, Wu M-H, Juang Y-J. Spin coating of polymer solution on polydimethylsiloxane mold for fabrication of microneedle patch. Journal of the Taiwan Institute of Chemical Engineers.
214. Jorgensen JH, Ferraro MJ. Antimicrobial susceptibility testing: a review of general principles and contemporary practices. Clin Infect Dis. 2009;49(11):1749-55.
215. InvivoGen. Polymyxin B 2015. Available from: http://www.invivogen.com/PDF/Polymyxin_B_TDS_09E27-MM.pdf.

216. Bartosova L, Bajgar J. Transdermal drug delivery in vitro using diffusion cells. Curr Med Chem. 2012;19(27):4671-7.
217. Steffansen B, Brodin B, Nielsen CU. Molecular Biopharmaceutics: Aspects of Drug Characterisation, Drug Delivery and Dosage Form Evaluation: Pharmaceutical Press; 2010.
218. Ruela ALM, Perissinato AG, Lino MEdS, Mudrik PS, Pereira GR. Evaluation of skin absorption of drugs from topical and transdermal formulations. Brazilian Journal of Pharmaceutical Sciences. 2016;52:527-44.
219. Cevc G, Mazgareanu S, Rother M, Vierl U. Occlusion effect on transcutaneous NSAID delivery from conventional and carrier-based formulations. International Journal of Pharmaceutics. 2008;359(1–2):190-7.
220. Pham QD, Björklund S, Engblom J, Topgaard D, Sparr E. Chemical penetration enhancers in stratum corneum — Relation between molecular effects and barrier function. Journal of Controlled Release. 2016;232:175-87.
221. Björklund S, Engblom J, Thuresson K, Sparr E. A water gradient can be used to regulate drug transport across skin. Journal of Controlled Release. 2010;143(2):191-200.
222. Baert B, Boonen J, Burvenich C, Roche N, Stillaert F, Blondeel P, et al. A new discriminative criterion for the development of Franz diffusion tests for transdermal pharmaceuticals. J Pharm Pharm Sci. 2010;13(2):218-30.
223. Inc. P. Diffusion Testing Fundamentals 2015 [updated 14/02/17]. Available from: http://permegear.com/wp-content/uploads/2015/08/primer.pdf.
224. Ng SF, Rouse JJ, Sanderson FD, Meidan V, Eccleston GM. Validation of a static Franz diffusion cell system for in vitro permeation studies. AAPS PharmSciTech. 2010;11(3):1432-41.
225. Prausnitz MR, Elias PM, Franz TJ, Schmuth M, Tsai J-C, Menon GK, et al. Skin barrier and transdermal drug delivery. Medical Therapy. 2012.
226. Larrañeta E, Moore J, Vicente-Pérez EM, González-Vázquez P, Lutton R, Woolfson AD, et al. A proposed model membrane and test method for microneedle insertion studies. International Journal of Pharmaceutics. 2014;472(1–2):65-73.
227. Hartmann XH, van der Linde P, Homburg EF, van Breemen LC, de Jong AM, Luttge R. Insertion Process of Ceramic Nanoporous Microneedles by Means of a Novel Mechanical Applicator Design. Pharmaceutics. 2015;7(4):503-22.
228. Sciences P. Development and Validation of *In Vitro* Release Testing Methods for Semisolid Formulations2009 [cited 2017 20/04/17]; 10. Available from: http://www.particlesciences.com/news/technical-briefs/2009/in-vitro-release-testing-methods.html.
229. Rahman A, Rizwan S, Waycaster C, Wall GM. Pooled analysis of two clinical trials comparing the clinical outcomes of topical ciprofloxacin/dexamethasone otic suspension and polymyxin B/neomycin/hydrocortisone otic suspension for the treatment of acute otitis externa in adults and children. Clinical Therapeutics. 2007;29(9):1950-6.
230. Adams E, Schepers R, Gathu LW, Kibaya R, Roets E, Hoogmartens J. Liquid chromatographic analysis of a formulation containing polymyxin, gramicidin and neomycin. Journal of Pharmaceutical and Biomedical Analysis. 1997;15(4):505-11.
231. Whall TJ. High-performance liquid chromatography of polymyxin B sulfate and colistin sulfate. Journal of Chromatography A. 1981;208(1):118-23.
232. Orwa JA, Govaerts C, Gevers K, Roets E, Van Schepdael A, Hoogmartens J. Study of the stability of polymyxins B1, E1 and E2 in aqueous solution using

liquid chromatography and mass spectrometry. Journal of Pharmaceutical and Biomedical Analysis. 2002;29(1–2):203-12.
233. Orwa JA, Van Gerven A, Roets E, Hoogmartens J. Liquid chromatography of polymyxin B sulphate. Journal of Chromatography A. 2000;870(1–2):237-43.
234. ICH. Validation of analytical procedures: text and methodology Q2(R1). ICH Harmonised Tripartite Guideline: 2005.
235. Sakabe J-i, Yamamoto M, Hirakawa S, Motoyama A, Ohta I, Tatsuno K, et al. Kallikrein-related Peptidase 5 Functions in Proteolytic Processing of Profilaggrin in Cultured Human Keratinocytes. The Journal of Biological Chemistry. 2013;288(24):17179-89.
236. Lapière CM, Pierard G. Skin Procollagen Peptidase in Normal and Pathologic Conditions. Journal of Investigative Dermatology. 1974;62(6):582-6.
237. Teixeira TSP, Freitas RF, Abrahão Jr O, Devienne KF, de Souza LR, Blaber SI, et al. Biological evaluation and docking studies of natural isocoumarins as inhibitors for human kallikrein 5 and 7. Bioorganic & Medicinal Chemistry Letters. 2011;21(20):6112-5.
238. Nair R, Nyamweya N, Gönen S, Martínez-Miranda LJ, Hoag SW. Influence of various drugs on the glass transition temperature of poly(vinylpyrrolidone): a thermodynamic and spectroscopic investigation. International Journal of Pharmaceutics. 2001;225(1):83-96.
239. Barbero AM, Frasch HF. Pig and guinea pig skin as surrogates for human in vitro penetration studies: A quantitative review. Toxicology in Vitro. 2009;23(1):1-13.
240. Godin B, Touitou E. Transdermal skin delivery: Predictions for humans from in vivo, ex vivo and animal models. Advanced Drug Delivery Reviews. 2007;59(11):1152-61.
241. Kielhorn J, Melching-Kollmuss S, Mangelsdorf I, United Nations Environment P, International Labour O, World Health O. Dermal absorption : first draft. Geneva: World Health Organization; 2006. xix, 197 : ill. ; 21 cm. p.
242. Sun WC, Araci Z, Inayathullah M, Manickam S, Zhang XX, Bruce MA, et al. Polyvinylpyrrolidone microneedles enable delivery of intact proteins for diagnostic and therapeutic applications. Acta Biomaterialia. 2013;9(8):7767-74.
243. Trommer H, Neubert RHH. Overcoming the stratum corneum: The modulation of skin penetration - A review. Skin Pharmacology and Physiology. 2006;19(2):106-21.
244. Shaikh HK, Kshirsagar, R.V., Patil, S.G. Mathematical models for drug release characterisation: a review. World Journal of Pharmacy and Pharmaceutical Sciences. 2015;4(04):324-38.
245. Christensen JM, Chuong MC, Le H, Pham L, Bendas E. Hydrocortisone Diffusion Through Synthetic Membrane, Mouse Skin, and Epiderm™ Cultured Skin. Archives of Drug Information. 2011;4(1):10-21.
246. Thakkar V, Shah P, Soni T, Parmar M, Gohel M, Gandhi T. Goodness-of-fit model-dependent approach for release kinetics of levofloxacin hemihydrates floating tablet. Dissolution Technologies. 2009;16(1):35-9.
247. Taylor LJ, Lee RS, Long M, Rawlings AV, Tubek J, Whitehead L, et al. Effect of occlusion on the percutaneous penetration of linoleic acid and glycerol. International Journal of Pharmaceutics. 2002;249(1–2):157-64.
248. Zhang S, Qiu Y, Gao Y. Enhanced delivery of hydrophilic peptides in vitro by transdermal microneedle pretreatment. Acta Pharmaceutica Sinica B. 2014;4(1):100-4.

249. Cherukuri S, Batchu UR, Mandava K, Cherukuri V, Ganapuram KR. Formulation and evaluation of transdermal drug delivery of topiramate. International Journal of Pharmaceutical Investigation. 2017;7(1):10-7.
250. Kumar De P, Mallick S, Mukherjee B, Sengupta S, Pattnaik S, Chakraborty S. Optimization of In-vitro Permeation Pattern of Ketorolac Tromethamine Transdermal Patches. Iranian Journal of Pharmaceutical Research : IJPR. 2011;10(2):193-201.
251. Silva LAD, Taveira SF, Lima EM, Marreto RN. In vitro skin penetration of clobetasol from lipid nanoparticles: drug extraction and quantitation in different skin layers. Brazilian Journal of Pharmaceutical Sciences. 2012;48:811-7.
252. Silva NC, Sarmento B, Pintado M. The importance of antimicrobial peptides and their potential for therapeutic use in ophthalmology. International Journal of Antimicrobial Agents. 2013;41(1):5-10.
253. Craik DJ, Fairlie DP, Liras S, Price D. The Future of Peptide-based Drugs. Chemical Biology & Drug Design. 2013;81(1):136-47.
254. Wu LC, Chen F, Lee SL, Raw A, Yu LX. Building parity between brand and generic peptide products: Regulatory and scientific considerations for quality of synthetic peptides. International Journal of Pharmaceutics. 2017;518(1–2):320-34.
255. Brayden DJ, Alonso M-J. Oral delivery of peptides: opportunities and issues for translation. Advanced Drug Delivery Reviews. 2016;106, Part B:193-5.
256. Kumar S, Zakrewsky M, Chen M, Menegatti S, Muraski JA, Mitragotri S. Peptides as skin penetration enhancers: Mechanisms of action. Journal of Controlled Release. 2015;199:168-78.
257. Hsu T, Mitragotri S. Delivery of siRNA and other macromolecules into skin and cells using a peptide enhancer. Proceedings of the National Academy of Sciences. 2011;108(38):15816-21.
258. Cohen-Avrahami M, Libster D, Aserin A, Garti N. Penetratin-induced transdermal delivery from HII mesophases of sodium diclofenac. Journal of Controlled Release. 2012;159(3):419-28.
259. Zhao X, Coulman SA, Hanna SJ, Susan Wong F, Dayan CM, Birchall JC. Formulation of hydrophobic peptides for skin delivery via coated microneedles. Journal of Controlled Release. 2017.
260. Book C. Benzoyl Glycylglycine 2017 [28/06/17]. Available from: http://www.chemicalbook.com/ChemicalProductProperty_EN_CB1770102.htm.
261. Pubchem. Glycylglycine 2017 [28/06/2017]. Available from: https://pubchem.ncbi.nlm.nih.gov/compound/Glycylglycine.
262. Advances in Molecular Biology : Synthetic Peptides : A User's Guide (2). Cary, GB: OUP Oxford; 2002.
263. Carpino LA, Han GY. 9-Fluorenylmethoxycarbonyl function, a new base-sensitive amino-protecting group. Journal of the American Chemical Society. 1970;92(19):5748-9.
264. Huang H, Rabenstein DL. A cleavage cocktail for methionine-containing peptides. J Pept Res. 1999;53(5):548-53.
265. Aldrich S. Fmoc chloride 2017 [cited 2017 27/06/17]. Available from: http://www.sigmaaldrich.com/catalog/product/aldrich/160512?lang=en&region=IE.

266. Aldrich S. Solid Phase Peptide Synthesis Scheme [3/02/17]. Available from: http://www.sigmaaldrich.com/life-science/custom-oligos/custom-peptides/learning-center/solid-phase-synthesis.html.
267. Scientific T. Cleavage, Deprotection, and Isolation of Peptides after Fmoc Synthesis 1998 [cited 2016 20/03/16]. Technical Bulletin]. Available from: https://tools.thermofisher.com/content/sfs/brochures/cms_040654.pdf.
268. Kosugi Y, Yamamoto S, Sano N, Furuta A, Igari T, Fujioka Y, et al. Evaluation of Acid Tolerance of Drugs Using Rats and Dogs Controlled for Gastric Acid Secretion. Journal of Pharmaceutical Sciences. 2015;104(9):2887-93.
269. Barbot N, Calmettes C, Schuffenecker I, Saint-Andre JP, Franc B, Rohmer V, et al. Pentagastrin stimulation test and early diagnosis of medullary thyroid carcinoma using an immunoradiometric assay of calcitonin: comparison with genetic screening in hereditary medullary thyroid carcinoma. J Clin Endocrinol Metab. 1994;78(1):114-20.
270. De Cort K, Schroijen M, Hurlemann R, Claassen S, Hoogenhout J, Van den Bergh O, et al. Modeling the development of panic disorder with interoceptive conditioning. European Neuropsychopharmacology. 2017;27(1):59-69.
271. Book C. Pentagastrin 2016 [01/12/16]. Available from: http://www.chemicalbook.com/ChemicalProductProperty_EN_CB4412263.htm.
272. Inc BD. Kinevac Sincalide for Injection 2014 [cited 2017 09/05/2017]. Available from: http://imaging.bracco.com/sites/braccoimaging.com/files/technica_sheet_pdf/us-en-2016-07-20-spc-kinevac.pdf.
273. Book C. Sincalide 2016 [01/12/16]. Available from: http://www.chemicalbook.com/ChemicalProductProperty_EN_CB7361692.htm.
274. Michels T, Dolling R, Haberkorn U, Mier W. Acid-mediated prevention of aspartimide formation in solid phase peptide synthesis. Org Lett. 2012;14(20):5218-21.
275. Shechter Y. Selective oxidation and reduction of methionine residues in peptides and proteins by oxygen exchange between sulfoxide and sulfide. J Biol Chem. 1986;261(1):66-70.
276. AAPPTEC. Practical Synthesis Guide to Solid Phase Peptide Chemistry: Advanced Automated Peptide Protein Technologies; 2008 [4th April 2016]. Available from: https://www.aapptec.com/custdocs/aapptec%20Synthesis%20Guide%202-0%20(2).pdf.
277. Ita K. Transdermal delivery of vaccines – Recent progress and critical issues. Biomedicine & Pharmacotherapy. 2016;83:1080-8.
278. Velkov T, Roberts KD, Nation RL, Thompson PE, Li J. Pharmacology of polymyxins: new insights into an 'old' class of antibiotics. Future Microbiol. 2013;8(6):711-24.
279. Rocco D, Ross J, Murray PE, Caccetta R. Acyl lipidation of a peptide: effects on activity and epidermal permeability in vitro. Drug Design, Development and Therapy. 2016;10:2203-9.
280. Namjoshi S, Toth I, Blanchfield JT, Trotter N, Mancera RL, Benson HA. Enhanced transdermal peptide delivery and stability by lipid conjugation: epidermal permeation, stereoselectivity and mechanistic insights. Pharm Res. 2014;31(12):3304-12.

281. Pagels RF, Prud'homme RK. Polymeric nanoparticles and microparticles for the delivery of peptides, biologics, and soluble therapeutics. Journal of Controlled Release. 2015;219:519-35.
282. Wan F, Yang M. Design of PLGA-based depot delivery systems for biopharmaceuticals prepared by spray drying. International Journal of Pharmaceutics. 2016;498(1–2):82-95.
283. Varypataki EM, Silva AL, Barnier-Quer C, Collin N, Ossendorp F, Jiskoot W. Synthetic long peptide-based vaccine formulations for induction of cell mediated immunity: A comparative study of cationic liposomes and PLGA nanoparticles. Journal of Controlled Release. 2016;226:98-106.
284. Ma G. Microencapsulation of protein drugs for drug delivery: Strategy, preparation, and applications. Journal of Controlled Release. 2014;193(0):324-40.
285. Malhaire H, Gimel J-C, Roger E, Benoît J-P, Lagarce F. How to design the surface of peptide-loaded nanoparticles for efficient oral bioavailability? Advanced Drug Delivery Reviews. 2016;106, Part B:320-36.
286. Dinarvand R, Sepehri N, Manoochehri S, Rouhani H, Atyabi F. Polylactide-co-glycolide nanoparticles for controlled delivery of anticancer agents. International Journal of Nanomedicine. 2011;6:877-95.
287. Schwendeman SP, Shah RB, Bailey BA, Schwendeman AS. Injectable controlled release depots for large molecules. Journal of Controlled Release. 2014;190:240-53.
288. Zhang Z, Tsai PC, Ramezanli T, Michniak-Kohn BB. Polymeric nanoparticles-based topical delivery systems for the treatment of dermatological diseases. Wiley Interdisciplinary Reviews-Nanomedicine and Nanobiotechnology. 2013;5(3):205-18.
289. Hans ML, Lowman AM. Biodegradable nanoparticles for drug delivery and targeting. Current Opinion in Solid State and Materials Science. 2002;6(4):319-27.
290. Chereddy KK, Her C-H, Comune M, Moia C, Lopes A, Porporato PE, et al. PLGA nanoparticles loaded with host defense peptide LL37 promote wound healing. Journal of Controlled Release. 2014;194:138-47.
291. Water JJ, Smart S, Franzyk H, Foged C, Nielsen HM. Nanoparticle-mediated delivery of the antimicrobial peptide plectasin against Staphylococcus aureus in infected epithelial cells. European Journal of Pharmaceutics and Biopharmaceutics. 2015;92:65-73.
292. McGinity JW, O'Donnell PB. Preparation of microspheres by the solvent evaporation technique. Adv Drug Deliv Rev. 1997;28(1):25-42.
293. Zambaux MF, Bonneaux F, Gref R, Maincent P, Dellacherie E, Alonso MJ, et al. Influence of experimental parameters on the characteristics of poly(lactic acid) nanoparticles prepared by a double emulsion method. J Control Release. 1998;50(1-3):31-40.
294. Fan J-B, Huang C, Jiang L, Wang S. Nanoporous microspheres: from controllable synthesis to healthcare applications. Journal of Materials Chemistry B. 2013;1(17):2222-35.
295. Vauthier C, Bouchemal K. Methods for the preparation and manufacture of polymeric nanoparticles. Pharm Res. 2009;26(5):1025-58.
296. Patzelt A, Mak WC, Jung S, Knorr F, Meinke MC, Richter H, et al. Do nanoparticles have a future in dermal drug delivery? Journal of Controlled Release. 2017;246:174-82.

297. Gomaa YA, Garland MJ, McInnes FJ, Donnelly RF, El-Khordagui LK, Wilson CG. Microneedle/nanoencapsulation-mediated transdermal delivery: Mechanistic insights. European Journal of Pharmaceutics and Biopharmaceutics. 2014;86(2):145-55.
298. Govender T, Stolnik S, Garnett MC, Illum L, Davis SS. PLGA nanoparticles prepared by nanoprecipitation: drug loading and release studies of a water soluble drug. Journal of Controlled Release. 1999;57(2):171-85.
299. Kristoffersen AS, Erga SR, Hamre B, Frette O. Testing fluorescence lifetime standards using two-photon excitation and time-domain instrumentation: rhodamine B, coumarin 6 and lucifer yellow. J Fluoresc. 2014;24(4):1015-24.
300. Najlah M, Ahmed Z, Iqbal M, Wang Z, Tawari P, Wang W, et al. Development and characterisation of disulfiram-loaded PLGA nanoparticles for the treatment of non-small cell lung cancer. European Journal of Pharmaceutics and Biopharmaceutics. 2017;112:224-33.
301. Finke JH, Richter C, Gothsch T, Kwade A, Büttgenbach S, Müller-Goymann CC. Coumarin 6 as a fluorescent model drug: How to identify properties of lipid colloidal drug delivery systems via fluorescence spectroscopy? European Journal of Lipid Science and Technology. 2014;116(9):1234-46.
302. Aldrich S. Coumarin 6 2017 [09/03/17]. Available from: http://www.sigmaaldrich.com/catalog/product/aldrich/546283?lang=en&region=IE.
303. Demuth PC, Garcia-Beltran WF, Ai-Ling ML, Hammond PT, Irvine DJ. Composite dissolving microneedles for coordinated control of antigen and adjuvant delivery kinetics in transcutaneous vaccination. Adv Funct Mater. 2013;23(2):161-72.